Ionic Liquid - Based Nanofluids for Thermal Application

A thesis submitted to The University of Manchester for the degree of
Doctor of Philosophy
in the Faculty of Science and Engineering

2018

Kamil Oster

School of Chemical Engineering and Analytical Science

Contents

Words count: 51968

List of Tables

List of Figures

List of Symbols

D	difussion coefficient
$\overline{z}^2$	mean square particle displacement
l	thickness
T	temperature or torque
∇	nabla operator
∇T	temperature gradient
S	area segment
t	time
Q	energy heat flux
w_U	unit vector
U	internal energy or potential energy
λ	thermal conductivity coefficient or wavelength
ρ	density
c_p	specific isobaric heat capacity
C_p	molar isobaric heat capacity
κ	thermal diffusivity coefficient
a, b	fitting parameters
ΔT	temperature difference
d	diameter
E	Euler's constant ($e^E = 1.78107$) or energy ground state/separation constant
K	calibration constant
W	work
H	enthalpy or Hamiltonian operator
p	pressure or momentum
V	volume or potential energy
Φ	heat flow

R	resistance
C	capacitance
m	mass or equipment type constant
ω	angular frequency
t_p	period
R^2	coefficient of determination
f	frequency or correction factor
τ	elasticity constant
A, B, C, D	adjustable parameters
η	dynamic viscosity coefficient
α_p	isobaric thermal expansion coefficient
x	mole fraction or distance or data points
ν	velocity
F	force
υ	kinematic viscosity coefficient
σ	shear stress
r	radius
γ	shear rate
w	mass fraction
M	molecular mass
$\overline{R}_M$	nuclei positions
Ψ	wavefunction
$\hbar$	Dirac's constant
$\overline{r}_N$	electrons positions
$\mu_i, \Delta\lambda_{o,j}, k_0$	parameters
n	number of groups
A_f	acentric factor
R	gas constant
φ	volume fraction
α	shape factor or fractional factor
ϕ	ratio of interfacial layer thermal conductivity and ionic liquid thermal conductivity
Γ	ratio of interfacial layer thickness and particle diameter

k	total number of data points
ε	absolute enhancement
c	concentration
U_0	overall heat transfer coefficient
A_0	heat transfer area
$(\Delta T)_{lm}$	logarithmic mean temperature difference
D	tube diameter
h	heat transfer coefficient
r	tube thermal resistance
Nu	Nusselt number
Pr	Prandtl number
Re	Reynolds number
u	mean velocity
C_E and C_B	heat transfer unit and reference equipment costs
X and X_B	capacity of the equipment and reference equipment

List of Abbreviations

IL(s)	Ionic Liquid(s)
$[R_1R_1Pyrr]^+$	pyrrolidinium-based cation
$[C_3C_1Pyrr]^+$	1-methyl-1-propylpyrrolidinium cation
$[C_4C_1Pyrr]^+$	1-butyl-1-methylpyrrolidinium cation
C_1Im	1-methylimidazole
$[R_1R_1Im]^+$	imidazolium-based cation
$[C_nC_1Im]^+$	1-alkyl-3-methylimidazolium cation
$[C_2C_1Im]^+$	1-methyl-3-ethylimidazolium cation
$[C_4C_1Im]^+$	1-butyl-3-methylimidazolium cation
$[C_6C_1Im]^+$	1-hexyl-3-ethylimidazolium cation
$[C_8C_1Im]^+$	1-octyl-3-methylimidazolium cation
$[R_1Pyr]^+$	pyridinium-based cation
$[P_{R1,R2,R3,R4}]^+$	quaternary phosphonium-based cation
$[P_{14,6,6,6}]^+$	trihexyl(tetradecyl)phosphonium cation
$[P_{4,4,4,(Al)}]^+$	allyltributylphosphonium cation
$[P_{4,4,4,3}]^+$	tributyl(propyl)phosphonium cation
$[P_{14,6,6,6}][RO]$	trihexyl(tetradecyl)phosphonium carboxylate
$[N_{R1,R2,R3,R4}]^+$	quaternary ammonium-based cation
$[Dca]^-$	dicyanamide anion
$[NTf_2]^-$	bis[(trifluoromethyl)sulfonyl]imide anion
Cl^-	chloride anion
$[Cyc]^-$	cysteinate anion
$[R_1SO_4]^-$	sulfate ester anion
X^-	halide anion
$[BF_4]^-$	tetrafluoroborate anion
$[PF_6]^-$	hexafluorophosphate anion
$[C_1SO_3]^-$	methanesulfonate anion

$[CF_3SO_3]^-$ or $[TfO]^-$	trifluoromethanesulfonate anion
I^-	iodide anion
Br^-	bromide anion
$[AcO]^-$	acetate anion
$[ButO]^-$	butanoate anion
$[HexO]^-$	hexanoate anion
$[OctO]^-$	octanoate anion
$[DecO]^-$	decanoate anion
$[C_2SO_4]^-$	ethylsulfate anion
R_2SO_4	alkylsulfate
R_2CO_3	alkylcarbonate
R_1X	haloalkane
TGA	thermogravimetric analysis
XRD	X-ray diffraction
TA	thermal analysis
DSC	differential scanning calorimetry
DTA	differential thermal analysis
MDSC	modulated differential scanning calorimetry
DFT	density functional theory
AARD	average absolute relative deviation
RD	relative deviation
RAD	relative absolute deviation
CSP	concentrated solar power
HTF(s)	heat transfer fluid(s)
PCM	phase change materials
LBE	Pb and Bi eutectic alloy
FOM	figure-of-merit
NP(s)	nanoparticle(s)
MWCNT	multiwalled carbon nanotubes
BN	boron nitride
G	graphite
MC	mesoporous carbon
INF	ionanofluids

Abstract

The University of Manchester

Kamil Oster

Doctor of Philosophy (PhD)

Ionic Liquid - Based Nanofluids for Thermal Application

July 2018

Heat transfer fluids are materials responsible for heat distribution, transfer and storage. Their significance is undeniable - many technological processes cannot be carried out without using heat transfer materials (for example due to overheating). These are usually mixtures of many compounds, for example glycols, silicones or water. Today's technologies constantly require more efficient, environmentally- and economically-friendly solutions for heat transfer applications. It is necessary to know the full physicochemical characteristics to design a new heat transfer fluid (mainly density, heat capacity, viscosity and thermal conductivity). Nanofluids (mixture of a basefluid and nanoparticles) were proposed as a solution for many industrial issues due to their enhanced thermophysical properties (*i.e.* thermal conductivity) than pure liquids. Moreover, these enhancements exhibit unusual features which make this group of materials interesting from molecular and industrial point of view. Ionic liquids, task specific materials with tuneable properties were repeatedly recommended as heat transfer fluids due to their specific properties (mainly low vapour pressure, wide liquidus range, or non-flammability) caused by the ionic structure. A very interesting material can be obtained by mixing ionic liquids and nanoparticles where specific properties of ionic liquids are preserved, and thermophysical properties are enhanced due to nanoparticles dispersion.

In this work, we investigated ionic liquid - based nanofluids from the experimental and theoretical point of view, including imidazolium-, pyrrolidinium- and phosphonium-based ionic liquids with several different anions, and multiwalled carbon nanotubes, graphite, boron nitride and mesoporous carbon as nanoparticles, and also in mixtures with water. As a final result, we assessed the molecular recognition of the thermophysical properties enhancements in ionanofluids, developed the predictive models for physical properties, compared all investigated systems to commercial heat transfer fluids.

The project was supported by King Faisal University (Saudi Arabia) through a research fund from the International Cooperation and Knowledge Exchange Administration department at KFU. Cytec are thanked for the generous donation of the trihexyl(tetradecyl)phosphonium chloride sample.

Declaration

No portion of the work referred to in the thesis has been submitted in support of an application for another degree or qualification of this or any other university or other institute of learning.

Copyright Statement

Acknowledgments

The last 3 years - completion of the PhD and life, were probably one of the most challenging in my life, with several ups and downs. I couldn't finish and achieve this all without quite a few, very important, people in my life.

A huge thank you to Chris who supervised me throughout the whole project. Before I began working with him, I didn't believe there's someone who knows everything. It was an honour to meet and work with him.

No less thanks to Johan who didn't only supervise my work but also has become a great friend of mine, supporting me, offering more ideas and challenging me.

A gratitude to Ana who didn't hesitate to tear apart my manuscripts (and it's hard to admit but she was right, most of the time). She also helped me by listening, understanding and advising me.

My everyday life would be extremely boring if not all my friends from the office. I would like to say a special thank you to Adam, who always listens to my moaning, Terri - I couldn't ask for better company sitting next to me every day, Janine, a friend that you can talk about everything and will always support you, and all my other colleagues - Rebecca, Marta, Tom, Helen and Cristina. Thanks to Peter for help in the lab, especially ionic liquids synthesis.

I wouldn't be where I currently am if not Mirosław C. and his wife Anna C. They are not only people I had a pleasure to work with, but they are friends of mine. They have always been in the side lines, cheering me on in my success and achievements, they have put my accomplishment above theirs and still are happy for me. Thank you is not enough to show how grateful I am.

My passion to physical chemistry was seeded by Monika G.-R. She was the best lecturer at University I could have ever had. I would like to say thank you for contributing

to my success as a scientist, being my science tutor.

I would like to thank to my parents and family for bringing me up, supporting in my decisions and help moving to the UK. A special gratitude to my grandmother Krystyna for inspiration and showing me the meaning of hard work.

Anna O. is one of the biggest support in my life. She listens, understands, helps, advises and cares. I couldn't go through the last 3 years, and more without her. She knows me better than anyone on this Planet (Hey! We've known each other for over 15 years!)

To Andrew, extremely huge thank you for the love you gave me, the support, being my person I could always rely on, making me proud of you (and also being proud of me), encouragement and motivation. I probably wouldn't complete the PhD without you during my meltdowns over the writing up.

Every revolutionary idea - in science, politics, art, or whatever - seems to evoke three stages of reaction. They may be summed up by the phrases:

(1) It's completely impossible - don't waste my time

(2) It's possible, but it's not worth doing

(3) I said it was a good idea all along

Arthur C. Clarke's Law of Revolutionary Ideas

Publications

K. Oster, P. Goodrich, J. Jacquemin, C. Hardacre, A. P. C. Ribeiro, A. Elsinawi, A New Insight Into Pure and Water-Saturated Quaternary Phosphonium-Based Carboxylate Ionic Liquids: Density, Heat Capacity, Ionic Conductivity, Thermogravimetric Analysis, Thermal Conductivity and Viscosity, *The Journal of Chemical Thermodynamics*, **2018**, 121, 97-111.

K. Oster, J. Jacquemin, C. Hardacre, A. P. C. Ribeiro, A. Elsinawi, Further Development of the Predictive Models for Physical Properties of Pure Ionic Liquids: Thermal Conductivity and Heat Capacity, *The Journal of Chemical Thermodynamics*, **2018**, 118, 1-15.

K. Oster, C. Hardacre, J. Jacquemin, A. P. C. Ribeiro, A. Elsinawi, Understanding the Heat Capacity Enhancement in Ionic Liquid-Based Nanofluids (Ionanofluids), *Journal of Molecular Liquids*, **2018**, 253, 326-339.

K. Oster, C. Hardacre, J. Jacquemin, A. P. C. Ribeiro, A. Elsinawi, Thermal Conductivity Enhancement Phenomena in Ionic Liquid-Based Nanofluids (Ionanofluids), *Australian Journal of Chemistry*, **2018**, doi.org/10.1071/CH18116, *In memory of Prof. Kenneth Seddon*

Chapter 1

Theoretical Background

1.1 Ionic Liquids

Nowadays' technologies and processes encounter a problem with chemicals that are not environmentally friendly, or their thermal properties are insufficient for many technical purposes. These factors drive chemists and engineers to search for new solutions for many technological and environmental issues. Ionic liquid (ILs) have been examined as alternative solvents and fluids which may provide a solution to these issues. [1–3] The first discovered and experimentally approved IL was ethylammonium nitrate, by Walden (**1914**). [4] There have been many studies on the molecular structure, properties and the application of ILs since this discovery. [5–11] ILs are thought to be prospective materials for many applications for example catalysis, [12] synthesis, [13] solar panels, [14] lubricants, [15] luminescent materials, [16] supercritical fluids, [17] *etc.* The literature for further reading on ILs include references [18–28].

1.1.1 Definition

During *the Faraday Discussions on Ionic Liquids: From Fundamental Properties to Practical Applications* meeting, Professor Douglas R. MacFarlane raised many issues related to ILs. [28] One of them was the definition of ILs. The most common definition is that ILs are salts with melting point below 373.15 K. This is not a fully correct approach

because of the following aspects: **a)** salt remains a single component while mixing several components lowers the liquidus point forming the liquid phase; **b)** melting point of 373.15 K seems to be very limiting factor, as most industrial applications consider the temperature higher than 373.15 K. Certainly it is beneficial if the medium has low melting point, for example room temperature (room temperature ILs, RTILs). The most reasonable definition proposed is that ILs consist entirely of ions. The ionicity can be induced by the purity of the ILs (also explained on the basis of Walden rule in Experimental Section 2.2.5), therefore, this is a very important property to be controlled and reported. MacFarlane *et al.* (**2009**) investigated several different types of ILs and reported distinctive degrees of ionicity, for example almost perfectly ionic ILs are $[C_3C_1Pyr][Dca]$ and $[C_2C_1Im][NTf_2]$ and a much less ionic IL is $[P_{14,6,6,6}][NTf_2]$. [29] Similar work was carried out by Fraser *et al.* (**2007**), with the same result for $[P_{14,6,6,6}][NTf_2]$, and reporting very weak ionic compounds, such as $[P_{14,6,6,6}]Cl$ or $[P_{14,6,6,6}][Cyc]$ (term *compounds* has been used specifically as the degree of ionicity is very low). [30]

1.1.2 Classification

ILs can be classified in order to their structure, type of anion or cation. The most commonly used cations are imidazolium, $[R_1R_2Im]^+$, pyridinium, $[R_1Pyr]^+$, pyrrolidinium, $[R_1R_2Pyrr]^+$, quaternary ammonium, $[N_{R1,R2,R3,R4}]^+$, and quaternary phosphonium, $[P_{R1,R2,R3,R4}]^+$ (**Figure 1.1.1**). [31] While the most commonly used anions are sulfate esters, $[R_1SO_4]^-$, halide, X^-, dicyanamide, $[Dca]^-$, tetrafluoroborate, $[BF_4]^-$, hexafluorophosphate, $[PF_6]^-$, or bis(trifluoromethylsulfonyl)imide, $[NTf_2]^-$ (**Figure 1.1.1**). [31] Moreover, ILs can be also classified in terms of the quantitative composition of cations and anions: dicationic, [32] or dianionic, [33] *etc.*

The research interest of scientists on ILs is classified into 4 evolutions. The 1st evolution, primarily developed by Angell, [34–36] and Moynihan, [37] reports the physical properties of RTILs. The 2nd evolution is the recognition of ILs tuneable properties, the 3rd evolution refers to the biological properties of ILs. Finally, the most recent 4th evolution treats the ILs in solutions with other solvents. [28]

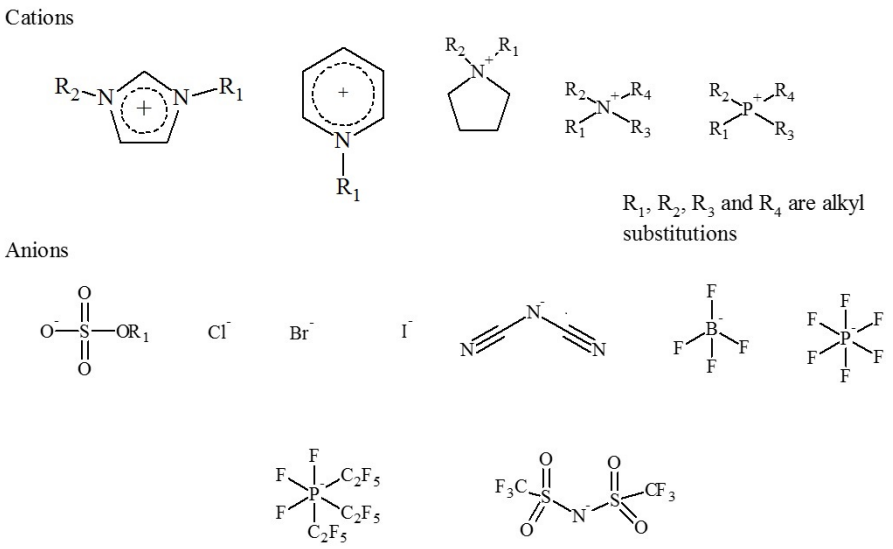

Figure 1.1.1. Most common used cations (upper) and anions (lower) in ILs.

1.1.3 Interactions and Properties

ILs are characterized by short-range order and long-range disorder. The short-range ordering is a combination of dominant Coulombic charge-charge interactions balanced against the rotational and vibrational freedom of ions. [21] They can be treated as an elaborate network of ions which is stabilized by electrostatic charges and hydrogen bonding. [31] Hunt *et al.* (**2015**) described plethora of types of hydrogen bonding which can be found in ILs, *i.e.* simply neutral, ionic, doubly ionic, bifurcated traditional, bifurcated-multiple anions, bifurcated/chelated single anion, chelated-traditional, chelated from positions within same molecule, anion-anion, *etc.* [38] Matthews *et al.* (**2015**) discussed the possibility of π-π interactions in imidazolium-chloride ILs clusters, and hydrogen bonding. [39] Their impact on physical properties is not negligible and is discussed herein.

Most ILs have relatively a wide liquidus range. This property is caused by the characteristic ionic structure of ILs, governed by Coulombic interactions and specific interactions, such as hydrogen bonding. As an example, the liquidus range for [C_nC_1Im] salts is typically over 573.15 K. [20] This range is much narrower for water (100 K) or ethanol (192.6 K). [40]

One of the characteristic features of ILs is their very low vapour pressure. This has

led to them being called green materials due to their low vapour toxicity/pollution and their reduced flammability. On the other hand, this class of compounds is more difficult to purify due to their low vapour pressure, in many cases impossible to distil under standard conditions. Earle *et al.* (**2006**) proved that it is possible to distil ILs but this process is very slow and occurs under very harsh conditions. [41] As described above, ILs are sometimes described as green solvents due to their negligible vapour pressure, which prevents the exposure of the solvent to the atmosphere and to the worker. However, it must be considered that a release of ILs from industrial process into environment (*i.e.* ground water) may be dangerous due to their toxicity. Moreover, the high stability of some ILs can make them persistent pollutants in wastewaters. [42] García *et al.* (**2005**) showed that ILs, in general, have very poor biodegradability. [43] This is an issue due to the harmful effect on bacteria, fungi or other organisms, instead of being degraded. This may also result in bioaccumulation making them difficult to remove from environmental cycles.

ILs are expected to have an ionic conductivity which makes them reliable materials for electrical applications. [44–46] This property depends directly on the structure of ILs. Bulky cations tend to have lower conductivities due to larger size what results in lower mobility (and ability to transport the charge). Overall, the ionic conductivity of ILs is lower than that of conventional aqueous electrolytes solutions but similar to those of solutions of inorganic electrolytes in aprotic organic solvents. [20]

Due to their low volatility, the upper limit temperature is reported as to thermal decomposition temperature (ILs decompose before boiling). There are two types of thermal stability: short-term and long-term. The first one is determined by applying a relatively high heating rate in thermogravimetric analysis (TGA; 10 K min^{-1} to 20 K min^{-1}). The second type of thermal stability is determined by applying a constant temperature for longer time (2, 15 or 20) h. [47] Nevertheless, any considerations of the long-term experiment must include the contribution of evaporation. It is well-known that ILs have low vapour pressure, however, application of high temperature for a long time may result in some weight loss. For instance, the vapour pressures at 500 K of $[C_2C_1Im][NTf_2]$, $[C_2C_1Im][MeSO_3]$ and $[C_2C_1Im][CF_3SO_3]$ are (0.10, 0.014 and 0.013) Pa, respectively. [48, 49] While the vapour pressure at 373 K for water is 10132 Pa, or 101325 Pa for ethylene glycol at 470 K. [40]

The thermal stability is cation- and anion-type dependent. In terms of cation

dependence on the thermal stability, the following sequence can be found (for compounds based on N-atom, from most stable to least stable): $[R_1R_2Pyrr]^+$, $[R_1R_2Im]^+$, $[R_1Pyr]^+$, $[N_{R1,R2,R3,R4}]^+$. [50–54] Increasing the alkyl chain length reduces the thermal stability. This trend is assigned to weaker Coulombic interactions between cation and anion with longer alkyl chain length leading to increased stability of the carbocation and carbon radicals. This has been proved for imidazolium Cl^-, $[BF_4]^-$, $[PF_6]^-$, $[NTf_2]^-$, $[TfO]^-$. [55–58] Imidazolium-based ILs with unsaturated alkyl chains exhibit lower stability than their analogues with fully saturated alkyl chains. [59] $[P_{R1,R2,R3,R4}]^+$-based ILs are more stable than their corresponding ammonium salts. In the series of phosphonium dicyanamide salts, the decomposition temperature at which 10% weight loss occurs is even 100 K higher than the corresponding ammonium salts. [49] Quaternary phosphonium ILs with fully saturated alkyl chains are less stable than their corresponding salts with some unsaturated alkyl chains, *i.e.* unsaturated allyltributylphosphonium salts $[P_{4,4,4,(Al)}][NTf_2]$ are more stable than the saturated analogues $[P_{4,4,4,3}][NTf_2]$. [49] The thermal stability of ILs with different anions can be well-correlated with the anion hydrophobicity, since this is a measure for the H-bonding capacity and often nucleophilicity. [55] The stability decreases in the following order: $[PF_6]^- > [NTf_2]^- > [BF_4]^- > [Me]^- > I^- > Cl^- > Br^- > F^- >$ $[MeSO_4]$-. [47]

1.1.4 Synthesis and Purification

The synthesis and purification of ILs were extensively described in the work of Wasserscheid *et al.* (**2002**), and the basic principles are presented herein. [21] The synthesis of ILs is divided into two steps: formation of the desired cation, and anion exchange (if needed).

The general procedure for imidazolium-based ILs is shown in **Figure 1.1.2**. Holbrey *et al.* (**2002**) proposed an efficient and halide-free synthesis (**Figure 1.1.2**, step 1.1) which is based on the reaction of 1-methylimidazole, C_1Im, with alkylsulfate, R_2SO_4, or alkylcarbonate, R_2CO_3. [60] The first step of the general and most commonly used procedure is shown in **Figure 1.1.2** (step 1.2), where C_1Im undergoes the reaction with haloalkane, R_1X, to form 1-alkyl-3-methylimidazolium halide, $[C_1R_1Im]X$. [60] This

product is then treated (if desired) in the second step (**Figure 1.1.2**, step 2), where the halide anion is exchanged with the salt containing the desired anion.

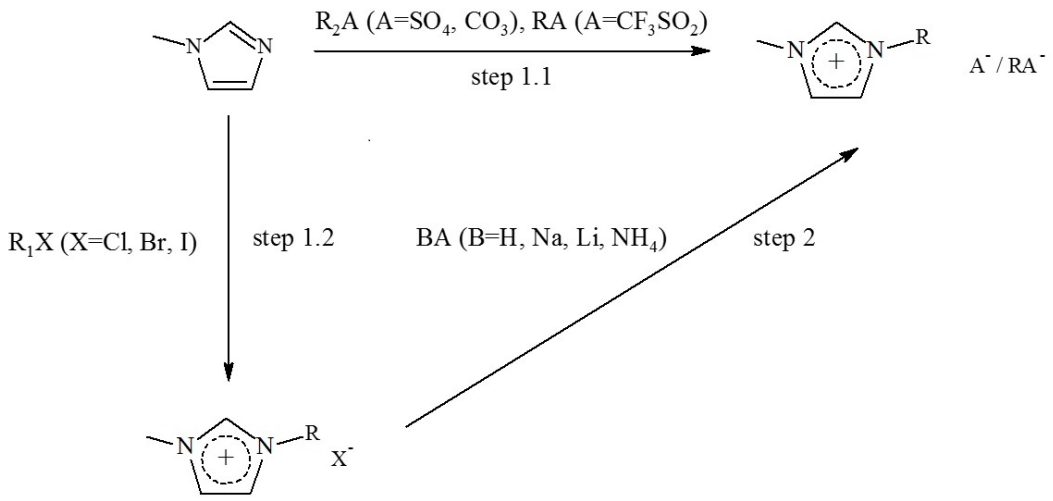

Figure 1.1.2. Schematic route of imidazolium-based ILs synthesis.

A similar procedure is applied for quaternary ammonium- and phosphonium-based ILs. [61] In the first step (**Figure 1.1.3a** - phosphonium-based ILs, **Figure 1.1.3b** - ammonium-based ILs), trialkylphosphine or trialkylamine undergoes reaction with a haloalkane, to form a quaternary phosphonium or ammonium halide salt. In the second step (**Figure 1.1.3a** - phosphonium-based ILs, **Figure 1.1.3b** - ammonium-based ILs), the previously obtained quaternary halide salt is treated with the desired halide anion salt, to obtain the desired quaternary cation-based ILs.

a)

$$PR_3 \xrightarrow[\text{step 1}]{R'X} [PR_3R']^+[X]^- \xrightarrow[\text{step 2}]{BA\ (B=H,\ Na,\ Li,\ NH_4)} [PR_3R']^+[A]^-$$

b)

$$NR_3 \xrightarrow[\text{step 1}]{R'X} [NR_3R']^+[X]^- \xrightarrow[\text{step 2}]{BA\ (B=H,\ Na,\ Li,\ NH_4)} [NR_3R']^+[A]^-$$

Figure 1.1.3. Schematic reactions for **a)** quaternary phosphonium-based ILs, **b)** ammonium-based ILs. [61]

It is of high importance to use starting materials as pure as possible, for example distilling or crystallising the reagents prior to use. In many cases, the main impurities in ILs are halides and water. [62] The most commonly used method to purify ILs is washing (with solvent in which the IL is immiscible) and extraction (with dichloromethane or other solvent, in which IL has excellent miscibility and the washing agent is immiscible). [21] It is recommended to repeat the washing-extraction process 3-5 times, until no halide is detected. This is commonly tested using silver nitrate titration of the washings/ILs. The last step of purification is drying under high vacuum, when water and other volatile solvents are removed.

Seddon *et al.* (2000) investigated the impact of impurities on the physical properties (density and viscosity). Firstly, even small amount of chloride can cause higher viscosity. [62] In contrast, the effect on density is smaller. [62] On the other hand, water is ubiquitous in ILs due to the impossibility of its complete removal. Moreover, ILs are hygroscopic (even if the IL is hydrophobic). Water (and other solvents) causes the viscosity to shift to lower values. [62] The impact with respect to the density of the ILs is not that straightforward, and it depends on the density of salt. If the IL density is higher than that of water, the presence of water lowers the density and *vice versa*.

1.2 Nanoparticles

Nanotechnology has significantly increased the interests of scientists over the last decade, mainly due to unique properties of such group of materials, described herein. But also, they can provide new resources of applications, and interestingly improve the efficiency of many processes. Even though it may seem that nanotechnology is a new branch of science, and the first report was published by Norio Taniguchi from Tokyo University in 1974, [63] it should be kept in mind that *'nanoparticles are not a new discovery of science, nor are they an innovation, as regards their definition based on their particle size or as a technical achievement. They have, however, always been components of smoke'*, as stated by Dirk Walter. [64] The literature for further reading on nanoparticles include references [65–73].

1.2.1 Definition

The term *'nanoparticles'* is defined ambiguously. For example Mohanraj and Chen (**2006**) defined them as particles with size below 1000 nm. [66] Whereas the pre-normative ISO nomenclature recommendations (ISO / TS 27687) state that:

- nano-definition considered the range of (1-100) nm dimension;
- nano-objects are considered as one, two or three external nano-domain dimensions, *i.e.* nano-plates have only one nano-sized dimension, nanofibers are two nano-sized dimensions, and the third dimensional are significantly longer.

Other definitions (*i.e.* Health Canada or The National Industrial Chemicals Notifications and Assessment Scheme) also fully cover the ISO definition. In 2010, the European commission also took part in such discussion, and modified the ISO definition, as follows:

- nanoparticles with (1-100) nm size for at least 1% of their number size distribution;
- internal or surface structure in at least one dimension is in the size of (1-100) nm;

- specific surface area (by volume) at least 60 m^2 cm^{-3}, excluding materials smaller than 1 nm.

1.2.2 Specific Properties

Important definitions were discussed by Walter (**2013**) concerning these are primary particles, agglomerates and aggregates. [64] Primary particles are recognized with many various shapes (spheres, cubes, rods), while those with undefined shape are called bulky. A natural process is that primary particles prone to create larger units, called agglomerates (usually due to adhesion forces, weak physical interactions). Agglomerates are an assembly of primary particles, while the total surface area of these objects does not differ from the summation of the surface areas of all primary particles. Therefore, many consequences can be pointed out: agglomerates depend on the conditions of environment (temperature and/or pressure), viability to destroy large agglomerates to smaller units. On the other hand, aggregates are also an assembly of primary particles but created when common crystalline structure of nanoparticles is formed (similarly to sintering). The particles are aggregated in alignment to each other, so consequently, the total surface area is smaller than the summation of all surface areas of all particles. The above consideration may be crucial when considering some materials as nano-sized because the size of particles can be reported as agglomerates. It can lead to wrong results, thus, attention must be paid to this issue.

One of the characteristic property of nanoparticles is their high specific surface area (the surface area per mass unit). The size of particles has a significant impact on the surface area, *i.e.* the smaller the particles size the larger the surface area (**Figure 1.2.1**). This, in turn, affects the thermal properties of such materials as the heat exchange is enhanced with larger contact areas. [74] Surface area has significant contribution to many other properties of nanoparticles, for example dispersity or, in case of TiO_2 solutions, the decrease of pH. [75] Heat transfer is a process in which the heat exchange occurs at the surface of nanoparticles, thus materials with large surface area are expected to have higher thermal conductivity and heat capacity. [74, 76] As Yurkov *et al.* (**2007**) proved, electrical properties depend on the size of nanoparticles. [77] As defined above, nanomaterials are expected to have size in the range of 1-100 nm. This definition is not always strictly

applied as many materials cannot be prepared in such a size range. Surface morphology is a term used to describe the nanoparticles shape, size, porosity, pores volume, pores width, *etc.* Shape is also an important factor which must always be taken into account while considering processes occurring at the surface of nanoparticles, such as heat exchange, liquid-solid and gas-solid adsorption, or optical properties. All matter tends to minimize their surface energy, and this is also observed in the case of nanomaterials in dispersion. Their surface energy is an increasing function of the particle size decreasing which means that they prone to form aggregates in which the surface energy is lower. [78]

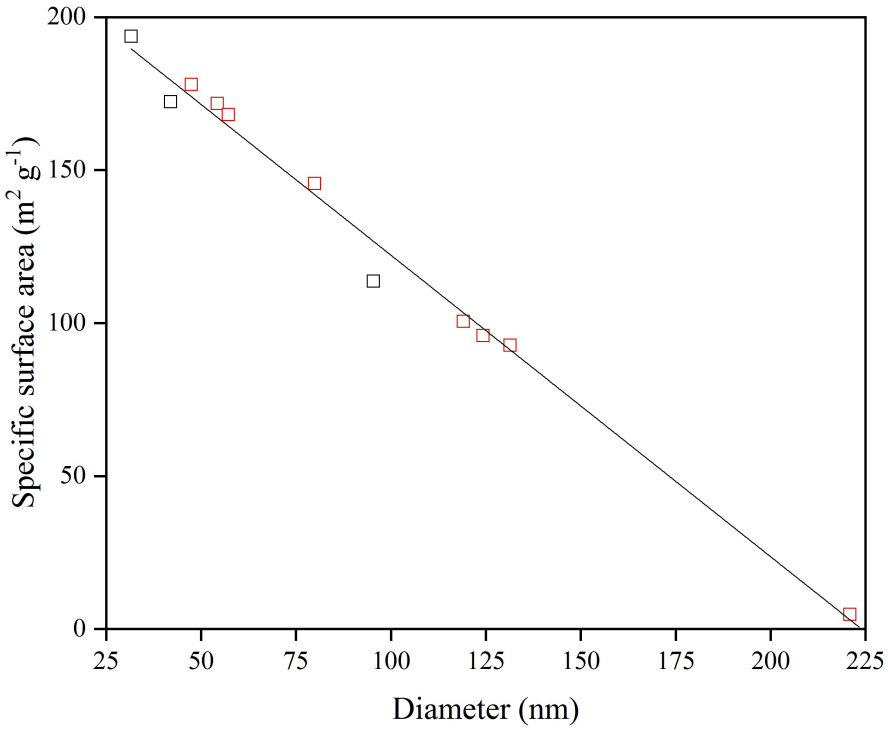

Figure 1.2.1. The dependence of specific surface area on diameter of nanoparticles for diamond, □, carbon black, □ [79, 80].

The properties of nanomaterials vary extensively and depend on the type of nanoparticles, their structure and individual factors. However, they exhibit unique properties in comparison to their micro-sized or bigger equivalents. Studies of Lu *et al.* (**2005**) proved that the structure of carbon nanotubes has significant impact on their electrical properties, they can be metallic or semiconductors. [81] Furthermore, Yurkov *et al.* (**2007**) showed that the electrical properties of nanoparticles containing iron and cobalt depend on

the particles size. [77] The thermal conductivity of nanomaterials is usually very high, for example Kim *et al.* (**2001**) showed that carbon nanotubes can have extremely high thermal conductivities. [82] Nanomaterials exhibit very high strength and strain moduli which makes them very good candidates for construction applications. Due to lattice defects, most materials are found to exhibit different properties, *i.e.* graphite is fragile. [83]

1.3 Nanofluids

The first notification of solid-liquid dispersion was reported in 1861 by Scottish chemist Thomas Graham. [84] A new branch of science was then named colloids chemistry with the investigated systems colloids. This branch of studies is very sophisticated in its molecular understanding, and, generally, the colloids are naturally occurring, for example wood (solid + liquid), asphalt (solid + liquid), milk (liquid + liquid) or styrofoam (solid + gas). The literature for further reading on nanofluids include references [85–91].

1.3.1 Definition

The dispersion system remains physically discontinuous and it consists of two or more phases: continuous phase (dispersing or dispersion medium) and fine suspended particles (dispersed phase). An important criterion for dispersion systems is the differentiation in fineness degree of the substance, a degree of dispersion. This parameter is defined as the ratio of dispersed phase surface to its volume: suspensions ($>10^{-5}$ m or 10^{-7}-10^{-5} m particles size for macroscopic or microscopic dispersions, respectively), colloids (10^{-9}-10^{-7} m particles size) and proper solutions ($<10^{-9}$ m particles size), for example nanofluids are colloids with dispersed particles of 10^{-9} m in size. However, the distinction between them is not strict, particularly, when the physical or chemical properties are considered. In the case of colloids, all dispersed fine particles remain separate phase with a specific phase volume and interface. However, every single particle is a kinetic unit with a particular shape and size. A dispersed phase is usually thermodynamically unstable in comparison to dispersing phase but it remains kinetic metastability (no observable changes within a relatively long time due to protective layer on the particle). There are several characteristic features of such defined systems:

- the particles of dispersed phase interact with each other *via* intermolecular forces which are not saturated on the interface, and their order is significantly longer than the interatomic distances;

- dispersed phase has highly resolved interfacial surface of which properties are determined by the interactions of system with the external electromagnetic or gravitational fields;

- the chemical nature of particles is the same as the substance from which they are originated. If the particles of the dispersed phase consists of many different molecules, the molecules conserve the individual chemical and physical properties, after they separate from each other.

1.3.2 Classification

Dispersion systems can be classified based on several criteria, *i.e.* the type of interface created between the dispersed phase and the dispersing phase, size, shape and physicochemical properties of dispersed phase. The thermodynamics of comminution can be another parameter used to distinguish between them (spontaneous or energetically supported). The most widely accepted classification is based on the physical states of dispersing and dispersed phases, thus, on the type of interface and the aggregation (**Table 1.3.1**).

Table 1.3.1. Classification of dispersion systems based on physical states of dispersing and dispersed phases.

		Dispersed phase		
		Gas	**Liquid**	**Solid**
Dispersing phase	**Gas**	Full miscibility	Liquid aerosol (fog)	Solid aerosol (smoke)
	Liquid	Foam (shaving cream)	Emulsion, microemulsion, colloidal solution (cosmetic creams)	Sol, micellar system, liposome, suspension, colloidal solution (ink)
	Solid	Solid foam (pumice)	Gel (asphalt)	Solid sol (pearl)

Another classification is based on the particle size distribution. As well as the average particle size, the size distribution function is an important parameter to describe particles in the dispersed phase. The system is called monodispersed when all particles are of the same size (**Figure 1.3.1a**), otherwise the system is polydispersed (**Figure 1.3.1c**). Nevertheless, the monodisperse systems do not occur so systems with relatively narrow size distribution are considered as monodispersion (**Figure 1.3.1b**).

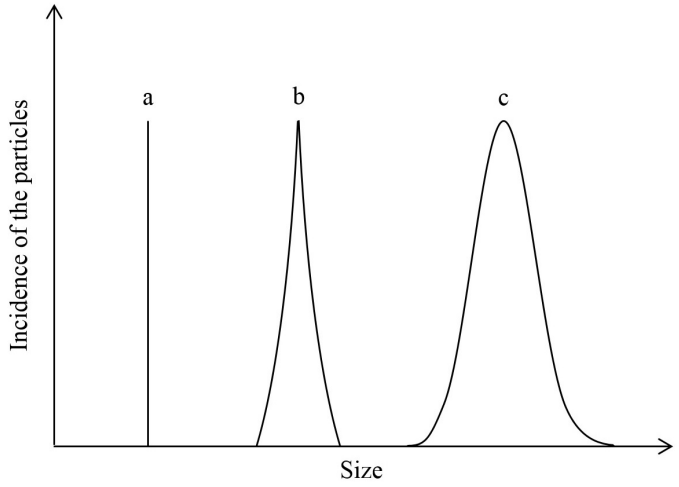

Figure 1.3.1. Size distribution functions of dispersion systems for **a)** strict monodispersion; **b)** monodispersion; **c)** polydispersion.

Dispersion systems can be also one-shape (balls, sticks, discs) or poly-shaped (several shapes in one sample, *i.e.* from spheres to discs-like). There can be distinguished lyophilic colloids (water as dispersing phase), and lyophobic colloids. Lyophilic systems exhibit high affinity to the solvent, and the solvation shell makes them more stable. Lyophobic systems are described as less attracting to the solvent, and they are stabilized mainly by the electrostatically charged layers. In the meaning of dispersion process thermodynamics, they can be divided into micellar systems (also called association colloids in which dispersed phase becomes scattered spontaneously due to weak intermolecular interactions) and phase systems (also called dispersion colloids in which dispersed phase becomes scattered by applying external forces, *i.e.* milling or ultrasound).

1.3.3 Specific Properties

A significant role is played by the chaotic thermal motions of the dispersed phase in dispersing medium, which is a result of the interaction of particles with dispersing phase components. These motions, with zigzag trajectory, are stronger (so the velocity of particles is also higher) with lower particle sizes, for example it is not possible to observe this effect for millimetre-sized materials. This phenomenon is called Brownian motion. This motion is insensitive to external stimuli (electrical, magnetic or gravitational fields), the physical state of the dispersing medium and the dispersed phase. However, temperature and viscosity have a significant impact. The mathematical foundations of Brownian motion were proposed by Einstein and Smoluchowski. The authors derived an equation which relates the mean square particle displacement in a direction, $\overline{z}^2$, occurring at the same time period, t, during chaotic motions, with a diffusion coefficient, D: [92, 93]

$$\overline{z}^2 = 2Dt \tag{1.3.1}$$

From the molecular point of view, the reason for the existence of diffusion is the same as for Brownian motion, *i.e.* thermal motion. The diffusion coefficient is related to the viscosity of the liquid, η, and the size of the particles (in this case radius), r, by the following Einstein-Smoluchowski equation:

$$D = \frac{kT}{6\pi\eta r} \tag{1.3.2}$$

Thus, it is possible to determine the diffusion coefficient experimentally, *i.e.* by scattering methods, nuclear magnetic resonance or electrochemistry.

The characteristic properties of colloids are assigned to a specific light scattering. Nevertheless, the light introduced to the system is both absorbed and scattered. However, for the purpose of colloids unique properties discussion, it will be limited to only scattering process, it means the changes in wave propagation direction without changing its length. The scattering of light by colloids particles was first observed by Irish physicist John Tyndall, thus, this phenomenon is called Tyndall effect (**Figure 1.3.2**). If the beam is passed through the colloid, its intensity is decreased not only due to absorption but also by the scattering on inhomogeneities (caused by the dispersed particles). This effect is

usually very strong and can be easily observed with *naked eye*.

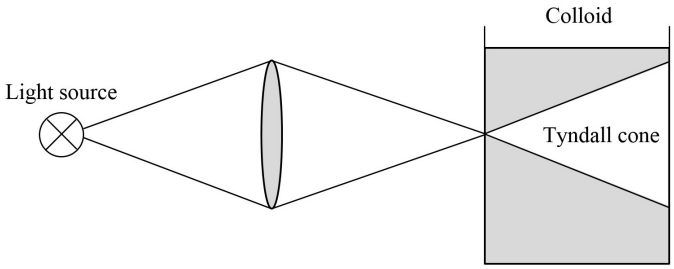

Figure 1.3.2. Tyndall effect.

Dispersion systems are usually thermodynamically unstable, and the only question is about the kinetics, *i.e.* the time after the particles of dispersed phase aggregate and create phase with a larger size, thereafter sedimentation occurs. If the attraction forces are dominant, the particles aggregate quicker. Otherwise, the repulsion forces are dominant, the particles move more freely, and system is usually more stable. The particles in a dispersed phase have defined structure, shape and interface surface. There is an electrostatic potential distribution near the interface of dispersed phase particles and dispersing phase due to the presence of ions, dipoles, *etc.* Charged particles can be found in almost every system, and it can be also caused by the ionic group dissociation, ions or dipoles adsorption onto the interface surface. The structure of dispersed phase particles and scheme of potential distribution are presented in **Figure 1.3.3**. The structure of this double layer is described by the model proposed by Stern which is based on elementary theories of Helmholtz, Gouy and Chapman. The term *electrical double layer* is an analogous to the parallel plate capacitor. In the meaning of Stern model, the double layer is divided into two parts. The first layer which is adhered to solid state particle, also called Helmholtz-Stern layer (or adsorption layer). It usually has a thickness of ions which means that the counterions accumulated close to the charged particle create bulk layer with a specific packing density. The potential changes approximately linearly with the distance from the interface, and on the border achieves some value, named electrokinetic potential (zeta potential). The second layer is called Gouy-Chapman layer (or diffuse layer), and because of thermal motions occurring in the system, the ordering becomes highly disturbed at some specific distance. The changes of potential with the distance in this layer are non-linear. From the above considerations, this phenomenon is called electrical double layer as it is built with

two layers: the first one on the surface of particle, and the second one is the diffuse layer.

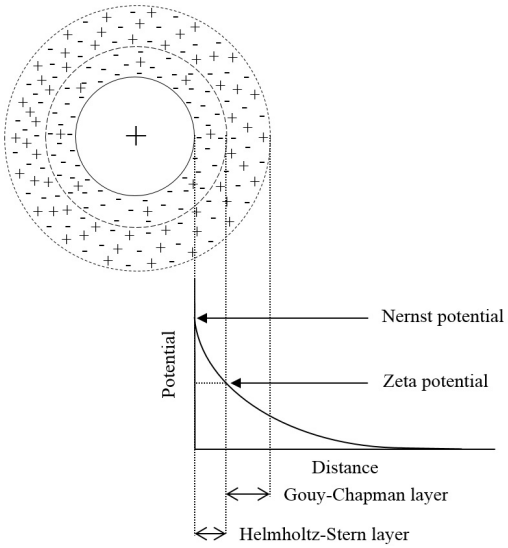

Figure 1.3.3. Structure of electrical double layer created on the surface of dispersed phase particle.

The thickness of the diffuse layer is one the most important parameters which characterizes the spatial range of electrostatic interactions, it depends on the concentration and type of ions in the solution, increases with temperature and relative permittivity. The stability of a dispersion system is not only dependent on the Coulombic interactions between charged particles but also electrostatic interactions of higher order, *i.e.* dipole-dipole or van der Waals. Nevertheless, a colloid's stability is strongly determined by the value of the zeta potential. The meaning of zeta potential for other characteristic properties of colloids is also discussed, herein. The absolute value of the zeta potential determines directly the stability of colloids where higher values are proportional to stronger repulsion forces and higher stability (**Table 1.3.2**).

Table 1.3.2. General description of colloids stability caused by the values of zeta potential.

Absolute zeta potential (mV)	Stability
< 10	Rapid coagulation/flocculation
10-30	Slight stability/almost unstable
30-40	Moderate stability
40-60	Good stability
> 61	Excellent stability

1.3.4 Heat Transfer in Nanofluids

The mechanism of thermal conduction in a gas is explained by a simple kinetic theory of gases. The temperature is directly related to the kinetic energy of molecules where higher temperatures result in higher kinetic energy (and higher velocity). Gas molecules are in a continuous flow, colliding with each other. While transported from a cooler region to a warmer region, they transport the kinetic energy and collide to molecules with lower kinetic energy. Upon collision with slower molecules, they give up some of their energy and increase the energy of lower energy molecules. The thermal conduction mechanism occurring in liquids is qualitatively similar to that of the gas but it is more complicated in the mathematical formalism. For most liquids, the thermal conductivity decreases with temperature, with water as an exception. The mechanism of thermal conduction in a solid is based on free electrons and atoms in a periodic lattice arrangement. The thermal conduction occurs with two mechanisms: migration of free electrons and lattice vibration. These two are additive but the migration is much more effective than vibration.

Nanofluids were repeatedly reported to have enhanced thermal conductivity and heat capacity, in contrary to mixing theory. This behaviour was not fully explained, so far. While thermal conductivity has been widely investigated in the literature and many theories were proposed, [94–99] heat capacity remained abandoned for a long time. The main point was focused about unusual enhancement caused by the addition of nanoparticles, which have usually lower heat capacity than liquids. [100] Following the first approach to describe this behaviour based on mixing theory for ideal gas mixtures, the heat capacity should be a decreasing function of nanoparticles loading, which was later proved to be wrong. [101] A further derivation leads to the assumption of thermal equilibrium between the particles and the surrounding fluid by including the density of liquid and nanoparticles. Still the reproducibility was very limited. [101] A meaningful theory was recommended by Shin and Banerjee (**2011**). [74] The authors assigned the enhancement due to the following three modes: **a)** resolved surface area of nanoparticles where the surface atoms are less constrained in terms of bonding, and these vibrate with a lower natural frequency and higher amplitude (resulting in higher surface energy); **b)** the interfacial interactions between nanoparticles surface atoms and liquid molecules act as an additional energy storage layer; **c)** the adhered nanolayers exhibit semi-solid higher physical properties than

bulk liquid (*i.e.* density and heat capacity). The most recent work, reported by Hentschke (**2016**), introduced the full mathematical fundamentals of the enhancement. [79] This includes the interfacial layering, and some type of overlapping mesolayers. The phenomena of thermal conductivity enhancement caused by the dispersion of nanoparticles into liquids has been widely discussed in the literature, for example the mechanism was explained by Brownian motion of nanoparticles, liquid layering at the liquid/particle interface, nature of heat transport across nanoparticles, nanoparticle clustering, while the interface layering was proven to be the most sensible explanation in a good agreement with experimental and theoretical works. [102–108] Different various models were also proposed to correlate the thermal conductivity enhancement and a number of reviews have been published. [102–106]

1.3.5 Preparation

Nanofluids are not simply liquid-solid mixtures. Stable and durable colloids require a specific and gentle preparation with a further treatment. For this reason, many techniques for the preparation of the nanofluids have been developed. Those are divided into two groups: one-step and two-step processes. [109]

In one-step methods, preparation of nanoparticles and their dispersing are being done simultaneously. The main advantage of this process is the minimization of nanoparticles agglomeration and increasing the stability of suspension. [109] Only low vapour pressure fluids are appropriate for this process which is the main disadvantage, [109] however, it is also associated with leaving the residual reactants (impurities) in the suspension, mainly due to the incomplete reaction, which are difficult to remove. [110] The major limitation is the oxidation of nanoparticles in contact with surrounding air. [111] The methods used to prepare nanofluids through one-step process include the thermal decomposition of organometallic precursors, [112] physical vapour condensation, [113] chemical reduction, [114] submerged arc nanoparticle synthesis, [115] laser ablation, [116] and microwave irradiation. [117]

In two-step methods nanoparticles are first prepared and then dispersed into the basefluid. The dispersion is made by intensive magnetic force agitation, ultrasonic agita-

tion, high-shear mixing, homogenizing, or ball milling. Two-step processes are the most widely used due to large scalability and cost effectiveness. Otherwise, this is associated with relatively high tendency to aggregate. It is mainly caused by very high surface area and surface activity of nanoparticles, which, on the other hand, are the properties desired for thermal application (causing enhancement of thermal properties). The first step is based on nanoparticles preparation and purification. It is usually done by transition metal salt reduction, ligand reduction and displacement from organometallics, microwave synthesis or precipitation.

1.4 Heat Transfer Fluids and Thermal Applications

The Romans are thought to be first people that used heat transfer fluids (HTFs) in hot-air distribution systems to heat homes and public baths. [118] These materials are probably one of the most important in everyday life, for example for heating and cooling buildings, responsible for cooling in the refrigerator and freezer, solar panels, power stations, *etc.* The literature for further reading on HTFs include references [119, 120].

1.4.1 Definition, Classification and Properties

HTFs are materials liable for absorption and transport of heat, storage of thermal energy, and heat exchange. This definition covers a wide range of applications including engines, radiators/air conditioners, electronics or welding, nuclear systems, solar water, drilling, refrigeration, space, high-power lasers and biomedical application. [103, 106, 121] The classification can be done in many different ways, for example temperature range of operation: low temperature, up to 563.15 K (water, silicone polymers, glycols), medium temperature, between 563.15 K and 863.15 K (mixture of phenylcyclohexane and bicyclohexyl, terphenyl, synthetic hydrocarbons, alkyl substituted aromatic compounds, white mineral oils), or high temperature, above 863.15 K (metals eutectics or liquid sodium).

The first consideration should be focused on the phase in which HTFs are being operated - liquid, solid or gas. For some applications, phase change materials (PCM) give the opportunity to modulate the heat transfer efficiency. [122, 123] The phase in which HTFs operate depends on the type of application. Another important property is the compatibility with the equipment, for example water is very corrosive, petroleum and synthetic hydrocarbons with seals and gaskets made of ethylene propylene diene M-class rubber and silicone. Another important factor is flammability, flash point and the type of heating source because some materials might have low flash point, therefore, highly flammable, which is not desired in, for example, gas fire boilers or electric resistance heaters. A high impact on the cost of operation can be found for pumpability which is influenced by the viscosity (materials with low dynamic viscosity are desired). The

prospective HTFs must be also accessible to produce, obtain or replace with the respective lowest cost. Moreover, these must not exhibit biotoxicity or the environmental impact should be minimized. Durability and maintenance are other properties that need to be considered, most HTFs are operated for at least 10 years with median of 20 years. The impact of thermophysical properties (thermal conductivity, heat capacity, density and viscosity) is also discussed in detail, herein.

1.4.2 Heat Transfer Fluids: State of the Art Review

The first group of HTFs are liquids. Almost all CSP plants incorporate HTFs based on synthetic oils (*i.e.* Therminol VP-1 or Dowtherm A). The main limitations of synthetic oils are low thermal stability (usually up to 673.15 K), high degradation over the time, high cost and flammability. Molten salts can be also used as HTFs in power plants. The most recognized liquid salt is Solar Salt composed of 60% $NaNO_3$ and 40% KNO_3 (by mass). [124] This mixture allows to operate from about 563.15 K (above solidification point of 495.15 K) up to 873.15 K. Even though, molten salts have high density, their specific heat capacity and thermal conductivity are low. The main issue in this type of molten salts is that during the non-operational periods, the HTF would solidify which causes serious damage to the equipment. Raade and Padowitz (**2011**) reported a quinary molten salt (8% $LiNO_3$, 6% $NaNO_3$, 23% KNO_3, 44% $CsNO_3$ and 19% $Ca(NO_3)_2$ by mass) with low melting point of 338.15 K and thermal stability of about 773.15 K. [125] On the other hand, all above limitations can be overcome by using liquid metals or alloys which have solidification point of usually below 273.15 K and thermal stability well over 1873.15 K. These also have outstanding thermal conductivity, heat capacity, density and low viscosity. The exemplary HTF in case of liquid metals is sodium. The first application of sodium was in 1988 by Small Solar Power Systems Project of the International Energy Agency at the Plataforma Solar de Almería. [126] The main disadvantage of liquid sodium is a very strong exothermic reaction with water in which hydrogen is created. 22.2% Na-77.8% K eutectic alloy is very attractive as HTF with melting point of 260.55 K and boiling point of 1058.15 K. [127] 44.5% Pb-55.5% Bi eutectic alloy (LBE) does not exhibit a disadvantage of chemical instability with water, it also has thermal stability of

up to 1943.15 K. [128] However, the solidification point is 398.15 K and the corrosivity are main drawbacks. [129] The other group of HTFs are gases. The main advantage is that there is no operation maximum temperature of gases, but it is dictated by the equipment limitations. The main drawback is that these have very low heat transfer efficiency. Therefore, these materials are not very favoured due to low efficiency (due to low density and thermal conductivity). The most popular gaseous HTF is air (available everywhere, environmentally-friendly, free and safe to use). Other gases used as HTFs are helium, CO_2 or nitrogen, and they have better properties than air, the corrosivity is also reduced, however, they are harder to work with and much more expensive. On the other hand, a very recent report of solids application as HTFs in direct absorption receivers, can be found in work of Wu *et al.* (**2011**). [130] The main difference in comparison to fluids is that the heat is directly absorbed and transferred by solid through convection. The main advantages are higher radiation absorption or significant heat capacity. [131] Solids are usually combined with fluids and the solar absorption with sufficient heat transfer are achieved. In terms of two-phase HTFs, phase change materials (PCM) were found useful, for example in steam generators. [131] Supercritical fluids have been used in the industry for decades, particularly supercritical H_2O, s-H_2O. [132] Due to high supercritical pressure (and as a result cost of the equipment), [133] supercritical CO_2, s-CO_2, is more favoured. [134] However, the evaporation process in case of s-H_2O is reduced, therefore, more efficient isobaric heat transfer occurs, and corrosivity is also lower. [133, 135]

Several authors included ILs in their general considerations for potential HTFs. [136–140] Wu *et al.* (**2001**) considered ILs consisting of 1-alkyl-3-methylimidazolium cations with various anions in terms of their heat capacity, and further heat storage capacity, structure-property relationship, feasibility and economic analyses. The authors showed that ILs might have very beneficial physical properties as HTFs. [141] Blake *et al.* (**2002**) clarified the future challenges for HTFs which are thermal stability over 673.15 K and acting as both heat transfer and storage fluid. [142] Moreover, the authors discussed the application of ILs in parabolic trough solar thermal electric plants, and shown that low freezing point is a very unique prospective property of ILs. Holbrey *et al.* (**2003**) presented the comparison of 1-alkyl-3-methylimidazolium ILs and commercial HTFs, particularly their heat capacities as prospective values. [143] Moens *et al.* (**2003**) showed key issues of ILs for the development of HTFs (availability, cost, purity specifications, material

compatibility, environmental safety and health issues, development costs and intellectual property). [144] Van Valkenburg *et al.* (**2005**) investigated 1-alkyl-3-methylimidazolium tetrafluoroborate ILs in terms of their physical properties (thermal stability, heat storage and transfer), and proved that they might be a suitable replacement for conventional HTFs. [145] França *et al.* (**2009**) carried out a careful economic analysis of ILs and commercial HTFs. [146] Unfortunately, the authors concluded that for some ILs the estimated cost for the shell and tube heat exchanger is twice higher than for commercial HTFs. Other very important conclusion made by the authors is that the viscosity is the limiting factor influencing the thermophysical cost of ILs as HTFs. A very extensive review prepared by Chernikova *et al.* (**2015**) discussed good thermal stability, desired extremely low vapour pressure, varied viscosity and corrosivity (for some ILs lower and for some higher). [147] The main drawback was high cost of production and maintenance. Musiał *et al.* (**2017**) presented the results of thermophysical properties of pyrrolidinium-based ILs and their comparison to commercial HTFs over a wide range of temperature and pressure, and showed that this class of ILs might be a real replacement for current HTFs. [148]

The first notification on ionic liquid-based nanofluids was published by Nieto de Castro *et al.* (**2010**), in which authors introduced a new solution with unique properties of ILs, along with enhanced thermal conductivity and heat capacity caused by dispersed nanoparticles (in that case multiwalled carbon nanotubes). [149] Even though this very specialized branch of nanofluids is relatively new, there are many publications on this subject. Aforementioned enhanced thermophysical properties were repeated in further reports for thermal conductivity, [14, 150–161] heat capacity, [14, 100, 152, 156, 160, 161] density, [100, 158, 162] or viscosity. [152, 158] One of the most widely investigated potential application of ionanofluids has been as lubrication materials due to their friction reduction and antiwear properties, [163–170] wettability (not always an advantage), [165] thermal stability, [165, 170] ionic liquid-induced stabilisation of nanofluids, [165, 170] prevention against a tribocorrosion and steel oxidation. [165] Few authors considered ionanofluids as HTFs, and the discussions were mainly based on thermophysical properties, [171–179] thermal stability, [171] rheological behaviour, [174, 180], thermal performance, [173, 178–184] or in collar collectors based on their radiative and optical properties. [177, 179, 185, 186]

1.4.3 Thermophysical Properties

The most important physical properties responsible for the heat transfer efficiency are volumetric heat capacity (specific heat capacity and density), thermal conductivity and viscosity. Generally, we tend to have materials with as high as possible volumetric heat capacity (so do specific heat capacity and density) and thermal conductivity, but low values of viscosity. The heat transfer performance is represented by the combination of all these properties instead of treating them separately. The most well-known approach was established by Mouromtseff (**1942**) based on the Dittus-Boelter correlation, by estimating so-called Mouromtseff heat transfer coefficient, M_o: [187]

$$M_o = \frac{\rho^{0.8} c_p^{0.33} \lambda^{0.67}}{\eta^{0.47}} \tag{1.4.1}$$

Unfortunately, Mouromtseff assumed radial direction of transfer characteristics. To properly describe the heat performance, thermal storage capacity, convective heat transfer and hydraulic performance of pumping power need to be included. Murakami and Mikic proposed other correlation by including all of the above factors in so-called figure-of-merit (FOM): [188]

$$\text{FOM} = \frac{\rho^{2.0} c_p^{1.6} \lambda^{1.8}}{\eta^{1.4}} \tag{1.4.2}$$

The comparison of all studied HTFs, to date, is summarized in **Table 1.4.1**. The FOM values for several currently used HTFs were calculated.

Table 1.4.1. Comparison of figure-of-merit (FOM) ranges for several materials.

FOM ($W^{2.4}$ $m^{-4.4}$ $K^{-3.4}$)	Material
10^{18}-10^{19}	Liquid sodium [189]
10^{17}-10^{18}	LBE [190]
10^{15}-10^{17}	Water [40]
10^{13}-10^{16}	Commercial HTFs [191]
10^{13}-10^{15}	Supercritical H_2O [40]
10^{11}-10^{14}	ILs [192]
10^{10}-10^{13}	Nanofluids [191]
10^{9}-10^{10}	Air [40]

It can be seen that liquid sodium exhibits the most efficient heat transfer, very similar to LBE. This is mainly caused by high thermal conductivity and low viscosity for liquid sodium, extremely high density, low viscosity and high thermal conductivity for LBE. The other, probably the most renown, material is water which shows high efficiency in terms of heat transfer due to very low viscosity, high heat capacity and thermal conductivity. There is a wide range of HTFs commonly used and commercially available, such as Therminol VP-1, Dynalene HC-series or Dowtherm Q. The range of FOM for these materials is classified as moderate and vary more than other groups due to several different compositions of those materials (synthetic, organic compounds or mixtures with water). Those based on synthetic and organic compounds have lower FOM, while water enhances FOM values. Supercritical fluids have similar FOM to commercial HTFs, however, the origin of this is different. In case of commercial HTFs, thermal conductivity, heat capacity and density have the main contribution, while for supercritical materials the viscosity is extremely low which influences FOM values significantly (even though other properties are not prospective in terms of heat transfer). On the other hand, it can be seen that ILs have lower FOM. The thermophysical properties of these are very similar to commercial HTFs but the dynamic viscosity values are much higher which is the biggest disadvantage of these materials. Nanofluids were also investigated in the same way. Even though the addition of nanoparticles increases the thermal conductivity, heat capacity and density of nanofluids in comparison to pure liquid, the viscosity also increases which overpowers the other enhancements. The worst material in case of FOM is air with very low thermal conductivity, heat capacity and density which are not comprised by low viscosity. It should be noted that discussion based on FOM is very generalized because it does not include the type of equipment but only physical properties.

Mendonça *et al.* (**1981**) presented a very detailed approach to compare the thermophysical properties of HTFs by economic estimation of heat transfer unit cost (for shell and tube heat exchanger). [193] The procedure is described in Section 2.3.3. As ILs and nanofluids are rather considered as replacements for commercial HTFs, the discussion was also limited to this class of compounds. França *et al.* (**2009**) used this method to compare ILs with commercial HTFs. The authors showed that the estimated heat transfer unit cost incorporating ILs is twice as large as common HTFs, and the driving force for that is significantly higher values of viscosity. The accuracy of determined thermophysical

properties have an enormous impact on the heat exchange units design. This was also investigated based on this methodology. For example, Mendonça *et al.* (**1981**) showed 25% of misestimation of the unit cost, [193] Nunes *et al.* (**2003**) studied the importance of viscosity and thermal conductivity accuracy which might result in the heat exchanger cost misestimation of 16%, [194] França *et al.* (**2009**) combined the uncertainties of all four thermophysical properties and reported the misestimation of 15%. [146]

Bibliography

[1] J. G. HUDDLESTON, H. D. WILLAUER, R. P. SWATLOSKI, A. E. VISSER, and R. D. ROGERS, *Chemical Communications* **16**, 1765 (1998).

[2] K. R. SEDDON, *Journal of Chemical Technology and BioTechnology* **68**, 351 (1997).

[3] H. XIE, S. LI, and S. ZHANG, *Green Chemistry* **7**, 606 (2005).

[4] P. WALDEN, *Bulletin de l'Académie Impériale des Sciences de St.-Pétersbourg* **1800**, 405 (1914).

[5] H. HAMAGUCHI and R. OZAWA, *Advances in Chemical Physics* **131**, 85 (2005).

[6] J. L. KUHLER, R. T. BROOKS, A. HARDY, M. E. HODGE, K. D. HOLLEY, R. R. PATEL, and T. R. SHORTER, Application of an Ionic Liquid Catalyst Toward the Synthesis of Meridianins, in *Abstracts of Papers of the American Chemical Society*, American Chemical Society, Washington, D.C., USA, 2009.

[7] J.-F. LIU, G.-B. JIANG, and J. Å. JÖNSSON, *TrAC Trends in Analytical Chemistry* **24**, 20 (2005).

[8] D. D. PATEL and J. LEE, *The Chemical Record* **12**, 329 (2012).

[9] P. A. Z. SUAREZ, S. EINLOFT, J. E. L. DULLIUS, R. F. DE SOUZA, and J. DUPONT, *Journal de Chimie Physique et de Physico-Chimie Biologique* **95**, 1626 (1998).

[10] S. M. URAHATA and M. C. C. RIBEIRO, *The Journal of Chemical Physics* **120**, 1855 (2004).

[11] S. ZHANG, N. SUN, X. HE, X. LU, and X. ZHANG, *Journal of Physical and Chemical Reference Data* **35**, 1475 (2006).

[12] C. M. GORDON, *Applied Catalysis A: General* **222**, 101 (2001).

[13] L. CROWHURST, R. FALCONE, N. L. LANCASTER, V. LLOPIS-MESTRE, and T. WELTON, *The Journal of Organic Chemistry* **71**, 8847 (2006).

[14] A. P. C. RIBEIRO, S. I. C. VIEIRA, J. M. FRANÇA, C. S. QUEIRÓS, E. LANGA, M. J. V. LOURENÇO, S. M. S. MURSHED, and C. A. N. DE CASTRO, *Thermal Properties of Ionic Liquids and Ionanofluids*, InTech, London, The United Kingdom, 2011.

[15] H. KAMIMURA, T. KUBO, I. MINAMI, and S. MORI, *Tribology International* **40**, 620 (2007).

[16] A.-V. MUDRING, A. BABAI, S. ARENZ, R. GIERNOTH, K. BINNEMANS, K. DRIESEN, and P. NOCKEMANN, *Journal of Alloys and Compounds* **418**, 204 (2006).

[17] C. P. FREDLAKE, M. J. MULDOON, S. N. V. K. AKI, T. WELTON, and J. F. BRENNECKE, *Physical Chemistry Chemical Physics* **6**, 3280 (2004).

[18] S. ZHANG and K. DONG, *Structures and Interactions of Ionic Liquids*, Springer-Verlag, Berlin, Germany, 2013.

[19] R. D. ROGERS, K. R. SEDDON, and S. VOLKOV, *Green Industrial Applications of Ionic Liquids*, Springer Science & Business Media, Dordrecht, Netherlands, 2012.

[20] M. FREEMANTLE, *An Introduction to Ionic Liquids*, Royal Society of Chemistry, London, The United Kingdom, 2010.

[21] J. H. DAVIS JR, C. M. GORDON, C. HILGERS, P. WASSERSCHEID, and T. WELTON, *Ionic Liquids in Synthesis*, Wiley-VCH Verlag GmbH & Co, New York City, New York, USA, 2003.

[22] W. E. ACREE and L. M. GRUBBS, *Encyclopedia of Analytical Chemistry*, John Wiley & Sons, New York City, New York, USA, 2012.

[23] M. GAUNE-ESCARD and K. R. SEDDON, *Molten Salts and Ionic Liquids: Never the Twain?*, John Wiley & Sons, New York City, New York, USA, 2012.

[24] A. A. J. TORRIERO and M. J. A. SHIDDIKY, *ElectroChemical Properties and Applications of Ionic Liquids*, Nova Science Publishers, Hauppauge, New York, USA, 2011.

[25] R. CAMINITI and L. GONTRANI, *The Structure of Ionic Liquids*, Springer-Verlag, Berlin, Germany, 2016.

[26] S. ZHANG, Q. ZHOU, X. LU, Y. SONG, and X. WANG, *PhysicoChemical Properties of Ionic Liquid Mixtures*, Springer-Verlag, Berlin, Germany, 2017.

[27] K. R. SEDDON and N. V. PLECHKOVA, *Ionic Liquids Uncoiled: Critical Expert Overviews*, John Wiley & Sons, New York City, New York, USA, 2012.

[28] D. R. MACFARLANE, A. L. CHONG, M. FORSYTH, M. KAR, R. VIJAYARAGHAVAN, A. SOMERS, and J. M. PRINGLE, *Faraday Discussions* **206**, 9 (2018).

[29] D. R. MACFARLANE, M. FORSYTH, E. I. IZGORODINA, A. P. ABBOTT, G. ANNAT, and K. FRASER, *Physical Chemistry Chemical Physics* **11**, 4962 (2009).

[30] K. J. FRASER, E. I. IZGORODINA, M. FORSYTH, J. L. SCOTT, and D. R. MACFARLANE, *Chemical Communications* , 3817 (2007).

[31] C. N. DE CASTRO, A. P. C. RIBEIRO, S. I. C. VIEIRA, J. M. P. FRANÇA, M. J. V. LOURENÇO, F. V. SANTOS, S. M. S. MURSHED, P. GOODRICH, and C. HARDACRE, *Synthesis, Properties and Physical Applications of IoNanofluids*, InTech, London, The United Kingdom, 2013.

[32] Q. Q. BALTAZAR, J. CHANDAWALLA, K. SAWYER, and J. L. ANDERSON, *Colloids and Surfaces A: PhysicoChemical and Engineering Aspects* **302**, 150 (2007).

[33] W. XU and C. A. ANGELL, *Science* **302**, 422 (2003).

[34] C. A. ANGELL, *The Journal of Physical Chemistry* **70**, 2793 (1966).

[35] C. A. ANGELL, *The Journal of Chemical Physics* **46**, 4673 (1967).

[36] C. A. ANGELL, Y. ANSARI, and Z. ZHAO, *Faraday Discussions* **154**, 9 (2012).

[37] C. T. MOYNIHAN, *The Journal of Physical Chemistry* **70**, 3399 (1966).

[38] P. A. HUNT, C. R. ASHWORTH, and R. P. MATTHEWS, *Chemical Society Reviews* **44**, 1257 (2015).

[39] R. P. MATTHEWS, T. WELTON, and P. A. HUNT, *Physical Chemistry Chemical Physics* **17**, 14437 (2015).

[40] J. R. RUMBLE, *CRC Handbook of Chemistry and Physics*, CRC Press Taylor & Francis Group, Boca Raton, Florida, USA, 2017.

[41] M. J. EARLE, J. M. S. S. ESPERANÇA, M. A. GILEA, J. N. C. LOPES, L. P. N. REBELO, J. W. MAGEE, K. R. SEDDON, and J. A. WIDEGREN, *Nature* **439**, 831 (2006).

[42] A. ROMERO, A. SANTOS, J. TOJO, and A. RODRIGUEZ, *Journal of Hazardous Materials* **151**, 268 (2008).

[43] M. T. GARCIA, N. GATHERGOOD, and P. J. SCAMMELLS, *Green Chemistry* **7**, 9 (2005).

[44] H. OHNO, *ElectroChemical Aspects of Ionic Liquids*, John Wiley & Sons, New York City, New York, USA, 2005.

[45] R. D. ROGERS and K. R. SEDDON, *Science* **302**, 792 (2003).

[46] T. SATO, G. MASUDA, and K. TAKAGI, *Electrochimica Acta* **49**, 3603 (2004).

[47] C. MATON, N. DE VOS, and C. V. STEVENS, *Chemical Society Reviews* **42**, 5963 (2013).

[48] F. HEYM, B. J. M. ETZOLD, C. KERN, and A. JESS, *Green Chemistry* **13**, 1453 (2011).

[49] K. TSUNASHIMA, S. KODAMA, M. SUGIYA, and Y. KUNUGI, *Electrochimica Acta* **56**, 762 (2010).

[50] J. L. ANDERSON, J. DING, T. WELTON, and D. W. ARMSTRONG, *Journal of the American Chemical Society* **124**, 14247 (2002).

[51] J. M. CROSTHWAITE, M. J. MULDOON, J. K. DIXON, J. L. ANDERSON, and J. F. BRENNECKE, *The Journal of Chemical Thermodynamics* **37**, 559 (2005).

[52] J. GOLDING, S. FORSYTH, D. R. MACFARLANE, M. FORSYTH, and G. B. DEACON, *Green Chemistry* **4**, 223 (2002).

[53] H. L. NGO, K. LECOMPTE, L. HARGENS, and A. B. MCEWEN, *Thermochimica Acta* **357**, 97 (2000).

[54] H. TOKUDA, K. ISHII, M. A. B. H. SUSAN, S. TSUZUKI, K. HAYAMIZU, and M. WATANABE, *The Journal of Physical Chemistry B* **110**, 2833 (2006).

[55] J. G. HUDDLESTON, A. E. VISSER, W. M. REICHERT, H. D. WILLAUER, G. A. BROKER, and R. D. ROGERS, *Green Chemistry* **3**, 156 (2001).

[56] M. KOSMULSKI, J. GUSTAFSSON, and J. B. ROSENHOLM, *Thermochimica Acta* **412**, 47 (2004).

[57] M. R. R. PRASAD and V. N. KRISHNAMURTHY, *Thermochimica Acta* **185**, 1 (1991).

[58] H. TOKUDA, K. HAYAMIZU, K. ISHII, M. A. B. H. SUSAN, and M. WATANABE, *The Journal of Physical Chemistry B* **109**, 6103 (2005).

[59] A. F. FERREIRA, P. N. SIMÕES, and A. G. M. FERREIRA, *The Journal of Chemical Thermodynamics* **45**, 16 (2012).

[60] J. D. HOLBREY, W. M. REICHERT, R. P. SWATLOSKI, G. A. BROKER, W. R. PITNER, K. R. SEDDON, and R. D. ROGERS, *Green Chemistry* **4**, 407 (2002).

[61] C. J. BRADARIC, A. DOWNARD, C. KENNEDY, A. J. ROBERTSON, and Y. ZHOU, *Green Chemistry* **5**, 143 (2003).

[62] K. R. SEDDON, A. STARK, and M.-J. TORRES, *Pure and Applied Chemistry* **72**, 2275 (2000).

[63] N. TANIGUCHI, On the Basic Concept of Nano-Technology, in *Proceedings of the International Conference on Production Engineering*, Japan Society of Precision Engineering, Tokyo, Japan, 1974.

[64] D. WALTER, *NanoMaterials*, John Wiley & Sons, New York City, New York, USA, 2013.

[65] G. SCHMID, *Nanoparticles: From Theory to Application*, John Wiley & Sons, New York City, New York, USA, 2005.

[66] V. J. MOHANRAJ and Y. CHEN, *Tropical Journal of Pharmaceutical Research* **5**, 561 (2006).

[67] C. DE MELLO DONEGÁ, *Nanoparticles: Workhorses of NanoScience*, Springer-Verlag, Berlin, Germany, 2014.

[68] M. ALIOFKHAZRAEI, *Handbook of Nanoparticles*, Springer-Verlag, Berlin, Germany, 2016.

[69] V. M. ROTELLO, *Nanoparticles: Building Blocks for NanoTechnology*, Springer Science & Business Media, Dordrecht, Netherlands, 2004.

[70] A. SENGUPTA and C. K. SARKAR, *Introduction to Nano: Basics to NanoScience and NanoTechnology*, Springer-Verlag, Berlin, Germany, 2015.

[71] Z. ABDULLAEVA, *Synthesis of Nanoparticles and NanoMaterials: Biological Approaches*, Springer, 2017.

[72] B. BHUSHAN, *Handbook of NanoTechnology*, Springer-Verlag, Berlin, Germany, 2017.

[73] B. BHUSHAN, D. LUO, S. R. SCHRICKER, W. SIGMUND, and S. ZAUSCHER, *Handbook of NanoMaterials Properties*, Springer Science & Business Media, Dordrecht, Netherlands, 2014.

[74] D. SHIN and D. BANERJEE, *International Journal of Heat and Mass Transfer* **54**, 1064 (2011).

[75] K. SUTTIPONPARNIT, J. JIANG, M. SAHU, S. SUVACHITTANONT, T. CHARINPANITKUL, and P. BISWAS, *Nanoscale Research Letters* **6**, 27 (2011).

[76] S. U. S. CHOI and J. A. EASTMAN, *Enhancing Thermal Conductivity of Fluids with Nanoparticles*, Argonne National Lab., Lemont, IL, USA, 1995.

[77] G. Y. YURKOV, A. S. FIONOV, Y. A. KOKSHAROV, V. V. KOLESO, and S. P. GUBIN, *Inorganic Materials* **43**, 834 (2007).

[78] J. J. SCHNEIDER, *NanoMaterials: Synthesis, Properties and Applications*, The Institute of Physics Publishing, Bristol, The United Kingdom, 1996.

[79] R. HENTSCHKE, *Nanoscale Research Letters* **11**, 88 (2016).

[80] F. RÖTHEMEYER and F. SOMMER, *Kautschuktechnologie: Werkstoffe-Verarbeitung-Produkte*, Hanser Fachbuchverlag, München, Germany, 2013.

[81] X. LU and Z. CHEN, *Chemical Reviews* **105**, 3643 (2005).

[82] P. KIM, L. SHI, A. MAJUMDAR, and P. L. MCEUEN, *Physical Review Letters* **87**, 215502 (2001).

[83] G. A. OZIN, A. C. ARSENAULT, and L. CADEMARTIRI, *NanoChemistry: a Chemical Approach to NanoMaterials*, Royal Society of Chemistry, London, The United Kingdom, 2009.

[84] T. GRAHAM, *Philosophical Transactions of the Royal Society of London* **151**, 183 (1861).

[85] J. EDEL, A. IVANOV, and M. KIM, *Nanofluidics*, Royal Society of Chemistry, London, The United Kingdom, 2016.

[86] S. K. DAS, S. U. CHOI, W. YU, and T. PRADEEP, *Nanofluids: Science and Technology*, John Wiley & Sons, New York City, New York, USA, 2007.

[87] J. LYKLEMA, *Fundamentals of Interface and Colloid Science: Soft Colloids*, Academic Press Elsevier, Cambridge, Massachusetts, USA, 2005.

[88] A. S. DUKHIN and P. J. GOETZ, *Fundamentals of Interface and Colloid Science*, Academic Press Elsevier, Cambridge, Massachusetts, USA, 2010.

[89] D. J. SHAW, *Introduction to Colloid and Surface Chemistry*, Butterworth-Heinemann, Oxford, The United Kingdom, 1966.

[90] W. B. RUSSEL, D. A. SAVILLE, and W. R. SCHOWALTER, *Colloidal Dispersions*, Cambridge University Press, Cambridge, The United Kingdom, 1989.

[91] D. FENNELL EVANS, H. WENNERSTROM, and R. RAJAGOPALAN, *Journal of Colloid and Interface Science* **172**, 541 (1995).

[92] A. EINSTEIN, *Annalen der Physik* **17**, 549 (1905).

[93] M. SMOLUCHOWSKI, *Essai d'une Théorie Cinétique du Mouvement Brownien et des Milieux Troublés*, Academie Litterarum Cracoviensis, Cracow, Poland, 1906.

[94] S. P. JANG and S. U. S. CHOI, *Applied Physics Letters* **84**, 4316 (2004).

[95] P. KEBLINSKI, S. R. PHILLPOT, S. U. S. CHOI, and J. A. EASTMAN, *International Journal of Heat and Mass Transfer* **45**, 855 (2002).

[96] S. M. S. MURSHED, K. C. LEONG, and C. YANG, *International Journal of Thermal Sciences* **47**, 560 (2008).

[97] R. PRASHER, P. BHATTACHARYA, and P. E. PHELAN, *Physical Review Letters* **94**, 25901 (2005).

[98] N. PUTRA, P. THIESEN, and W. ROETZEL, *Journal of Heat Transfer* **125**, 567 (2003).

[99] W. YU and S. U. S. CHOI, *Journal of Nanoparticle Research* **5**, 167 (2003).

[100] M. P. SHEVELYOVA, Y. U. PAULECHKA, G. J. KABO, A. V. BLOKHIN, A. G. KABO, and T. M. GUBAREVICH, *The Journal of Physical Chemistry C* **117**, 4782 (2013).

[101] H. O'HANLEY, J. BUONGIORNO, T. MCKRELL, and L.-W. HU, Measurement and Model Correlation of Specific Heat Capacity of Water-Based Nanofluids with Silica, Alumina and Copper Oxide Nanoparticles, in *ASME 2011 International Mechanical Engineering Congress and Exposition*, American Society of Mechanical Engineers, New York City, New York, USA, 2011.

[102] W. YU, D. M. FRANCE, J. L. ROUTBORT, and S. U. S. CHOI, *Heat Transfer Engineering* **29**, 432 (2008).

[103] S. KAKAÇ and A. PRAMUANJAROENKIJ, *International Journal of Heat and Mass Transfer* **52**, 3187 (2009).

[104] S. ÖZERINÇ, S. KAKAÇ, and A. G. YAZICIOĞLU, *Microfluidics and Nanofluidics* **8**, 145 (2010).

[105] C. KLEINSTREUER and Y. FENG, *Nanoscale Research Letters* **6**, 1 (2011).

[106] X.-Q. WANG and A. S. MUJUMDAR, *International Journal of Thermal Sciences* **46**, 1 (2007).

[107] V. TRISAKSRI and S. WONGWISES, *Renewable and Sustainable Energy Reviews* **11**, 512 (2007).

[108] J. FRANÇA, C. A. N. DE CASTRO, and A. A. H. PADUA, *Physical Chemistry Chemical Physics* **19**, 17075 (2017).

[109] Y. LI, S. TUNG, E. SCHNEIDER, and S. XI, *Powder Technology* **196**, 89 (2009).

[110] S. ANGAYARKANNI and J. PHILIP, *Advances in Colloid and Interface Science* **225**, 146 (2015).

[111] S. A. KUMAR, K. S. MEENAKSHI, B. NARASHIMHAN, S. SRIKANTH, and G. ARTHANAREESWARAN, *Materials Chemistry and Physics* **113**, 57 (2009).

[112] Y. CHEN, D.-L. PENG, D. LIN, and X. LUO, *NanoTechnology* **18**, 505703 (2007).

[113] H. AKOH, Y. TSUKASAKI, S. YATSUYA, and A. TASAKI, *Journal of Crystal Growth* **45**, 495 (1978).

[114] J. ZHU, D. LI, H. CHEN, X. YANG, L. LU, and X. WANG, *Materials Letters* **58**, 3324 (2004).

[115] M. KASSAEE, F. BUAZAR, and E. MOTAMEDI, *Journal of NanoMaterials* **2010**, 7 (2010).

[116] H. J. KIM, I. C. BANG, and J. ONOE, *Optics and Lasers in Engineering* **47**, 532 (2009).

[117] H. WANG, J.-Z. XU, J.-J. ZHU, and H.-Y. CHEN, *Journal of Crystal Growth* **244**, 88 (2002).

[118] H. F. GREINER and F. P. BUSSICK, *Tribology & Lubrication Technology* **56**, 17 (2000).

[119] N. CANTER, *Tribology & Lubrication Technology* **65**, 28 (2009).

[120] A. LENERT and E. N. WANG, *Solar Energy* **86**, 253 (2012).

[121] E. FERRANNINI, *Metabolism* **37**, 287 (1988).

[122] B. ZALBA, J. M. MARIN, L. F. CABEZA, and H. MEHLING, *Applied Thermal Engineering* **23**, 251 (2003).

[123] F. AGYENIM, N. HEWITT, P. EAMES, and M. SMYTH, *Renewable and Sustainable Energy Reviews* **14**, 615 (2010).

[124] H. E. REILLY and G. J. KOLB, *An Evaluation of Molten-Salt Power Towers Including Results of the Solar Two Project*, Sandia National Labs., Albuquerque, New Mexico, USA, 2001.

[125] J. W. RAADE and D. PADOWITZ, *Journal of Solar Energy Engineering* **133**, 31013 (2011).

[126] W. J. C. SCHIEL and M. A. GEYER, *Solar Energy* **41**, 255 (1988).

[127] O. J. FOUST, *Sodium-NaK Engineering Handbook*, Gordon & Breach Science Publishers, Philadelphia, Pennsylvania, USA, 1972.

[128] J. PACIO and T. WETZEL, *Solar Energy* **93**, 11 (2013).

[129] T. FURUKAWA, G. MÜLLER, G. SCHUMACHER, A. WEISENBURGER, A. HEINZEL, F. ZIMMERMANN, and K. AOTO, *Journal of Nuclear Science and Technology* **41**, 265 (2004).

[130] W. WU, B. GOBEREIT, C. SINGER, L. AMSBECK, and R. PITZ-PAAL, *Direct Absorption Receivers for High Temperatures*, 17th SolarPACES Conference, Granada, Spain, 2011.

[131] L. HELLER, *Literature Review on Heat Transfer Fluids and Thermal Energy Storage Systems in CSP Plants*, Stellenbosch University, Stellenbosch, South Africa, 2013.

[132] M. BOSS, T. GADOURY, S. FEENY, and M. MONTGOMERY, *Recent Advances in Ultra Super Critical Steam Turbine Technology*, GE Energy, Schenectady, New York, USA, 2002.

[133] J. COVENTRY and J. PYE, *Coupling Supercritical and Superheated Direct Steam Generation with Thermal Energy Storage*, 15th SolarPACES Conference, Berlin, Germany, 2009.

[134] S. A. WRIGHT, T. M. CONBOY, and G. E. ROCHAU, *Overview of Supercritical CO_2 Power Cycle Development at Sandia National Laboratories*, 2011 University Turbine Systems Research Workshop, Columbus, Ohio, USA, 2011.

[135] F. ROUILLARD, G. MOINE, and F. CHARTON, Corrosion Behavior of Different Metallic Materials In Supercritical CO_2 at 550°C And 250 bars, CORROSION 2010 - NACE International, San Antonio, Texas, USA, 2010.

[136] J. F. BRENNECKE and E. J. MAGINN, *AIChE Journal* **47**, 2384 (2001).

[137] H. ZHAO, *Chemical Engineering Communications* **193**, 1660 (2006).

[138] D. R. MACFARLANE, N. TACHIKAWA, M. FORSYTH, J. M. PRINGLE, P. C. HOWLETT, G. D. ELLIOTT, J. H. DAVIS, M. WATANABE, P. SIMON, and C. A. ANGELL, *Energy & Environmental Science* **7**, 232 (2014).

[139] J. F. WISHART, *Energy & Environmental Science* **2**, 956 (2009).

[140] S. APARICIO, M. ATILHAN, and F. KARADAS, *Industrial & Engineering Chemistry Research* **49**, 9580 (2010).

[141] B. WU, R. REDDY, and R. ROGERS, *Novel Ionic Liquid Thermal Storage for Solar Thermal Electric Power Systems*, Proceedings of Solar Forum 2001 Solar Energy: The Power to Choose, Washington, D.C., USA, 2001.

[142] D. M. BLAKE, L. MOENS, M. J. HALE, H. PRICE, D. KEARNEY, and U. HERRMANN, *New Heat Transfer and Storage Fluids for Parabolic Trough Solar Thermal Electric Plants*, Proceedings of the 11th SolarPACES International Symposium on Concentrated Solar Power and Chemical Energy Technologies, Zurich, Switzerland, 2002.

[143] J. D. HOLBREY, W. M. REICHERT, R. G. REDDY, and R. D. ROGERS, *Ionic Liquids as Green Solvents*, ACS Publications, Washington, D.C., USA, 2003.

[144] L. Moens, D. M. Blake, D. L. Rudnicki, and M. J. Hale, *Journal of Solar Energy Engineering* **125**, 112 (2003).

[145] M. E. Van Valkenburg, R. L. Vaughn, M. Williams, and J. S. Wilkes, *Thermochimica Acta* **425**, 181 (2005).

[146] J. M. P. França, C. A. Nieto de Castro, M. M. Lopes, and V. M. B. Nunes, *Journal of Chemical & Engineering Data* **54**, 2569 (2009).

[147] E. A. Chernikova, L. M. Glukhov, V. G. Krasovskiy, L. M. Kustov, M. G. Vorobyeva, and A. A. Koroteev, *Russian Chemical Reviews* **84**, 875 (2015).

[148] M. Musiał, K. Malarz, A. Mrozek-Wilczkiewicz, R. Musiol, E. Zorębski, and M. Dzida, *ACS Sustainable Chemistry & Engineering* **5**, 11024 (2017).

[149] C. A. N. de Castro, E. Langa, A. L. Morais, M. L. M. Lopes, M. J. V. Lourenço, F. J. V. Santos, M. S. C. S. Santos, J. N. C. Lopes, H. I. M. Veiga, and M. Macatrão, *Fluid Phase Equilibria* **294**, 157 (2010).

[150] B. Wang, J. Hao, Q. Li, and H. Li, *International Journal of Thermal Sciences* **83**, 89 (2014).

[151] C. T. Siong, R. Daik, and M. A. A. Hamid, *Thermally Conductive of Nanofluid from Surfactant Doped Polyaniline Nanoparticle and Deep Eutectic Ionic Liquid*, AIP Conference Proceedings, Melville, New York, USA, 2014.

[152] A. G. M. Ferreira, P. N. Simões, A. F. Ferreira, M. A. Fonseca, M. S. A. Oliveira, and A. S. M. Trino, *The Journal of Chemical Thermodynamics* **64**, 80 (2013).

[153] B. Wang, X. Wang, W. Lou, and J. Hao, *Journal of Colloid and Interface Science* **362**, 5 (2011).

[154] N. Y. J. B. Nikapitiya and H. Moon, Thermal Conductivity Enhancement of Room Temperature Ionic Liquids (RTILS) with Various Magnetic Nanoparticles, Proceedings of the ASME Micro/Nanoscale Heat and Mass Transfer International Conference, Atlanta, Georgia, USA, 2012.

[155] F. Wang, L. Han, Z. Zhang, X. Fang, J. Shi, and W. Ma, *Nanoscale Research Letters* **7** (2012).

[156] C. A. N. De Castro, S. M. S. Murshed, M. J. V. Lourenço, F. J. V. Santos, M. L. M. Lopes, and J. M. P. França, *International Journal of Thermal Sciences* **62**, 34 (2012).

[157] J. M. P. França, S. I. C. Vieira, M. J. V. Lourenço, S. M. S. Murshed, and C. A. Nieto de Castro, *Journal of Chemical & Engineering Data* **58**, 467 (2013).

[158] H. Xie, Z. Zhao, J. Zhao, and H. Gao, *Chinese Journal of Chemical Engineering* **24**, 331 (2016).

[159] C. Li, Z. Zhao, X. Zhang, and T. Li, *International Journal of Thermophysics* **39**, 1 (2018).

[160] H. Tiznobaik, D. Banerjee, and D. Shin, *International Journal of Heat and Mass Transfer* **91**, 342 (2015).

[161] H. Tiznobaik and D. Shin, *Applied Physics Letters* **102**, 1 (2013).

[162] I. Rodriguez-Palmeiro, B. Rodriguez-Cabo, E. Rodil, A. Arce, J. M. Saiz-Jabardo, and A. Soto, *Journal of Nanoparticle Research* **15**, 1 (2013).

[163] B. Wang, X. Wang, W. Lou, and J. Hao, *Journal of Physical Chemistry C* **114**, 8749 (2010).

[164] B. Wang, X. Wang, W. Lou, and J. Hao, *Nanoscale Research Letters* **6**, 259 (2011).

[165] C. Espejo, F.-J. Carrion, D. Martinez, and M.-D. Bermudez, *Tribology Letters* **50**, 127 (2013).

[166] N. Saurin, T. Espinosa, J. Sanes, F.-J. Carrion, and M.-D. Bermudez, *Lubricants* **3**, 650 (2015).

[167] C. Yegin, W. Lu, B. Kheireddin, M. Zhang, P. Li, Y. Min, H.-J. Sue, M. M. Sari, and M. Akbulut, *Journal of Tribology* **139**, 1 (2017).

[168] J. Sanes, M.-D. Aviles, N. Saurin, T. Espinosa, F.-J. Carrion, and M.-D. Bermudez, *Tribology International* **116**, 371 (2017).

[169] Y. Guo, L. Zhang, G. Zhang, D. Wang, T. Wang, and Q. Wang, *Journal of Materials Chemistry A* **6**, 2817 (2018).

[170] X. Shi, W. Huang, and X. Wang, *Lubrication Science* **30**, 73 (2018).

[171] E. B. Fox, A. E. Visser, N. J. Bridges, and J. W. Amoroso, *Energy & Fuels* **27**, 3385 (2013).

[172] T. C. Paul, A. K. M. M. Morshed, E. B. Fox, and J. A. Khan, *APPLIED Thermal Engineering* **110**, 1 (2017).

[173] T. C. PAUL, A. K. M. M. MORSHED, E. B. FOX, A. E. VISSER, N. J. BRIDGES, and J. A. KHAN, *Natural Convection in Rectangular Cavity with Nanoparticle Enhanced Ionic Liquids (NEILs)*, Proceedings of the ASME International Mechanical Engineering Congress and Exposition, Houston, Texas, USA, 2013.

[174] T. C. PAUL, A. K. M. M. MORSHED, E. B. FOX, and J. A. KHAN, *International Journal of Heat and Mass Transfer* **85**, 585 (2015).

[175] T. C. PAUL, A. K. M. M. MORSHED, and J. A. KHAN, *Effect of Nanoparticle Dispersion on Thermophysical Properties of Ionic Liquids for its Potential Application in Solar Collector*, 10th International Conferece on Mechanical Engineering (ICME 2013), Dhaka, Bangladesh, 2014.

[176] T. C. PAUL, A. M. MORSHED, and J. A. KHAN, *Nanoparticle Enhanced Ionic Liquids (NEILS) as Working Fluid for the Next Generation Solar Collector*, 5th BSME International Conference on Thermal Engineering, Dhaka, Bangladesh, 2013.

[177] W. CHEN, C. ZOU, and X. LI, *Solar Energy Materials and Solar Cells* **163**, 157 (2017).

[178] T. C. PAUL, A. K. M. M. MORSHED, E. B. FOX, and J. A. KHAN, *International Journal of Heat and Mass Transfer* **83**, 753 (2015).

[179] J. LIU, C. XU, L. CHEN, X. FANG, and Z. ZHANG, *Solar Energy Materials and Solar Cells* **170**, 219 (2017).

[180] T. C. PAUL, A. K. M. M. MORSHED, E. B. FOX, A. E. VISSER, N. J. BRIDGES, and J. A. KHAN, *Enhanced Thermal Performance of Ionic Liquid-Al_2O_3 Nanofluid as Heat Transfer Fluid for Solar Collector*, Proceedings of the ASME 7th International Conference on Energy Sustainability, Minneapolis, Minnesota, USA, 2014.

[181] T. C. PAUL, A. K. M. M. MORSHED, E. B. FOX, A. E. VISSER, N. J. BRIDGES, and J. A. KHAN, *Heat Transfer and Flow Behavior of Nanoparticle Enhanced Ionic Liquids (NEILs)*, Proceedings of the ASME Summer Heat Transfer Conference, Rio Grande, Puerto Rico, 2012.

[182] T. C. PAUL, A. M. MORSHED, and J. A. KHAN, *Numerical Investigation of Natural Convection of Nanoparticle Enhanced Ionic Liquids (NEILs) in Enclosure Heated from Below*, Proceedings of the 11th International Conference on Mechanical Engineering (ICME 2015), Dhaka, Bangladesh, 2016.

[183] A.-A. MINEA and W. M. EL-MAGHLANY, *Chemical Engineering Science* **174**, 13 (2017).

[184] E. I. CHERECHES, K. V. SHARMA, and A. A. MINEA, *Continuum Mechanics and Thermodynamics* **30**, 657 (2018).

[185] J. LIU, Z. YE, L. ZHANG, X. FANG, and Z. ZHANG, *Solar Energy Materials and Solar Cells* **136**, 177 (2015).

[186] L. ZHANG, J. LIU, G. HE, Z. YE, X. FANG, and Z. ZHANG, *Solar Energy Materials and Solar Cells* **130**, 521 (2014).

[187] I. E. MOUROMTSEFF, *Proceedings of the IRE* **30**, 190 (1942).

[188] Y. MURAKAMI and B. B. MIKIC, *IEEE Transactions on Components and Packaging Technologies* **24**, 2 (2001).

[189] J. K. FINK and L. LEIBOWITZ, *Thermodynamic and Transport Properties of Sodium Liquid and Vapor*, Argonne National Lab., Lemont, IL, USA, 1995.

[190] V. SOBOLEV, *Database of Thermophysical Properties of Liquid Metal Coolants for GEN-IV*, Belgian Nuclear Research Centre, Mol, Belgium, 2010.

[191] A. LENERT, Y. NAM, and E. N. WANG, *Annual Review of Heat Transfer* **15**, 93 (2012).

[192] R. GE, C. HARDACRE, P. NANCARROW, and D. W. ROONEY, *Journal of Chemical & Engineering Data* **52**, 1819 (2007).

[193] A. J. F. MENDONCA, C. A. NIETO DE CASTRO, M. J. ASSAEL, and W. A. WAKEHAM, *Revista Portuguesa de Química* **23**, 7 (1981).

[194] V. M. B. NUNES, M. J. V. LOURENÇO, F. J. V. SANTOS, and C. A. NIETO DE CASTRO, *Journal of Chemical & Engineering Data* **48**, 446 (2003).

Chapter 2

Experimental

2.1 Materials

2.1.1 Trihexyl(tetradecyl)phosphonium Carboxylate Ionic Liquids

Trihexyl(tetradecyl)phosphonium carboxylate ILs, $[P_{14,6,6,6}][RO]$, were synthesized using the general anion exchange reaction (**Figure 2.1.1**). In this reaction, a quaternary phosphonium chloride salt undergoes the reaction with an anion exchange resin, and the chloride anion is exchanged into hydroxide anion. To prevent the undesired reaction of quaternary-phosphonium ILs in the presence of such nucleophilic species as hydroxide (**Figure 2.1.2**), this process should be carried out in highly dielectric medium (ethanol, methanol or water), where the hydroxide anion is stabilized by solvation. In the second step, the hydroxide salt undergoes acid-base reaction with the appropriate carboxylic acid.

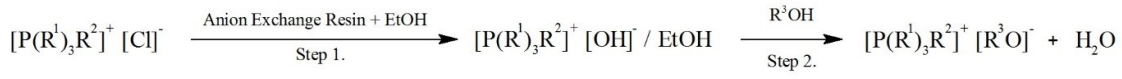

Figure 2.1.1. General reaction of carboxylate ILs preparation using the anion exchange resin.

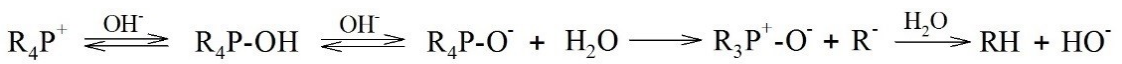

Figure 2.1.2. General reaction of quaternary phosphonium salts in the presence of hydroxide anion. [1]

Trihexyl(tetradecyl)phosphonium acetate, $[P_{14,6,6,6}][AcO]$ (CAS: 872700-58-8), butanoate, $[P_{14,6,6,6}][ButO]$ (CAS: 1393375-56-8), hexanoate, $[P_{14,6,6,6}][HexO]$ (CAS: 1393375-57-9), octanoate, $[P_{14,6,6,6}][OctO]$ (CAS: 1393375-58-0), and decanoate, $[P_{14,6,6,6}][DecO]$ (CAS: 465527-65-5), were synthesized using the above described method. Trihexyl(tetradecyl)phosphonium chloride, $[P_{14,6,6,6}]Cl$ (Cytec Industries Inc., product code: Cyphos IL-101, CAS: 258864-54-9, purity: >95%) was diluted with ethanol (Sigma-Aldrich, absolute, CAS: 64-17-5, purity: ≥99.8%) to a concentration of 30 wt%. Thereafter, the reaction mixture was treated with 60 cm^3 of strongly basic anion exchange resin (Alfa Aesar, product code: IRN-78, CAS: 11128-95-3). This was repeated at least 3 times (after each run, the resin in the column was replaced with a new portion) until no precipitation using a silver nitrate test (CAS: 7761-88-8, Sigma-Aldrich, Purity ≥99.9999%) was obtained confirming complete anion exchange. In the second step, the relevant carboxylic acid (acetic acid, SigmaAldrich, ReagentPlus, CAS: 64-19-7, purity: ≥99%, butanoic acid, Sigma-Aldrich, CAS: 107-92-6, purity: ≥99%, hexanoic acid, Sigma-Aldrich, CAS: 142-62-1, purity: ≥99.5%, octanoic acid, Sigma-Aldrich, CAS: 124-07-2, purity: ≥99%, decanoic acid, Sigma-Aldrich, CAS: 334-48-5, purity: ≥98%) was added in slight molar excess to the amount of chloride salt used in the first step to solution of hydroxide salt in ethanol to obtain the acetate, butanoate, hexanoate, octanoate or decanoate-based ILs, respectively,. The mixture was then heated at 328 K overnight with stirring. The final product was purified under rotary evaporation and then dried under high vacuum (10^{-3} Pa) at 338 K for at least 72 h. The description of all chemicals has been summarized in **Table A1** (Appendix A).

2.1.2 Imidazolium- and Pyrrolidinium-Based Ionic Liquids

The procedure for the synthesis of 1-octyl-3-methylimidazolium bis[(trifluoromethyl)sulfonyl]imide (CAS: 178631-04-4), $[C_8C_1Im][NTf_2]$, can be found in reference [2]. The structure of this IL can be found in **Figure 2.1.3**. Following the synthesis, the IL was washed with deionised water (18 MΩ cm) 5 times (until no precipitation using a silver nitrate test was obtained) and dried under reduced pressure at 328.15 K. The $[C_8C_1Im][NTf_2]$ was then dried under high vacuum (10^{-3} Pa) at 328.15 K for at least 72 h. The purity

of this compound was summarized in **Table A1** (Appendix A). This IL was selected to calibrate the KD2 Pro Thermal Properties Analyzer (thermal conductivity measurement) as the properties of this compound have been accurately investigated in the literature. [3] 1-Butyl-3-methylimidazolium dicyanamide (CAS: 448245-52-1), $[C_4C_1Im][Dca]$, and 1-butyl-3-methylimidazolium bis[(trifluoromethyl)sulfonyl]imide (CAS: 174899-83-3), $[C_4C_1Im][NTf_2]$, were bought from Merck (purity ≥98%, ≥0.01% halides, catalogue number: 4900150500) and Sigma-Aldrich (purity ≥98%, catalogue number: 711713), respectively. 1-Butyl-1-methylpyrrolidinium bis[(trifluoromethyl)sulfonyl]imide (CAS: 223437-11-4), $[C_4C_1Pyrr][NTf_2]$, 1-hexyl-3-methylimidazolium hexafluorophosphate (CAS: 304680-35-1), $[C_6C_1Im][PF_6]$, and 1-ethyl-3-methylimidazolium ethylsulfate (CAS: 342573-75-5), $[C_2C_1Im][C_2SO_4]$, were synthesized in-house following the procedures available in the literature. [4–6] All the ILs were washed 3-5 times with ultrapure water (18 MΩ cm), and extracted with dichloromethane. Thereafter, the ILs were dried under high vacuum (10^{-3} Pa) and elevated temperature (333.15 K) for at least 72 h. All the IL structures are presented in **Figure 2.1.3**

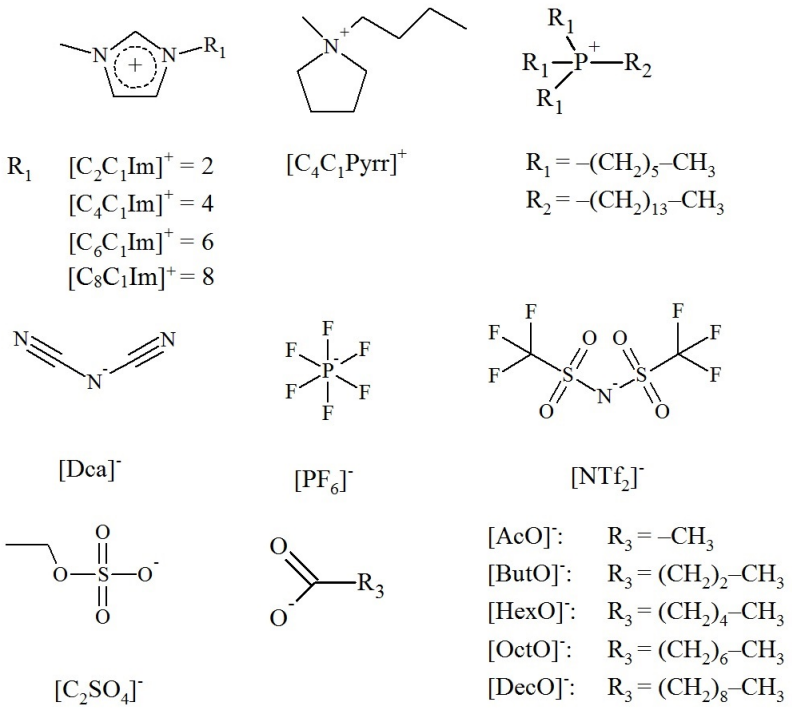

Figure 2.1.3. Structures of the investigated ionic liquids.

2.1.3 Purity Assessment of Ionic Liquids

The final purity of the ILs was assessed by ^{1}H, ^{13}C and ^{31}P NMR (B400 Bruker Avance III 400 MHz, ILs dissolved in $CDCl_3$), Karl Fisher titration (Metrohm 899 Coulometer with 803 Ti Stand and Hydranal Coulomat AG) and CHNS elemental analysis (for carbon and hydrogen content, Perkin Elmer PE2400CHNS). The water content was checked prior to and after each of the thermophysicochemical measurements. To determine the standard uncertainty of the measurement, 3 independent measurements of water were carried out, and the error was assigned as the standard deviation. However, no significant changes in the case of the water content after the measurement were observed (the measurement cells were completely sealed against the atmosphere), even in case of mixtures with water. The results of the NMR and elemental analyses are included in **Table A2** (Appendix A).

The water content for the trihexyl(tetradecyl)phosphonium carboxylate ILs and their mixtures with water are presented in Section 4.1, those used in ionanofluids have water content of < 100 ppm. In case of imidazolium- and pyrrolidinium-based ILs and ionanofluids with these ILs, the water content was < 200 ppm. The halide content in the ILs was checked by the silver nitrate test (< 5 ppm). [7–9]

2.1.4 Nanomaterials

Multiwalled carbon nanotubes (MWCNT) used in this work are Bayer Material Science Baytubes C150 HP (CAS: 308068-56-6, purity ≥99%, 3-15 number of walls, 13-16 nm outer mean diameter, 5-20 nm outer diameter distribution, 4 nm inner mean diameter, 2-6 nm inner diameter distribution, 1-10 mm length, 140-230 kg m^{-3} bulk density; according to the specifications provided by the supplier). Hexagonal boron nitride (BN, CAS: 10043-11-5, purity ≥99.8%, 70-80 nm size, 2290 kg m^{-3} theoretical true density, <0.03% Fe_2O_3, <0.002% CaO, <0.04% MgO, <0.1% B_2O_3), graphite (G, CAS: 7782-42-5, ≥99.9% purity, 400-1200 nm size, <0.1% impurities, ~0.2% water) and mesoporous carbon (MC, CAS: 7440-44-0, purity: 95%, 20-40 nm APS, <5% water, <2 % ash, 7-10 pH) were obtained from US Research Nanomaterials, Inc. Before the

preparation of nanofluids, boron nitride and graphite were processed by using ball milling to reduce the particles size (Retsch Mixer Mill MM 400, frequency 20 Hz, 3 times for 1800 s). The size of the particles was ascertained using scanning electron microscopy (650 FEI Quanta FEG, 15-20, <90, <100, and <50 nm for carbon nanotubes, boron nitride, graphite and mesoporous carbon, respectively, **Figure 2.1.4**), and with light scattering (Malvern Mastersizer, dispersion with water, stabilized with sodium laureth sulfate as anionic surfactant, refractive index of 1.330 for water, 1.650 for boron nitride and 2.420 for all carbon-based nanomaterials; 26.60 ± 0.15 nm, 154.5 ± 1.7 nm, 159.1 ± 3.1 nm and 46.23 ± 0.62 nm for carbon nanotubes, boron nitride, graphite and mesoporous carbon, respectively, **Figure 2.1.5a**). The purity of nanomaterials was checked with X-ray diffractometry (X'Pert Powder PANalytical, 15-90°scan range, 0.0084°scan step size, **Figure 2.1.5b**). The specification of nanomaterials is summarized in **Table A1** (Appendix A).

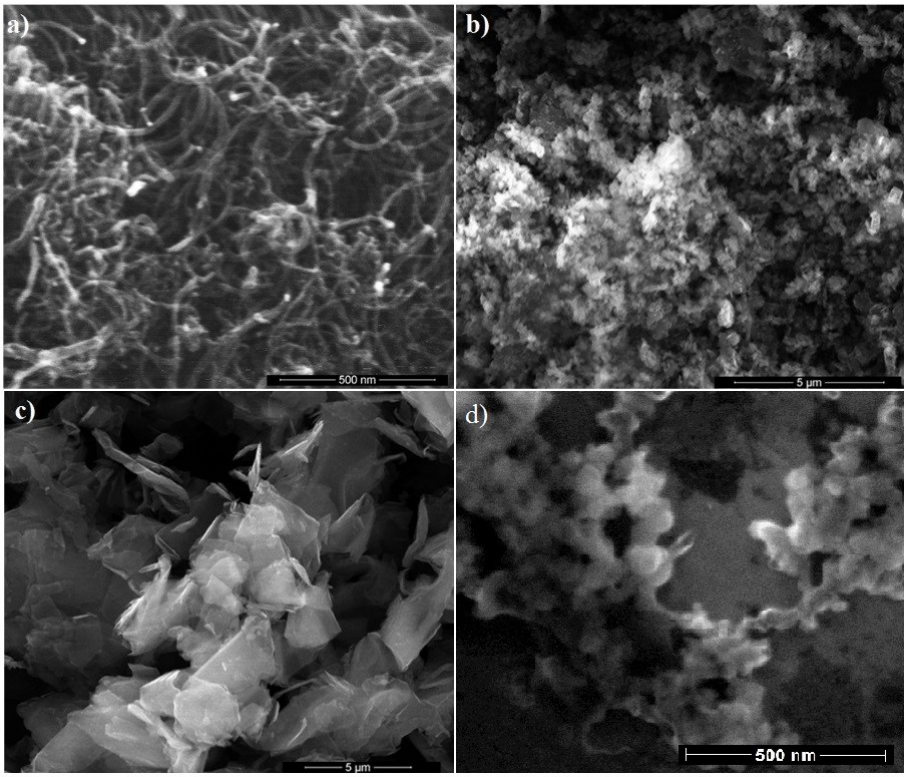

Figure 2.1.4. Scanning electron microscope images for: **a)** carbon nanotubes; **b)** boron nitride; **c)** graphite; **d)** mesoporous carbon.

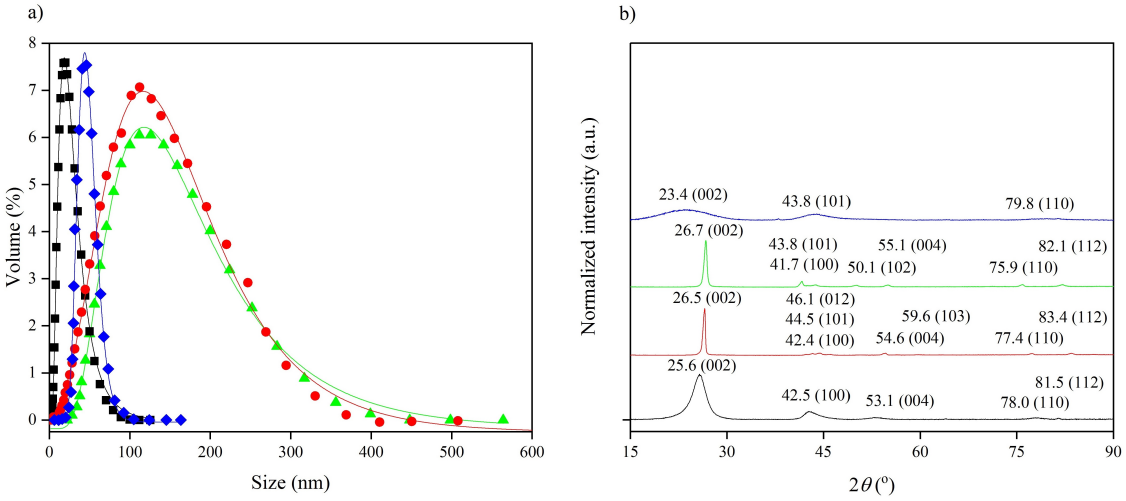

Figure 2.1.5. a) Nanoparticles size distribution derived from laser diffraction; **b)** XRD patterns with maximum of the diffraction peaks and assigned characteristic Miller indices in the brackets; for multiwalled carbon nanotubes, ■ and —, graphite, ● and —, boron nitride, ▲ and —, mesoporous carbon, ♦ and —.

2.1.5 Ionanofluids and Mixtures with Water

Manufacture of ionanofluids is a very delicate process and requires careful treatment. The same protocols used previously to produce reproducible nanofluids have been applied, herein. This was also applied in this work: after the nanoparticles were added to ILs, 30 min of magnetic stirring was applied, prior to the 1 h of sonication required to the formation of nanofluids instead of so-called bucky gels, and the nanoparticles agglomerates breaking down. To protect the mixtures against water absorption from the air, the whole procedure was performed under high vacuum: after the addition of nanoparticles to ILs, the mixture is subjected to the high vacuum to remove trapped air in nanoparticles and some residues of water introduced, afterwards, the mixture is transported to measuring cells in the glovebox purged with inert gas nitrogen. To produce the water-saturated ILs, the same volume of IL and deionised water (18 MΩ cm) were mixed together and sealed to prevent evaporation. After stirring vigorously for 30 min, the mixture was left for 48 h to fully saturate and phase separation at 298.2 K using a thermostatic oil bath. The water content was checked in a regular basis, and 48h were found enough to fully saturate the ILs (no change in the water content in IL phase). The IL layer was then separated by decantation, and water content measured by the Karl Fischer titration.

2.2 Techniques

2.2.1 Thermal Conductivity

Basic Principles

When a constant temperature difference on the medium layer borders of thickness l is caused by a contact with heater (T_1) on the first side, and cooler (T_2) on the other side (**Figure 2.2.1**), the temperature gradient, ∇T, is made, where ∇ is the Nabla operator, and the value of ∇T is, generally, changing from point to point.

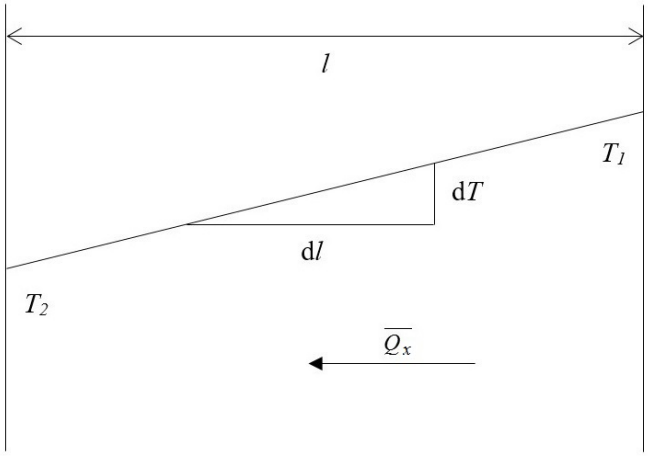

Figure 2.2.1. Schematic definition of heat transfer on the basis of Fourier's law.

If the medium is homogenous on the thickness of l, the gradient is constant:

$$|\nabla T| = \frac{T_2 - T_1}{l} \tag{2.2.1}$$

The heat is transferred through medium flat parallel layer of area segment in direction x in time t, and is expressed with the energy flux flow, $\overline{Q}_x$:

$$\overline{Q}_x = -\lambda \frac{dT}{dx} \tag{2.2.2}$$

where λ is thermal conductivity coefficient. Or the amount of heat transferred through a homogenous layer:

$$|\overline{Q}_U| = -\lambda \frac{T_2 - T_1}{l} \tag{2.2.3}$$

The thermal conductivity coefficient, λ, is a characteristic property of each substance in its physical state, as well as its phase. The thermal conductivity coefficient is also temperature dependent. Materials with the highest thermal conductivity are solids, then liquids and the worst conductive are gases.

Techniques

There is a wide range of many techniques which allows the determination of the thermal conductivity coefficient. Steady-state methods are performed when the temperature of studied material is constant, or the temperature difference is statistically negligible over the time. This makes the data analysis simpler to obtain a value of thermal conductivity coefficient. While the main disadvantage is the difficulty in constructing a proper equipment for this type of measurement. Within this group, we can distinguish cylindrical cell [10] and steady-state parallel-plate. [11] Thermal comparator, the basis of this technique is a calibration curve of thermal conductivity as a function of voltage caused by the temperature increase. [12] Non-steady state methods (transient techniques) are based on the studies of a signal as a function of time, instead of obtaining constant signal. The main advantage is that the measurement can be done relatively quickly. But the analysis of signal as a function of time is a complex issue. Within this group, we can distinguish thermal constants analyser, [13] temperature oscillation, [14] 3ω technique, [15] and transient hot-wire. [16]

Transient Hot-Wire Method

The transient hot-wire method has been primarily invented by Horrocks and McLaughlin (**1963**), [16] and established by Healy *et al.* (**1976**), [17] with further development by Watanabe (**2002**). [18] A model of transient hot-wire is based on an infinite line source of constant energy flux, Q, per unit length applied step-wise at $t = 0$, infinite incompressible medium with constant density, ρ, thermal conductivity, λ, and specific heat capacity, c_p, of constant thermal diffusivity, κ:

$$\kappa = \frac{\lambda}{\rho c_p} \tag{2.2.4}$$

The basic problem is ruled by the general Fourier heat-conduction equation:

$$\rho c_p \frac{\partial T}{\partial t} = \lambda \nabla^2 T \tag{2.2.5}$$

where c_p, ρ, λ are the functions of temperature:

$$\lambda = \lambda_{t=0}(1 + a\Delta T) \tag{2.2.6}$$

$$c_p \rho = (c_p \rho)_{t=0}(1 + b\Delta T) \tag{2.2.7}$$

$$\kappa = \frac{\lambda}{\rho c_p} = \kappa_{t=0}[1 + (a - b)\Delta T] \tag{2.2.8}$$

where a and b are fitting parameters, and ΔT is the temperature rise relative to $T_{t=0}$. After applying these functions, the heat equation has the following form:

$$\frac{\partial (c_p \rho T)}{\partial t} = \nabla[\kappa \nabla (c_p \rho T)] \tag{2.2.9}$$

The above equation is also known as the diffusion equation for the flux of heat energy distributed in the medium. As described above, ρc_p usually remains constant, then:

$$c_p \rho \frac{\partial T}{\partial t} = \nabla(\lambda \nabla T) \tag{2.2.10}$$

It is worth mentioning that equation (2.2.9) is more accurate than equation (2.2.10) due to the ρc_p assumption. When equations (2.2.6), (2.2.7) and (2.2.8) are inserted into equation (2.2.10), and the temperature is expressed as ΔT=T-$T_{t=0}$:

$$(c_p \rho)_{t=0}(1 + 2b\Delta T)\frac{\partial \Delta T}{\partial t} = \lambda_{t=0}[1 + (a + b)\Delta T]\nabla^2(\Delta T) + \lambda_{t=0}(b + a)\left(\frac{\partial \Delta T}{\partial 0.5d}\right)^2 \tag{2.2.11}$$

where d is the diameter of the wire. Equation (2.2.11) is equivalent to the equation obtained after revising equation (6.50) in work of Watanabe (**2002**) [18] – it means introducing factor $2b$ instead of b on the left-hand side and $(a + b)$ instead of a on the right-hand side of the equation. Commonly $\lambda_{t=0}$ is omitted and then equation (2.2.11) takes the following form:

$$\frac{\partial \Delta T}{\partial t} = \kappa_{t=0}\left\{[1 + (a + b)\Delta T]\nabla^2 \Delta T + (a + b)\left(\frac{\partial \Delta T}{\partial 0.5d}\right)^2\right\} \tag{2.2.12}$$

It can then be found that, that for certain boundary conditions, the equation for the temperature rise in the hot wire for times t such that the Fourier number,

$(16\kappa_{t=0}\, t)/(d^2\, e^E\,) \gg 1$, where $e^E = 1.78107$, E is Euler's constant:

$$\Delta T(t) = \frac{Q}{4\pi\lambda_{t=0}}\left(\ln\frac{16\kappa_{t=0}t}{d^2e^E}\right) - 0.5(a+b)\left(\frac{Q}{4\pi\lambda_{t=0}}\right)^2\left(\ln\frac{16\kappa_{t=0}t}{d^2e^E}\right)^2 + (a-b)\left(\frac{Q}{4\pi\lambda_{t=0}}\right)^2 \ln 4 \tag{2.2.13}$$

The above equation can be used to calculate $\kappa_{t=0}$, $\lambda_{t=0}$ at the temperature $T_{t=0}$ by fitting experimental data. The final values of experimental thermal conductivity, λ_{exp}, and experimental thermal diffusivity, κ_{exp}, are usually calculated from the following approximate expression:

$$\Delta T(t) = \left(\frac{Q}{4\pi\lambda_{exp}}\right)\left(\ln\frac{16\kappa_{exp}t}{d^2e^E}\right) \tag{2.2.14}$$

Experimental Procedure

The equipment used for the thermal conductivity measurement was a KD2 Pro Thermal Properties Analyzer (Decagon company), based on the transient hot-wire principle. The sensor used was KS-1 (6 cm length, 1.3 mm diameter). The sensor was inserted into a vial containing the sample (~30 cm^3) during measurement. The whole system was sealed to prevent any leakage to the environment or water absorption. The whole system was wrapped with cotton wool in case of any vibrations caused by the flowing fluid. Then the wrapped system was immersed in an oil bath circulator (Grant TC120, filled with 50 vol% ethylene glycol/water, thermal stability ± 0.05 K and uniformity ± 0.1 K). The time gap between each measurement was at least 15 min. To obtain valuable and precise data on the thermal conductivity, a calibration was performed. Whereas the standard uncertainty u of temperature is $u(T) = 0.05$ K.

A range of methods for the thermal conductivity have been reported previously and, in the present work, special attention was paid to the calibration and measurement of the reported materials, herein. [19, 20] It is well-known that the results of the thermal conductivity measurement may be affected by many factors, *i.e.* temperature, viscosity, electrical and ionic conductivity. Thus, for the calibration purpose, a series of different liquids were chosen – water (ultrapure obtained by using Barnstead Nanopure Diamond, purity: 18 MΩ cm), toluene (Sigma-Aldrich, ACS Reagent, CAS: 108-88-3, purity:

≥99.5%, water content: 0.150 wt%), glycerine (Sigma-Aldrich, for molecular biology, CAS: 56-81-5, purity: ≥99%, water content: 0.138 wt%), 50 wt% glycerine/water, 2.702 mol kg^{-1} sodium chloride/water (Sigma-Aldrich, ACS Reagent, CAS: 7647-14-5, purity: ≥99%). In the final step, the calibration procedure was checked by thermal conductivity measurement of $[C_8C_1Im][NTf_2]$. 10 measurements of each substance at each temperature were performed. The output data from KD2 Pro contain, *inter alia*, temperature, thermal conductivity and error of the thermal conductivity. These data are further used for the calibration. The calibration constant, K, is defined using equation:

$$K = \frac{\lambda_{exp}}{\lambda_{real}} \tag{2.2.15}$$

where subscripts *exp* and *real* refer to experimental and real values, respectively. The final experimental value is given as the average (and the standard uncertainty as the average of those determined in the measurement). The standard uncertainty of K is calculated based on the chain rules of differentiation as shown in the following equation:

$$\delta K = \left|\frac{\partial K}{\partial \lambda_{exp}}\right| \delta\lambda_{exp}^2 + \left|\frac{\partial K}{\partial \lambda_{real}}\right| \delta\lambda_{real}^2 = \left|\frac{\delta\lambda_{exp}^2}{\lambda_{real}}\right| + \left|\frac{\lambda_{exp}\delta\lambda_{real}^2}{-\lambda_{real}^2}\right| \tag{2.2.16}$$

where δ indicates the standard uncertainty. The final value of K is used as the average of all determined constants (as well as the standard uncertainty). To use the above considerations in practical issues, it is recommended to do at least 3 measurements of thermal conductivity at each temperature. The thermal conductivity was then calculated as the average of values determined by the equation (2.2.15), and the standard uncertainty is also the average of values calculated by the following equation:

$$\delta\lambda_{real} = \left|\frac{\partial \lambda_{real}}{\partial \lambda_{exp}}\right| \delta\lambda_{exp}^2 + \left|\frac{\partial \lambda_{real}}{\partial K}\right| \delta K^2 = \left|\frac{\delta\lambda_{exp}^2}{K}\right| + \left|\frac{\lambda_{exp}\delta K^2}{-K^2}\right| \tag{2.2.17}$$

This approach leads to accurate values for the calibration constant with a very low standard uncertainty. The results are shown in **Table 2.2.1**. As can be seen, all K values are approximately equal to 1. The value of K was found to be 0.9932 ± 0.0075 (a relative deviation of 1.52%). The δK reported by the manufacturer is ± 0.01.

The calibration constant was checked to ascertain its dependence on the temperature and the thermal conductivity (**Figure 2.2.2a** and **Figure 2.2.2b**, respectively). To properly illustrate these dependencies, the confidence level was set as 95% with coverage

factor equal to 2 (in general, it means the multiplication of the average standard deviation by the value of coverage factor, while the confidence level is as set).

The results indicate that the calibration constant was temperature and thermal conductivity independent. To check whether any value was out of confidence level, five additional lines were added to **Figure 2.2.2**. Two of these correspond to $K \pm 2\delta K$, two of these correspond to $K \pm \delta K$, and one corresponds to K. As can be seen, there was only one data point (of water at 298.16 K) which was close to $K \pm 2\delta K$ upper line, however, it did not exceed this value. The procedure also proved that the sensor (and measurement methodology) is viscosity, thermal, ionic and electrical conductivity independent.

Table 2.2.1. Results of KD2 Pro Thermal Properties Analyzer calibration, including temperature, T, experimental thermal conductivity and its standard uncertainty, λ_{exp} and $\delta\lambda_{exp}$, literature thermal conductivity, λ_{real}, calibration constant and its standard uncertainty, K and δK, at 101 kPa.

	T (K)	$\lambda_{exp} \pm \delta\lambda_{exp}$ (mW m^{-1} K^{-1})	λ_{real} (mW m^{-1} K^{-1})	$K \pm \delta K$
Glycerine [21]	284.59	283 ± 1	281.4	1.0053 ± 0.0031
	293.15	280 ± 1	282.5	0.9922 ± 0.0029
	321.82	284 ± 1	286.3	0.9913 ± 0.0032
	357.98	286 ± 2	291.2	0.9818 ± 0.0062
Glycerine + Water (50.0 wt%) [21]	293.15	414 ± 1	419.8	0.9864 ± 0.0021
	308.57	427 ± 1	431.6	0.9903 ± 0.0027
Water [22]	278.45	562 ± 2	568.2	0.9893 ± 0.0032
	293.50	597 ± 4	598.2	0.9987 ± 0.0071
	298.16	611 ± 2	606.4	1.0078 ± 0.0030
Water + NaCl (2.702 mol kg^{-1}) [23]	288.23	569 ± 2	572.0	0.9865 ± 0.0033
	297.02	585 ± 2	585.0	0.9944 ± 0.0033
Toluene [24]	286.45	133 ± 1	134.5	0.9896 ± 0.0055
	296.79	131 ± 1	131.4	0.9977 ± 0.0067

The thermal conductivity values of the references used for the calibration were slightly out of the range of values of the investigated ILs. Only toluene exhibits similar values. However, as can be seen later this did not affect the measurement.

The final check of the calibration was done by the thermal conductivity measurement of $[C_8C_1Im][NTf_2]$, and the values were compared with previously reported data (**Figure 2.2.3** and **Table CD2.1**, Appendix CD2).

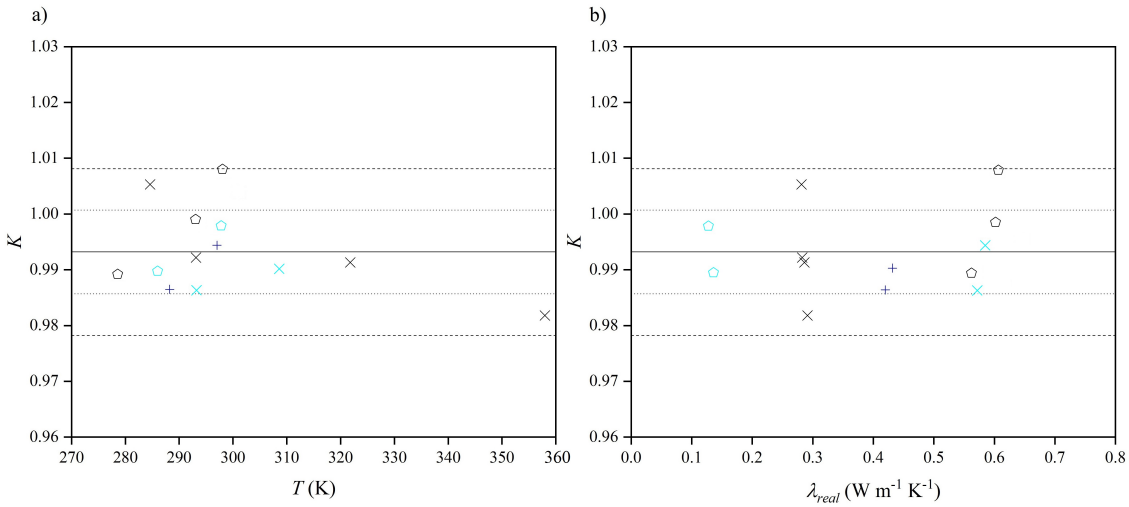

Figure 2.2.2. Calibration constant, K, of KD2 Pro Thermal Properties Analyzer as a function of **a)** the temperature, T; **b)** the literature thermal conductivity coefficient, λ_{real}, for water, ⬠, toluene, ⬠, glycerine, ×, glycerine/water 50 wt%, +, water/NaCl 2.702 mol kg^{-1}, ×.

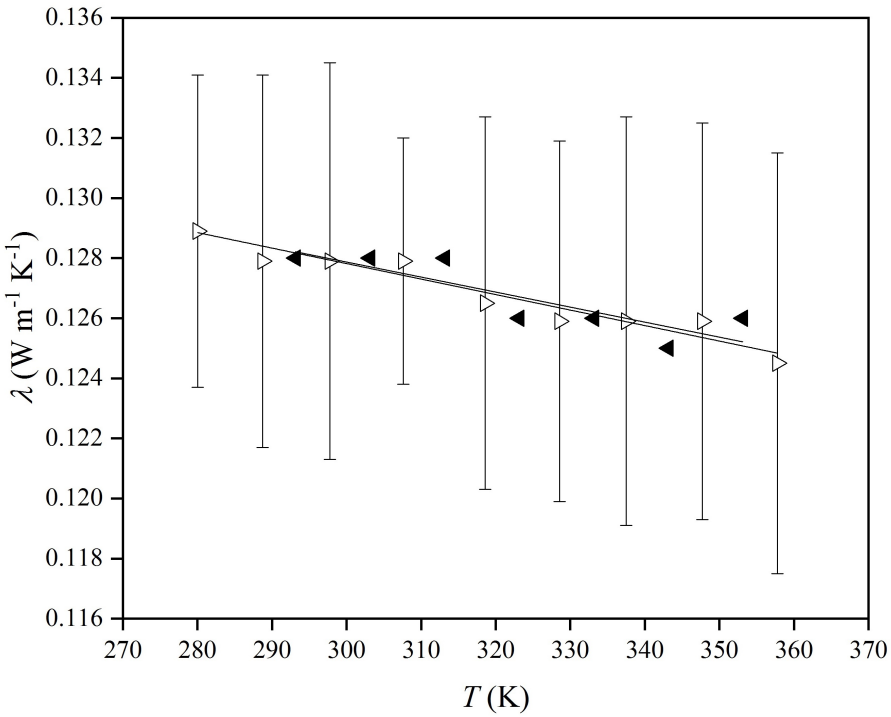

Figure 2.2.3. Thermal conductivity, λ, as a function of the temperature, T, for $[C_8C_1Im][NTf_2]$ experimental data, ▷, literature data, ◀ [25].

As can be seen, the results from this work agreed well with previously reported data (maximum relative deviation of 0.43%). [25] The water content of the sample was

checked by Karl Fisher titration prior to each measurement undertaken (in this work 0.020 wt%). The water content reported previously was 0.08 wt% which is higher than the sample used in this work. [25] However, it did not affect the values of thermal conductivity, while the deviations between both series of data were negligible. If water would influence the thermal conductivity of ILs, it should raise these values (as water has higher thermal conductivity in comparison to ILs). The parameters of equation (2.2.18), $\lambda(T)$, are a_0=(143 ± 61) × 10^3 W m^{-1} K^{-1} and a_1=-(50 ± 190) × 10^6 W m^{-1} K^{-2} in this work, a_0=(143 ± 26) × 10^3 W m^{-1} K^{-1} and a_1=-(52 ± 82) × 10^6 W m^{-1} K^{-2} in the literature reference [25]. As can be seen, the errors of a_1 parameters are higher than the values of these parameters. It means that, according to experimental errors, the thermal conductivity of $[C_8C_1Im][NTf_2]$ seems to be temperature independent over the temperature range investigated during this work. To correlate the thermal conductivity coefficient as a function of the temperature, equation (2.2.18) was used:

$$\lambda(T) = \sum_{i=0}^{1} a_i T^i \tag{2.2.18}$$

2.2.2 Thermal Analysis

In accordance to the International Confederation for Thermal Analysis and Calorimetry (ICTAC), *thermal analysis (TA) refers to a group of techniques in which a property of a sample is monitored against time or temperature while the temperature of the sample, in a specified atmosphere, is programmed* with a further modification *thermal analysis (TA) means the analysis of a change in a property of a sample, which is related to an imposed temperature alteration*. [26] Therefore, many different properties can be studied, for example temperature, [27] pressure, [28] temperature difference, [29] optical properties, [30–34] heat, [27] electrical properties, [35–37] mass, [38] acoustic properties, [39] magnetic properties, [40] deformation mechanical properties. [41–44]

The exchange of the internal energy, U, between system and environment can occur by heat transfer, Q, or work, W, done on the system:

$$\Delta U = Q + W \tag{2.2.19}$$

$$dU = dQ + dW = dQ - pdV \tag{2.2.20}$$

for finite, ΔU, and infinitesimal, $\mathrm{d}U$, internal energy changes, respectively. Internal energy is a state function which means that only a difference between the final and beginning states can be determined, instead of absolute values in the final and beginning states. Generally, internal energy is associated to all types of energies accumulated in the system. Enthalpy, H, other state function, defined as follows:

$$\Delta H = U + pV = Q + W + pV \tag{2.2.21}$$

$$dH = dU + pdV + Vdp = dQ + Vdp \tag{2.2.22}$$

where p is pressure and V is volume. One of the most important thermophysical property, isobaric heat capacity, c_p, can be derived based upon the above expressions (assumptions: p = const. which reduces $V\mathrm{d}p = 0$):

$$\left(\frac{\partial H}{\partial T}\right)_p = \left(\frac{\partial Q}{\partial T}\right)_p = c_p \tag{2.2.23}$$

Generally, heat capacity property describes the heat required to decrease/increase the temperature for 1 K. It must be noted, that the nomenclature and thermodynamic approach distinguish two types of isobaric heat capacity, these are specific heat capacity, which corresponds to the amount of substance per mass (c_p), and molar heat capacity, which corresponds to the amount of substance per moles (C_p). The main technique used to determine the heat capacity is calorimetry, particularly, differential scanning calorimetry (DSC).

Differential Scanning Calorimetry: Basic Principles

The main aim of calorimetric techniques is the measurement of heat, more specifically the heat exchange. This heat exchange directly affects the temperature change in a body inducing a heat flow. Most reactions or physical transitions are associated with heat exchange which means that calorimetry is a very useful technique to investigate these behaviours. Moreover, the heat capacity of sample also influences the heat flow during the measurement, therefore, it is possible to determine this property through the measurement of heat flow. The most commonly used technique is DSC and is followed by the very accurate definition: the measurement of the change of the difference in the heat flow rate to the sample and to a reference sample while they are subjected to a controlled temperature program. In comparison to differential thermal analysis (DTA),

DSC is a quantitative technique, while DTA is counted as qualitative technique in which the temperature difference between the sample and the reference is measured. It is more dynamic technique which enables wider temperature characteristic.

The principle of DSC is the registering of heat flow differences between measured sample, Φ_s, and reference (empty pan), Φ_r:

$$\Phi = \Phi_s + \Phi_r \tag{2.2.24}$$

The construction of the system is presented in **Figure 2.2.4**. The heat flows of sample and reference are represented by the following relations:

$$\Phi_s = \frac{T_0 - T_s}{R_s} - C_s \frac{dT_s}{dt} \tag{2.2.25}$$

$$\Phi_s = \frac{T_0 - T_r}{R_r} - C_r \frac{dT_r}{dt} \tag{2.2.26}$$

for sample and reference, respectively. Where T_0 is DSC enclosure temperature (constantan and chromel wires), T_s and T_r are temperature of sample and reference (chromel and alumel wires), respectively, R_s, C_s and R_r, C_r are the sensor thermal parameters (resistance and capacitance) of sample and reference, respectively.

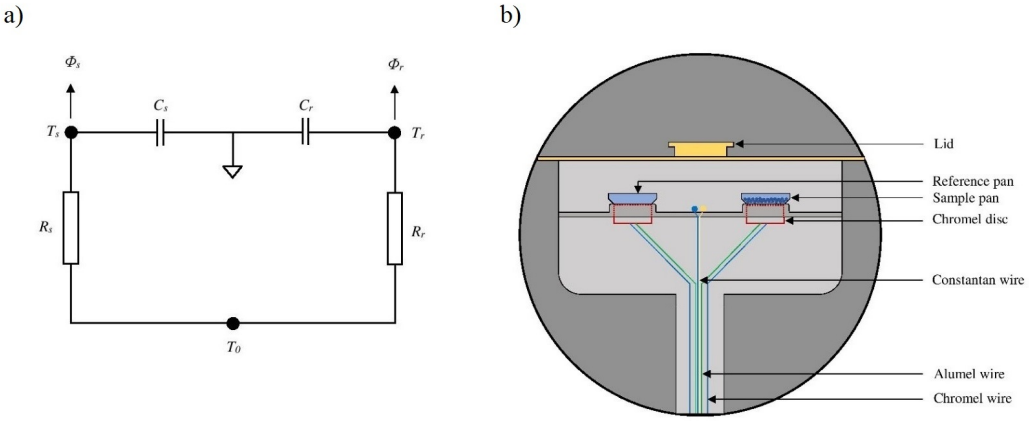

Figure 2.2.4. The construction of DSC: **a)** electrical circuit; **b)** chamber.

The final form of heat flux is:

$$\Phi = -\frac{\Delta T}{R_r} + \frac{\Delta T_0}{R_s - R_r} + (C_r - C_s)\frac{dT_s}{dt} - C_r \frac{d(\Delta T)}{dt} \tag{2.2.27}$$

where ΔT=T_s-T_r and ΔT_0=T_0-T_s. This four-term heat flux equation is widely applied in DSC equipment. The first term is classical equation in which the heat flow is determined

based on the proportionality factor. The second and third terms are related to equipment asymmetry and reflect the imbalances between thermal resistances and heat capacities of reference and sample. The last term corrects the differences in heating rate between sample and reference. The thermal parameters of sensors, R and C, are determined within the calibration procedure on empty pans (as a baseline) and a pan with sapphire (material with known heat capacity).

Isobaric Heat Capacity Measurement

As a result, the calibration of signal is performed, as well the possibility of heat capacity determination is enabled:

$$c_{p,s} = \frac{\Phi_s}{\Phi_r}\frac{m_r}{m_s}c_{p,r} \tag{2.2.28}$$

where m is mass, or with modulated differential scanning calorimetry (MDSC), as another technique used to determine the heat capacity. The principle of this method is the small sinusoidal temperature changes, and the following term is introduced to the linear temperature-time function:

$$c_{p,s} = \frac{\Phi_A}{T_A\omega} \tag{2.2.29}$$

where Φ_A is the heat flow rate amplitude, T_A is temperature modulation temperature, ω is the angular frequency ($2\pi/t_p$, where t_p is the period).

The calibration of this equipment is divided into 3 steps: **a)** measurement within the whole range of temperature without any pans (neither sample nor reference) to characterize the background and reduce the impact of asymmetry of the system; **b)** after the baseline subtraction, signal calibration on the sample of known heat capacity and mass is performed (usually ultrapure sapphire pellets) on both sample and reference sides; **c)** as a last step, the final calibration on melting point is performed (usually indium) to correct the temperature reading (melting temperature) and to confirm accurate signal calibration (enthalpy change of melting).

Thermogravimetric Analysis

Another extensively used thermal analysis technique is thermogravimetry in which the weight loss against temperature and time is measured. The scheme of equipment is presented in **Figure 2.2.5**. The most accurate mechanism of working is so-called null-point weighing (sensitivity of 1 μg). The sample is kept in the sample position in furnace, independent of weight change. An electrooptical device (LED and photo cell) has a shutter attached which detects any weight changes (beam alters the light intensity on photo cell, whereas the enhanced output from photocell induces the balance to restore the equilibrium between sample and reference, as equal to the weight change).

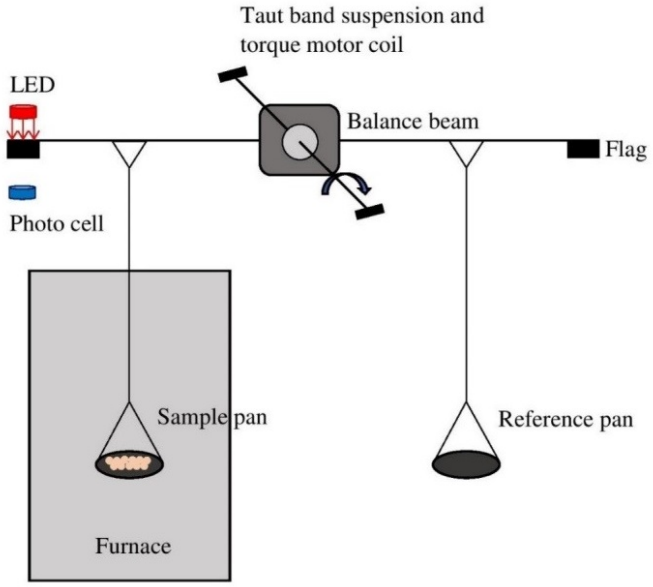

Figure 2.2.5. A general scheme of equipment used for thermogravimetric analysis (based on null-point weighing mechanism).

An important factor influencing the significance of thermogravimetric results is the methodology to determine the onset temperature (**Figure 2.2.6**). The differentiation of obtained thermogravimetric curve produces a Gaussian-like peak function, which is used to determine the onset temperature as the crossing point of baseline and extrapolated linear function (as presented in **Figure 2.2.6**), while the percentage of weight loss is an equivalent to curve area. Furthermore, as indicated by Maton *et al.* (**2013**), [45] T_{on} is determined by the derivative function (dm/dT *vs.* T) which has been recognized as a sufficiently accurate parameter of thermal stability, and this is commonly used to describe

the thermal decomposition. [46, 47] Moreover, the overestimation of the onset temperature is reduced.

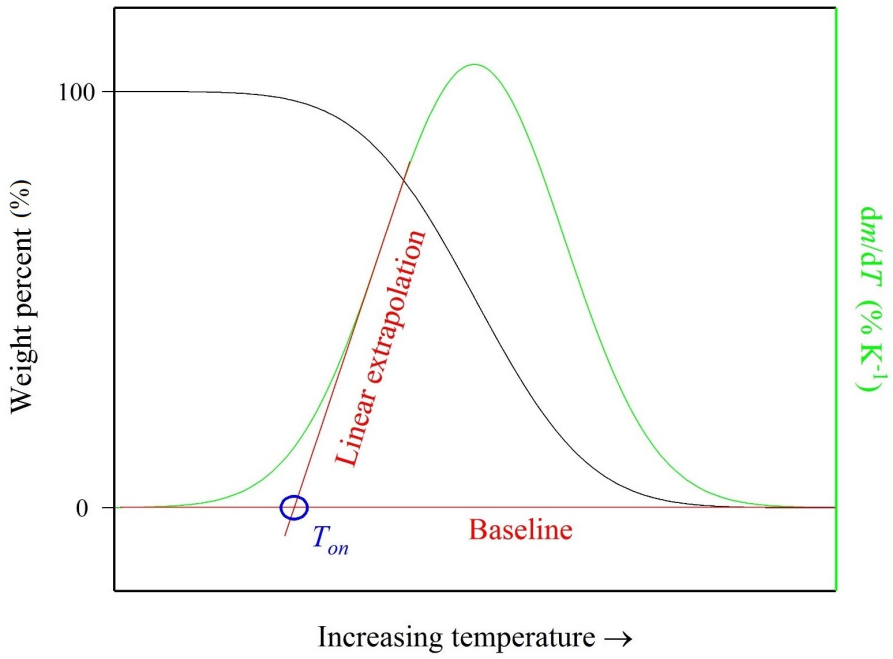

Figure 2.2.6. Determination of onset temperature, T_{on}, based on thermogravimetric curve.

Experimental Procedure

Two types of machine were used in this work to perform the calorimetric studies (in the meaning of heat capacity and phase transition). However, both of them produce the same accurate results with no numerical differences.

The first equipment used for heat capacity determination was TA Instruments DSC Q2000, using Tzero Aluminum Hermetic Pan, with a nitrogen gas flow (50 cm^3 min^{-1}), and a heating rate of 5 K min^{-1}. Relative standard uncertainty of measurement $u_r(c_p)$ = 3% (declared by the equipment company and confirmed within the calibration), while the temperature standard uncertainty, $u(T)$ = 0.01 K. The calibration of this equipment was done using sapphire as a reference material (CAS: 1317-82-4, TA Instruments, ultrapure in accordance to the reference standards NIST SRM 720, **Table A1**, Appendix A) with further checking on 1-hexyl-3-methylimidazolium bis(trifluoromethylsulfonyl)imide as a NIST standard. [48] The temperature range was (298.15-363.15) K. To obtain the most accurate values of the heat capacity, 3 independent measurements on each sample were per-

formed with 5% repeatability. In order to determine the melting point of investigated ILs, the temperature scan was performed in the temperature range of (193.15-383.15) K and heating rate of 5 K min^{-1}. For all ILs studied, herein, no first order transition was recorded. This equipment was used for pure and water-saturated trihexyl(tetradecyl)phosphonium carboxylate ILs.

The second equipment was a differential scanning calorimeter, Q100 TA instruments (modulated differential scanning calorimetry technique, calibration on sapphire with further checking on 1-hexyl-3-methylimidazolium bis(trifluoromethylsulfonyl)imide as a NIST standard. [48] Relative standard uncertainty of measurement $u_r(c_p) = 3\%$, while the temperature relative standard uncertainty, $u_r(T) = 0.01$ K, nitrogen gas flow rate of 50 cm^3 min^{-1}, heating rate $dT/dt = 2$ K min^{-1}, amplitude ± 0.5 K, modulation period 60 s, 3 independent repeats of the measurement with 5% repeatability). This machine was used for every measurement excluding pure and water-saturated trihexyl(tetradecyl)phosphonium carboxylate ILs.

It has been reported that a second order equation is sufficient to define the heat capacity as a function of the temperature: [49, 50]

$$c_p(T) = \sum_{i=0}^{2} a_i T^i \tag{2.2.30}$$

where the coefficients of this equation, a_i, and their fitting errors, were determined by the least-square procedure. To describe the fit of this equation, R^2 coefficient was used. These data was then used to calculate the molar excess heat capacity, $C^E_{p,m}$ using the following equation:

$$C^E_{p,m} = c_{p,1+2}\,(x_1 M_1 + x_2 M_2) - c_{p,1} x_1 M_1 - c_{p,2} x_2 M_2 \tag{2.2.31}$$

where x is mole fraction, M is molecular mass.

The thermogravimetric analysis (TGA) was investigated on two machines: **a)** TA Instruments TGA Q5000 on the platinum-HT pan, weighing standard uncertainty 0.01%, standard uncertainty of signal resolution 0.01 μg, standard uncertainty of temperature $u(T) = 0.5$ K, for trihexyl(tetradecyl)phosphonium carboxylate ILs and their mixtures with water; **b)** TA Instruments TGA 550 on the platinum-HT pan, weighing standard uncertainty 0.01%, standard uncertainty of signal resolution 0.01 μg, standard uncertainty of temperature $u(T) = 0.5$ K, for all samples excluding trihexyl(tetradecyl)phosphonium

carboxylate ILs and their mixtures with water. All measurements were done under a nitrogen gas flow of 25 cm^3 min^{-1} and heating rate of 5 K min^{-1} (high heating rates increases the registered decomposition temperature), about 25 mg of sample was used (as larger sample mass increases the registered decomposition temperature).

The calibration procedure is divided into two steps. In the first step, the signal generated by mass is calibrated on the reference material mass (100 mg), assessed within the whole temperature range for 2 points, with further linear interpolation. The temperature scale is calibrated on Curie point determination (temperature at which material loses its magnetic properties) due to the magnet placed in the furnace (which also assures the same position of sample during each measurement). The materials used for calibration are alumel (T_{curie} = 426.15 K) and nickel (T_{curie} = 631.15 K).

2.2.3 Density and Viscosity

Density

Density is a thermophysical parameter which is classified to the group of properties essential to know. It is easily measurable and sensitive enough to detect any contaminations. The definition of this is as follows:

$$\rho = \frac{m}{V} \tag{2.2.32}$$

As can be seen, it correlates the mass and volume of compound. Thus, it is necessary to know as a function of temperature for many purposes, especially in chemical and engineering processes, simulations, or to make a recalculation between different types of concentrations. There are many types of density determination techniques, for example pycnometer (mass measurement in a container with known volume), refractometry (beam diffraction angle measurement in relation to sample's density), however, the most commonly used technique is called vibrating U-tube.

Density Measurement: Oscillating U-Tube

The basic principle of vibrating U-tube is that every material has its own natural vibration frequency represented by the following equation:

$$f = \frac{1}{2\pi}\sqrt{\frac{\tau}{m + V\rho}} \tag{2.2.33}$$

where f is frequency ($f = t_p$-1, t_p is oscillation period), τ is elasticity constant. The scheme of exemplary equipment construction is presented in **Figure 2.2.7**.

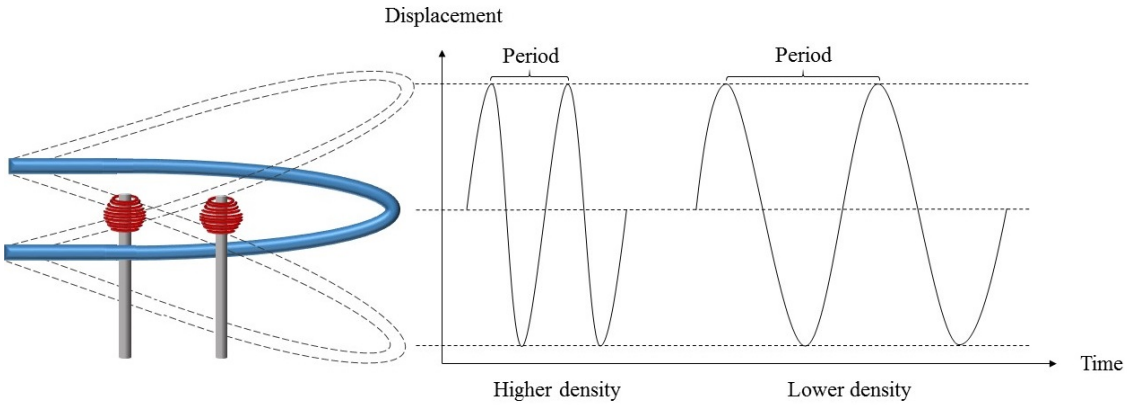

Figure 2.2.7. Oscillating U-tube densitymeter working principle.

The electrical alternating voltage is transformed into alternating magnetic field in the electric coil. This causes the excitation in the coil which makes the U-tube vibrate with a unique frequency of the fluid inside. This magnet's oscillation frequency is then measured with an amplifier. The first correlation between density, densitometer properties and fluid properties was proposed by Stabinger with the following well-known equation:

$$\rho = \frac{\tau^2 - B}{A} \tag{2.2.34}$$

where A and B are adjustable parameters dependent on the measuring machine (incorporating the volume, mass and spring constant of the oscillating tube). Another important factor which needs to be taken into account during the density measurement is viscosity. The density correction factor, ρ_{corr}, is described with the following equation:

$$\rho_{corr} = 11.6 + 109\ln\eta - 21.4\,(\ln\eta)^2 + 4.92\,(\ln\eta)^3 \tag{2.2.35}$$

where η is dynamic viscosity. This equation was reported to contribute to density changes of ± 0.035 kg m^{-3}. [51] The final form of equation used for density determination including the correction factor is as follows:

$$\rho = \left(\frac{\tau^2 - B}{A}\right)\left(\frac{1 - \rho_{corr}}{10^6}\right) \tag{2.2.36}$$

One of the most popular density-based property is isobaric thermal expansion coefficient, α_p:

$$\alpha_p = V^{-1}\left(\frac{\partial V}{\partial T}\right)_p = -\rho^{-1}\left(\frac{\partial \rho}{\partial T}\right)_p \tag{2.2.37}$$

α_p describes the thermal behaviour of system, more specifically its volume expansion because density correlates the mass and volume of the system, and mass is constant over the temperature, therefore, the volume is the only variable.

Viscosity

Viscosity is a property describing the ability of liquid to flow explained by the frictional forces occurring between moving liquid layers (**Figure 2.2.8**).

Figure 2.2.8. Viscosity as the friction forces between liquid layers.

Two liquid layers surfaces S with distance dx are moving with different velocities in relation to each other. To make two layers move with different velocity, v, a force, F, must be applied:

$$F = \eta S\frac{dv}{dx} \tag{2.2.38}$$

Generally, dynamic viscosity determines the liquid's resistance to flow upon the external force. The other way to describe the viscosity is kinematic viscosity coefficient, υ, is

defined as follows:

$$\upsilon = \frac{\eta}{\rho} \tag{2.2.39}$$

The kinematic viscosity, in contrary to dynamic viscosity, is a property describing the resistance to flow where no external forces act on the liquid, excluding the gravity. The equation (2.2.38) is valid for laminar flow in which the liquid velocity vectors are parallel. When the liquid velocity is becoming higher, the laminar flow becomes chaotic.

Viscosity Measurement: Rotational Rheometer

There are a few methods used to determine the dynamic viscosity of liquids, for example capillary viscometer (flowing time between two points assigned to specific viscosity), falling sphere (falling time of sphere inside the liquid based on Stokes equation), or rotational rheometer. One of the types of rotational rheometer is a parallel-plate orientation in which two plates (one stationary and one rotating) are filled with measured liquid (**Figure 2.2.9**).

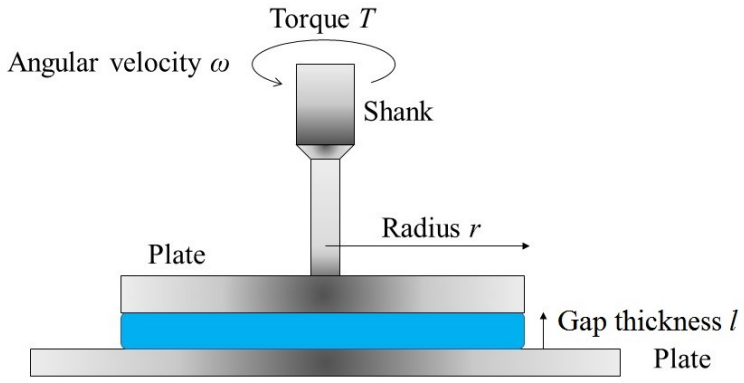

Figure 2.2.9. Parallel-plate rotational rheometer.

The viscosity is correlated with the torque (in respective to force applied), T, measured within the experiment, and therefore shear stress, σ, is calculated as follows:

$$\sigma = \frac{2T}{\pi r^3} \tag{2.2.40}$$

where r is the plate radius. The other property related to the characteristics of the plate

and rotation speed, so-called shear rate, γ:

$$\gamma = \frac{\omega r}{l} \tag{2.2.41}$$

where ω is angular velocity and l is the liquid thickness (or plates distance). The viscosity is then calculated as the ratio of shear stress to shear rate, $\eta = \sigma/\gamma$.

Density: Experimental Procedure

The density was measured by using two instruments. For pure trihexyl(tetradecyl)-phosphonium carboxylate ILs and their mixtures with water, a Mettler-Toledo DM40 densitometer was used (relative standard uncertainty of density, $u_r(\rho) = 0.1\%$, standard uncertainty of temperature, $u(T) = 0.05$ K, viscosity-induced errors reduced). This equipment works on the principle of oscillating U-tube. The calibration was conducted using ultrapure water (18.2 MΩ cm) and dry air. The temperature range used during the measurements was (298.15-363.15) K. The ionanofluids were measured as a function of the temperature, using an Anton Paar DMA 4500M densitometer (calibration on ultrapure degassed water and dry air, relative standard uncertainty of density, $u_r(\rho) = 0.1\%$, relative standard uncertainty of temperature, $u_r(T) = 0.01$ K, viscosity-induced errors reduced). These equipment work on the principle of oscillating U-tube where approximately 1.5 cm^3 sample volume is used within 3 independent repeats of the measurement. The temperature range of each measurement was set as (298.15 to 363.15) K.

To correlate the density with temperature, the following linear equation was then used:

$$\rho(T) = \sum_{i=0}^{1} a_i T^i \tag{2.2.42}$$

where a_i is the regression parameter determined by the least-square method, along with the standard uncertainty, δa_i. The coefficient of determination, R^2, was used to describe the fit. The nanoparticle densities were calculated using the following empirical formulae: [52]

$$\rho_{NP} = \frac{\rho_{IL+NP} - \rho\,(1 - w_{NP})}{w_{NP}} \tag{2.2.43}$$

where w is mass fraction, *IL* and *NP* refer to ILs and nanoparticles, respectively. The densities were also used to calculate the excess molar volumes of mixtures with water and nanoparticles. This was undertaken using the elementary definition of excess molar

properties, given by the following equation:

$$V_m^E = V_{m,1+2} - \left(x_1 V_{m,1} + x_2 V_{m,2}\right) = \frac{x_1 M_1 + x_2 M_2}{\rho_{1+2}} - \left(\frac{x_1 m_1}{\rho_1} + \frac{x_2 m_2}{\rho_2}\right) \tag{2.2.44}$$

where the subscripts *1* and *2* correspond to (*1* = water and *2* = ILs, or *1* = nanoparticles and *2* = ILs, in the mixture, respectively), superscript E corresponds to excess property, subscript m corresponds to molar property, x is the mole fraction, M is the molecular mass.

Viscosity: Experimental Procedure

The viscosity was measured using two instruments, both working on the same principle of rotational rheometer. The viscosity of pure trihexyl(tetreadecyl)phosphonium ILs and mixtures with water were determined by using Malvern Bohlin Gemini HRnano equipment (torque resolution better than 1 nN m, position resolution 50 nrad, temperature standard uncertainty, $u(T) = 0.1$ K). The principle of this equipment is based on parallel-plate viscosity measurement technique. The measurement temperature range was (298.2-363.2) K. The viscosity standard (ASTM Oil Standard S600 of CANNON, 1053 mPa s at 298.15 K) and ultrapure water were used to calibrate the viscometer. Based on these measurements, the reported viscosity relative standard uncertainty is $u_r(\eta) = 3\%$. The latter equipment was TA Instruments AR2000 rheometer (angular displacement resolution 40 nRad, torque resolution 0.1 nN m, temperature standard uncertainty $u(T) = 0.01$ K) with stainless steel 20 mm parallel plate geometry. The measurement temperature range was (298.15-363.15) K. The viscosity standard Cannon S600 oil and ultrapure water were used to ascertain the reported viscosity relative standard uncertainty, $u_r(\eta) = 3\%$.

The viscosity was correlated with temperature by using Vogel-Fulcher-Tammann (VFT) equation:

$$\eta(T) = \eta_0 \exp \frac{\beta}{T - T_0} \tag{2.2.45}$$

where η_0, β and T_0 are fitting parameters, determined by the nonlinear curve fitting algorithm in OriginPro 2017 software.

2.2.4 Ionic Conductivity

The ionic conductivity was measured by using Hach sensION+ EC71 Conductivity Benchtop Meter (conductivity relative standard uncertainty $u_r(\sigma)$ = 2%, temperature standard uncertainty $u(T)$ = 0.2 K, calibration on KCl (CAS: 7447-40-7, Sigma-Aldrich, Purity ≥99%) standard solutions of concentration as follows: 0.001 mol dm^{-3} (147 μS cm^{-1}), 0.01 mol dm^{-3} (1413 μS cm^{-1}), 0.1 mol dm^{-3} (12.88 mS cm^{-1}), **Table A1** in Appendix A, direct current, DC) with Hach sensION+ 5070 laboratory platinum conductivity cell. The temperature range of measurement was (298.2-363.2) K. The temperature of probe and electrode was stabilized in oil bath within accuracy close to 0.5 K.

To describe the relationship between ionic conductivity, σ, and temperature, the Vogel-Fulcher-Tammann-like (VFT) equation (2.2.46) was used:

$$\sigma(T) = \sigma_0 \exp \frac{-\beta}{T - T_0} \tag{2.2.46}$$

where σ_0, β and T_0 are fitting parameters, determined by the nonlinear curve fitting algorithm in OriginPro 2015 software.

2.2.5 Walden Plot

Electrolytes are associated with their ions mobility, u, which is related with the electrical field force applied and internal friction force (viscosity):

$$u = \frac{|z_i|\, e}{6\pi\eta r_i} \tag{2.2.47}$$

where z_i is the charge value of ion, e is elementary charge, r_i is ion radius. The radius of ions do not change significantly with the temperature change, so the ion mobility (or limiting molar conductivity, Λ^0), and viscosity product is constant:

$$\Lambda^0\eta = C = \text{constant} \tag{2.2.48}$$

where C is constant also known as the Walden product. The data of ionic conductivity, density and viscosity were used to construct the Walden plot. This rule was used to

describe the degree of ionicity of neat ILs and mixtures with water. The logarithmic form was used:

$$\log(\Lambda^0) = \log C + \log \eta^{-1} \tag{2.2.49}$$

There can be also found the extension of equation (2.2.48) and equation (2.2.49). These include the fractional Walden rule which introduces the fractional factor, α: [53]

$$\Lambda^0 \eta^\alpha = C' = \text{constant} \tag{2.2.50}$$

$$\log(\Lambda^0) = \log C + \alpha \log \eta^{-1} \tag{2.2.51}$$

Two approaches were used to describe the degree of ionicity, herein. The first is based on ΔW factor, which describes the vertical distance between the ideal 0.01 mol dm^{-3} KCl line and experimental data. The second is based on the fractional factor comparison with the 0.01 mol dm^{-3} KCl line. The molar conductivity was calculated using the following equation:

$$\Lambda = \sigma c^{-1} \tag{2.2.52}$$

where c is the IL concentration in water (in mol cm^{-3}), and for pure ILs it transforms into $V_m = M\rho^{-1}$.

Due to intermolecular interactions, the mobility of ions can be affected. Walden rule is a useful approach to describe the interactions between cations and anions, particularly in ILs. Highly associated ions (for example due to strong Coulombic interactions) would exhibit lower mobility, and resulted in higher values of Walden product (as a deviation from ideally dissociated 0.01 mol dm^{-3} KCl). Moreover, the effect of solvents on the cation-anion interactions can be studied.

2.3 Theoretical Calculations and Modelling

2.3.1 Quantum Chemistry

The basic principles of quantum chemistry are presented herein, while the literature for further reading includes the references [54–56].

A macroscopic representation can be visualised by classical mechanics in which the position of a particle at any given time is studied, $x(t)$. Based on that, several other properties can be figured out, for example the velocity (v=dx/dt), the momentum (mv), or the kinetic energy ($0.5mv^2$). However, to determine $x(t)$, the Newton's second law is applied, F=ma= $\partial V/\partial x$ (as potential energy function derivative). The same problem is considered differently in quantum mechanics, more specifically the case is wave function, $\Psi(x,t)$, of the particle, which is obtained by solving the so-called Schrödinger equation:

$$i\hbar\frac{\partial\Psi}{\partial t} = -\frac{\hbar^2}{2m}\frac{\partial^2\Psi}{\partial x^2} + V\Psi \tag{2.3.1}$$

where i is a square root of -1, $\hbar$ is Planck's constant.

The wavefunction gives a valuable answer based on Born's statistical interpretation which says that $|\Psi(x,t)|^2$ gives the probability to find the particle within the wavefunction at point x, at time t. The conclusion from this interpretation is that the prediction of the exact position of the particle is impossible and unmeasurable, however, the information provided is the statistical probability. A direct result of that is the integration of $|\Psi(x,t)|^2$ must be 1 (as the particle exist and must be somewhere within the wavefunction):

$$\int_{-\infty}^{+\infty} |\Psi(x,t)|^2 \,\mathrm{d}x = 1 \tag{2.3.2}$$

The other issue in quantum mechanics is that wavefunction determined by the Schrödinger equation must be checked in terms of consistency between these. A normalisation factor was introduced, therefore:

$$\frac{\mathrm{d}}{\mathrm{d}t}\int_{-\infty}^{+\infty} |\Psi(x,t)|^2 \,\mathrm{d}x = \int_{-\infty}^{+\infty} \frac{\partial}{\partial t}|\Psi(x,t)|^2 \,\mathrm{d}x = 0 \tag{2.3.3}$$

The particles are also described by momentum, p:

$$\langle p\rangle = -i\hbar\int\left(\Psi^*\frac{\partial\Psi}{\partial x}\right)\mathrm{d}x \tag{2.3.4}$$

where $|\Psi|^2 = \Psi^*\Psi$, and Ψ^* is imaginary part of the wave function, Ψ is real part of the wave function.

Wavelength, λ, and momentum can be related with de Broglie formulae:

$$p = \frac{2\pi\hbar}{\lambda} \tag{2.3.5}$$

A conclusion from this equation is that changes in momentum spreads over the changes in wavelength, which lead to Heisenberg's uncertainty principle:

$$\delta x \delta p \geq \frac{\hbar}{2} \tag{2.3.6}$$

where δ is uncertainty of the property. It says that increasing the precision of position results in decreasing the precision of momentum, and *vice versa*.

As presented above, the Schrödinger equation provides the wave function as variable of time, $\Psi(x,t)$. The issue which arises is: how to solve this equation? The assumption is that potential energy function, V, is time-independent. Then, the Schrödinger equation can be represented by the separation of variables:

$$\Psi(x,t) = \psi(x)f(t) \tag{2.3.7}$$

where ψ is a function of x alone, and f of t alone. This gives the following solutions:

$$\frac{\partial\Psi}{\partial t} = \psi\frac{\mathrm{d}f}{\mathrm{d}t}, \frac{\partial^2\Psi}{\partial x^2} = \frac{\mathrm{d}^2\psi}{\mathrm{d}x^2}f \tag{2.3.8}$$

After rearrangements, and comparing to original Schrödinger equation:

$$i\hbar\frac{1}{f}\frac{\mathrm{d}f}{\mathrm{d}t} = -\frac{\hbar^2}{2m}\frac{1}{\psi}\frac{\mathrm{d}^2\psi}{\mathrm{d}x^2} + V = E \tag{2.3.9}$$

where E is so-called separation constant. This leads to the following expression:

$$-\frac{\hbar^2}{2m}\frac{1}{\psi}\frac{\mathrm{d}^2\psi}{\mathrm{d}x^2} + V\psi = E\psi \tag{2.3.10}$$

The above equation is called time-independent Schrödinger equation. In classical mechanics, the total energy of the system (kinetic and potential energies) is called Hamiltonian, H:

$$H(x,p) = \frac{p^2}{2m} + V(x) \tag{2.3.11}$$

$$\hat{H} = -\frac{\hbar^2}{2m}\frac{\partial^2}{\partial x^2} + V(x) \tag{2.3.12}$$

The final well-known time-independent Schrödinger equation is presented in the following form:

$$\hat{H}\psi = E\psi \tag{2.3.13}$$

where the expected value of the Hamiltonian (total energy) is:

$$\langle H \rangle = \int \psi^* \hat{H} \psi \mathrm{d}x = E \int |\psi|^2 \, \mathrm{d}x = E \tag{2.3.14}$$

The other issue for time-independent Schrödinger equation is that a numerous solution of $(\psi_1(x), \psi_2(x), \psi_3(x), ...)$ with the associated constant value (E_1, E_2, E_3, ...), can be found. The linear combination of separable solutions was introduced to overcome this problem:

$$\psi(x) = \sum_{n=1}^{\infty} c_n \psi_n(x) \tag{2.3.15}$$

where c_n are constants fitted for the initial conditions.

Two-particle issue can be solved in terms of exact solution (*i.e.* hydrogen atom). When more complicated systems (for example two-electron atoms) are considered, approximate methods need to be applied. One of them is perturbation theory in which the more complicated systems are solved based on simpler exemplary and known systems by perturbing them with '*small deformations*':

$$\hat{H} = \hat{H}_0 + \lambda \hat{H}' \tag{2.3.16}$$

where $\hat{H}_0$ is the Hamiltonian of the unperturbed system, $\hat{H}'$ is the Hamiltonian after perturbation, λ perturbation parameter (from 0 for no perturbation to 1 for full perturbation).

On the other hand, the variational method is based on guessing a '*trial*' wavefunction which consists of adjustable parameters (namely variational parameters). By changing these parameters, the wavefunction is recalculated and the minimum of the energy obtained. The trial wavefunction, Φ, can be represented by the linear combination of exact wavefunction, ψ_i:

$$\Phi = \sum_i c_i \psi_i \tag{2.3.17}$$

Therefore, the approximate energy of this wavefunction is:

$$E[\Phi] = \frac{\int \Phi^* \hat{H} \Phi}{\int \Phi^* \Phi} \tag{2.3.18}$$

By including the ground state energy, ε_0, the following expression can be used:

$$E\left[\Phi\right] - \varepsilon_0 = \frac{\sum_i c_i^* c_i(\varepsilon_i - \varepsilon_0)}{\sum_i c_i^* c_i} \tag{2.3.19}$$

The variational methods are optimizing the wavefunctions until:

$$E\left[\Phi\right] \geq \varepsilon_0 \tag{2.3.20}$$

One of central approximations in quantum mechanics is related to the motions of electrons and nuclei, so-called Born-Oppenheimer, which says that atomic nuclei are much heavier than electrons, as a result, their motion is slower than electrons and, therefore, their motions in a molecule can be separated).

The molecule electrons wavefunction with N electrons consists of $3N$ cartesian coordinates and N spin coordinates. It is an object of $4N$-dimension made by molecular spin orbitals and each of them is a function of 3 cartesian coordinates and one spin of one electron. It is extremely hard to solve. The linear combination of atomic orbitals is used to represent the molecular orbitals, also called algebraic approximation, where every molecular orbital is represented as a linear combination of atomic orbitals, χ_j:

$$\varphi(1) = \sum_j^M c_j \chi_j(1) \tag{2.3.21}$$

where (1) highlights that every atomic orbital and every molecular orbital depend on the spatial coordinates of one electron (electron number 1), and c_j are coefficients. A wavefunction in its pure form would need an infinite grid of points which is computationally impossible, moreover, the outcome is discontinuous.

In case of linear combination, the solution would consist of $4N$ numbers which simplifies the calculation. The set of atomic orbitals, $g(r)$, are defined within a basis set:

$$g(r) = f(x, y, z) \exp -\zeta r^n \tag{2.3.22}$$

where $f(x, y, z)$ is a polynomial, ζ is the orbital width, r is a distance from nucleus (centre of the atomic orbital). This given atomic orbital is localised (focused) at point (0,0,0). If n=1, then the orbitals are called Slater orbitals (STO – slater type orbitals), or n=1 for Gaussian orbitals (GTO – Gaussian type orbitals). STO are very similar to hydrogen atom orbitals, and they produce excellent results similar to '*real*' orbitals.

However, in the expression for Hamiltonian (particularly electron-electron interactions), the solution including STO is extremely hard. For this reason, GTO gained an incredible popularity. Other basis sets are based mainly on GTO, for example by adding more basis functions to atomic orbitals (double-zeta with two basis functions, triple-zeta with three basis functions), polarisation functions (as other atom's orbitals might shift from one place to another by polarisation, s orbital with p orbital, p orbital with d orbital), diffuse functions (with small ζ which means the electrons are located further from the nucleus). The following basis sets can be distinguished:

- STO-3G: contracted gaussian-type orbitals (good for C and H atoms);
- 6-31G (DZVP): contracted gaussian-type orbitals with double-zeta split-valence (from He to Kr atoms);
- 6-311G (or TZVP): contracted gaussian-type orbitals with triple-zeta split-valence (from He to Kr atoms);
- 6-31G*(d): 6-31G with added d polarization function (non-hydrogen atoms);
- 6-31G**(d,p): 6-31G with added d and p polarization functions (included hydrogen atoms);
- 6-31+G: 6-31G with diffuse s and p functions (non-hydrogen atoms);
- 6-31++G: 6-31G with diffuse s and p functions (including hydrogen atoms).

The first method used in quantum chemical calculations is Hartree-Fock. The main focus is on so-called Slater determinant, ψ:

$$\psi = \frac{1}{\sqrt{N!}} \begin{vmatrix} \phi_1(1) & \phi_1(2) & \dots & \phi_1(N) \\ \phi_2(1) & \phi_2(2) & \dots & \phi_2(N) \\ \dots & \dots & \dots & \dots \\ \phi_N(1) & \phi_N(2) & \dots & \phi_N(N) \end{vmatrix} \tag{2.3.23}$$

where ϕ_i are orthonormal one-electron functions – molecular spin orbitals. There are a few conclusions from the Slater determinant: electrons with the same spins cannot approach each other, and electron with different spins can approach each other.

Hartree-Fock method is a variational method with the Slater determinant as the trial function. This is an estimation of Schrödinger equation solution without any possibility to achieve the exact solution. The way to obtain the global optimum of the energy is the iterative method called self-consistent field: arbitral molecular orbitals are taken as initial conditions, solving the Slater determinant, estimating the energy from Schrödinger equation based on this Slater determinant, changing the orbitals and reiterating. This procedure is repeated until no changes in the energy are obtained. The self-consistent field is usually used alongside linear combination of atomic orbitals.

From the quantum point of view, we are not able to strictly determine the exact coordinates of electrons but the quantity we can establish is the probability to find an electron in the certain coordinate:

$$n(\overline{r}) = 2 \sum_i \psi_i^*(\overline{r})\psi_i(\overline{r}) \tag{2.3.24}$$

where $\overline{r}$ is a vector of electron coordinates. The principles of density function theory (DFT) are based on two theorems of Kohn and Hohenberg. The first fully proved is *the ground-state energy from Schrödinger's equation is a unique functional of the electron density*, in that meaning it shows that there is a one-to-one relation between ground-state wave function and the ground-state electron density. The restated Hohenberg and Kohn's theory can be expressed as $E[n(\overline{r})]$ which says that the ground-state energy, E, is expressed as the electron density, $n(\overline{r})$. Unfortunately, this does not explain what the functional is, and in the second theorem, the important property is explained – the electron density that minimizes the energy of the overall functional is the true electron density corresponding to the full solution of the Schrödinger equation. This state is practically used in DFT, with some pre-defined forms of functionals. As the wave function density, $n(\overline{r})$, is expressed by the wave functions, ψ, the following expression defines the electron density:

$$E[\psi_i] = E_{known}[\psi_i] + E_{XC}[\psi_i] \tag{2.3.25}$$

where the functional is separated into two terms: $E_{known}[\psi_i]$ representing the analytical form, and $E_{XC}[\psi_i]$ other unknown contribution, so-called exchange-correlation functional

(including the quantum mechanical effects). The analytical form can be expressed as:

$$E_{known}[\psi_i] = -\frac{\hbar^2}{m}\sum_i \psi_i^* \nabla^2 \psi_i d^2 r + \int V(\overline{r}) n(\overline{r}) d^3 r + \frac{e^2}{2} \iint \frac{n(\overline{r}) n(\overline{r}')}{\left|\overline{r} - \overline{r}'\right|} d^3 r d^3 r' + E_{ion} \tag{2.3.26}$$

This equation includes four terms (from left) electron kinetic energies, electrons-nuclei Coulombic interactions, electrons pairs Coulombic interactions, nuclei pairs Coulombic interactions. The above approach still implies some difficulties, and the task of energy optimization is not much easier than solving the Schrödinger equation. The solution for this problem was proposed by Kohn and Sham who showed that the electron density can be defined in a way of solving a set of equations in which only a single electron is included:

$$\left[-\frac{\hbar^2}{2m}\nabla^2 + V(\overline{r}) + V_H(\overline{r}) + V_{XC}(\overline{r})\right] \psi_i(\overline{r}) = \varepsilon_i \psi_i(\overline{r}) \tag{2.3.27}$$

It can be seen that this expression is very similar to the Hamiltonian operator inserted into original Schrödinger equation. The first potential, V, is defined as the *known* part of the total energy in equation (2.3.26). The other potential, V_H, called Hartree potential defined by the following equation:

$$V_H(\overline{r}) = e^2 \int \frac{n(\overline{r}')}{\left|\overline{r} - \overline{r}'\right|} d^3 r' \tag{2.3.28}$$

describes the repulsion forces between electrons. The last part, exchange-correlation potential, V_{XC}:

$$V_{XC}(\overline{r}) = \frac{\delta E_{XC}(\overline{r})}{\delta n(\overline{r})} \tag{2.3.29}$$

where δ is a functional derivative. Because of the primary assumption of calculations based on one electron, the exchange - correlation term defines the unphysical self - interaction correction. The main focus in DFT is on the exchange-correlation potential functional selection:

- local density approximation (LDA): exchange-correlation energy density is the at every position in the molecule, as for uniform electron gas;

- generalised gradient approximation (GGA): introduction of electron density gradient into LDA, these can include empirical parameters fitted to reproduce the experiment

(exchange: B, CAM, FT97, O, PW, mPW, X; correlation: B88, P86, LYP), or without empirical parameters (exchange: B86, LG, P, PBE, mPBE; correlation: PW91);

- Meta-GGA: introduction of second derivative of the density (for example B95, B98, ISM, KCIS, PKZB, TPSS, VSXC);

- adiabatic connection method (ACM) hybrid: including the exact Hartree-Fock exchange energy, determined as a functional of the Kohn-Sham molecular orbitals (B3LYP, B1PW91, B1LYP, B1B95, mPW1PW91, PBE1PBE).

A very useful visualisation of atoms in the molecule, particularly their properties can be obtained by calculating Mulliken charges. Mulliken atomic populations are based on a first-order density function of linear combination of atomic orbitals. To explain Mulliken charges, two normalized atomic orbitals are taken into consideration:

$$\psi_i = c_{ij}\chi_j + c_{ik}\chi_k \tag{2.3.30}$$

The charge distribution:

$$\psi_i^2 = c_{ij}^2\chi_j^2 + c_{ik}^2\chi_k^2 + 2c_{ik}\chi_i\chi_j \tag{2.3.31}$$

After integrating over all coordinates of electrons, and after normalization:

$$1 = c_{ij}^2 + c_{ik}^2 + 2c_{ij}c_{ik}S_{jk} \tag{2.3.32}$$

where S_{jk} is an overlap integral of the two orbitals. Assumption of Mulliken's theory is that one electron in molecular orbital, ψ, contributes c_{ij}^2 to the atomic orbital χ_j, c_{ik}^2 to the atomic orbital χ_k, and $2c_{ij}c_{ik}S_{jk}$ the the overlap region. These properties can be presented in Mulliken population matrix:

$$P_i = \begin{pmatrix} c_{ij}^2 & 2c_{ij}c_{ik}S_{jk} \\ 2c_{ij}c_{ik}S_{jk} & c_{ik}^2 \end{pmatrix} \tag{2.3.33}$$

Net population matrix, NP, described the sum of all the population matrices:

$$NP = \sum_i P_i \tag{2.3.34}$$

Calculations Procedure

Ground-state DFT was used to examine the charge distribution on the atoms of ILs, as an input information for further development of heat capacity predictive models. The approach to study the charge was based on Mulliken charge distribution (shortly, incorporation of molecular orbitals calculated on the basis of a linear combination of atomic orbitals, LCAO MO). Because the partial atomic charge is not a molecular descriptor in DFT, and Mulliken charges are defined by LCAO MO, the selection of set of functions describing the electronic wave functions (basis set) is very important process. Several different basis sets were used (TZVP, DGDZVP, DGTZVP, SVP, STO-3G) for the geometry optimization. After the Mulliken charges were assessed, there was no effect of the basis set and qualitative results of Mulliken charges. Even though the results were quantitatively deviated. For the purpose of this work, the quantitative relationship is not necessary, only qualitative results are needed. Therefore, based on the literature review and convenient methods, DGTZVP basis set was presented in this work. [57–59] B3LYP hybrid functional is a standard used for DFT calculations in case of ILs, therefore, this was used. [60–62] The software in which calculations were carried out was Gaussian 09W-A02.

2.3.2 Physical Properties Prediction

Pure Ionic Liquids

To predict the thermal conductivity the model proposed by Wu was used, defined by the following equation: [63]

$$\lambda(T) = \sum_{i=0}^{2} \mu_i \left(\sum_{j=1}^{k} n_j \Delta\lambda_{0,j} \right)^i \left[1 + k_0 (1 - T_r)^{\frac{2}{3}} \right] \tag{2.3.35}$$

where μ_i, $\Delta\lambda_{0,j}$ and k_0 are parameters, [63] n_j is the number of j group in the molecule, and:

$$T_r = \frac{T}{T_c} \tag{2.3.36}$$

$$T_c = \frac{T_b}{0.5703 + 1.0121 \sum_{j=1}^{k} n_j \Delta T_c - \left(\sum_{j=1}^{k} n_j \Delta T_c \right)^2} \tag{2.3.37}$$

$$T_b = 198.2 + \sum_{j=1}^{k} n_j \Delta T_b \tag{2.3.38}$$

where T_c is so-called critical temperature and T_b is the boiling temperature. In this case, Valerrama's critical and boiling temperature are used; ΔT_b and ΔT_c are the contributions to the boiling and critical temperature, respectively. [64–66] The prediction of heat capacity from the model of Ge *et al.* (**2008**) [3] and Nancarrow *et al.* (**2015**) [67] is done by the following equations:

$$\begin{aligned} C_p^0(T) = &\left(\sum_{i=1}^{k} n_k A_{C_{p,i}} - 37.93\right) + \left(\sum_{i=1}^{k} n_k B_{C_{p,i}} + 0.210\right) T \\ &+ \left(\sum_{i=1}^{k} n_k C_{C_{p,i}} - 3.91 \times 10^{-4}\right) T^2 + \left(\sum_{i=1}^{k} n_k A_{D_{p,i}} + 2.06 \times 10^{-7}\right) T^3 \end{aligned} \tag{2.3.39}$$

$$\frac{C_p - C_p^0}{\mathrm{R}} = 1.586 + \frac{0.49}{1 - T_r} + A_f \left[4.2775 + \frac{6.3(1 - T_r)^{\frac{1}{3}}}{T_r} + \frac{0.4355}{1 - T_r}\right] \tag{2.3.40}$$

$$\begin{aligned} A_f = &\frac{(T_b - 43)(T_c - 43)}{(T_c - T_b)(0.7T_c - 43)} \log\left[\frac{p_c}{0.101325}\right] - \frac{(T_c - 43)}{(T_c - T_b)} \log\left[\frac{p_c}{0.101325}\right] + \\ &\log\left[\frac{p_c}{0.101325}\right] - 1 \end{aligned} \tag{2.3.41}$$

where A_f is the acentric factor and A_{C_p}, B_{C_p}, C_{C_p}, D_{C_p} are the group contribution parameters, R is the gas constant (8.314 J mol^{-1} K^{-1}), and p_c is the critical pressure, in this case Valderrama's critical pressure: [3, 67]

$$p_c = \frac{M}{\left(0.2573 + \sum_{j=1}^{k} n_j \Delta p_c\right)^2} \tag{2.3.42}$$

The group contribution coefficients re-optimization of models was performed in Microsoft Excel using the Solver add-in and generalized reduced gradient (GRG) nonlinear optimization method (minimization of AARD as set objective up to 10 consistent iterations with central derivatives, constraints precision of 10^{-6}, and convergence of 10^{-6}).

Ionanofluids

The thermal conductivity experimental data presented in this work were compared to values calculated based on the available models in the literature. [19, 68, 69] The very first model, derived by Maxwell (**1881**) from the definition of the effective thermal

conductivity of two-component mixture, λ_{eff}: [70]

$$\lambda_{eff} = \frac{\lambda_{NP}\varphi_{NP}\left(\frac{\partial T}{\partial x}\right)_{NP} + \lambda_{IL}\varphi_{IL}\left(\frac{\partial T}{\partial x}\right)_{IL}}{\varphi_{NP}\left(\frac{\partial T}{\partial x}\right)_{NP} + \varphi_{IL}\left(\frac{\partial T}{\partial x}\right)_{IL}} \tag{2.3.43}$$

where $(\partial T/\partial x)$ is overall average temperature gradient, φ is volume fraction, subscript *NP* and *IL* refer to nanoparticles and ILs, respectively. The volume fraction is defined as follows:

$$\varphi = \frac{V_{NP}}{V_{NP} + V_{IL}} = \frac{\frac{m_{NP}}{\rho_{NP}}}{\frac{m_{NP}}{\rho_{NP}} + \frac{m_{IL}}{\rho_{IL}}} = \frac{\frac{w_{m,NP}}{\rho_{NP}}}{\frac{w_{m,NP}}{\rho_{NP}} + \frac{1-w_{m,NP}}{\rho_{IL}}} \tag{2.3.44}$$

w_m is mass fraction (densities for nanomaterials were also characterized).

Application of the effective medium approximation of randomly dispersed, and uniformly sized spherical particles leads to:

$$\frac{\left(\frac{\partial T}{\partial x}\right)_{NP}}{\left(\frac{\partial T}{\partial x}\right)_{IL}} = \frac{\alpha\lambda_{NP}}{\lambda_{IL} + (\alpha - 1)\lambda_{NP}} \tag{2.3.45}$$

where α is a shape factor of the dispersed particles, (assumption: spherical particles, α = 3), which finally gives the following formulae:

$$\frac{\lambda_{Maxwell}}{\lambda_{IL}} = \frac{\lambda_{NP} + 2\lambda_{IL} + 2(\lambda_{NP} - \lambda_{IL})\varphi_{NP}}{\lambda_{NP} + 2\lambda_{IL} - (\lambda_{NP} - \lambda_{IL})\varphi_{NP}} \tag{2.3.46}$$

Further improvements were performed by Hamilton and Crosser (**1962**) where the shape factor, α, was not replaced with a set value of 3 (equal to sphericity), and different nanoparticles shapes were investigated. [71] Finally, the following formula was proposed:

$$\frac{\lambda_{Hamilton-Crosser}}{\lambda_{IL}} = \frac{\lambda_{NP} + (\alpha - 1)\lambda_{IL} - (\alpha - 1)(\lambda_{IL} - \lambda_{NP})\varphi_{NP}}{\lambda_{NP} + (\alpha - 1)\lambda_{IL} + (\lambda_{IL} - \lambda_{NP})\varphi_{NP}} \tag{2.3.47}$$

Another widely investigated and extended model of Tinga *et al.* (**1973**) [72] was developed by Leong *et al.* (**2006**) [73] and Murshed *et al.* (**2008**). [74] The final form of this model is divided into spherical- and cylindrical-shaped nanoparticles: [74]

$$\frac{\lambda_{TLM-Spherical}}{\lambda_{IL}} = \frac{\varphi_{NP}\phi(\lambda_{NP} - \phi\lambda_{IL})(2\Gamma_1^3 - \Gamma^3 + 1) + (\lambda_{NP} + 2\phi\lambda_{IL})2\Gamma_1^3(\varphi_{NP}\Gamma^3(\phi - 1) + 1)}{\Gamma_1^3(\lambda_{NP} + 2\phi\lambda_{IL}) - (\lambda_{NP} - \phi\lambda_{IL})\varphi_{NP}(\Gamma_1^3 - \Gamma^3 - 1)} \tag{2.3.48}$$

$$\frac{\lambda_{TLM-Cylindrical}}{\lambda_{IL}} = \frac{\varphi_{NP}\phi(\lambda_{NP}-\phi\lambda_{IL})(\Gamma_1^2-\Gamma^3+1)+(\lambda_{NP}+\phi\lambda_{IL})\Gamma_1^2(\varphi_{NP}\Gamma^2(\phi-1)+1)}{\Gamma_1^2(\lambda_{NP}+2\phi\lambda_{IL})-(\lambda_{NP}-\phi\lambda_{IL})\varphi_{NP}(\Gamma_1^2-\Gamma^3-1)} \tag{2.3.49}$$

where ϕ is the ratio of interfacial layer thermal conductivity, λ_{lr}, and IL thermal conductivity, λ_{IL}, $\lambda_{LR}/\lambda_{IL}$, Γ is the ratio of interfacial layer thickness, l, and particle diameter, r, defined as $\Gamma = 1 + l/r$ and $\Gamma_1 = 1 + l/2r$. The thickness and thermal conductivity of interfacial nanolayer are impossible to be measured experimentally, thus, some assumptions are necessary. Leong *et al.* (**2006**) showed that the predictions are the most reliable for ϕ equals to 2, and that the interfacial nanolayer equals to 1 nm. [73] Furthermore, Timofeeva *et al.* (**2007**) investigated the shape, size and motions of nanoparticles. [75] Finally, in a good agreement with the effective medium theory, the authors proposed the following formulae:

$$\frac{\lambda_{Timofeeva}}{\lambda_{IL}} = 1 + 3\varphi_{NP} \tag{2.3.50}$$

To the best of our knowledge, there is only one model developed for ionanofluids. Atashrouz *et al.* (**2015**) developed an equation based on the Maxwell model and modified geometric mean, with better correlative capability than Maxwell model (mean absolute relative deviation of below 5.7%) in case of ionic liquid-based nanofluid: [76]

$$\frac{\lambda_{Atashrouz}}{\lambda_{IL}} = \left(\frac{\lambda_{NP}}{\lambda_{IL}}\right)^{\varphi_{NP}} \tag{2.3.51}$$

Undoubtedly there are more models available for such systems with molecular solvents, however, those discussed herein are the most recognized with a solid elementary description, and widely studied for several different systems. Also, many reviews have been published. [77–82] The limitation is made by the thermal conductivity of nanoparticles. To perform the modelling as a function of temperature, the thermal conductivity of nanoparticles is required at elevated temperature. However, this type of study is very rare, and only performed at low temperatures, to date. [83–85]

The density of ionanofluids was calculated with the following additivity formulae:

$$\rho_{INF} = \rho_{IL}w_{IL} + \rho_{NP}w_{NP} = \rho_{IL}(1 - w_{NP}) + \rho_{NP}w_{NP} \tag{2.3.52}$$

Statistical Analysis

To check how reliable the predicted values are, the relative deviation (RD) and average absolute relative deviation (AARD) were calculated as follows:

$$RD = \frac{100(x_{calc,i} - x_{exp,i})}{x_{exp,i}} \tag{2.3.53}$$

$$AARD = \frac{100}{k} \sum_{i=1}^{n} \left| \frac{x_{calc,i} - x_{exp,i}}{x_{exp,i}} \right| \tag{2.3.54}$$

where k is the total number of data points, $x_{calc,i}$ and $x_{exp,i}$ are the calculated and experimental data points, respectively.

The errors of thermal conductivity enhancement were assessed based on the neglected covariance (as the values of thermal conductivity and those errors are similar and relatively small), therefore, the errors do not propagate excessive numerical artefacts:

$$\delta\varepsilon = \sqrt{\left(\frac{\partial\varepsilon}{\partial\lambda_{INF}}\right)^2 (\delta\lambda_{INF})^2 + \left(\frac{\partial\varepsilon}{\partial\lambda_{IL}}\right)^2 (\delta\lambda_{IL})^2} \tag{2.3.55}$$

where ε is the absolute enhancement of the property, x_{INF}/x_{IL}.

To determine the errors of isobaric heat capacity, density and viscosity enhancements, ε, the chain rules of differentiation can be used:

$$\delta\varepsilon = \left|\frac{\partial\varepsilon}{\partial x_{INF}}\right| \delta x_{INF} + \left|\frac{\partial\varepsilon}{\partial x_{IL}}\right| \delta x_{IL} \tag{2.3.56}$$

2.3.3 Economic Analysis

The procedure to assess the transport coefficient of the fluids involved in heat transfer process was primarily described by Mendonca *et al.* (**1981**). [86] The authors made some assumptions to simplify the calculation by degree of freedom reduction. In the first instance, it is reduced to two by selecting a specific type of device (usually shell and tube type), prescribing the external constraints and neglecting the pressure drop across the fluid ducts as it does not affect the performance. Then the only factor which has the influence is heat transfer area expressed by Newton′s law of cooling:

$$Q = U_0 A_0 (\Delta T)_{lm} \tag{2.3.57}$$

where Q is rate of heat transfer (Q = 1 MW), U_0 is overall heat transfer coefficient, A_0 is heat transfer area, and $(\Delta T)_{lm}$ is logarithmic mean temperature difference between inlet and outlet stream temperatures $(\Delta T)_{lm}$ = 20 K. In case of circular tubes, U_0 can be calculated by the following equation:

$$U_0^{-1} = \frac{D_o}{h_i D_i} + h_o^{-1} + r_w + r_o + \frac{r_i D_o}{D_i} \tag{2.3.58}$$

where D_o is outside tube diameter (D_o = 0.020 m), h_i is heat transfer coefficient for the inside film of fluid, D_i is inside tube diameter (D_i = 0.018 m), h_o is heat transfer coefficient for the outside film of fluid (h_o = 2000 W m^{-2} K^{-1}), r_w is thermal resistance of the tube wall, r_o is outside fouling resistance, r_i is inside fouling resistance. This can be also simplified into the following form:

$$U_0^{-1} = \frac{D_o}{h_i D_i} + h_o^{-1} + R \tag{2.3.59}$$

where R stands for all the factors related to the resistance (R = 0 as ideal flow). The major assumption in this methodology is the turbulent flow required for the efficient and accurate optimization. The most recognized correlation for the heat transfer coefficients for smooth circular tube was proposed by Sieder and Tate: [87]

$$Nu = \frac{h_i D_i}{\lambda} = 0.027 Re^{0.8} Pr^{\frac{1}{3}} \left(\frac{\eta}{\eta_w}\right)^{0.14} \tag{2.3.60}$$

where Nu is Nusselt number, λ is thermal conductivity coefficient, η is dynamic viscosity, η_w is dynamic viscosity at the wall temperature (assumption: $\eta_w = \eta$), Re is Reynolds number, Pr is Prandtl number. Pr can be calculated by the following equation:

$$Pr = \frac{c_p \eta}{\lambda} \tag{2.3.61}$$

where c_p is the specific isobaric heat capacity. Whereas the Reynolds number can be determined as follows:

$$Re = \frac{\rho u D_i}{\eta} \tag{2.3.62}$$

where ρ is density, u is mean velocity over the tube cross section (u = 0.5 m s^{-1}).

França *et al.* (**2009**) proposed an efficient way to study the cost of a new design which was divided into five parts, namely battery limits, utility, off-site, engineering fees and working capital. [88] The main concern is on the battery limits investment, which is

related to the cost of individual parts of the equipment, along with the installation. This cost, C_E, is a function of the size (as heat transfer area), material of the construction, design pressure, temperature:

$$C_E = C_B \left(\frac{X}{X_B} \right)^m \tag{2.3.63}$$

where C_B is the cost of a reference equipment, X capacity of the equipment (in this case heat transfer area, A_0), X_B capacity of the reference equipment (heat transfer area of reference) and m is a constant depending on the equipment type ($m = 0.68$). Following the work of França *et al.* (**2009**), the reference equipment is carbon steel shell and tube heat exchanger with the reference heat transfer area of 80 m^2 and cost of (3.28×10^4) US$. When the factors of materials type, pressure and temperature are included in equation 2.3.63), the following equation is obtained:

$$C_E = C_B^{'} \left(\frac{X}{X_B} \right)^m f_M f_p f_T \tag{2.3.64}$$

where C_B' is the cost of the above described reference equipment (C_B' = 3.28×10^4 US$), f_M is the correction factor for materials type ($f_M = 3.4$), f_P is the correction factor for pressure ($f_P = 1.5$), and f_T is the correction factor for temperature ($f_T = 1.3$). Finally, the equation for the cost of the heat exchange unit is derived as follows:

$$C_E = 3.28 \times 10^4 \left(\frac{A_0}{80} \right)^{0.68} \times 3.4 \times 1.5 \times 1.3 = 2.18 \times 10^5 \left(\frac{A_0}{80} \right)^{0.68} \tag{2.3.65}$$

Nevertheless, the short description of this approach is described herein, the full explanation can be found in the literature. [86, 88–90]

Bibliography

[1] W. E. McEwen, G. Axelrad, M. Zanger, and C. A. VanderWerf, *Journal of the American Chemical Society* **87**, 3948 (1965).

[2] J. D. Holbrey, K. R. Seddon, and R. Wareing, *Green Chemistry* **3**, 33 (2001).

[3] R. Ge, C. Hardacre, J. Jacquemin, P. Nancarrow, and D. W. Rooney, *Journal of Chemical & Engineering Data* **53**, 2148 (2008).

[4] A. K. Burrell, R. E. Del Sesto, S. N. Baker, T. M. McCleskey, and G. A. Baker, *Green Chemistry* **9**, 449 (2007).

[5] M. J. Earle, C. M. Gordon, N. V. Plechkova, K. R. Seddon, and T. Welton, *Analytical Chemistry* **79**, 758 (2007).

[6] J. D. Holbrey, W. M. Reichert, R. P. Swatloski, G. A. Broker, W. R. Pitner, K. R. Seddon, and R. D. Rogers, *Green Chemistry* **4**, 407 (2002).

[7] L. S. P. De Gelder, *Handbook of Water Analysis*, CRC Press Taylor & Francis Group, Boca Raton, Florida, USA, 2013.

[8] W. L. Hough and M. Smiglak, *New Journal of Chemistry* **31**, 1429 (2007).

[9] K. Shimojo and M. Goto, *Analytical Chemistry* **76**, 5039 (2004).

[10] H. Kurt and M. Kayfeci, *Applied Energy* **86**, 2244 (2009).

[11] A. R. Challoner and R. W. Powell, *Proceedings of the Royal Society of London A* **238**, 90 (1956).

[12] R. W. Powell, *Journal of Scientific Instruments* **34**, 485 (1957).

[13] W. Jiang, G. Ding, and H. Peng, *International Journal of Thermal Sciences* **48**, 1108 (2009).

[14] W. Czarnetzki and W. Roetzel, *International Journal of Thermophysics* **16**, 413 (1995).

[15] D. G. Cahill, *Review of Scientific Instruments* **61**, 802 (1990).

[16] J. K. Horrocks and E. McLaughlin, *Proceedings of the Royal Society of London A* **273**, 259 (1963).

[17] J. J. Healy, J. J. De Groot, and J. Kestin, *Physica B + C* **82**, 392 (1976).

[18] H. Watanabe, *Metrologia* **39**, 65 (2002).

[19] J. M. P. França, S. I. C. Vieira, M. J. V. Lourenço, S. M. S. Murshed, and C. A. Nieto de Castro, *Journal of Chemical & Engineering Data* **58**, 467 (2013).

[20] A. Ghadimi and I. H. Metselaar, *Experimental Thermal and Fluid Science* **51**, 1 (2013).

[21] L. Riedel, *Chemie Ingenieur Technik* **23**, 465 (1951).

[22] M. L. V. Ramires, C. A. Nieto de Castro, Y. Nagasaka, A. Nagashima, M. J. Assael, and W. A. Wakeham, *Journal of Physical and Chemical Reference Data* **24**, 1377 (1995).

[23] M. L. V. Ramires, C. A. N. Decastro, J. M. N. A. Fareleira, and W. A. Wakeham, *Journal of Chemical and Engineering Data* **39**, 186 (1994).

[24] M. L. V. Ramires, C. A. Nieto de Castro, R. A. Perkins, Y. Nagasaka, A. Nagashima, M. J. Assael, and W. A. Wakeham, *Journal of Physical and Chemical Reference Data* **29**, 133 (2000).

[25] R. Ge, C. Hardacre, P. Nancarrow, and D. W. Rooney, *Journal of Chemical & Engineering Data* **52**, 1819 (2007).

[26] M. E. BROWN, *Introduction to Thermal Analysis: Techniques and Application*, Kluwer Academic Publishers, Dordrecht, Netherlands, 2001.

[27] G. HÖHNE, W. HEMMINGER, and H. J. FLAMMERSHEIM, *Differential Scanning Calorimetry: An Introduction for Practitioners*, Springer-Verlag, Berlin, Germany, 1996.

[28] S. P. CHOW and G. L. HARDING, *Solar Energy Materials* **11**, 123 (1984).

[29] M. J. VOLD, *Analytical Chemistry* **21**, 683 (1949).

[30] R. CHEN and S. W. S. MCKEEVER, *Theory of Thermoluminescence and Related Phenomena*, World Scientific, Singapore, 1997.

[31] M. TAKAHASHI, *Thermophotometric Phase Shifter and Method for Fabricating the Same*, US Patent US7333679B2 2008-02-19, 2008.

[32] T. SAKAI, S. WATANABE, and S. YAMAMOTO, *Analytical Chemistry* **69**, 1766 (1997).

[33] B. B. VILENCHITS, V. K. POPOV, and D. S. UMREIKO, *Journal of Engineering Physics and Thermophysics* **51**, 979 (1986).

[34] M. MARCHETTI, M. FOIS, L. IBOS, J. DUMOULIN, P. BOURSON, and J.-M. PIAU, *Applied Thermal Engineering* **130**, 49 (2018).

[35] H. C. WRIGHT and G. A. ALLEN, *British Journal of Applied Physics* **17**, 1181 (1966).

[36] W. H. M. CRAANE-VAN HINSBERG, J. C. VERHOEF, H. E. JUNGINGER, and H. E. BODDE, *Thermochimica Acta* **248**, 303 (1995).

[37] U. SCHNEIDER, P. LUNKENHEIMER, R. BRAND, and A. LOIDL, *Physical Review E* **59**, 6924 (1999).

[38] J. H. FLYNN and L. A. WALL, *Journal of Research of the National Bureau of Standards* **70**, 487 (1966).

[39] T. YAZAKI and A. TOMINAGA, *Proceedings of the Royal Society of London A: Mathematical, Physical and Engineering Sciences* **454**, 2113 (1998).

[40] Y. MAEDA and M. TAKAHASHI, *Journal of Applied Physics* **68**, 4751 (1990).

[41] G.-H. SHI, *Engineering Computations* **9**, 157 (1992).

[42] K. P. MENARD, *Dynamic Mechanical Analysis: A Practical Introduction*, CRC Press Taylor & Francis Group, Boca Raton, Florida, USA, 2008.

[43] A. HAMMICHE, D. M. PRICE, E. DUPAS, G. MILLS, A. KULIK, M. READING, J. M. R. WEAVER, and H. M. POLLOCK, *Journal of Microscopy* **199**, 180 (2000).

[44] N. BEKKEDAHL, *Journal of Research of the National Bureau of Standards* **43**, 145 (1949).

[45] C. MATON, N. DE VOS, and C. V. STEVENS, *Chemical Society Reviews* **42**, 5963 (2013).

[46] H. L. NGO, K. LECOMPTE, L. HARGENS, and A. B. MCEWEN, *Thermochimica Acta* **357**, 97 (2000).

[47] J. G. HUDDLESTON, A. E. VISSER, W. M. REICHERT, H. D. WILLAUER, G. A. BROKER, and R. D. ROGERS, *Green Chemistry* **3**, 156 (2001).

[48] N. G. POLIKHRONIDI, R. G. BATYROVA, I. M. ABDULAGATOV, J. W. MAGEE, and J. T. WU, *Physics and Chemistry of Liquids* **52**, 657 (2014).

[49] M. E. VAN VALKENBURG, R. L. VAUGHN, M. WILLIAMS, and J. S. WILKES, *Thermochimica Acta* **425**, 181 (2005).

[50] J. M. CROSTHWAITE, M. J. MULDOON, J. K. DIXON, J. L. ANDERSON, and J. F. BRENNECKE, *The Journal of Chemical Thermodynamics* **37**, 559 (2005).

[51] S. J. ASHCROFT, D. R. BOOKER, and J. C. R. TURNER, *Journal of the Chemical Society, Faraday Transactions* **86**, 145 (1990).

[52] R. S. VAJJHA, D. K. DAS, and B. M. MAHAGAONKAR, *Petroleum Science and Technology* **27**, 612 (2009).

[53] C. SCHREINER, S. ZUGMANN, R. HARTL, and H. J. GORES, *Journal of Chemical & Engineering Data* **55**, 1784 (2009).

[54] D. SHOLL and J. A. STECKEL, *Density Functional Theory: A Practical Introduction*, John Wiley & Sons, New York City, New York, USA, 2011.

[55] W. KOCH and M. C. HOLTHAUSEN, *A Chemist's Guide to Density Functional Theory*, John Wiley & Sons, New York City, New York, USA, 2015.

[56] F. GIUSTINO, *Materials Modelling Using Density Functional Theory: Properties and Predictions*, Oxford University Press, Oxford, The United Kingdom, 2014.

[57] L. TIMPERMAN, F. BÉGUIN, E. FRACKOWIAK, and M. ANOUTI, *Journal of The Electrochemical Society* **161**, A228 (2014).

[58] N. A. MANAN, C. HARDACRE, J. JACQUEMIN, D. W. ROONEY, and T. G. YOUNGS, *Journal of Chemical & Engineering Data* **54**, 2005 (2009).

[59] B. GORSKA, L. TIMPERMAN, M. ANOUTI, J. PERNAK, and F. BÉGUIN, *RSC Advances* **6**, 55144 (2016).

[60] M. DIEDENHOFEN, A. KLAMT, K. MARSH, and A. SCHÄFER, *Physical Chemistry Chemical Physics* **9**, 4653 (2007).

[61] C. WANG, H. LUO, D. JIANG, H. LI, and S. DAI, *Angewandte Chemie International Edition* **49**, 5978 (2010).

[62] S. ZAHN, D. R. MACFARLANE, and E. I. IZGORODINA, *Physical Chemistry Chemical Physics* **15**, 13664 (2013).

[63] K.-J. WU, C.-X. ZHAO, and C.-H. HE, *Fluid Phase Equilibria* **339**, 10 (2013).

[64] J. O. VALDERRAMA, L. A. FORERO, and R. E. ROJAS, *Industrial & Engineering Chemistry Research* **51**, 7838 (2012).

[65] J. O. VALDERRAMA, L. A. FORERO, and R. E. ROJAS, *Industrial & Engineering Chemistry Research* **54**, 3480 (2015).

[66] J. O. VALDERRAMA and P. A. ROBLES, *Industrial & Engineering Chemistry Research* **46**, 1338 (2007).

[67] P. NANCARROW, M. LEWIS, and L. ABOUCHACRA, *Chemical Engineering & Technology* **38**, 632 (2015).

[68] J. M. P. FRANÇA, F. REIS, S. I. C. VIEIRA, M. J. V. LOURENÇO, F. J. V. SANTOS, C. A. N. DE CASTRO, and A. A. H. PADUA, *The Journal of Chemical Thermodynamics* **79**, 248 (2014).

[69] C. A. NIETO DE CASTRO, M. J. V. LOURENÇO, A. P. C. RIBEIRO, E. LANGA, S. I. C. VIEIRA, P. GOODRICH, and C. HARDACRE, *Journal of Chemical & Engineering Data* **55**, 653 (2009).

[70] J. C. MAXWELL, *A Treatise on Electricity and Magnetism*, Clarendon Press, Wotton-Under-Edge, The United Kingdom, 1881.

[71] R. L. HAMILTON and O. K. CROSSER, *Industrial & Engineering Chemistry Fundamentals* **1**, 187 (1962).

[72] W. R. TINGA, W. A. G. VOSS, and D. F. BLOSSEY, *Journal of Applied Physics* **44**, 3897 (1973).

[73] K. C. LEONG, C. YANG, and S. M. S. MURSHED, *Journal of Nanoparticle Research* **8**, 245 (2006).

[74] S. M. S. MURSHED, K. C. LEONG, and C. YANG, *International Journal of Thermal Sciences* **47**, 560 (2008).

[75] E. V. TIMOFEEVA, A. N. GAVRILOV, J. M. MCCLOSKEY, Y. V. TOLMACHEV, S. SPRUNT, L. M. LOPATINA, and J. V. SELINGER, *Physical Review E* **76**, 61203 (2007).

[76] S. ATASHROUZ, M. MOZAFFARIAN, and G. PAZUKI, *Industrial & Engineering Chemistry Research* **54**, 8600 (2015).

[77] W. YU, D. M. FRANCE, J. L. ROUTBORT, and S. U. S. CHOI, *Heat Transfer Engineering* **29**, 432 (2008).

[78] S. KAKAÇ and A. PRAMUANJAROENKIJ, *International Journal of Heat and Mass Transfer* **52**, 3187 (2009).

[79] S. ÖZERINÇ, S. KAKAÇ, and A. G. YAZICIOĞLU, *Microfluidics and Nanofluidics* **8**, 145 (2010).

[80] X.-Q. WANG and A. S. MUJUMDAR, *International Journal of Thermal Sciences* **46**, 1 (2007).

[81] V. TRISAKSRI and S. WONGWISES, *Renewable and Sustainable Energy Reviews* **11**, 512 (2007).

[82] J. FAN and L. WANG, *Journal of Heat Transfer* **133**, 40801 (2011).

[83] R. TAYLOR, *Philosophical Magazine* **13**, 157 (1966).

[84] E. K. SICHEL, R. E. MILLER, M. S. ABRAHAMS, and C. J. BUIOCCHI, *Physical Review B* **13**, 4607 (1976).

[85] P. KIM, L. SHI, A. MAJUMDAR, and P. L. MCEUEN, *Physica B: Condensed Matter* **323**, 67 (2002).

[86] A. J. F. MENDONCA, C. A. NIETO DE CASTRO, M. J. ASSAEL, and W. A. WAKEHAM, *Revista Portuguesa de Química* **23**, 7 (1981).

[87] E. N. SIEDER and G. E. TATE, *Industrial & Engineering Chemistry* **28**, 1429 (1936).

[88] J. M. P. FRANÇA, C. A. NIETO DE CASTRO, M. M. LOPES, and V. M. B. NUNES, *Journal of Chemical & Engineering Data* **54**, 2569 (2009).

[89] V. M. B. NUNES, M. J. V. LOURENÇO, F. J. V. SANTOS, and C. A. NIETO DE CASTRO, *Journal of Chemical & Engineering Data* **48**, 446 (2003).

[90] S. APARICIO, M. ATILHAN, and F. KARADAS, *Industrial & Engineering Chemistry Research* **49**, 9580 (2010).

Chapter 3

Imidazolium- and Pyrrolidinium-Based Ionic Liquids and Ionanofluids

3.1 Pure Ionic Liquids

3.1.1 Density and Isobaric Heat Capacity

The density and heat capacity were measured for pure ILs and the purity before and after each measurement was studied, in particular the water content which may increase during/after the data collection. Thus, the water content after heat capacity assessments was checked by weighing the mass of the pan, and directly by using Karl Fischer titration after density measurement. No changes were recorded which means that the pans containing studied samples were sealed from the environment and water absorption. It was previously reported that water may influence the physical properties. [1] In the case of heat capacity, 1% of water shifts the heat capacity by about 1.6% (1-butyl-3-methylimidazolium tetrafluoroborate). [2] Nevertheless, density is much less dependent on the water content – 20% of water content changes the density of 1-butyl-3-methylimidazolium bis(trifluoromethylsulfonyl)imide for about 1%. [3]

The experimental data for the density and the heat capacity of the pure ILs are shown in **Figure 3.1.1a** and **Figure 3.1.2a**, respectively, and collected in **Tables CD3.1-CD3.9** (Appendix CD3). Their values were also compared to those previously reported in the literature. An extensive comparison to NIST ILs database was performed by taking into account all available literature positions, the relative deviations are presented in **Figure 3.1.1b** and **Figure 3.1.2b** for pure IL density and heat capacity, respectively.

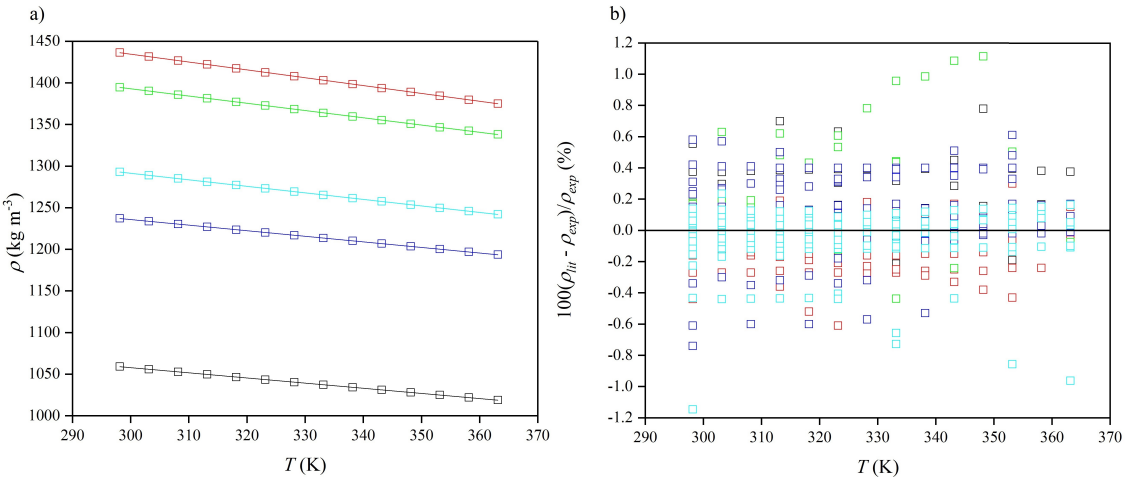

Figure 3.1.1. a) Density, ρ, as a function of the temperature, T, for pure ILs; **b)** density deviations, $100(\rho_{lit} - \rho_{exp})/\rho_{exp}$, between values in this work, ρ_{exp}, and literature data, ρ_{lit}, for $[C_4C_1Im][Dca]$, □ [4–25], $[C_4C_1Im][NTf_2]$, □ [3, 6, 17, 20, 23, 26–80], $[C_2C_1Im][C_2SO_4]$, □ [3, 6, 20, 43, 43, 44, 48, 52, 56, 71, 81–126], $[C_4C_1Pyrr][NTf_2]$, □ [6, 9, 47, 55, 66, 92, 127–144], $[C_6C_1Im][PF_6]$, □ [34, 39, 41, 52, 145–166].

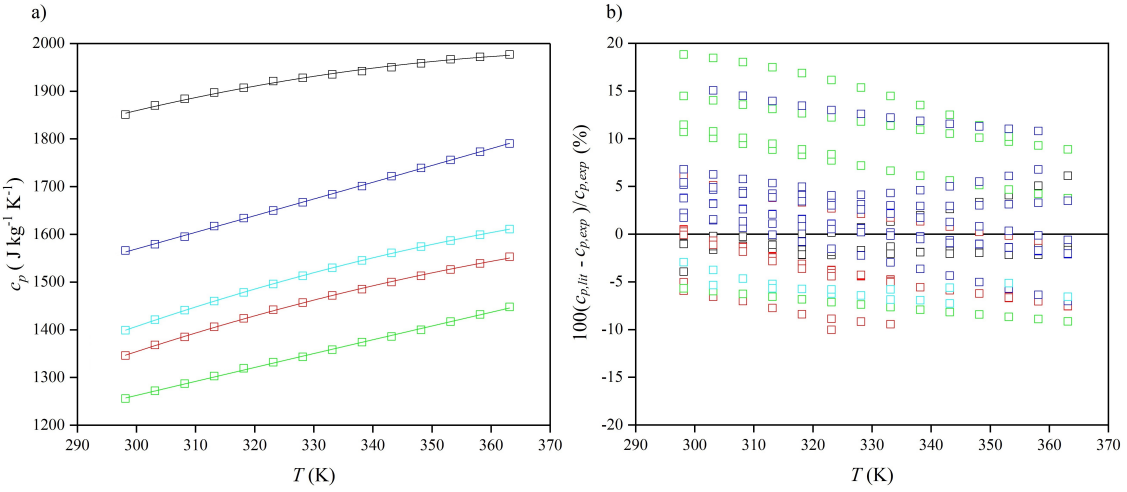

Figure 3.1.2. a) Isobaric heat capacity, c_p, as a function of the temperature, T, for pure ILs; **b)** isobaric heat capacity deviations, $100(c_{p,lit} - c_{p,exp})/c_{p,exp}$, between values in this work, $c_{p,exp}$, and literature data, $c_{p,lit}$, for $[C_4C_1Im][Dca]$, □ [2, 20, 23, 24, 167, 168], $[C_4C_1Im][NTf_2]$, □ [20, 23, 38, 67, 146, 169–175], $[C_2C_1Im][C_2SO_4]$, □ [2, 20, 89, 93, 146, 176–180], $[C_4C_1Pyrr][NTf_2]$, □ [2, 146, 173, 181, 182], $[C_6C_1Im][PF_6]$, □ [158, 175].

As can be seen, the density is a very extensively investigated property of ILs. The deviations observed were approximately (-1.2 – 1.2) % while the main concentration

of them is between (-0.2 – 0.2) % as it could be expected regarding solely the standard uncertainty of each equipment used, with maximum of -1.15%. [145] In the case of heat capacity, the deviations were about (-10 – 20) %, with maximum of 19.06%. [146] Whereas the standard uncertainty of density measurement is 0.1% and heat capacity of 3%. Such high deviations may be related to different impurity levels and measurement methodology (technique, heating rate, gas flow rate, crucibles used, samples preparation and treatment, calibration). Moreover, such deviations (1% and 20% for density and heat capacity, respectively, or even 40% for heat capacity) are commonly observed in the literature for ILs. [2, 26] Diedrichs and Gmehling (**2006**) critically reviewed the heat capacity measurement approaches, including different techniques and parameters. [183] To the best of our knowledge, and following the above and others' recommendations, the heat capacity values determined in this work are highly accurate. [2, 146, 183, 184] The deviations of pure ILs properties can be observed, nevertheless.

Four different cations, $[C_4C_1Im]^+$, $[C_4C_1Pyrr]^+$, $[C_2C_1Im]^+$, $[C_6C_1Im]^+$, and four different anions, $[Dca]^-$, $[NTf_2]^-$, $[C_2SO_4]^-$, $[PF_6]^-$, were used as the constituents of the investigated ILs. Zhao *et al.* (**2016**) calculated the volume of several cations and anions by COSMO-RS modelling – 154 Å^3 for $[C_2C_1Im]^+$, 197 Å^3 for $[C_4C_1Im]^+$, 242 Å^3 for $[C_6C_1Im]^+$, 214 Å^3 for $[C_4C_1Pyrr]^+$, 222 Å^3 for $[NTf_2]^-$, 104 Å^3 for $[PF_6]^-$, 82 Å^3 for $[Dca]^-$ and 104 Å^3 for $[C_1SO_4]^-$ (value for $[C_2SO_4]^-$ was not reported, therein). [185] This given, the volume of cation + anion is in the following order: $[C_2C_1Im][C_1SO_4]$ (258 Å^3) < $[C_4C_1Im][Dca]$ (279 Å^3) < $[C_6C_1Im][PF_6]$ (346 Å^3) < $[C_4C_1Im][NTf_2]$ (419 Å^3) < $[C_4C_1Pyrr][NTf_2]$ (436 Å^3). As can be seen in **Figure 3.1.1a** and **Figure 3.1.2a** for density and heat capacity, respectively, the values of those properties clearly depend on the type of cation/anion. More specifically, increasing the size of anion and cation results in lower density (less number of bulky molecules in a volume unit, however, the density is a combination of cation and anion instead of them treated separately), and higher specific heat capacity (as an effect of molecules energy represented by bonds). Moreover, the density is decreasing with temperature, (3.8, 4.3, 4.1, 3.5 and 3.9) % of decrease between 298.15 K and 363.15 K for $[C_4C_1Im][Dca]$, $[C_4C_1Im][NTf_2]$, $[C_4C_1Pyrr][NTf_2]$, $[C_2C_1Im][C_2SO_4]$ and $[C_6C_1Im][PF_6]$, respectively, whereas the heat capacity is increasing with temperature, (6.8, 15.4, 15.3, 14.3 and 15.2) % of increase between 298.15 K and 363.15 K for $[C_4C_1Im][Dca]$, $[C_4C_1Im][NTf_2]$, $[C_4C_1Pyrr][NTf_2]$, $[C_2C_1Im][C_2SO_4]$ and

$[C_6C_1Im][PF_6]$, respectively.

3.1.2 Thermal Conductivity

The thermal conductivity was measured in the temperature range of about (278 – 358) K, at atmospheric pressure (101 kPa), for pure ILs, in the first instance, and compared to literature data, as shown in **Figure 3.1.3**. The experimental data were collected in **Tables CD3.10-CD3.12** (Appendix CD3).

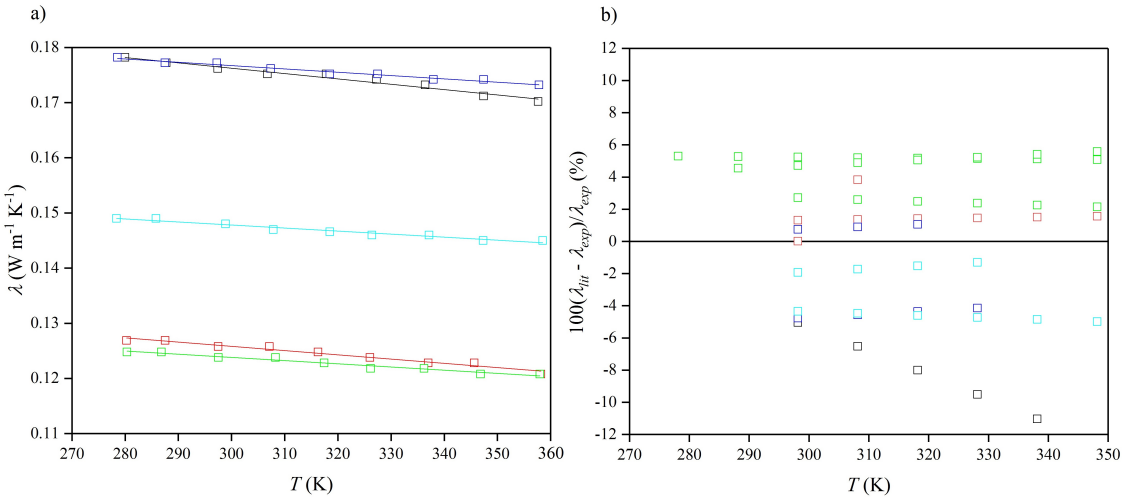

Figure 3.1.3. a) Thermal conductivity, λ, as a function of the temperature, T, for pure ionic liquids; **b)** relative deviations, $100(\lambda_{lit} - \lambda_{exp})/\lambda_{exp}$, between values reported in this work, λ_{exp}, and those in the literature, λ_{lit}, for $[C_4C_1Im][Dca]$, □ [4], $[C_4C_1Im][NTf_2]$, □ [186, 187], $[C_2C_1Im][C_2SO_4]$, □ [186, 188, 189], $[C_4C_1Pyrr][NTf_2]$, □ [186, 190], $[C_6C_1Im][PF_6]$, □ [190, 191].

Thermal conductivity, as a transport property, should be dependent on the volume/mass of molecules. As shown in **Figure 3.1.3a**, this follows the order of $[C_2C_1Im][C_1SO_4]$ (258 Å^3) < $[C_4C_1Im][Dca]$ (279 Å^3) < $[C_6C_1Im][PF_6]$ (346 Å^3) < $[C_4C_1Im][NTf_2]$ (419 Å^3) < $[C_4C_1Pyrr][NTf_2]$ (436 Å^3). Therefore, the thermal conductivity could be easily predicted qualitatively based purely on the size of cation/anion.

The thermal conductivity was found to decrease with temperature, as expected. Moreover, the slope for each IL is similar which means that the thermal conductivity is

governed by the same mechanism with a reduced contribution of convection. The difference between lowest and highest temperature is relatively small, (4.70, 5.05, 2.89, 3.31 and 2.76) % for $[C_4C_1Im][Dca]$, $[C_4C_1Im][NTf_2]$, $[C_2C_1Im][C_2SO_4]$, $[C_4C_1Pyrr][NTf_2]$ and $[C_6C_1Im][PF_6]$, respectively.

Differences of about (-12 - 6) % can be found between values in this work and those reported in the literature, while the maximum for $[C_2C_1Im][C_2SO_4]$ (5.33% between 0.1742 W m^{-1} K^{-1} in this work and 0.184 W m^{-1} K^{-1} in [189], at 348.15 K), and $[C_4C_1Im][Dca]$ (-11.74% between 0.1725 W m^{-1} K^{-1} in this work and 0.153 W m^{-1} K^{-1} in [4], at 338.15 K). All deviations with literature data for pure ILs are presented in **Figure 3.1.3b**, [4, 186–190, 192, 193] while selected positions were taken for further discussion (the same references as those used for the comparison of ionanofluids results). [4, 190, 193]

The standard uncertainties of measurements in the literature are (7.1, 6.5, 6.4, 4.2 and 3.5) % for $[C_4C_1Im][NTf_2]$, [193] $[C_4C_1Im][Dca]$, [4] $[C_2C_1Im][C_2SO_4]$, [193] $[C_4C_1Pyrr][NTf_2]$, [190] and $[C_6C_1Im][PF_6]$, [190] respectively. Calibration of the equipment used for thermal conductivity measurement is a significant process because it is possible to introduce a range of factors which results in an increase of the uncertainty in this property, for example viscosity (different liquids of various viscosity values should be used, *i.e.* toluene, water, glycerol and its water solutions), electrical conductivity (this factor can be included by using water solutions of sodium chloride or ILs), thermal conductivity (to ensure the proper calibration along the whole range of thermal conductivity measurement, *i.e.* toluene, glycerol, water), and temperature (in order to ensure that the calibration is reliable over the whole range of temperatures investigated). [4, 193–195] All of these factors were included in the calibration of the equipment in this work. Moreover, the calibration was also validated with one IL, $[C_8C_1Im][NTf_2]$, and the values obtained are in an excellent agreement with literature (average absolute relative deviation below 1%), [186] as presented and disccused in Section 2.2.1. This issue can be addressed to work of Nieto de Castro *et al.* (**2009**) where only water and glycerol were used to perform the calibration. [190] Also, as can be seen, the data for $[C_4C_1Pyrr][NTf_2]$ and $[C_6C_1Im][PF_6]$ originated from work of Nieto de Castro *et al.* (**2009**) are consistently deviated which explains the excessive deviations from the results in this work, (0.118 and 0.1238) W m^{-1} K^{-1} or relative deviation of 4.9% for $[C_4C_1Pyrr][NTf_2]$ at 298.15 K, (0.142 and 0.1480) W m^{-1} K^{-1} or relative deviation of 4.2% for $[C_6C_1Im][PF_6]$ at

298.15 K. Moreover, to ensure the proper heat transfer occurring in the investigated system, a minimum volume of the sample is required (depending on the construction of cell, minimum of 30 cm^3). [4] While in work of Nieto de Castro *et al.* (**2009**) the volume of sample is approximately 15 cm^3. [190] Unlike other properties, such as heat capacity or viscosity, water has less impact on thermal conductivity – those with 800 ppm of water in ILs do not differ significantly in comparison to those with 400 ppm of water in ILs. [196] Therefore, this is not an issue of consideration herein due to very low amounts of water in each literature position and this work.

Another significant deviation can be found for $[C_4C_1Im][Dca]$ (up to -11.03% of relative deviation, 0.1725 W m^{-1} K^{-1} in this work and 0.153 W m^{-1} K^{-1} in [4], at 338.15 K), however, in the work of França *et al.* (**2014**), the proper calibration was presented, along with high purity chemicals. [4] França *et al.* (**2014**) compared their results of 1-ethyl-3-methylimidazolium dicyanamide with literature and reported relative deviation of (10 – 15) %, [188] increasing with temperature. [4] Similar relative deviations can be found between this work and França *et al.* (**2014**). [4] It might appear as some systematic error being propagated in the work of França *et al.* (**2014**), [4] whereas the data in this work represent better accuracy. However, the origin of such deviations is unknown, and the value of the error starts to be higher than the standard uncertainty above approximately 318 K.

3.2 Ionanofluids

3.2.1 Density

The density of ionanofluids containing different loadings of carbon nanotubes, boron nitride or graphite nanoparticles dispersed in selected ILs, was measured as a function of temperature. The results are shown in **Figure 3.2.1a**, **Figure 3.2.1b** and **Figure 3.2.1c** for ionanofluids with carbon nanotubes, boron nitride and graphite, respectively. The parameters of equation (2.2.42), $\rho(T)$, are summarized in **Table 3.2.1**.

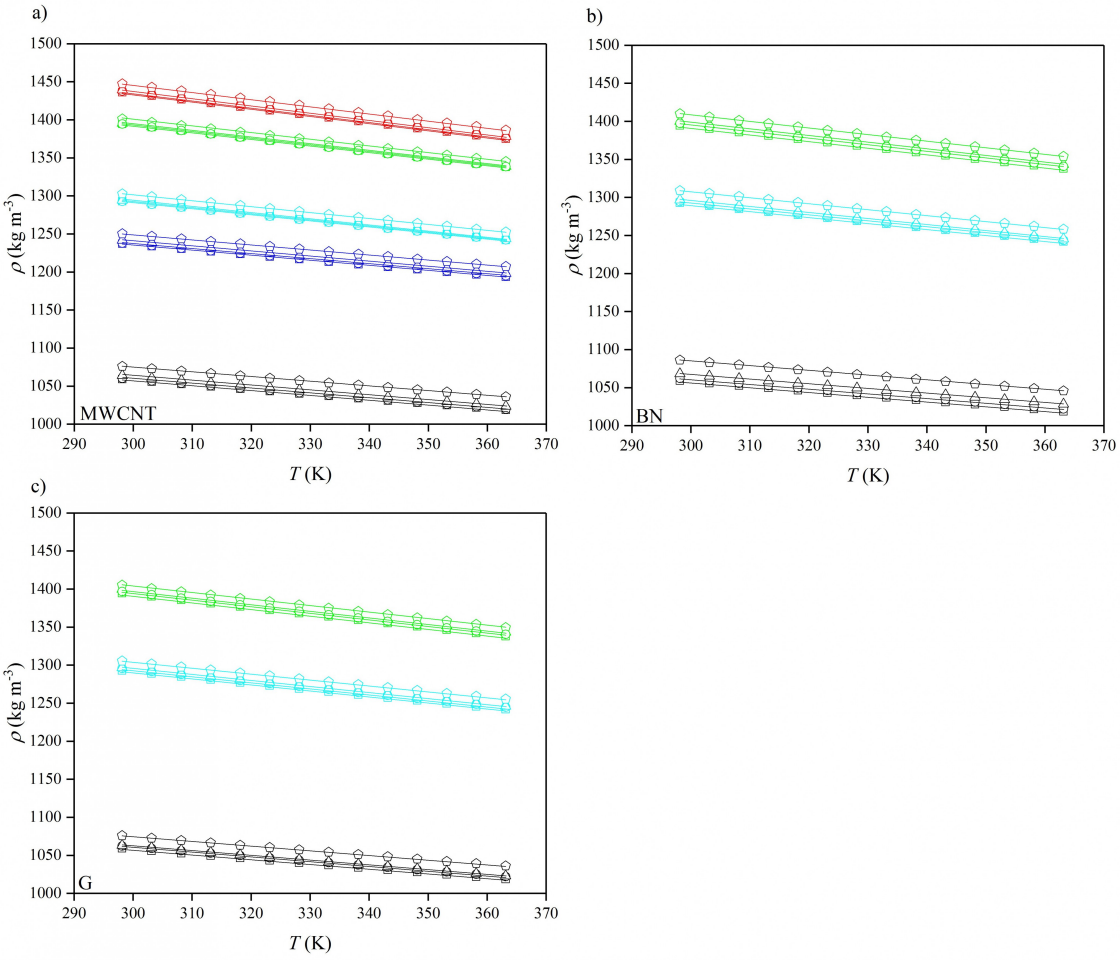

Figure 3.2.1. Temperature, T, dependence of the density, ρ, of investigated ionanofluids with **a)** multiwalled carbon nanotubes (MWCNT); **b)** boron nitride (BN); **c)** graphite (G), for neat ILs, squares □, 0.5 wt% NP, circles ○, 1.0 wt% NP, triangles △, 3.0 wt% NP, pentagons ⬠, $[C_4C_1Im][Dca]$, black, $[C_4C_1Im][NTf_2]$, red, $[C_4C_1Pyrr][NTf_2]$, green, $[C_2C_1Im][C_2SO_4]$, blue, $[C_6C_1Im][PF_6]$, cyan.

Table 3.2.1. The parameters, a_0 and a_1, with their standard uncertainties, δa_0 and δa_1, for equation (2.2.42), $\rho(T)$.

	$a_0 \pm \delta a_0$ (kg m^{-3})	$-(a_1 \pm \delta a_1) \times 10^{-3}$ (kg m^{-3} K^{-1})	R^2
[C_4C_1Im][Dca] neat	1243.6 ± 0.4	619 ± 1	0.99995
[C_4C_1Im][Dca] + 0.5% MWCNT	1244.5 ± 0.4	619 ± 1	0.99995
[C_4C_1Im][Dca] + 0.5% BN	1243.4 ± 0.4	619 ± 1	0.99994
[C_4C_1Im][Dca] + 0.5% G	1243.1 ± 0.4	618 ± 1	0.99995
[C_4C_1Im][Dca] + 1.0% MWCNT	1248.4 ± 0.5	619 ± 1	0.99994
[C_4C_1Im][Dca] + 1.0% BN	1248.5 ± 0.5	615 ± 1	0.99993
[C_4C_1Im][Dca] + 1.0% G	1244.4 ± 0.4	618 ± 1	0.99996
[C_4C_1Im][Dca] + 3.0% MWCNT	1259.2 ± 0.4	614 ± 1	0.99994
[C_4C_1Im][Dca] + 3.0% BN	1268.3 ± 0.5	622 ± 2	0.99992
[C_4C_1Im][Dca] + 3.0% G	1254.5 ± 0.5	610 ± 2	0.99992
[C_4C_1Im][NTf_2] neat	1717.4 ± 0.4	943 ± 1	0.99998
[C_4C_1Im][NTf_2] + 0.5% MWCNT	1718.1 ± 0.4	941 ± 1	0.99998
[C_4C_1Im][NTf_2] + 1.0% MWCNT	1719.3 ± 0.4	940 ± 1	0.99997
[C_4C_1Im][NTf_2] + 3.0% MWCNT	1727.4 ± 0.2	939 ± 1	0.99999
[C_4C_1Pyrr][NTf_2] neat	1654.4 ± 0.3	872 ± 1	0.99998
[C_4C_1Pyrr][NTf_2] + 0.5% MWCNT	1654.0 ± 0.8	870 ± 1	0.99992
[C_4C_1Pyrr][NTf_2] + 0.5% BN	1657.1 ± 0.4	871 ± 1	0.99997
[C_4C_1Pyrr][NTf_2] + 0.5% G	1655.5 ± 0.4	868 ± 1	0.99998
[C_4C_1Pyrr][NTf_2] + 1.0% MWCNT	1654.9 ± 0.3	871 ± 1	0.99998
[C_4C_1Pyrr][NTf_2] + 1.0% BN	1654.8 ± 0.4	870 ± 1	0.99998
[C_4C_1Pyrr][NTf_2] + 1.0% G	1654.3 ± 0.4	869 ± 1	0.99998
[C_4C_1Pyrr][NTf_2] + 3.0% MWCNT	1657.3 ± 0.4	859 ± 1	0.99998
[C_4C_1Pyrr][NTf_2] + 3.0% BN	1664.1 ± 0.4	866 ± 1	0.99997
[C_4C_1Pyrr][NTf_2] + 3.0% G	1655.5 ± 0.4	855 ± 1	0.99997
[C_2C_1Im][C_2SO_4] neat	1436.9 ± 0.3	670 ± 1	0.99998
[C_2C_1Im][C_2SO_4] + 0.5% MWCNT	1435.6 ± 0.5	663 ± 2	0.99992
[C_2C_1Im][C_2SO_4] + 1.0% MWCNT	1440.4 ± 0.3	667 ± 1	0.99997
[C_2C_1Im][C_2SO_4] + 3.0% MWCNT	1448.3 ± 0.4	664 ± 1	0.99997
[C_6C_1Im][PF_6] neat	1526.7 ± 0.3	784 ± 1	0.99999
[C_6C_1Im][PF_6] + 0.5% MWCNT	1526.3 ± 0.3	783 ± 1	0.99998
[C_6C_1Im][PF_6] + 0.5% BN	1524.3 ± 0.3	784 ± 1	0.99998
[C_6C_1Im][PF_6] + 0.5% G	1524.9 ± 0.3	782 ± 1	0.99998
[C_6C_1Im][PF_6] + 1.0% MWCNT	1528.0 ± 0.2	783 ± 1	0.99999
[C_6C_1Im][PF_6] + 1.0% BN	1527.0 ± 0.2	786 ± 1	0.99999
[C_6C_1Im][PF_6] + 1.0% G	1530.4 ± 0.2	783 ± 1	0.99999
[C_6C_1Im][PF_6] + 3.0% MWCNT	1533.9 ± 0.4	775 ± 1	0.99998
[C_6C_1Im][PF_6] + 3.0% BN	1538.3 ± 0.4	782 ± 1	0.99997
[C_6C_1Im][PF_6] + 3.0% G	1531.1 ± 0.4	770 ± 1	0.99997

It can be seen that, for all cases, the density decreased as a function of temperature, whereas the loading of nanoparticles caused the density shift to higher density values, as expected. The slopes were not found to be changed significantly by the addition of nanoparticles, therefore, the changes between maximum and minimum temperature are similar to pure ILs. It also indicates that the bulk density of all solid materials exhibits higher values. The experimental data were collected in **Tables CD3.1-CD3.6** (Appendix CD3). The changes of density for mixtures are consistent and clearly depend on the

type of nanoparticles. In the literature, it can be found that the density of nanofluids could be then determined by using the empirical equation (2.3.52) originally proposed by Pak and Cho (**1998**) or by using an ideal excess molar volume-based approach, equation (2.2.44). [197, 198] In other words, the assumption made during the calculation of nanoparticles density in the case of the ideal excess molar volume-based approach is that the ideal molar volume is equal to the real molar volume of each nanofluid at investigated temperature. These two methods were applied during this work and the results of both nanoparticles density calculations are summarized in **Tables CD3.1-CD3.6** (Appendix CD3) and shown in **Figure B1** (Appendix B).

Interestingly, the overall AARD for the density prediction of ionanofluids by using the empirical equation (2.3.52) model is close to 0.10 % in each case, while larger deviations are observed using the ideal excess molar volume-based approach, close to (0.44, 0.79 and 0.60) % for carbon nanotubes, boron nitride and graphite based ionanofluids, respectively. Herein, average absolute relative deviations observed using the ideal excess molar volume-based approach are presented in **Figure B2a**, **Figure B3a** and **Figure B4a** (Appendix B) for ionanofluids with carbon nanotubes, boron nitride and graphite, respectively. In fact, this latter approach does not lead to better results of ionanofluids density prediction (higher AARD) than that proposed by Pak and Cho. However, as shown in **Figure B2b**, **Figure B3b** and **Figure B4b** (Appendix B), the hypothetical excess molar volumes calculated using the NPs density values determined from this empirical equation (2.3.52) model resulted in larger absolute values (all negatives in the present cases) than those observed using the ideal excess molar volume-based approach. This finding is also in a good agreement with previous assessments about the molecular meaning of excess properties of systems consisting of more than two phases in solution. From a thermodynamic perspective, in such a case, this excess property is meaningless as an ideal reference state cannot be truly defined. [199] Therefore, the empirical equation (2.3.52) model originally proposed by Pak and Cho seems to be more reliable to determine nanofluids density. [200] Moreover, negative values of excess molar volume indicate the possible contribution of higher density of interfacial nanolayers.

Density is a highly accurate property which may give a useful information about interfacial structure of nanoparticles. Shin and Banarjee (**2011**) showed that there is a specific interfacial organization occurring between fluid and nanoparticles. [201] Hentschke

(**2016**) gave a full theoretical interpretation of the interfacial layer on nanoparticles with including the density and mass fraction of interfacial layer. [202] However, the assumption made in his work was that the density of interfacial layer is similar to this of bulk liquid. Based on the results reported in this work (for example the empirical equation (2.3.52)), it can be seen that the density of interfacial layer is higher. Finally, the most recent theoretical and experimental work of França *et al.* (**2017**) proved the existence of interfacial layer. [203]

Using this recommended approach, the density values at 298.15 K are (1626.34, 1911.89 and 1711.99) kg m^{-3} for carbon nanotubes, boron nitride and graphite, respectively, with the standard uncertainty as described in the experimental part for density (Section 2.2.3). It can be seen that carbon nanotubes and graphite have similar density values which indicates similarity in the packing of particle structure. These data are necessary for efficient and accurate nanofluids properties prediction while most of these are correlated to volumetric concentration of nanomaterials, for example thermal conductivity. [193]

The values of calculated density were further used to calculate the theoretical density of ionanofluids with equation (2.3.52). The results are summarized in the **Tables CD3.1-CD3.3** (Appendix CD3). The representation of calculated density values against the experimental data is shown in **Figure 3.2.2**, while the deviations can be found in **Figure 3.2.3a**, **Figure 3.2.3b** and **Figure 3.2.3c** for ionanofluids containing carbon nanotubes, boron nitride and graphite doped, respectively. The AARD values were 0.10% in each case, which indicated high correlative capability, and the absolute values did not exceed 0.3% deviation, apart from the system containing $[C_4C_1Im][NTf_2]$ + 3 wt% MWCNT where absolute deviations close to (0.3-0.4) % are observed.

França *et al.* (**2014**) studied the physical properties of dicyanamide ILs (*i.e.* density). [4] Based on these density values of ionanofluids containing carbon nanotubes, one can calculate the density of ionanofluids with equation (2.3.52), within RAD values close to (0.11, 0.09, 0.17, 0.25, 0.03, 0.17) % for $[C_2C_1Im][Dca]$ + 0.5 wt% MWCNT , $[C_2C_1Im][Dca]$ + 1.0 wt% MWCNT, $[C_4C_1Im][Dca]$ + 0.5 wt% MWCNT, $[C_4C_1Im][Dca]$ + 1.0 wt% MWCNT, $[C_4C_1Pyrr][Dca]$ + 0.5 wt% MWCNT, $[C_4C_1Pyrr][Dca]$ + 1.0 wt% MWCNT, respectively. [4]

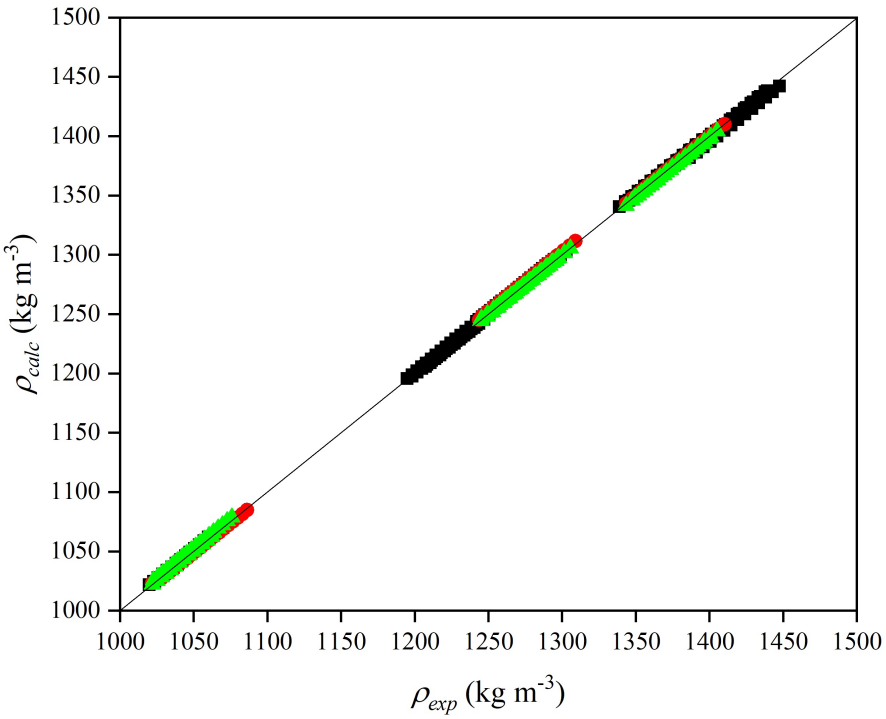

Figure 3.2.2. Calculated density, ρ_{calc}, over the experimental values, ρ_{exp}, for ionanofluids (INF) incorporating multiwalled carbon nanotubes (MWCNT), ■, boron nitride (BN), ●, and graphite (G), ▲, by empirical equation (2.3.52).

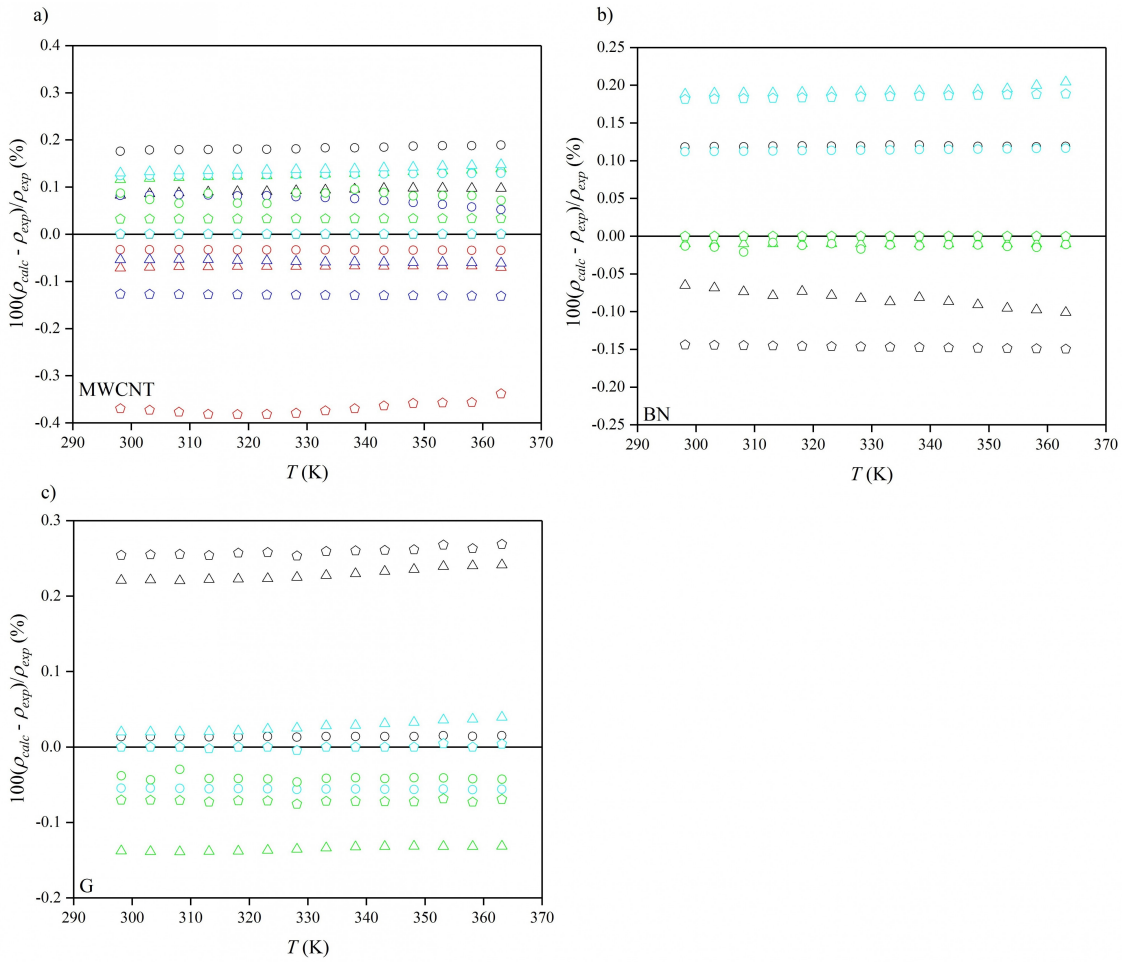

Figure 3.2.3. Relative deviations, $100(\rho_{calc} - \rho_{exp})/\rho_{exp}$, between calculated, ρ_{calc}, and experimental, ρ_{exp}, values of density for ionanofluids with **a)** multiwalled carbon nanotubes (MWCNT); **b)** boron nitride (BN); **c)** graphite (G), by empirical equation (2.3.52), for neat ILs, squares □, 0.5 wt% NP, circles ○, 1.0 wt% NP, triangles △, 3.0 wt% NP, pentagons ⬠, $[C_4C_1Im][Dca]$, black, $[C_4C_1Im][NTf_2]$, red, $[C_4C_1Pyrr][NTf_2]$, green, $[C_2C_1Im][C_2SO_4]$, blue, $[C_6C_1Im][PF_6]$, cyan.

3.2.2 Isobaric Heat Capacity

The results of the heat capacity measurements for all investigated systems are shown in **Figure 3.2.4a**, **Figure 3.2.4b** and **Figure 3.2.4c** for carbon nanotubes-, boron nitride- and graphite-doped ionanofluids, respectively, while the parameters of second-order equation (2.2.30) are summarized in **Table 3.2.2**. The experimental data are collected in **Tables CD3.7-CD3.9 (Appendix CD3)**. Unfortunately, very few datasets have been previously reported for similar systems, to date, which limits the comparison that can be

made. As can be seen the heat capacity of all data increases with temperature, as expected.

Table 3.2.2. The parameters, a_0, a_1 and a_2, with their standard uncertainties, δa_0, δa_1 and δa_2, for equation (2.2.30), $c_p(T)$.

	$-(a_0 \pm \delta a_0)$ (J kg^{-1} K^{-1})	$a_1 \pm \delta a_1$ (J kg^{-1} K^{-2})	$-(a_2 \pm \delta a_2) \times 10^{-3}$ (J kg^{-1} K^{-3})	R^2
[C_4C_1Im][Dca] neat	530 ± 160	13 ± 1	17 ± 2	0.99693
[C_4C_1Im][Dca] + 0.5% MWCNT	920 ± 180	16 ± 1	22 ± 2	0.99497
[C_4C_1Im][Dca] + 0.5% BN	530 ± 160	13 ± 1	17 ± 2	0.99693
[C_4C_1Im][Dca] + 0.5% G	690 ± 110	14 ± 1	17 ± 1	0.99951
[C_4C_1Im][Dca] + 1.0% MWCNT	560 ± 78	14.6 ± 0.5	20 ± 1	0.99867
[C_4C_1Im][Dca] + 1.0% BN	210 ± 140	12 ± 1	15 ± 1	0.99775
[C_4C_1Im][Dca] + 1.0% G	-1060 ± 12	4.0 ± 0.4		0.99874
[C_4C_1Im][Dca] + 3.0% MWCNT	610 ± 110	15 ± 1	21 ± 1	0.99737
[C_4C_1Im][Dca] + 3.0% BN	1800 ± 200	22 ± 1	29 ± 2	0.99719
[C_4C_1Im][Dca] + 3.0% G	-1121 ± 14	4.2 ± 0.4		0.99863
[C_4C_1Im][NTf_2] neat	1190 ± 100	13 ± 1	15 ± 1	0.99956
[C_4C_1Im][NTf_2] + 0.5% MWCNT	2520 ± 110	22 ± 1	29 ± 1	0.99944
[C_4C_1Im][NTf_2] + 1.0% MWCNT	2150 ± 110	20 ± 1	25 ± 1	0.99943
[C_4C_1Im][NTf_2] + 3.0% MWCNT	2980 ± 120	25 ± 1	33 ± 1	0.99942
[C_4C_1Pyrr][NTf_2] neat	-391 ± 7	2.9 ± 0.2		0.99919
[C_4C_1Pyrr][NTf_2] + 0.5% MWCNT	1480 ± 160	16 ± 1	17 ±2	0.99786
[C_4C_1Pyrr][NTf_2] + 0.5% BN	220 ± 12	6.5 ± 0.4	4.2 ± 0.3	0.99909
[C_4C_1Pyrr][NTf_2] + 0.5% G	194 ± 29	4.0 ± 0.2	2.1 ± 0.3	0.99791
[C_4C_1Pyrr][NTf_2] + 1.0% MWCNT	1460 ± 180	15 ± 1	19 ±2	0.99786
[C_4C_1Pyrr][NTf_2] + 1.0% BN	330 ± 10	3.7 ± 0.3		0.99909
[C_4C_1Pyrr][NTf_2] + 1.0% G	-191 ± 18	4.6 ± 0.4		0.99791
[C_4C_1Pyrr][NTf_2] + 3.0% MWCNT	1760 ± 160	17 ± 1	22 ± 2	0.99848
[C_4C_1Pyrr][NTf_2] + 3.0% BN	2360 ± 230	-8.5 ± 0.3	-19 ± 2	0.99850
[C_4C_1Pyrr][NTf_2] + 3.0% G	570 ± 280	9 ± 2	7.1 ± 0.3	0.99868
[C_2C_1Im][C_2SO_4] neat	-519 ± 6	3.5 ± 0.2		0.99956
[C_2C_1Im][C_2SO_4] + 0.5% MWCNT	780 ± 58	3.2 ± 0.4	0.82 ± 0.51	0.99979
[C_2C_1Im][C_2SO_4] + 1.0% MWCNT	-741 ± 1	3.1 ± 0.3		0.99998
[C_2C_1Im][C_2SO_4] + 3.0% MWCNT	-746 ± 17	3.3 ± 0.5		0.99676
[C_6C_1Im][PF_6] neat	1284 ± 34	13.7 ± 0.2	16 ± 3	0.99995
[C_6C_1Im][PF_6] + 0.5% MWCNT	2210 ± 160	20 ± 1	26 ± 2	0.99883
[C_6C_1Im][PF_6] + 0.5% BN	1517 ± 98	16 ± 1	18 ± 1	0.99966
[C_6C_1Im][PF_6] + 0.5% G	3450 ± 150	27 ± 1	34 ± 1	0.99957
[C_6C_1Im][PF_6] + 1.0% MWCNT	2250 ± 220	20 ± 1	26 ± 2	0.99793
[C_6C_1Im][PF_6] + 1.0% BN	2650 ± 110	23 ± 1	30 ± 1	0.99958
[C_6C_1Im][PF_6] + 1.0% G	3250 ± 310	26 ± 2	33 ± 3	0.99820
[C_6C_1Im][PF_6] + 3.0% MWCNT	2360 ± 250	22 ± 2	28 ± 2	0.99720
[C_6C_1Im][PF_6] + 3.0% BN	3270 ± 150	27 ± 1	36 ± 1	0.99925
[C_6C_1Im][PF_6] + 3.0% G	3760 ± 260	30 ± 2	37 ± 2	0.99894

The specific heat capacity was also found to increase with nanomaterials loading (with restriction up to 3% in nanoparticles mass fraction units, as investigated), as can be clearly seen in **Figure 3.2.4a**, **Figure 3.2.4b** and **Figure 3.2.4c** for carbon nanotubes-, boron nitride- and graphite-doped ionanofluids, respectively. **Figure 3.2.5a**, **Figure**

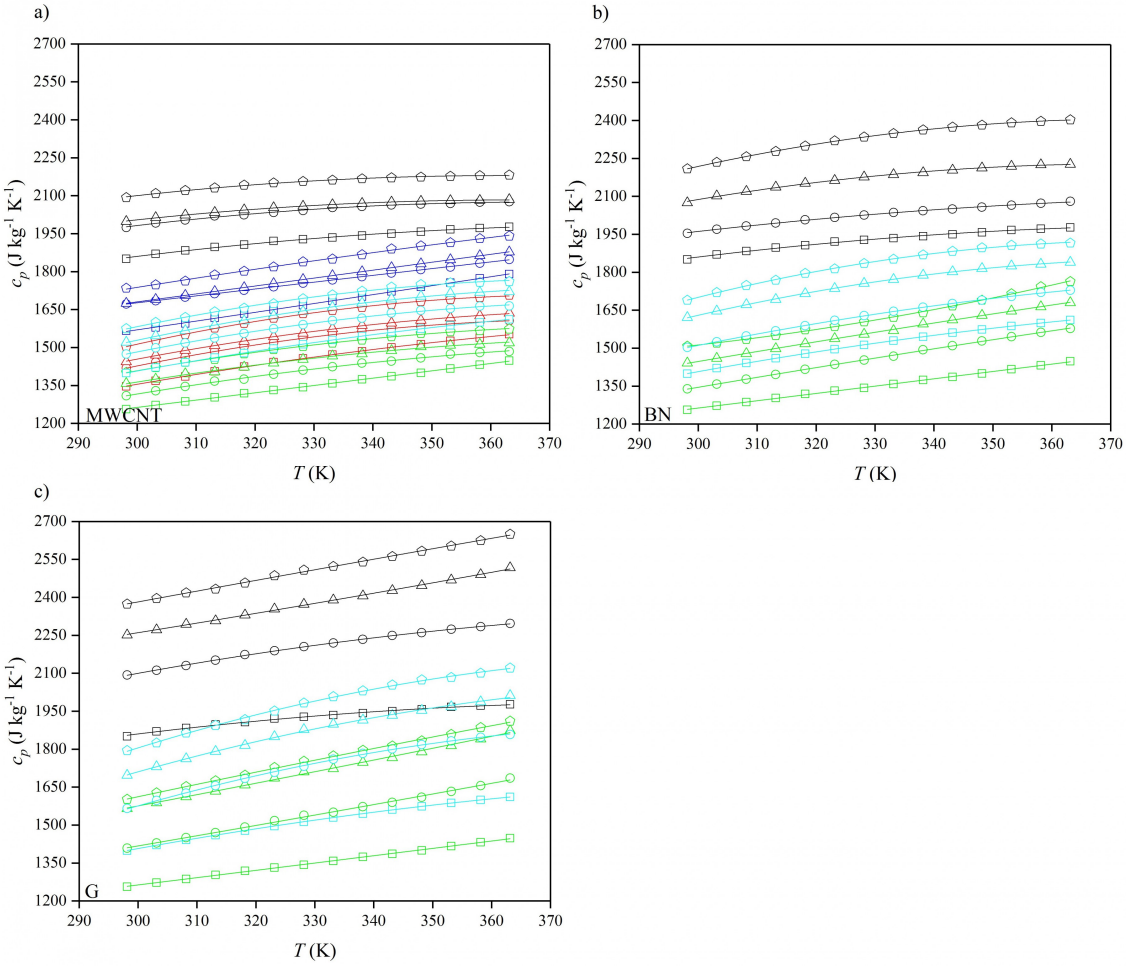

Figure 3.2.4. Temperature, T, dependence of the isobaric heat capacity, c_p, of investigated ionanofluids with **a)** multiwalled carbon nanotubes (MWCNT); **b)** boron nitride (BN); **c)** graphite (G), for neat ILs, squares □, 0.5 wt% NP, circles ○, 1.0 wt% NP, triangles △, 3.0 wt% NP, pentagons ⬠, $[C_4C_1Im][Dca]$, black, $[C_4C_1Im][NTf_2]$, red, $[C_4C_1Pyrr][NTf_2]$, green, $[C_2C_1Im][C_2SO_4]$, blue, $[C_6C_1Im][PF_6]$, cyan.

3.2.5b and **Figure 3.2.5c** show the heat capacity enhancement (in comparison to pure ILs) as a function of nanoparticles loading (volume fraction) for carbon nanotubes-, boron nitride- and graphite-doped nanofluids, respectively. The enhancements observed were in the ranges of (5 – 13, 5 – 21 and 12 – 28) % for carbon nanotubes-, boron nitride- and graphite-based ionanofluids. As can be seen, the effect of the addition of carbon nanotubes was the smallest and compared with graphite which showed the largest changes.

The mechanism of the heat capacity enhancement has been widely discussed and proposed to be based on the mixing theory for ideal gas mixtures. [204] However, it has been shown that this approach is not relevant for nanofluids, where the specific heat

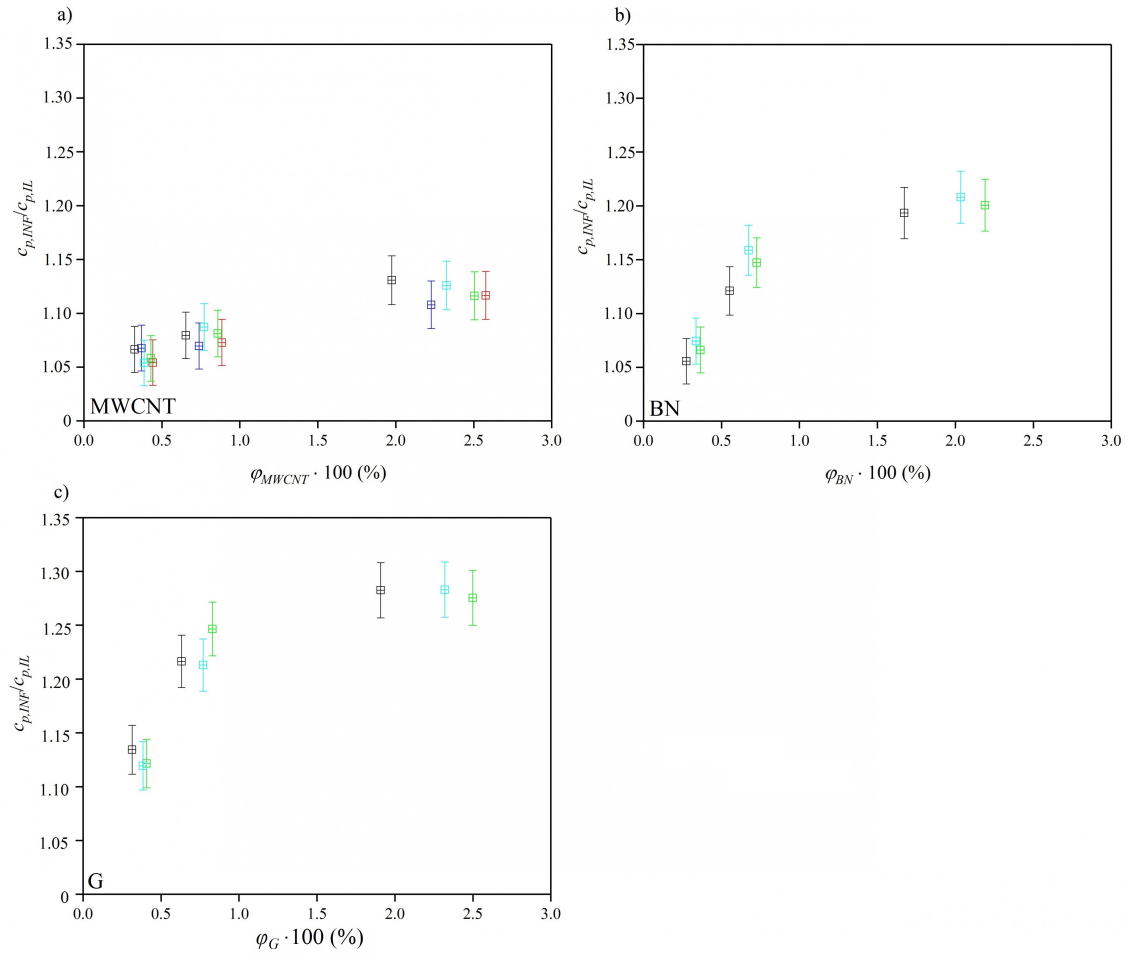

Figure 3.2.5. Heat capacity enhancement, $c_{p,INF}/c_{p,IL}$, in comparison to pure ionic liquids as a function of the nanoparticles volume fraction, φ, for **a)** multiwalled carbon nanotubes-doped (MWCNT) ionanofluids; **b)** boron nitride-doped (BN) ionanofluids; **c)** graphite-doped (G) ionanofluids, for $[C_4C_1Im][Dca]$, black, $[C_4C_1Im][NTf_2]$, red, $[C_4C_1Pyrr][NTf_2]$, green, $[C_2C_1Im][C_2SO_4]$, blue, $[C_6C_1Im][PF_6]$, cyan.

capacity of nanoparticles (as studied for carbon nanotubes) is lower than liquids and the enhancement of heat capacity is observed. [202] Another theory proposed is based on the assumption of thermal equilibrium between the fluid and nanoparticles. [204] It was shown that it reproduces better values, however, is still not accurate enough, and the specific mechanism is not explained within this theory. The first attempt to explain the heat capacity increasing was proposed by Shin *et al.* (**2011**). [201] The authors discussed three different modes: **a)** higher specific heat capacity of nanoparticles in comparison to their bulk equivalents (based on Al_2O_3, up to 25%) [205] which is related to the quantization of phonon spectrum with discrete values, which is not limited by the size of

nanoparticles (due to resolved surface area); **b)** high solid-fluid interaction energy caused by the high surface area per unit mass of nanoparticles which increases the interfacial thermal resistance and acts as additional thermal storage; **c)** layering of liquid molecules at the surface of nanoparticles due to the liquid molecules adsorption as semi-solid layer with larger thermal properties than the bulk liquid (usually 2-5 nm).

The most recent work of Hentschke (**2016**) discussed the possible mechanism of the heat capacity enhancement, including the mathematical foundation. [202] It was shown that the observed enhancement may be caused by one or both of the following factors: **a)** nanolayering of nanoparticles with liquid molecules, with the layer of higher heat capacity in comparison to liquids and dependent on the nanoparticles type; **b)** the new phenomenological theory based on the attendant mesolayer interacting with other mesolayers with the assumption that the enhancement occurs until some specific loading of nanoparticles, and then becomes a decreasing function of nanoparticles concentration (a few parameters were introduced while the maximum mass fraction concentration was always below 3%). Nevertheless, all of these theories are based on molecular solvents-like nanofluids, and none of them considered ILs as basefluids.

The observed enhancement clearly indicated the existence of interfacial nanolayers. Moreover, as can be seen in **Figure 3.2.5a**, **Figure 3.2.5b** and **Figure 3.2.5c** for carbon nanotubes-, boron nitride- and graphite-doped ionanofluids, respectively, the values of the enhancement observed are different in the case of each type of nanoparticle. This shows that the mechanism is based on the type of nanoparticles instead of type of IL. These dependencies were also correlated with temperature and nanoparticles concentration based on the following assumptions: **a)** $c_p(T)$ is a second-order dependence; **b)** $c_p(\varphi)$ is clearly not a linear equation, and can be easily described by a second order equation. Therefore, the following equations are proposed:

$$\frac{c_{p,INF}}{c_{p,IL}} = (6.00 \pm 0.43)\varphi_{MWCNT} + (32.6 \pm 8.7) \times 10^{-4}T - (109 \pm 14)\varphi_{MWCNT}^2 - (5.5 \pm 1.3) \times 10^{-6}T^2 + (0.55 \pm 0.14) \quad (3.2.1)$$

$$\frac{c_{p,INF}}{c_{p,IL}} = (28.99 \pm 0.85)\varphi_{BN} + (17.0 \pm 1.5) \times 10^{-4}T - (894 \pm 34)\varphi_{BN}^2 - (2.5 \pm 2.1) \times 10^{-6}T^2 + (0.70 \pm 0.24) \quad (3.2.2)$$

$$\frac{c_{p,INF}}{c_{p,IL}} = (29.5 \pm 1.2)\varphi_G + (23.4 \pm 2.3) \times 10^{-4} T - (829 \pm 42)\varphi_G^2 \\ -(2.5 \pm 1.3) \times 10^{-6} T^2 + (0.58 \pm 0.38) \tag{3.2.3}$$

with coefficient of determination, R^2, (0.91848, 0.97047 and 0.93451) for multiwalled carbon nanotubes-, boron nitride- and graphite-doped ionanofluids, respectively.

As shown by Hentschke (**2016**) a maximum enhancement is maintained by the existence of overlapping mesolayers. [202] In this work, this was not recorded (as no significant maximum of the enhancement was observed below 3 wt%) which may indicate a smaller impact of this type of interactions caused by stronger interactions between ILs and nanoparticles, and as a result more compact interfacial layer. The different types of ILs used in this work provide the information about impact of the base fluid on the enhancement. However, it can be assumed that the base fluid type and structure is not an influencing factor (based on the dependency upon the nanoparticles concentration). While different values of enhancements prove the fact that enhancement depends on the type of nanoparticles. Moreover, as pointed out by Hentschke (**2016**) the heat capacity enhancement depends on the particle size, and thus, the surface area, it can be observed that the enhancement intensity depends in the following sequence: graphite > boron nitride > carbon nanotubes, as well as the nanoparticle size (and reverse order for surface areas), which is in a good agreement with experimental data. [202]

The most likely mechanism for the enhancement in case of ionic liquid-based nanofluids is based on the semi-solid-like liquid ordering on the nanoparticles surface which was described in the work of Shin and Banerjee (**2011**), [201] with further extension by Hentschke (**2016**), [202] excluding the interacting mesolayers as no experimental result indicates such a behavior in this work. Similar work was carried out by França *et al.* (**2017**) with molecular dynamics simulations of surface nanolayering including the thermal conductivity modelling. [203] The results presented in this work clearly indicate the existence of liquid nanolayers on the nanoparticles surface which is mainly responsible for the enhancement of the thermal properties when nanoparticles are dispersed in a fluid base. As well, no mesolayer interaction was observed. The results presented herein are in a good agreement with those published by França *et al.* (**2017**). [203]

From an industrial perspective, the prior knowledge of the specific heat capacity as a function of temperature is crucial. More specifically, the enhancement in the heat capac-

ity caused by the presence of nanoparticles in base fluids as the function of composition and temperature is of high interest. **Figure 3.2.6** shows that the enhancements obtained for carbon nanotubes-, boron nitride- and graphite-doped ionanofluids are ranged from (3.1 to 13.2, 5.3 to 22.0, 10.9 to 34.2) %, respectively. The maximum of enhancement observed were (13.2, 22.0 and 34.2) % for $[C_4C_1Im][Dca]$ + 3 wt% MWCNT at 293.15 K, $[C_4C_1Im][Dca]$ + 3 wt% BN at 343.15 K and $[C_4C_1Im][Dca]$ + 3 wt% G at 363.15 K, respectively. It can be seen that for carbon nanotubes the enhancement decreases with temperature (related to increasing hydrophobicity, less favoured attraction of liquid molecules), [206] graphite is increasing with temperature (decreasing hydrophobicity, therefore, easier creation of nanolayers), [207] boron nitride (more or less constant with temperature, stabilized by the diversely charged surface of charge distribution between nitrogen and boron). [208] This also reflects in different type of prospective industrial applications in case of desired temperature profile of HTFs.

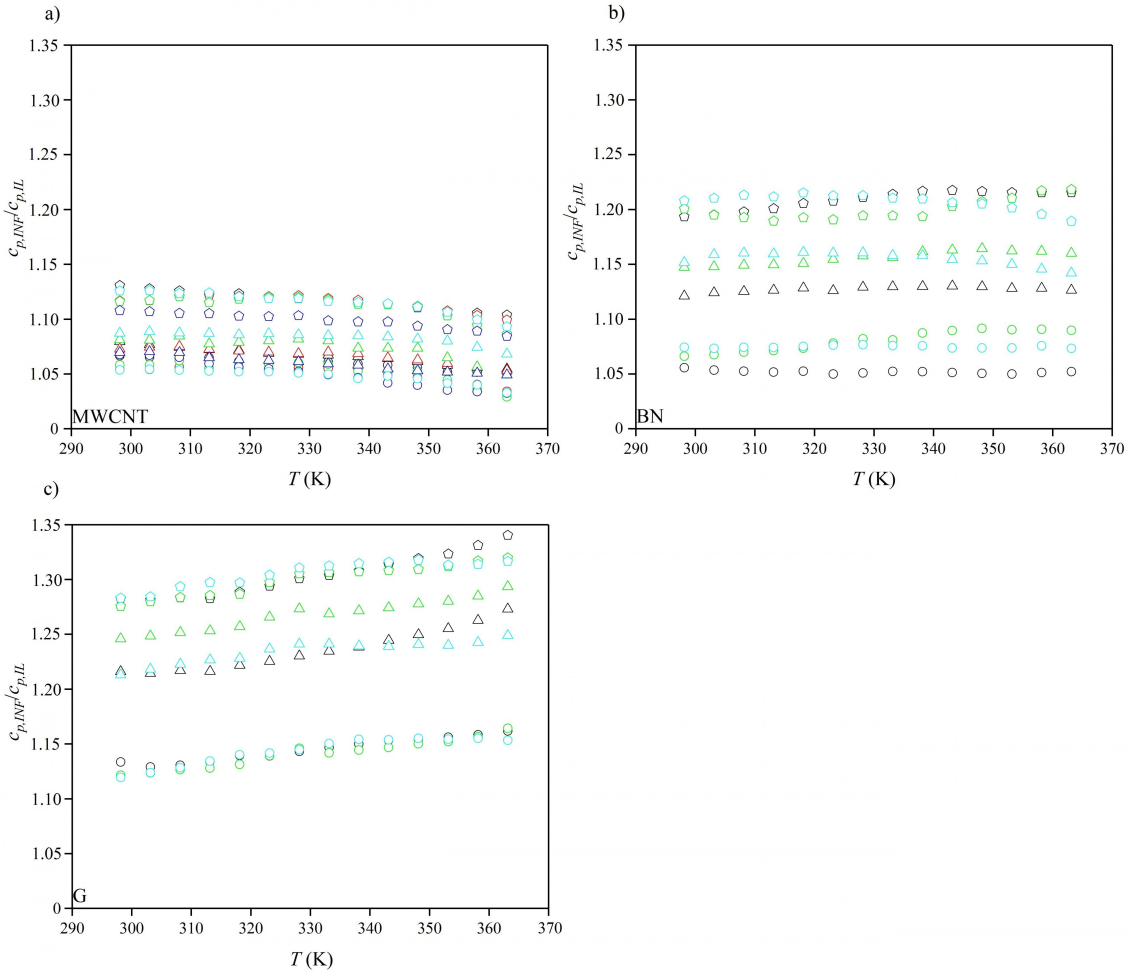

Figure 3.2.6. Heat capacity enhancement, $c_{p,INF}/c_{p,IL}$, in comparison to pure ionic liquids as a function of the temperature, T, for **a)** multiwalled carbon nanotubes-doped (MWCNT) ionanofluids; **b)** boron nitride-doped (BN) ionanofluids; **c)** graphite-doped (G) ionanofluids, for 0.5 wt% NP, circles ○, 1.0 wt% NP, triangles △, 3.0 wt% NP, pentagons ⬠, $[C_4C_1Im][Dca]$, black, $[C_4C_1Im][NTf_2]$, red, $[C_4C_1Pyrr][NTf_2]$, green, $[C_2C_1Im][C_2SO_4]$, blue, $[C_6C_1Im][PF_6]$, cyan.

3.2.3 Thermal conductivity

The thermal conductivity of each investigated ionanofluid was measured in the temperature range of (278 – 358) K, at atmospheric pressure (101 kPa). The experimental data were collected in **Tables CD3.10-CD3.12** (Appendix CD3), and presented in **Figure 3.2.7**. The coefficients of linear fitting, equation (2.2.18), $\lambda(T)$, have been collected in **Table 3.2.3**.

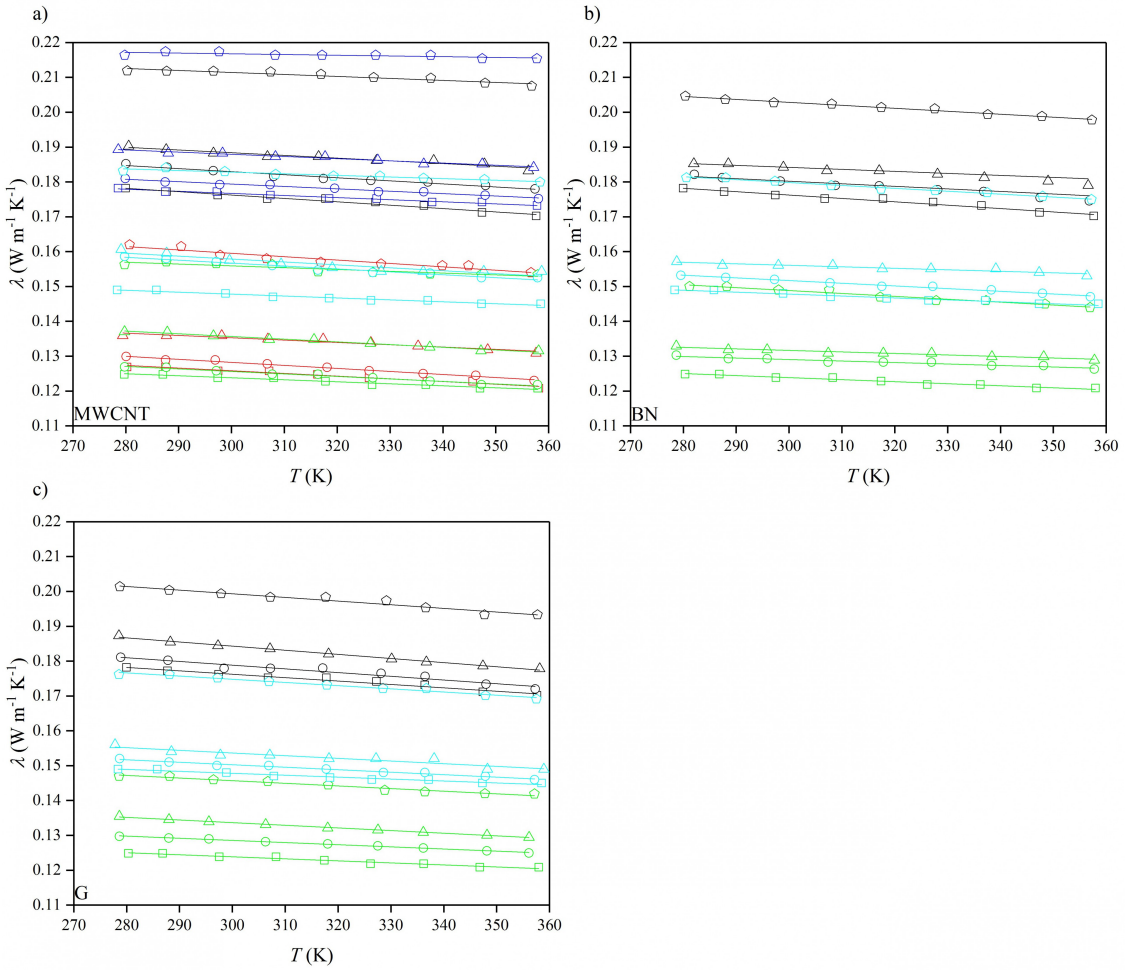

Figure 3.2.7. Temperature, T, dependence of thermal conductivity, λ, of investigated ionanofluids with **a)** multiwalled carbon nanotubes (MWCNT); **b)** boron nitride (BN); **c)** graphite (G), for neat ILs, squares □, 0.5 wt% NP, circles ○, 1.0 wt% NP, triangles △, 3.0 wt% NP, pentagons ⬠, $[C_4C_1Im][Dca]$, black, $[C_4C_1Im][NTf_2]$, red, $[C_4C_1Pyrr][NTf_2]$, green, $[C_2C_1Im][C_2SO_4]$, blue, $[C_6C_1Im][PF_6]$, cyan.

The thermal conductivity of solids is generally higher than that of liquids, moreover the thermal conductivity of nanoparticles is particularly higher. [209] Various effects could explain this behavior in case of nanoparticles, for example when considering the theory of the phonon transport, more porous materials have shorter effective size of nanoparticles in which this phonon transport occurs, the specific surface area is increased, or the wavelength of incident radiation (namely de Broglie wavelength) is comparable to the nanoparticles diameter.

This affects the electron properties of such materials in which the electron conduc-

Table 3.2.3. The parameters, a_0 and a_1, with their standard uncertainties, δa_0 and δa_1, for equation (2.2.18), $\lambda(T)$.

	$(a_0 \pm \delta a_0) \times 10^{-3}$ (W m^{-1} K^{-1})	$-(a_1 \pm \delta a_1) \times 10^{-5}$ (W m^{-1} K^{-2})	R^2
[C_4C_1Im][Dca] neat	205 ± 2	9.7 ± 0.7	0.96412
[C_4C_1Im][Dca] + 0.5% MWCNT	209 ± 2	8.8 ± 0.5	0.97230
[C_4C_1Im][Dca] + 0.5% BN	209 ± 1	9.5 ± 0.4	0.98237
[C_4C_1Im][Dca] + 0.5% G	211 ± 3	11 ± 1	0.93922
[C_4C_1Im][Dca] + 1.0% MWCNT	212 ± 2	7.8 ± 0.7	0.93154
[C_4C_1Im][Dca] + 1.0% BN	209 ± 2	8.3 ± 0.5	0.97347
[C_4C_1Im][Dca] + 1.0% G	220 ± 1	11.8 ± 0.4	0.99122
[C_4C_1Im][Dca] + 3.0% MWCNT	228 ± 2	5.7 ± 0.7	0.89274
[C_4C_1Im][Dca] + 3.0% BN	229 ± 1	8.6 ± 0.4	0.98549
[C_4C_1Im][Dca] + 3.0% G	233 ± 3	11 ± 1	0.94703
[C_4C_1Im][NTf_2] neat	149 ± 2	7.7 ± 0.5	0.96230
[C_4C_1Im][NTf_2] + 0.5% MWCNT	154 ± 1	8.7 ± 0.4	0.98517
[C_4C_1Im][NTf_2] + 1.0% MWCNT	155 ± 2	6.7 ± 0.7	0.92061
[C_4C_1Im][NTf_2] + 3.0% MWCNT	185 ± 2	8.5 ± 0.7	0.94693
[C_4C_1Pyrr][NTf_2] neat	141 ± 1	5.5 ± 0.4	0.95550
[C_4C_1Pyrr][NTf_2] + 0.5% MWCNT	147 ± 1	7.2 ± 0.4	0.97644
[C_4C_1Pyrr][NTf_2] + 0.5% BN	142 ± 1	4.3 ± 0.4	0.93217
[C_4C_1Pyrr][NTf_2] + 0.5% G	147 ± 6	6.2 ± 0.2	0.99201
[C_4C_1Pyrr][NTf_2] + 1.0% MWCNT	159 ± 1	7.8 ± 0.4	0.97763
[C_4C_1Pyrr][NTf_2] + 1.0% BN	145 ± 1	4.3 ± 0.4	0.93217
[C_4C_1Pyrr][NTf_2] + 1.0% G	156 ± 5	7.6 ± 0.2	0.99596
[C_4C_1Pyrr][NTf_2] + 3.0% MWCNT	171 ± 3	5.2 ± 0.8	0.81851
[C_4C_1Pyrr][NTf_2] + 3.0% BN	174 ± 2	8.3 ± 0.6	0.96063
[C_4C_1Pyrr][NTf_2] + 3.0% G	168 ± 2	7.6 ± 0.5	0.96270
[C_2C_1Im][C_2SO_4] neat	195 ± 1	6.0 ± 0.4	0.97086
[C_2C_1Im][C_2SO_4] + 0.5% MWCNT	200 ± 1	6.8 ± 0.4	0.97650
[C_2C_1Im][C_2SO_4] + 1.0% MWCNT	207 ± 1	6.3 ± 0.4	0.96331
[C_2C_1Im][C_2SO_4] + 3.0% MWCNT	223 ± 2	2.1 ± 0.6	0.96455
[C_6C_1Im][PF_6] neat	164 ± 1	5.5 ± 0.4	0.95453
[C_6C_1Im][PF_6] + 0.5% MWCNT	174 ± 2	8.3 ± 0.6	0.96522
[C_6C_1Im][PF_6] + 0.5% BN	175 ± 1	7.7 ± 0.3	0.98520
[C_6C_1Im][PF_6] + 0.5% G	172 ± 1	7.1 ± 0.4	0.97909
[C_6C_1Im][PF_6] + 1.0% MWCNT	179 ± 3	7.1 ± 0.8	0.86666
[C_6C_1Im][PF_6] + 1.0% BN	169 ± 2	4.3 ± 0.6	0.86349
[C_6C_1Im][PF_6] + 1.0% G	174 ± 2	6.6 ± 0.7	0.92133
[C_6C_1Im][PF_6] + 3.0% MWCNT	197 ± 2	4.6 ± 0.5	0.91603
[C_6C_1Im][PF_6] + 3.0% BN	205 ± 1	8.3 ± 0.4	0.98492
[C_6C_1Im][PF_6] + 3.0% G	198 ± 1	7.7 ± 0.4	0.98007

tion can be trapped (called quantum trapping), resulting in modification of the bandgap. For example, in 10 nm particles, about 10% of atoms are at the surface, and they are more active than the atoms in the volume. As a result, their electron energy levels are higher which is caused by the imperfections or active sites due to the partially saturated bonds. When the electromagnetic wave reaches these electrons, the polarization of the free electrons is induced. When the energy of the electromagnetic wave is high enough, the oscillation energy of these electrons is achieved and causes surface plasmon absorption. [210]

A short but conclusive description of mathematical fundamentals of nanotechnology was given by Marchiori (**2016**). [211] The previously reported values of thermal conductivity at 298.15 K for investigated nanomaterials are (3223.4, 874.1 and 35.7) W m^{-1} K^{-1} for carbon nanotubes, [212] boron nitride, [213] and graphite, [214] respectively, whereas those for liquids are values of 10^{-1} W m^{-1} K^{-1} order. The addition of nanoparticles shifts the thermal conductivity to higher values than pure ILs. The dependence of IL structure on the thermal conductivity was discussed in the previous section. As can be seen in **Figure 3.2.7**, the thermal conductivity behaviour as a function of temperature remains linear and is similar to this of pure ILs.

As a result, the thermal conductivity of nanofluids exhibits higher values than in comparison to pure fluids, and an enhancement is observed, as shown in **Figure 3.2.8a**, **Figure 3.2.8b** and **Figure 3.2.8c** for carbon nanotubes-, boron nitride- and graphite-doped ionanofluids, respectively. The results were also collected in **Tables CD3.10-CD3.12** (Appendix CD3).

As a consequence, the thermal conductivity enhancement was found to be an increasing function of nanoparticles concentration in solution. Even though the exact mechanism of heat transfer is still a subject of intensive investigation, there were a number of attempts to describe the enhancement, for example the mechanism was explained by Brownian motion of nanoparticles, liquid layering at the liquid/particle interface, nature of heat transport across nanoparticles, nanoparticle clustering, while the interface layering was proven to be most sensible explanation. [215–220] However, the most recent work of França *et al.* (**2017**) described these phenomena based on experimental and theoretical studies, and revealed the enhancement based on the ILs adsorption layering onto the surface of nanoparticles. [203]

As shown in **Figure 3.2.8**, the values of the enhancements are dependent on the type of nanoparticles, the highest for carbon nanotubes-doped (up to 27.48%, for 0.1541 W m^{-1} K^{-1} of $[C_4C_1Im][NTf_2]$ + 3.0 wt% MWCNT and 0.1213 W m^{-1} K^{-1} of pure $[C_4C_1Im][NTf_2]$, at 358.15 K), lower for boron nitride-doped (up to 21.77%, for 0.1800 W m^{-1} K^{-1} of $[C_6C_1Im][PF_6]$ + 3.0 wt% BN and 0.1479 W m^{-1} K^{-1} of pure $[C_6C_1Im][PF_6]$, at 298.15 K), and the lowest for graphite-doped (up to 18.49%, for 0.1742 W m^{-1} K^{-1} of $[C_6C_1Im][PF_6]$ + 3.0 wt% BN and 0.1474 W m^{-1} K^{-1} of pure $[C_6C_1Im][PF_6]$, at 308.15 K) ionanofluids. This is in an agreement with the size of nanoparticles and their values

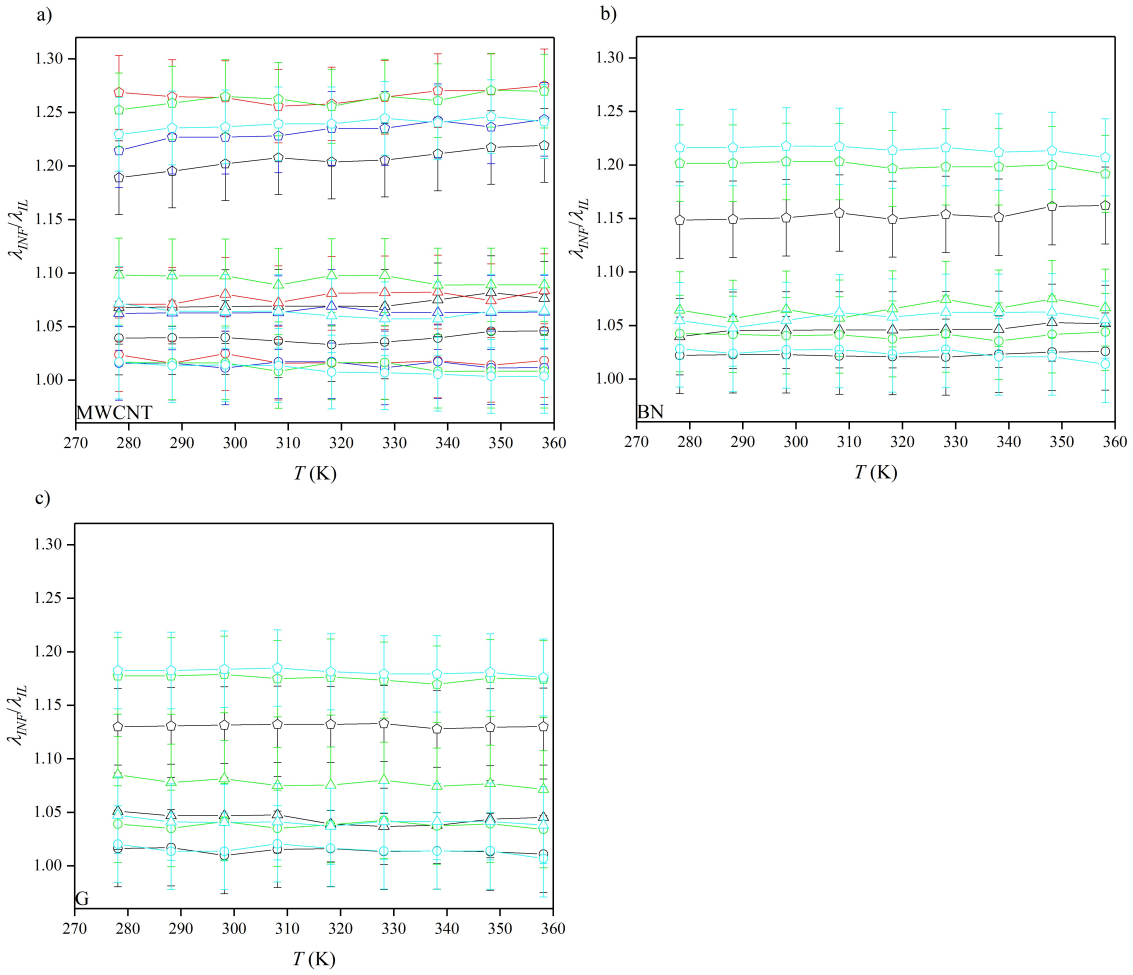

Figure 3.2.8. Thermal conductivity enhancement, $\lambda_{INF}/\lambda_{IL}$, in comparison to pure ionic liquids as a function of the temperature, *T*, for **a)** multiwalled carbon nanotubes-doped (MWCNT) ionanofluids; **b)** boron nitride-doped (BN) ionanofluids; **c)** graphite-doped (G) ionanofluids, for 0.5 wt% NP, circles ○, 1.0 wt% NP, triangles △, 3.0 wt% NP, pentagons ⬠, $[C_4C_1Im][Dca]$, black, $[C_4C_1Im][NTf_2]$, red, $[C_4C_1Pyrr][NTf_2]$, green, $[C_2C_1Im][C_2SO_4]$, blue, $[C_6C_1Im][PF_6]$, cyan.

of thermal conductivity: carbon nanotubes < boron nitride < graphite. Moreover, the enhancement calculated using IL as a reference (in this case the value of λ_{INF} divided by λ_{IL}, $\lambda_{INF}/\lambda_{IL}$) shows the dependence on the nanoparticles type (as well as the size and chemical nature). The following relationship is in good agreement with the thermal conductivity of nanoparticles, and it was also reflected in almost linear dependence on the nanoparticles concentration. As can be seen, these enhancements are more or less constant over the whole temperature range, with some deviations from the linearity, however, still remaining similarity in terms of those errors. The enhancement is still consistent in terms

of the enhancement and thermal conductivity of pure nanomaterials, in the decreasing sequence – nanofluids consisting of carbon nanotubes, boron nitride and graphite.

From an engineering perspective, a knowledge of thermal conductivity dependence over the temperature is very important as it reflects the heat transfer efficiency which occurs in the system. Carbon nanotubes, boron nitride and graphite were objects of investigation in terms of surface charge, in the meaning of zeta potential. All of them were represented with negative zeta potential caused by the adsorption of negatively charged ions (the positive surface charge of nanoparticles). [221–223] Therefore, the expectation was that the enhancement in this work would depend on the type of anions. It can be observed in **Figure 3.2.8a**, **Figure 3.2.8b** and **Figure 3.2.8c** that there is a dependence on the type of IL. Including the volumes of ILs constituents from COSMO-RS methodology, it can be observed that the enhancement is in the following order: $[C_4C_1Im][Dca]$ ($V_{[C_4C_1Im]^+}$=197 Å^3, $V_{[Dca]^-}$=82 Å^3, $V_{[C_4C_1Im][Dca]}$=279 Å^3) < $[C_2C_1Im][C_1SO_4]$ ($V_{[C_2C_1Im]^+}$=154 Å^3, $V_{[C_1SO_4]^-}$=104 Å^3, $V_{[C_2C_1Im][C_1SO_4]}$=258 Å^3) < $[C_6C_1Im][PF_6]$ ($V_{[C_6C_1Im]^+}$=242 Å^3, $V_{[PF_6]^-}$=104 Å^3, $V_{[C_6C_1Im][PF_6]}$=346 Å^3) < $[C_4C_1Im][NTf_2]$ ($V_{[C_4C_1Im]^+}$=197 Å^3, $V_{[NTf_2]^-}$=222 Å^3, $V_{[C_4C_1Im][NTf_2]}$=419 Å^3) < $[C_4C_1Pyrr][NTf_2]$ ($V_{[C_4C_1Pyrr]^+}$=214 Å^3, $V_{[NTf_2]^-}$=222 Å^3, $V_{[C_4C_1Pyrr][NTf_2]}$=436 Å^3). Clearly, the enhancement is dependent on the type of anion and increasing the volume of anion results in a larger enhancement. As explained above, bigger molecules (with larger molecular size/volume) tend to have smaller thermal conductivity. Bulkier anions have also less possibilities to adsorb onto the surface of nanoparticles, therefore, the effective molecular volume/size of nanoparticle-liquid molecules complex is smaller (and also observed, as presented above). On the other hand, there was no dependence on type of cation found, herein. This is also in a good agreement with the zeta potential discussion presented herein. Carbon-based materials tend to have positive charge, therefore, exhibiting negative zeta potential (caused by the adsorption of anions). The surface of boron nitride is described with negative charge from N-atom (electrons acceptor) and positive charge from B-atom (electrons donor). [224] However, in this work an adsorption of anions seems to be dominant and also observed in the results (as presented above).

Interestingly, many methods for nanofluids preparation can be used, including different nanomaterials pre-treatment, their average size, or agitation and ultrasonication time. [225–227] Moreover, the studies on the influence of these differences in case of ionic

liquid – based nanofluids have not been investigated previously, in particular the effect on the enhancement of thermal conductivity. The comparison between thermal conductivity in this work and literature data can be performed based on the enhancement as several aspects can influence the values of thermal conductivity – particularly the value of pure ILs as base fluids. This comparison is shown in **Figure 3.2.9**.

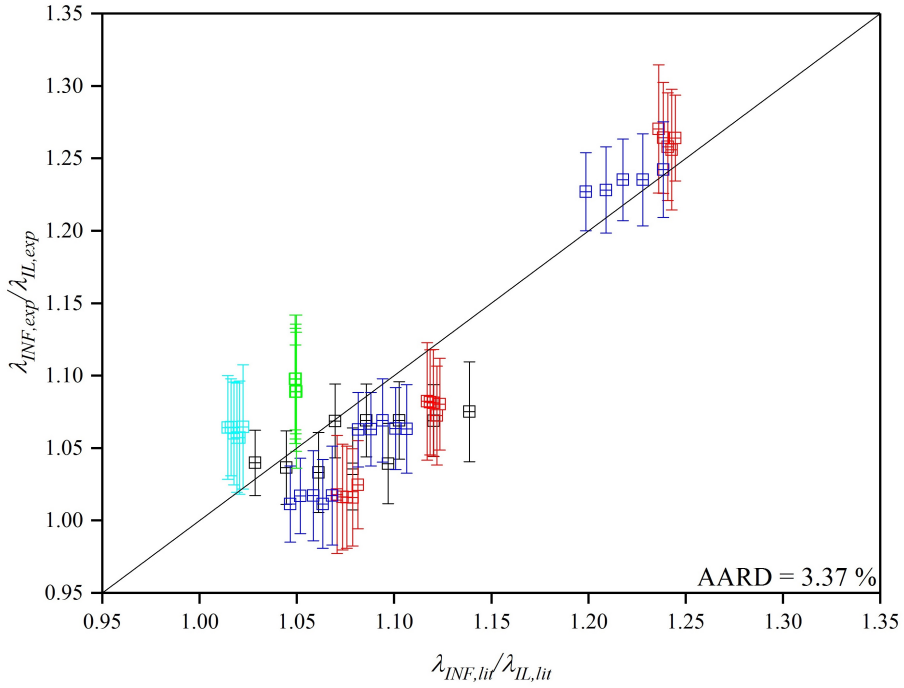

Figure 3.2.9. Thermal conductivity enhancement, $\lambda_{INF}/\lambda_{IL}$, from this work, over the results from literature, for $[C_4C_1Im][Dca]$, black [4], $[C_4C_1Im][NTf_2]$, red [193], $[C_4C_1Pyrr][NTf_2]$, green [193], $[C_2C_1Im][C_2SO_4]$, blue [190], $[C_6C_1Im][PF_6]$, cyan [190], with multiwalled carbon nanotubes (MWCNT) at 298.15 K.

Unfortunately, the comparison is possible for only ionanofluids containing multiwalled carbon nanotubes, as boron nitride and graphite have not been used before in such studies. Therefore, further assumption in the nomenclature of (io)nanofluids is that the carbon nanotubes are used, instead of boron nitride and graphite, in terms of enhancement comparison to the literature analysis. The first deliberation should be done for the methodology of ionanofluids preparation. All literature positions are consistent in terms of the ionanofluids preparation, as described in the Experimental Section 2.1.5. The other factor influencing the results is the source of nanomaterials. In this case (multiwalled carbon nanotubes) are from the same source (Baytubes C150 HP from Bayer Material

Science). Another source of deviations can be the purity of pure ILs, in particular the thermal conductivity values. This was discussed in the previous Section 3.1.2 devoted to the deviations of pure ILs thermal conductivity observed in this work and the literature.

On the other hand, the treatment of the sample is another influencing factor (including the transportation, storage, *etc.*). Probably the most important source of deviations is the measurement methodology (also described in Section 2.2.1), as various techniques, methodologies or calibration might shift the values of thermal conductivity. To quantify the deviations between the thermal conductivity in this work and literature, the absolute average relative deviation was ascertained as 3.37%. The most deviated points were for $[C_4C_1Im][NTf_2]$ + 0.5 wt% MWCNT at 308.15 K (6.19% relative deviation, 1.0159 in this work and 1.0788 in [193]) and $[C_6C_1Im][PF_6]$ + 0.5 wt% MWCNT at 328.15 K (-4.66% relative deviation, 1.0642 in this work and 1.0146 in [190]). Moreover, 31 points out of 52 were above the standard uncertainty of determined enhancement. This shows that the reported thermophysical properties (in particular the thermal conductivity) might vary in the literature, which is very important for the engineering application and further theoretical modelling.

More work on the unification of the thermophysical properties needs to be performed, since it is pivotal for the proper application in industry and related areas where the economical factor is determinant for the utilization in processes where heat transfer is very important. The first influence is made by the values of pure IL thermal conductivity which is further propagated into the thermal conductivity of ionanofluid. Therefore, the comparison of absolute thermal conductivity of ionanofluids obtained in literature is impossible, and thus, the enhancement seems to be a better property to compare.

The calculated thermal conductivity values for ionanofluids can be found in **Tables CD3.10-CD3.12** (Appendix CD3). The enhancement of ionanofluids thermal conductivity in comparison to pure ILs was also tested in case of theoretical modelling. Overall, 6 models were used, while only one was designed for ionic liquid–based nanofluids (Atashrouz). As also shown in **Figure 3.2.10**, the pure non-ionic-solvent-based-like models (Maxwell, Hamilton-Crosser, both versions of Tinga-Leong-Murshed, and Timofeeva models) were highly deviated from the experimental data .

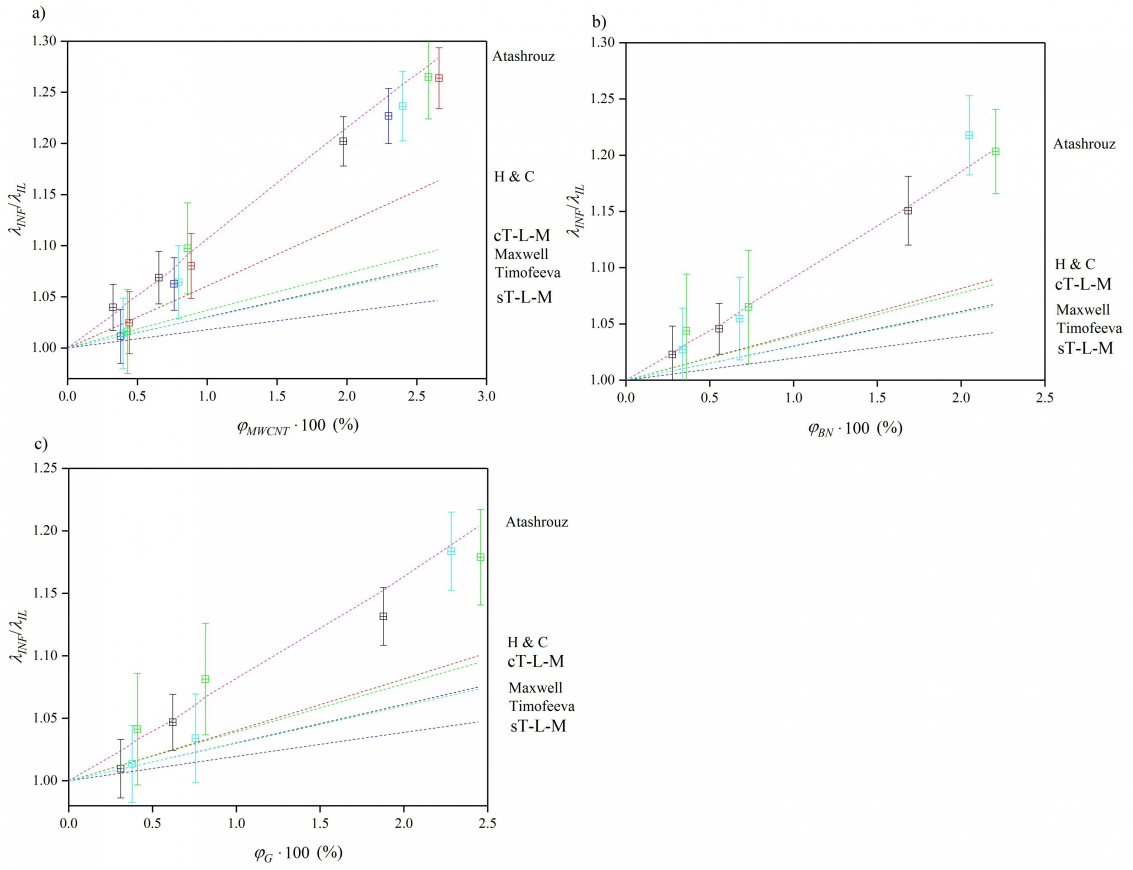

Figure 3.2.10. Thermal conductivity enhancement, $\lambda_{INF}/\lambda_{IL}$, in comparison to pure ILs as a function of the nanoparticles volume fraction, φ, for **a)** multiwalled carbon nanotubes-doped (MWCNT) ionanofluids; **b)** boron nitride-doped (BN) ionanofluids; **c)** graphite-doped (G) ionanofluids, for $[C_4C_1Im][Dca]$, black, $[C_4C_1Im][NTf_2]$, red, $[C_4C_1Pyrr][NTf_2]$, green, $[C_2C_1Im][C_2SO_4]$, blue, $[C_6C_1Im][PF_6]$, cyan, including Atashrouz, Hamilton and Crosser (H & C), cylindrical Tinga-Leong-Murshed (cT-L-M), spherical Tinga-Leong-Murshed (sT-L-M), Maxwell, and Timofeeva models.

This is not surprising in the case of the Maxwell model because of the assumption of spherical nanoparticles. [228] The possible explanation of the failure of other models may be due to the fact that they do not describe the interactions between nanoparticles and liquid which might shift the thermal conductivity (to higher values, as observed). The model of Atashrouz is based on the modified geometric mean in which the interactions between ILs and nanoparticles are included. [229] Moreover, different types of ILs and nanoparticles were analyzed. As can be observed, this model produces accurate values of enhancement – all of those modelled are statistically comparable to experimental data.

Therefore, this approach seems to be the most reliable and versatile. Moreover, apart from the original work of Atashrouz *et al.* (**2015**), this model is used in this work for the first time, along with the performance evaluation. [229]

After the initial assessment of most reliable model for the ionanofluids thermal conductivity modelling, the calculations as a function of temperature were also performed using the Atashrouz model. Nevertheless, the thermal conductivity of nanoparticles is needed to perform such calculations. The impact of nanoparticles thermal conductivity in Atashrouz model was estimated, and the results are shown in **Figure 3.2.11**.

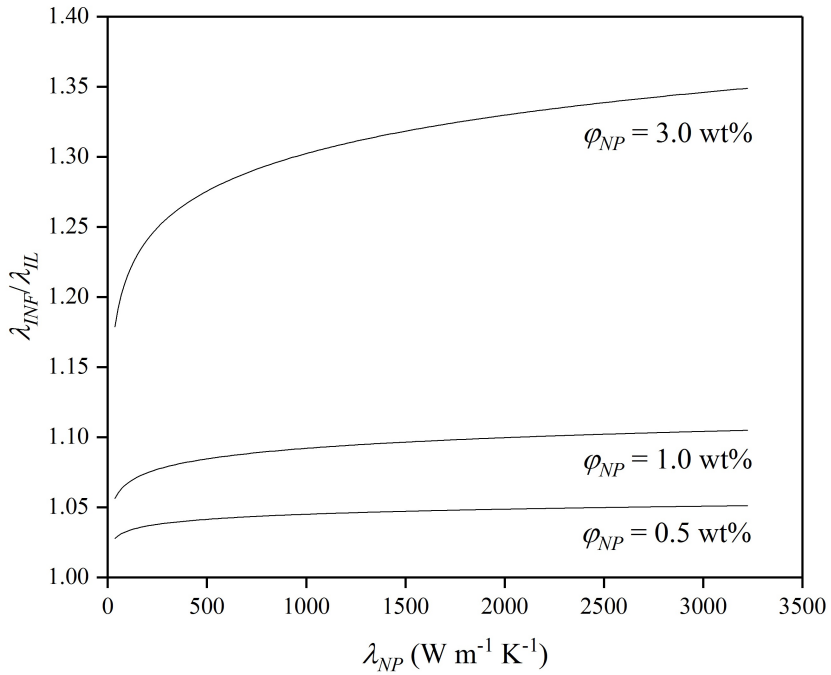

Figure 3.2.11. Impact of nanoparticles thermal conductivity, λ_{NP}, onto the thermal conductivity enhancement, $\lambda_{INF}/\lambda_{IL}$, for investigated volume concentrations of nanoparticles, φ_{NP}. Simulation for Atashrouz model.

As expected, the impact of nanoparticles thermal conductivity is increasing with increasing the concentration, in the logarithmic-function-like shape, becoming less dependent at high nanoparticle thermal conductivity values. Based on the literature on the thermal conductivity as a function of temperature, [212–214, 230] in the range of investigated temperature, (278 – 358) K, the changes in thermal conductivity of nanoparticles are negligible. Therefore, the values of thermal conductivity of nanoparticles at 298.15 K are used for the calculations at higher temperature, up to 358 K, (3223.4, 874.1 and 35.7) W

m^{-1} K^{-1} for carbon nanotubes, [212] boron nitride, [213] and graphite, [214] respectively.

This is also a reasonable explanation for the weak dependence of temperature on the thermal conductivity enhancement values observed in **Figure 3.2.8a**, **Figure 3.2.8b** and **Figure 3.2.8c**. The results of the modelling as a function of temperature are presented in **Figure 3.2.12a**, where the comparison of experimental *vs.* calculated values can be found. The deviations between experimental and calculated values are presented in **Figure 3.2.12b**. The absolute average relative deviation was found as 1.44%, and maximum relative deviations were found as (4.19, -2.06 and 3.92) % for $[C_4C_1Im][NTf_2]$ + 3 wt% MWCNT at 308.15 K, $[C_6C_1Im][PF6]$ + 3 wt% BN at 298.15 K and $[C_4C_1Pyrr][NTf_2]$ + 3 wt% G at 338.15 K, respectively. It should be noticed that the thermal conductivity standard uncertainty was about 3.44%, therefore, the modelled values of enhancement with Atashrouz model were reasonable.

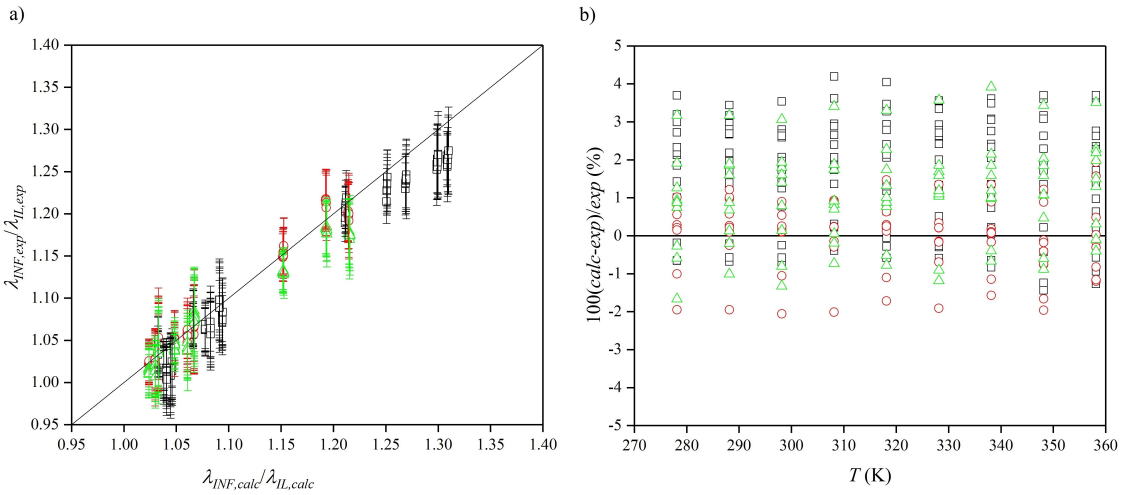

Figure 3.2.12. a) Thermal conductivity enhancement, $\lambda_{INF}/\lambda_{IL}$, calculated *vs.* experimental for whole range of investigated temperature, T; **b)** deviation between calculated and experimental thermal conductivity enhancement, $\lambda_{INF}/\lambda_{IL}$, as a function of the temperature, T. Used model: Atashrouz, for ionanofluids (INF) incorporating multiwalled carbon nanotubes (MWCNT), □, boron nitride (BN), ○, and graphite (G), △.

3.3 Conclusions

In this chapter, an extensive study on density, heat capacity and thermal conductivity of ionic liquid-based nanofluids was carried out. ILs with different cations and anions combinations were chosen for investigations, moreover, as well as using multi-walled carbon nanotubes, which have been studied previously, other nanoparticles types were selected, namely boron nitride and graphite that have not been investigated in such manners, resulting in the deeper insight into the physical properties, in particular the heat capacity and thermal conductivity enhancements.

In terms of density studies, two different models (empirical additive and excess molar volume) were studied, herein. Empirical additive model (primarily proposed by Pak and Cho) was found to be the most reliable in case of ionanofluids. The density of nanoparticles was determined based on the density measurements with the original empirical model proposed by Pak and Cho. Further ionanofluids density calculations were also based on this model. The overall predictive ability was established as accurate enough (near the relative standard uncertainty of density measurement).

Further mechanism of the heat capacity enhancement was also studied. Based on the previous reports on the simple molecular solvents-based nanofluids, the mechanism of the heat capacity enhancement of ionanofluids is probably driven by the existing interfacial nanolayering occurring on the surface of nanoparticles. The possibility of mesolayers overlapping, which was also proposed previously, was not found to be present in this study. Moreover, the heat capacity enhancement is determined by the type of nanoparticles, instead of type of IL. As a bridge to the industrial application of such results, the heat capacity enhancement as a function of temperature showed a high improvement, even up to about 34% in case of graphite-doped ionanofluids, whereas different type of temperature profile of enhancements were presented.

Based on the measurements carried out, the thermal conductivity enhancement of ionic liquid–based nanofluids with carbon nanotubes, boron nitride and graphite, in comparison to pure IL equivalents, was discussed. The enhancements observed were up to about 27% for carbon nanotubes, 22% for boron nitride, and 18% for graphite. The driving force of the enhancement was the type of nanoparticles and the magnitude was dependent on their thermal conductivity (the highest for carbon nanotubes, smaller for boron nitride

and the weakest of graphite). On the other hand, the type of anion in ILs was observed to be another factor influencing the thermal conductivity with more bulky anions leading to higher enhancement values (with $[NTf_2]^-$ as highest, and the weakest for $[Dca]^-$). The enhancements were also compared to literature with average absolute relative deviation of 3.37%. This work also shown that the thermal conductivity enhancement caused by the dispersion of nanoparticles is related to nanoparticles-liquid nanolayering. A theoretical modelling was used to calculate the theoretical enhancement in ionanofluids. Several models were used, however, only one model which was constructed for ionic liquid-based nanofluids (Atashrouz) was found to be the most accurate. As an extension, this model was also used to predict the enhancement at elevated temperature and successfully achieved average absolute relative deviation of 1.44% (with the assumption of independence of nanoparticles thermal conductivity over the temperature).

Bibliography

[1] K. R. SEDDON, A. STARK, and M.-J. TORRES, *Pure and Applied Chemistry* **72**, 2275 (2000).

[2] Y. U. PAULECHKA, A. G. KABO, A. V. BLOKHIN, G. J. KABO, and M. P. SHEVELYOVA, *Journal of Chemical & Engineering Data* **55**, 2719 (2010).

[3] J. JACQUEMIN, P. HUSSON, A. A. H. PADUA, and V. MAJER, *Green Chemistry* **8**, 172 (2006).

[4] J. M. P. FRANÇA, F. REIS, S. I. C. VIEIRA, M. J. V. LOURENÇO, F. J. V. SANTOS, C. A. N. DE CASTRO, and A. A. H. PADUA, *The Journal of Chemical Thermodynamics* **79**, 248 (2014).

[5] M. S. CALADO, A. S. H. BRANCO, J. C. F. DIOGO, J. M. N. A. FARELEIRA, and Z. P. VISAK, *The Journal of Chemical Thermodynamics* **80**, 79 (2015).

[6] G. MCHALE, C. HARDACRE, R. GE, N. DOY, R. W. K. ALLEN, J. M. MACINNES, M. R. BOWN, and M. I. NEWTON, *Analytical Chemistry* **80**, 5806 (2008).

[7] C. M. S. S. NEVES, K. A. KURNIA, J. A. P. COUTINHO, I. M. MARRUCHO, J. N. C. LOPES, M. G. FREIRE, and L. P. N. REBELO, *The Journal of Physical Chemistry B* **117**, 10271 (2013).

[8] L. G. SANCHEZ, J. R. ESPEL, F. ONINK, G. W. MEINDERSMA, and A. B. DE HAAN, *Journal of Chemical & Engineering Data* **54**, 2803 (2009).

[9] R. G. SEOANE, S. CORDERÍ, E. GÓMEZ, N. CALVAR, E. J. GONZÁLEZ, E. A. MACEDO, and Á. DOMÍNGUEZ, *Industrial & Engineering Chemistry Research* **51**, 2492 (2012).

[10] M. B. SHIFLETT, B. A. ELLIOTT, and A. YOKOZEKI, *Fluid Phase Equilibria* **316**, 147 (2012).

[11] A. STOPPA, J. HUNGER, and R. BUCHNER, *Journal of Chemical & Engineering Data* **54**, 472 (2008).

[12] F. XU, H. GAO, H. DONG, Z. WANG, X. ZHANG, B. REN, and S. ZHANG, *Fluid Phase Equilibria* **365**, 80 (2014).

[13] R. YUSOFF, M. K. AROUA, A. SHAMIRI, A. AHMADY, N. S. JUSOH, N. F. ASMUNI, L. C. BONG, and S. H. THEE, *Journal of Chemical & Engineering Data* **58**, 240 (2013).

[14] N. ZEC, M. BEŠTER-ROGAČ, M. VRANEŠ, and S. GADŽURIĆ, *The Journal of Chemical Thermodynamics* **97**, 307 (2016).

[15] O. ZECH, A. STOPPA, R. BUCHNER, and W. KUNZ, *Journal of Chemical & Engineering Data* **55**, 1774 (2010).

[16] N. CALVAR, E. J. GONZÁLEZ, Á. DOMÍNGUEZ, and E. A. MACEDO, *The Journal of Chemical Thermodynamics* **50**, 19 (2012).

[17] S. N. V. K. AKI, B. R. MELLEIN, E. M. SAURER, and J. F. BRENNECKE, *The Journal of Physical Chemistry B* **108**, 20355 (2004).

[18] G. V. S. M. CARRERA, C. A. M. AFONSO, and L. C. BRANCO, *Journal of Chemical and Engineering Data* **55**, 609 (2010).

[19] P. J. CARVALHO, T. REGUEIRA, L. M. SANTOS, J. FERNANDEZ, and J. A. P. COUTINHO, *Journal of Chemical & Engineering Data* **55**, 645 (2009).

[20] C. A. N. DE CASTRO, E. LANGA, A. L. MORAIS, M. L. M. LOPES, M. J. V. LOURENÇO, F. J. V. SANTOS, M. S. C. S. SANTOS, J. N. C. LOPES, H. I. M. VEIGA, and M. MACATRÃO, *Fluid Phase Equilibria* **294**, 157 (2010).

[21] M. ENGELMANN, H. SCHMIDT, J. SAFAROV, J. NOCKE, and E. HASSEL, *Acta Chimica Slovaca* **5**, 86 (2012).

[22] C. K. FOO, C. Y. LEO, R. ARAMESH, M. K. AROUA, N. AGHAMOHAMMADI, M. S. SHAFEEYAN, and A. SHAMIRI, *Journal of Molecular Liquids* **209**, 596 (2015).

[23] C. P. Fredlake, J. M. Crosthwaite, D. G. Hert, S. N. V. K. Aki, and J. F. Brennecke, *Journal of Chemical & Engineering Data* **49**, 954 (2004).

[24] E. J. González, Á. Domínguez, and E. A. Macedo, *Journal of Chemical & Engineering Data* **57**, 2165 (2012).

[25] M. Larriba, P. Navarro, J. García, and F. Rodríguez, *Industrial & Engineering Chemistry Research* **52**, 2714 (2013).

[26] M. Tariq, P. A. S. Forte, M. F. C. Gomes, J. N. C. Lopes, and L. P. N. Rebelo, *The Journal of Chemical Thermodynamics* **41**, 790 (2009).

[27] I. Bahadur, K. Osman, C. Coquelet, P. Naidoo, and D. Ramjugernath, *The Journal of Physical Chemistry B* **119**, 1503 (2015).

[28] M. L. S. Batista, L. I. N. Tomé, C. M. S. S. Neves, J. R. B. Gomes, and J. A. P. Coutinho, *Journal of Molecular Liquids* **192**, 26 (2014).

[29] N. Calvar, I. Domínguez, E. Gómez, J. Palomar, and Á. Domínguez, *The Journal of Chemical Thermodynamics* **67**, 5 (2013).

[30] N. Calvar, B. González, E. Gómez, and Á. Domínguez, *Journal of Chemical & Engineering Data* **53**, 820 (2008).

[31] Y.-Y. Choi, I.-C. Hwang, S.-H. Shin, and S.-J. Park, *Fluid Phase Equilibria* **354**, 59 (2013).

[32] S. Corderí and B. González, *The Journal of Chemical Thermodynamics* **55**, 138 (2012).

[33] I. Domínguez, E. J. González, R. González, and Á. Domínguez, *Journal of Chemical & Engineering Data* **56**, 3376 (2011).

[34] S. V. Dzyuba and R. A. Bartsch, *ChemPhysChem* **3**, 161 (2002).

[35] M. Geppert-Rybczyńska, A. Heintz, J. K. Lehmann, and A. Golus, *Journal of Chemical & Engineering Data* **55**, 4114 (2010).

[36] M. Geppert-Rybczyńska and M. Sitarek, *Journal of Chemical & Engineering Data* **59**, 1213 (2014).

[37] M. F. C. Gomes, L. Pison, A. S. Pensado, and A. A. H. Pádua, *Faraday Discussions* **154**, 41 (2012).

[38] R. Hamidova, I. Kul, J. Safarov, A. Shahverdiyev, and E. Hassel, *Brazilian Journal of Chemical Engineering* **32**, 303 (2015).

[39] K. R. Harris, M. Kanakubo, and L. A. Woolf, *Journal of Chemical & Engineering Data* **52**, 1080 (2007).

[40] Y. Hiraga, A. Kato, Y. Sato, and R. L. Smith Jr, *Journal of Chemical & Engineering Data* **60**, 876 (2015).

[41] J. G. Huddleston, A. E. Visser, W. M. Reichert, H. D. Willauer, G. A. Broker, and R. D. Rogers, *Green Chemistry* **3**, 156 (2001).

[42] J. Jacquemin, P. Husson, V. Majer, and M. F. C. Gomes, *Journal of Solution Chemistry* **36**, 967 (2007).

[43] J. Jacquemin, R. Ge, P. Nancarrow, D. W. Rooney, M. F. Costa Gomes, A. A. H. Pádua, and C. Hardacre, *Journal of Chemical & Engineering Data* **53**, 716 (2008).

[44] J. Jacquemin, P. Husson, V. Mayer, and I. Cibulka, *Journal of Chemical & Engineering Data* **52**, 2204 (2007).

[45] M. Kanakubo and K. R. Harris, *Journal of Chemical & Engineering Data* **60**, 1408 (2015).

[46] M. Kanakubo, T. Makino, and T. Umecky, *Journal of Molecular Liquids* **217**, 112 (2016).

[47] S. Katsuta, Y. Shiozawa, K. Imai, Y. Kudo, and Y. Takeda, *Journal of Chemical & Engineering Data* **55**, 1588 (2009).

[48] M. Krummen, P. Wasserscheid, and J. Gmehling, *Journal of Chemical & Engineering Data* **47**, 1411 (2002).

[49] H. Liu, E. Maginn, A. E. Visser, N. J. Bridges, and E. B. Fox, *Industrial & Engineering Chemistry Research* **51**, 7242 (2012).

[50] N. I. Malek and S. P. Ijardar, *The Journal of Chemical Thermodynamics* **93**, 75 (2016).

[51] H. Matsuda, Y. Norizuki, M. Kawai, K. Kurihara, K. Tochigi, and K. Ochi, *Journal of Solution Chemistry* **43**, 1561 (2014).

[52] M. G. Montalban, C. L. Bolivar, D. Baños, F. Guillermo, and G. Villora, *Journal of Chemical & Engineering Data* **60**, 1986 (2015).

[53] M. B. Oliveira, M. Domínguez-Pérez, O. Cabeza, J. A. Lopes-da Silva, M. G. Freire, and J. A. P. Coutinho, *The Journal of Chemical Thermodynamics* **64**, 22 (2013).

[54] M. B. Oliveira, M. Domínguez-Pérez, M. G. Freire, F. Llovell, O. Cabeza, J. A. Lopes-da Silva, L. F. Vega, and J. A. P. Coutinho, *The Journal of Physical Chemistry B* **116**, 12133 (2012).

[55] A. Pal, M. Saini, and B. Kumar, *Fluid Phase Equilibria* **411**, 66 (2016).

[56] J. Palgunadi, J. E. Kang, D. Q. Nguyen, J. H. Kim, B. K. Min, S. D. Lee, H. Kim, and H. S. Kim, *Thermochimica Acta* **494**, 94 (2009).

[57] M. A. A. Rocha, C. M. S. S. Neves, M. G. Freire, O. Russina, A. Triolo, J. A. P. Coutinho, and L. M. Santos, *The Journal of Physical Chemistry B* **117**, 10889 (2013).

[58] J. Salgado, T. Regueira, L. Lugo, J. Vijande, J. Fernández, and J. García, *The Journal of Chemical Thermodynamics* **70**, 101 (2014).

[59] R. Salinas, J. Pla-Franco, E. Lladosa, and J. B. Montón, *Journal of Chemical & Engineering Data* **60**, 525 (2015).

[60] D. Santos, M. Santos, E. Franceschi, C. Dariva, A. Barison, and S. Mattedi, *Journal of Chemical & Engineering Data* **61**, 348 (2015).

[61] R. G. Seoane, E. J. González, and B. González, *The Journal of Chemical Thermodynamics* **53**, 152 (2012).

[62] H. Shirota, T. Mandai, H. Fukazawa, and T. Kato, *Journal of Chemical & Engineering Data* **56**, 2453 (2011).

[63] S. Singh, I. Bahadur, P. Naidoo, G. Redhi, and D. Ramjugernath, *Journal of Molecular Liquids* **220**, 33 (2016).

[64] M. Součková, J. Klomfar, and J. Pátek, *The Journal of Chemical Thermodynamics* **77**, 31 (2014).

[65] M. Tariq, A. P. Serro, J. L. Mata, B. Saramago, J. M. S. S. Esperança, J. N. C. Lopes, and L. P. N. Rebelo, *Fluid Phase Equilibria* **294**, 131 (2010).

[66] H. Tokuda, S. Tsuzuki, M. A. B. H. Susan, K. Hayamizu, and M. Watanabe, *The Journal of Physical Chemistry B* **110**, 19593 (2006).

[67] J. Troncoso, C. A. Cerdeiriña, Y. A. Sanmamed, L. Romaní, and L. P. N. Rebelo, *Journal of Chemical & Engineering Data* **51**, 1856 (2006).

[68] M. Vraneš, S. Dozic, V. Djeric, and S. Gadžurić, *Journal of Chemical & Engineering Data* **57**, 1072 (2012).

[69] M. Vraneš, S. Papović, A. Tot, N. Zec, and S. Gadžurić, *The Journal of Chemical Thermodynamics* **76**, 161 (2014).

[70] M. Vraneš, N. Zec, A. Tot, S. Papović, S. Dožić, and S. Gadžurić, *The Journal of Chemical Thermodynamics* **68**, 98 (2014).

[71] A. Wandschneider, J. K. Lehmann, and A. Heintz, *Journal of Chemical & Engineering Data* **53**, 596 (2008).

[72] L. Xue, E. Gurung, G. Tamas, Y. P. Koh, M. Shadeck, S. L. Simon, M. Maroncelli, and E. L. Quitevis, *Journal of Chemical & Engineering Data* **61**, 1078 (2016).

[73] Y. Zhang, T. Zhang, P. Gan, H. Li, M. Zhang, K. Jin, and S. Tang, *Journal of Chemical & Engineering Data* **60**, 1706 (2015).

[74] E. Widowati and M.-J. Lee, *The Journal of Chemical Thermodynamics* **63**, 95 (2013).

[75] M. R. Currás, P. Husson, A. A. H. Pádua, M. F. Costa Gomes, and J. García, *Industrial & Engineering Chemistry Research* **53**, 10791 (2014).

[76] J. N. Canongia Lopes, T. C. Cordeiro, J. M. S. S. Esperança, H. J. R. Guedes, S. Huq, L. P. N. Rebelo, and K. R. Seddon, *The Journal of Physical Chemistry B* **109**, 3519 (2005).

[77] J.-M. Andanson, X. Meng, M. Traïkia, and P. Husson, *The Journal of Chemical Thermodynamics* **94**, 169 (2016).

[78] A. E. Andreatta, A. Arce, E. Rodil, and A. Soto, *Journal of Solution Chemistry* **39**, 371 (2010).

[79] A. E. Andreatta, M. Francisco, E. Rodil, A. Soto, and A. Arce, *Fluid Phase Equilibria* **300**, 162 (2011).

[80] A. E. Andreatta, E. Rodil, A. Arce, and A. Soto, *Journal of Solution Chemistry* **43**, 404 (2014).

[81] A. Arce, H. Rodríguez, and A. Soto, *Green Chemistry* **9**, 247 (2007).

[82] L. A. BLANCHARD, Z. GU, and J. F. BRENNECKE, *The Journal of Physical Chemistry B* **105**, 2437 (2001).

[83] N. CALVAR, E. GÓMEZ, B. GONZÁLEZ, and Á. DOMÍNGUEZ, *Journal of Chemical & Engineering Data* **52**, 2529 (2007).

[84] N. CALVAR, B. GONZÁLEZ, E. GÓMEZ, and á. DOMÍNGUEZ, *Journal of Chemical & Engineering Data* **54**, 1004 (2009).

[85] A. P. CARNEIRO, O. RODRÍGUEZ, C. HELD, G. SADOWSKI, and E. A. MACEDO, *Journal of Chemical & Engineering Data* **59**, 2942 (2014).

[86] A. P. CARNEIRO, O. RODRÍGUEZ, and E. A. MACEDO, *The Journal of Chemical Thermodynamics* **55**, 184 (2012).

[87] J. C. F. DIOGO, F. J. P. CAETANO, J. M. N. A. FARELEIRA, and W. A. WAKEHAM, *Fluid Phase Equilibria* **353**, 76 (2013).

[88] J. C. F. DIOGO, F. J. P. CAETANO, J. M. N. A. FARELEIRA, and W. A. WAKEHAM, *International Journal of Thermophysics* **35**, 1615 (2014).

[89] U. DOMAŃSKA and M. LASKOWSKA, *Journal of Solution Chemistry* **37**, 1271 (2008).

[90] A. FERNÁNDEZ, J. GARCÍA, J. S. TORRECILLA, M. OLIET, and F. RODRÍGUEZ, *Journal of Chemical & Engineering Data* **53**, 1518 (2008).

[91] A. P. FRÖBA, H. KREMER, and A. LEIPERTZ, *The Journal of Physical Chemistry B* **112**, 12420 (2008).

[92] F. M. GACIÑO, T. REGUEIRA, L. LUGO, M. J. P. COMUÑAS, and J. FERNÁNDEZ, *Journal of Chemical & Engineering Data* **56**, 4984 (2011).

[93] G. GARCÍA-MIAJA, J. TRONCOSO, and L. ROMANÍ, *Fluid Phase Equilibria* **274**, 59 (2008).

[94] E. GÓMEZ, B. GONZÁLEZ, N. CALVAR, E. TOJO, and Á. DOMÍNGUEZ, *Journal of Chemical & Engineering Data* **51**, 2096 (2006).

[95] B. GONZÁLEZ, N. CALVAR, E. GONZÁLEZ, and Á. DOMÍNGUEZ, *Journal of Chemical & Engineering Data* **53**, 881 (2008).

[96] E. J. GONZÁLEZ, N. CALVAR, I. DOMÍNGUEZ, and Á. DOMÍNGUEZ, *The Journal of Chemical Thermodynamics* **43**, 562 (2011).

[97] E. J. GONZÁLEZ, N. CALVAR, B. GONZÁLEZ, and á. DOMÍNGUEZ, *Journal of Chemical & Engineering Data* **55**, 4931 (2010).

[98] E. J. GONZÁLEZ, B. GONZÁLEZ, N. CALVAR, and Á. DOMÍNGUEZ, *Journal of Chemical & Engineering Data* **52**, 1641 (2007).

[99] T. HOFMAN, A. GOŁDON, A. NEVINES, and T. M. LETCHER, *The Journal of Chemical Thermodynamics* **40**, 580 (2008).

[100] I. C. HWANG, S. J. PARK, and R. H. KWON, *Fluid Phase Equilibria* **316**, 11 (2012).

[101] H.-D. KIM, I.-C. HWANG, and S.-J. PARK, *Journal of Chemical & Engineering Data* **55**, 2474 (2010).

[102] M. LARRIBA, S. GARCÍA, J. GARCÍA, J. S. TORRECILLA, and F. RODRÍGUEZ, *Journal of Chemical & Engineering Data* **56**, 3589 (2011).

[103] D. MATKOWSKA, A. GOŁDON, and T. HOFMAN, *Journal of Chemical & Engineering Data* **55**, 685 (2009).

[104] D. MATKOWSKA and T. HOFMAN, *Journal of Molecular Liquids* **165**, 161 (2012).

[105] A. B. PEREIRO, F. J. DEIVE, J. ESPERANÇA, and A. RODRÍGUEZ, *Fluid Phase Equilibria* **294**, 49 (2010).

[106] A. B. PEREIRO, J. M. M. ARAÚJO, F. S. OLIVEIRA, C. E. S. BERNARDES, J. M. S. S. ESPERANÇA, J. N. C. LOPES, I. M. MARRUCHO, and L. P. N. REBELO, *Chemical Communications* **48**, 3656 (2012).

[107] A. M. PINTO, H. RODRÍGUEZ, A. ARCE, and A. SOTO, *The Journal of Chemical Thermodynamics* **77**, 197 (2014).

[108] E. QUIJADA-MALDONADO, S. VAN DER BOOGAART, J. H. LIJBERS, G. W. MEINDERSMA, and A. B. DE HAAN, *The Journal of Chemical Thermodynamics* **51**, 51 (2012).

[109] D. RABARI, N. PATEL, M. JOSHIPURA, and T. BANERJEE, *Journal of Chemical & Engineering Data* **59**, 571 (2014).

[110] M. S. REDDY, S. M. NAYEEM, K. RAJU, and B. H. BABU, *Journal of Thermal Analysis and Calorimetry* **124**, 959 (2016).

[111] T. REGUEIRA, L. LUGO, and J. FERNÁNDEZ, *The Journal of Chemical Thermodynamics* **48**, 213 (2012).

[112] G. Reyes, M. Cartes, C. Rey-Castro, H. Segura, and A. Mejía, *Journal of Chemical & Engineering Data* **58**, 1203 (2013).

[113] E. Rilo, M. Domínguez-Pérez, J. Vila, L. M. Varela, and O. Cabeza, *The Journal of Chemical Thermodynamics* **49**, 165 (2012).

[114] E. Rilo, L. M. Varela, and O. Cabeza, *Journal of Chemical & Engineering Data* **57**, 2136 (2012).

[115] H. Rodríguez and J. F. Brennecke, *Journal of Chemical & Engineering Data* **51**, 2145 (2006).

[116] S. Seki, S. Tsuzuki, K. Hayamizu, Y. Umebayashi, N. Serizawa, K. Takei, and H. Miyashiro, *Journal of Chemical & Engineering Data* **57**, 2211 (2012).

[117] M. R. Shah, R. Anantharaj, T. Banerjee, and G. D. Yadav, *The Journal of Chemical Thermodynamics* **62**, 142 (2013).

[118] H. Shekaari, M. T. Zafarani-Moattar, and N. J. Behrooz, *The Journal of Chemical Thermodynamics* **86**, 188 (2015).

[119] S. Singh, I. Bahadur, G. G. Redhi, E. E. Ebenso, and D. Ramjugernath, *Journal of Molecular Liquids* **199**, 518 (2014).

[120] L. I. N. Tomé, P. J. Carvalho, M. G. Freire, I. M. Marrucho, I. M. A. Fonseca, A. G. M. Ferreira, J. A. P. Coutinho, and R. L. Gardas, *Journal of Chemical & Engineering Data* **53**, 1914 (2008).

[121] J. S. Torrecilla, J. Palomar, J. García, and F. Rodríguez, *Journal of Chemical & Engineering Data* **54**, 1297 (2009).

[122] J. Vila, P. Gines, E. Rilo, O. Cabeza, and L. M. Varela, *Fluid Phase Equilibria* **247**, 32 (2006).

[123] C.-L. Wong, A. N. Soriano, and M.-H. Li, *Fluid Phase Equilibria* **271**, 43 (2008).

[124] J.-Z. Yang, X.-M. Lu, J.-S. Gui, W.-G. Xu, and H.-W. Li, *The Journal of Chemical Thermodynamics* **37**, 1250 (2005).

[125] H. Schmidt, M. Stephan, J. Safarov, I. Kul, J. Nocke, I. M. Abdulagatov, and E. Hassel, *The Journal of Chemical Thermodynamics* **47**, 68 (2012).

[126] L. Alonso, A. Arce, M. Francisco, and A. Soto, *Fluid Phase Equilibria* **270**, 97 (2008).

[127] E. J. González, P. F. Requejo, Á. Domínguez, and E. A. Macedo, *Journal of Solution Chemistry* **42**, 746 (2013).

[128] K. R. Harris, L. A. Woolf, M. Kanakubo, and T. Rüther, *Journal of Chemical & Engineering Data* **56**, 4672 (2011).

[129] J. Jacquemin, P. Nancarrow, D. W. Rooney, M. F. Costa Gomes, P. Husson, V. Majer, A. A. H. Pádua, and C. Hardacre, *Journal of Chemical & Engineering Data* **53**, 2133 (2008).

[130] R. Kato and J. Gmehling, *The Journal of Chemical Thermodynamics* **37**, 603 (2005).

[131] J. Kumełan, D. Tuma, Á. Pérez-Salado Kamps, and G. Maurer, *Journal of Chemical & Engineering Data* **55**, 165 (2009).

[132] T. Makino, M. Kanakubo, T. Umecky, A. Suzuki, T. Nishida, and J. Takano, *Journal of Chemical & Engineering Data* **57**, 751 (2012).

[133] F. Mutelet, E.-S. R. E. Hassan, T. W. Stephens, W. E. Acree Jr, and G. A. Baker, *Journal of Chemical & Engineering Data* **58**, 2210 (2013).

[134] A. B. Pereiro, H. I. M. Veiga, J. M. S. S. Esperança, and A. Rodríguez, *The Journal of Chemical Thermodynamics* **41**, 1419 (2009).

[135] T. Regueira, L. Lugo, and J. Fernández, *The Journal of Chemical Thermodynamics* **58**, 440 (2013).

[136] R. G. Seoane, E. Gómez, E. J. González, and Á. Domínguez, *The Journal of Chemical Thermodynamics* **47**, 402 (2012).

[137] M. Shamsipur, A. A. M. Beigi, M. Teymouri, S. M. Pourmortazavi, and M. Irandoust, *Journal of Molecular Liquids* **157**, 43 (2010).

[138] M. Vraneš, A. Tot, S. Papović, N. Zec, S. Dožić, and S. Gadžurić, *The Journal of Chemical Thermodynamics* **81**, 66 (2015).

[139] D. R. MacFarlane, P. Meakin, J. Sun, N. Amini, and M. Forsyth, *The Journal of Physical Chemistry B* **103**, 4164 (1999).

[140] K. Řehák, P. Morávek, and M. Strejc, *Fluid Phase Equilibria* **316**, 17 (2012).

[141] J. L. Anthony, J. L. Anderson, E. J. Maginn, and J. F. Brennecke, *The Journal of Physical Chemistry B* **109**, 6366 (2005).

[142] Y. Deng, P. Husson, A.-M. Delort, P. Besse-Hoggan, M. Sancelme, and M. F. Costa Gomes, *Journal of Chemical & Engineering Data* **56**, 4194 (2011).

[143] R. L. Gardas, H. F. Costa, M. G. Freire, P. J. Carvalho, I. M. Marrucho, I. M. A. Fonseca, A. G. M. Ferreira, and J. A. P. Coutinho, *Journal of Chemical & Engineering Data* **53**, 805 (2008).

[144] M. Geppert-Rybczyńska, J. K. Lehmann, and A. Heintz, *The Journal of Chemical Thermodynamics* **71**, 171 (2014).

[145] T. M. Letcher and P. Reddy, *The Journal of Chemical Thermodynamics* **37**, 415 (2005).

[146] R. Ge, C. Hardacre, J. Jacquemin, P. Nancarrow, and D. W. Rooney, *Journal of Chemical & Engineering Data* **53**, 2148 (2008).

[147] N. I. Malek, A. Singh, R. Surati, and S. P. Ijardar, *The Journal of Chemical Thermodynamics* **74**, 103 (2014).

[148] A. Muhammad, M. I. A. Mutalib, C. D. Wilfred, T. Murugesan, and A. Shafeeq, *The Journal of Chemical Thermodynamics* **40**, 1433 (2008).

[149] H. Ning, M. Hou, Q. Mei, Y. Liu, D. Yang, and B. Han, *Science China Chemistry* **55**, 1509 (2012).

[150] A. Pal and B. Kumar, *Fluid Phase Equilibria* **334**, 157 (2012).

[151] A. B. Pereiro and A. Rodriguez, *The Journal of Chemical Thermodynamics* **39**, 978 (2007).

[152] A. B. Pereiro, E. Tojo, A. Rodriguez, J. Canosa, and J. Tojo, *The Journal of Chemical Thermodynamics* **38**, 651 (2006).

[153] A. B. Pereiro and A. Rodríguez, *Journal of Chemical & Engineering Data* **52**, 600 (2007).

[154] M. A. A. Rocha, F. M. S. Ribeiro, A. I. M. C. L. Ferreira, J. A. P. Coutinho, and L. M. Santos, *Journal of Molecular Liquids* **188**, 196 (2013).

[155] M. S. AlTuwaim, K. H. A. E. Alkhaldi, A. S. Al-Jimaz, and A. A. Mohammad, *Journal of Chemical & Engineering Data* **59**, 1955 (2014).

[156] R. L. Gardas, M. G. Freire, P. J. Carvalho, I. M. Marrucho, I. M. A. Fonseca, A. G. M. Ferreira, and J. A. P. Coutinho, *Journal of Chemical & Engineering Data* **52**, 80 (2007).

[157] J. Klomfar, M. Součková, and J. Pátek, *Journal of Chemical & Engineering Data* **59**, 2263 (2014).

[158] J.-G. Li, Y.-F. Hu, S. Ling, and J.-Z. Zhang, *Journal of Chemical & Engineering Data* **56**, 3068 (2011).

[159] J. Saien, M. M. S. Badieh, M. Norouzi, and S. Salehzadeh, *The Journal of Chemical Thermodynamics* **91**, 404 (2015).

[160] K. R. Seddon, A. Stark, and M.-J. Torres, *ACS Publications* **819**, 34 (2002).

[161] R. Taguchi, H. Machida, Y. Sato, and R. L. Smith Jr, *Journal of Chemical & Engineering Data* **54**, 22 (2008).

[162] D. Tomida, A. Kumagai, S. Kenmochi, K. Qiao, and C. Yokoyama, *Journal of Chemical & Engineering Data* **52**, 577 (2007).

[163] Z. Vaid, U. More, S. P. Ijardar, and N. I. Malek, *The Journal of Chemical Thermodynamics* **86**, 143 (2015).

[164] Z. Vaid, U. U. More, R. L. Gardas, N. I. Malek, and S. P. Ijardar, *Journal of Solution Chemistry* **44**, 718 (2015).

[165] G. Vakili-Nezhaad, M. Vatani, M. Asghari, and I. Ashour, *The Journal of Chemical Thermodynamics* **54**, 148 (2012).

[166] B. D. Fitchett, T. N. Knepp, and J. C. Conboy, *Journal of the ElectroChemical Society* **151**, E219 (2004).

[167] N. Calvar, E. Gómez, E. A. Macedo, and Á. Domínguez, *Thermochimica Acta* **565**, 178 (2013).

[168] P. Navarro, M. Larriba, E. Rojo, J. García, and F. Rodríguez, *Journal of Chemical & Engineering Data* **58**, 2187 (2013).

[169] E. Gómez, N. Calvar, Á. Domínguez, and E. A. Macedo, *Industrial & Engineering Chemistry Research* **52**, 2103 (2013).

[170] T. Makino, M. Kanakubo, Y. Masuda, and H. Mukaiyama, *Journal of Solution Chemistry* **43**, 1601 (2014).

[171] M. A. A. Rocha, M. Bastos, J. A. P. Coutinho, and L. M. Santos, *The Journal of Chemical Thermodynamics* **53**, 140 (2012).

[172] Y. Shimizu, Y. Ohte, Y. Yamamura, and K. Saito, *Chemistry Letters* **36**, 1484 (2007).

[173] E. Zorębski, M. Zorębski, M. Dzida, P. Goodrich, and J. Jacquemin, *Industrial & Engineering Chemistry Research* **56**, 2592 (2017).

[174] A. V. Blokhin, Y. U. Paulechka, A. A. Strechan, and G. J. Kabo, *The Journal of Physical Chemistry B* **112**, 4357 (2008).

[175] J. D. Holbrey, W. M. Reichert, R. G. Reddy, and R. D. Rogers, *Ionic Liquids as Green Solvents*, ACS Publications, Washington, D.C., USA, 2003.

[176] L. E. Ficke, H. Rodríguez, and J. F. Brennecke, *Journal of Chemical & Engineering Data* **53**, 2112 (2008).

[177] Y. U. Paulechka, A. V. Blokhin, and G. J. Kabo, *Thermochimica Acta* **604**, 122 (2015).

[178] Y.-H. Yu, A. N. Soriano, and M.-H. Li, *The Journal of Chemical Thermodynamics* **41**, 103 (2009).

[179] Z.-H. Zhang, Z.-C. Tan, L.-X. Sun, Y. Jia-Zhen, X.-C. Lv, and Q. Shi, *Thermochimica Acta* **447**, 141 (2006).

[180] A. Fernandez, J. S. Torrecilla, J. García, and F. Rodríguez, *Journal of Chemical & Engineering Data* **52**, 1979 (2007).

[181] G. Chatel, L. Leclerc, E. Naffrechoux, C. Bas, N. Kardos, C. Goux-Henry, B. Andrioletti, and M. Draye, *Journal of Chemical & Engineering Data* **57**, 3385 (2012).

[182] C. J. Rao, R. V. Krishnan, K. A. Venkatesan, K. Nagarajan, and T. G. Srinivasan, *Journal of Thermal Analysis and Calorimetry* **97**, 937 (2009).

[183] A. Diedrichs and J. Gmehling, *Fluid Phase Equilibria* **244**, 68 (2006).

[184] G. Höhne, W. Hemminger, and H. J. Flammersheim, *Differential Scanning Calorimetry: An Introduction for Practitioners*, Springer-Verlag, Berlin, Germany, 1996.

[185] N. Zhao, J. Jacquemin, R. Oozeerally, and V. Degirmenci, *Journal of Chemical & Engineering Data* **61**, 2160 (2016).

[186] R. Ge, C. Hardacre, P. Nancarrow, and D. W. Rooney, *Journal of Chemical & Engineering Data* **52**, 1819 (2007).

[187] H. Chen, Y. He, J. Zhu, H. Alias, Y. Ding, P. Nancarrow, C. Hardacre, D. Rooney, and C. Tan, *International Journal of Heat and Fluid Flow* **29**, 149 (2008).

[188] A. P. Fröba, M. H. Rausch, K. Krzeminski, D. Assenbaum, P. Wasserscheid, and A. Leipertz, *International Journal of Thermophysics* **31**, 2059 (2010).

[189] Q.-L. Chen, K.-J. Wu, and C.-H. He, *Journal of Chemical & Engineering Data* **58**, 2058 (2013).

[190] C. A. Nieto de Castro, M. J. V. Lourenço, A. P. C. Ribeiro, E. Langa, S. I. C. Vieira, P. Goodrich, and C. Hardacre, *Journal of Chemical & Engineering Data* **55**, 653 (2009).

[191] D. Tomida, S. Kenmochi, T. Tsukada, K. Qiao, and C. Yokoyama, *International Journal of Thermophysics* **28**, 1147 (2007).

[192] D. Tomida, S. Kenmochi, T. Tsukada, and C. Yokoyama, *Heat Transfer—Asian Research* **36**, 361 (2007).

[193] J. M. P. França, S. I. C. Vieira, M. J. V. Lourenço, S. M. S. Murshed, and C. A. Nieto de Castro, *Journal of Chemical & Engineering Data* **58**, 467 (2013).

[194] C.-J. Ho, M. W. Chen, and Z. W. Li, *International Journal of Heat and Mass Transfer* **51**, 4506 (2008).

[195] E. Abu-Nada, *International Journal of Heat and Fluid Flow* **30**, 679 (2009).

[196] C. N. de Castro, A. P. C. Ribeiro, S. I. C. Vieira, J. M. P. França, M. J. V. Lourenço, F. V. Santos, S. M. S. Murshed, P. Goodrich, and C. Hardacre, *Synthesis, Properties and Physical Applications of IoNanofluids*, InTech, London, The United Kingdom, 2013.

[197] R. S. VAJJHA, D. K. DAS, and B. M. MAHAGAONKAR, *Petroleum Science and Technology* **27**, 612 (2009).

[198] M. T. ZAFARANI-MOATTAR and R. MAJDAN-CEGINCARA, *The Journal of Chemical Thermodynamics* **54**, 55 (2012).

[199] M. J. PASTORIZA-GALLEGO, L. LUGO, J. L. LEGIDO, and M. M. PIÑEIRO, *Journal of Applied Physics* **110**, 14309 (2011).

[200] B. C. PAK and Y. I. CHO, *Experimental Heat Transfer an International Journal* **11**, 151 (1998).

[201] D. SHIN and D. BANERJEE, *International Journal of Heat and Mass Transfer* **54**, 1064 (2011).

[202] R. HENTSCHKE, *Nanoscale Research Letters* **11**, 88 (2016).

[203] J. FRANÇA, C. A. N. DE CASTRO, and A. A. H. PADUA, *Physical Chemistry Chemical Physics* **19**, 17075 (2017).

[204] S.-Q. ZHOU and R. NI, *Applied Physics Letters* **92**, 93123 (2008).

[205] L. WANG, Z. TAN, S. MENG, D. LIANG, and G. LI, *Journal of Nanoparticle Research* **3**, 483 (2001).

[206] G. HUMMER, J. C. RASAIAH, and J. P. NOWORYTA, *Nature* **414**, 188 (2001).

[207] T. MORIMOTO and K. MIURA, *Langmuir* **1**, 658 (1985).

[208] G. GIOVANNETTI, P. A. KHOMYAKOV, G. BROCKS, P. J. KELLY, and J. VAN DEN BRINK, *Physical Review B* **76**, 73103 (2007).

[209] R. C. ZELLER and R. O. POHL, *Physical Review B* **4**, 2029 (1971).

[210] I. H. EL-SAYED, X. HUANG, and M. A. EL-SAYED, *Nano Letters* **5**, 829 (2005).

[211] R. MARCHIORI, *Nanostructures*, Elsevier, Amsterdam, Netherlands, 2016.

[212] P. KIM, L. SHI, A. MAJUMDAR, and P. L. MCEUEN, *Physica B: Condensed Matter* **323**, 67 (2002).

[213] E. K. SICHEL, R. E. MILLER, M. S. ABRAHAMS, and C. J. BUIOCCHI, *Physical Review B* **13**, 4607 (1976).

[214] R. TAYLOR, *Philosophical Magazine* **13**, 157 (1966).

[215] X.-Q. WANG and A. S. MUJUMDAR, *International Journal of Thermal Sciences* **46**, 1 (2007).

[216] S. KAKAÇ and A. PRAMUANJAROENKIJ, *International Journal of Heat and Mass Transfer* **52**, 3187 (2009).

[217] V. TRISAKSRI and S. WONGWISES, *Renewable and Sustainable Energy Reviews* **11**, 512 (2007).

[218] W. YU, D. M. FRANCE, J. L. ROUTBORT, and S. U. S. CHOI, *Heat Transfer Engineering* **29**, 432 (2008).

[219] S. ÖZERINÇ, S. KAKAÇ, and A. G. YAZICIOĞLU, *Microfluidics and Nanofluidics* **8**, 145 (2010).

[220] C. KLEINSTREUER and Y. FENG, *Nanoscale Research Letters* **6**, 1 (2011).

[221] V. K. PARUCHURI, A. V. NGUYEN, and J. D. MILLER, *Colloids and Surfaces A: PhysicoChemical and Engineering Aspects* **250**, 519 (2004).

[222] W. LEI, V. N. MOCHALIN, D. LIU, S. QIN, Y. GOGOTSI, and Y. CHEN, *Nature Communications* **6**, 8849 (2015).

[223] B. WHITE, S. BANERJEE, S. O'BRIEN, N. J. TURRO, and I. P. HERMAN, *The Journal of Physical Chemistry C* **111**, 13684 (2007).

[224] B. OUYANG and J. SONG, *Applied Physics Letters* **103**, 102401 (2013).

[225] W. YU and H. XIE, *Journal of NanoMaterials* **2012**, 1 (2012).

[226] Y. LI, S. TUNG, E. SCHNEIDER, and S. XI, *Powder Technology* **196**, 89 (2009).

[227] Z. HADDAD, C. ABID, H. F. OZTOP, and A. MATAOUI, *International Journal of Thermal Sciences* **76**, 168 (2014).

[228] J. C. MAXWELL, *A Treatise on Electricity and Magnetism*, Clarendon Press, Wotton-Under-Edge, The United Kingdom, 1881.

[229] S. ATASHROUZ, M. MOZAFFARIAN, and G. PAZUKI, *Industrial & Engineering Chemistry Research* **54**, 8600 (2015).

[230] S. BERBER, Y.-K. KWON, and D. TOMÁNEK, *Physical Review Letters* **84**, 4613 (2000).

Chapter 4

Pure and Water-Saturated Trihexyl(tetradecyl)phosphonium Ionic Liquids

4.1 Water Solubility

The results of liquid-liquid equilibrium (LLE) experiment at 298.2 K are reported in **Table 4.1.1**. The trend in the water mass fraction in the ILs is as follows: $[ButO]^-$ > $[HexO]^-$ > $[OctO]^-$ > $[DecO]^-$. As expected, there is a small decrease in the solubility of water in the ILs with the elongation of anion carbon chain length due to increasing hydrophobicity. The LLE results for $[P_{14,6,6,6}][AcO]$ were not included in these studies because this IL was found to be significantly more soluble in water than other investigated ILs limiting its use as a HTF (*i.e.* liquid range or freezing point). To the best of our knowledge, there are only two reports on the solubility of only one of the investigated ILs, namely $[P_{14,6,6,6}][DecO]$. Freire *et al.* (**2008**) [1] reported the LLE point as 0.864 ± 0.005 (water mole fraction), Neves *et al.* (**2011**) [2] established this point as 0.872 ± 0.040 (water mole fraction), while in this work the value is 0.8570 ± 0.0022 (water mole fraction). Nevertheless, the LLE point was only measured at 298.2 K, whereas the physical properties were investigated over a wide temperature range (up to 368.2 K). Thus, the physical properties are reported from 298.15 K as the lowest temperature. Moreover, Neves *et al.* (**2011**) [2] investigated water solubility in ILs as a function of temperature, and therein it was shown that this increased with temperature. Therefore, there is no need to investigate the solubility for ILs in this work at the higher temperatures, and the physical properties can be still reported at these temperatures as no heterogeneous mixture were observed, as expected. Furthermore, as the LLE point at elevated temperature is higher than at determined at 298.15 K, the water-saturated term is not applicable at temperatures

higher than 298.15 K.

Table 4.1.1. Water contents for pure and IL+water mixtures (including liquid-liquid equilibrium points) used in this work, at T = (298.2 ± 0.1) K, and p = (101 ± 2) kPa

	Mass fraction × 10^2	Mole fraction
$[P_{14,6,6,6}][AcO]$	0.050 ± 0.022	0.0148 ± 0.0065
$[P_{14,6,6,6}][ButO]$	0.090 ± 0.017	0.0278 ± 0.0051
$[P_{14,6,6,6}][ButO] + H_2O$	16.680 ± 0.060	0.8638 ± 0.0010
$[P_{14,6,6,6}][HexO]$	0.061 ± 0.013	0.0199 ± 0.0042
$[P_{14,6,6,6}][HexO] + H_2O$	15.825 ± 0.057	0.8621 ± 0.0010
$[P_{14,6,6,6}][OctO]$	0.055 ± 0.011	0.0188 ± 0.0037
$[P_{14,6,6,6}][OctO] + H_2O$	14.783 ± 0.049	0.8579 ± 0.0092
$[P_{14,6,6,6}][DecO]$	0.030 ± 0.009	0.0108 ± 0.0032
$[P_{14,6,6,6}][DecO] + H_2O$	14.150 ± 0.051	0.8570 ± 0.0022

4.2 Density and Derived Properties

The experimental data for density of neat ILs and mixtures with water are reported in **Table CD4.1** (Appendix CD4). To the best of our knowledge, there are only four reports of the density for pure $[P_{14,6,6,6}][AcO]$ and pure $[P_{14,6,6,6}][DecO]$, and mixture with water. [2–5] The relative deviations between data in this work and those reported in the literature are (-0.37 [3], -0.45 [4], -0.98 [5]) % for pure $[P_{14,6,6,6}][AcO]$, 0.38% for pure $[P_{14,6,6,6}][DecO]$ [8], and 0.23% for $[P_{14,6,6,6}][DecO] + H_2O$ [2], at 298.15 K, also shown in **Figure 4.2.1a**. Nevertheless, it was reported that residual solvent and/or halide can affect the density, see for example Seddon *et al.* (**2000**). [6] Only the work of Tariq *et al.* (**2009**) [3] reports the chloride content (which was from 20 to 150 ppm, in comparison to values in this work – below 5 ppm). Moreover, the $[P_{14,6,6,6}][AcO]$ from the work of Esperança *et al.* (**2006**) [4] has been acquired from the same source as in Tariq *et al.* (**2009**), [3] which results in consistent results of high chloride content (*e.g.* inducing a potential decrease on the IL density especially by comparing the density of $[P_{14,6,6,6}]Cl$ *vs.* those reported herein). [7] Similar trends can be observed in work of Fillion *et al.* (**2016**) [5] In contrast, the density in work of Neves *et al.* (**2011**) [2] is higher, together with the water content (almost 3 times higher), which is in a good agreement with work of Seddon *et al.* (**2000**) [6] and the dependence of density on water content. The data reported in this work represent the highest quality with a very low amount of chloride, as well as water content reported, to date. The data are shown in **Figure 4.2.1b** for all the pure ILs and mixtures with water studied, herein.

The coefficients of equation (2.2.42), $\rho(T)$, are reported in **Table 4.2.1**. Based on the previous literature reports, the linear equation is sufficient enough to describe such dependence. [2, 8, 9] The density was a decreasing function of temperature, while the difference between the lowest (298.15 K) and the highest temperature (363.15 K) are similar for all ILs, (4.67, 4.72, 4.74, 4.73 and 4.76) % for $[P_{14,6,6,6}][AcO]$, $[P_{14,6,6,6}][ButO]$, $[P_{14,6,6,6}][HexO]$, $[P_{14,6,6,6}][OctO]$ and $[P_{14,6,6,6}][DecO]$, respectively.

In comparison to other ILs, the density in this work represent relatively low values, for example (1437.9, 1253.9, 1015.7 or 1181.8) kg m^{-3} for 1-butyl-3-methylimidazolium bis[(trifluoromethyl)sulfonyl]imide, [10] 1-butyl-1-methylpyrrolidinium trifluoromethanesulfonate, [11] tributylmethylammonium L-serinate, [12] or trihexyl(tetradecyl)phosphonium

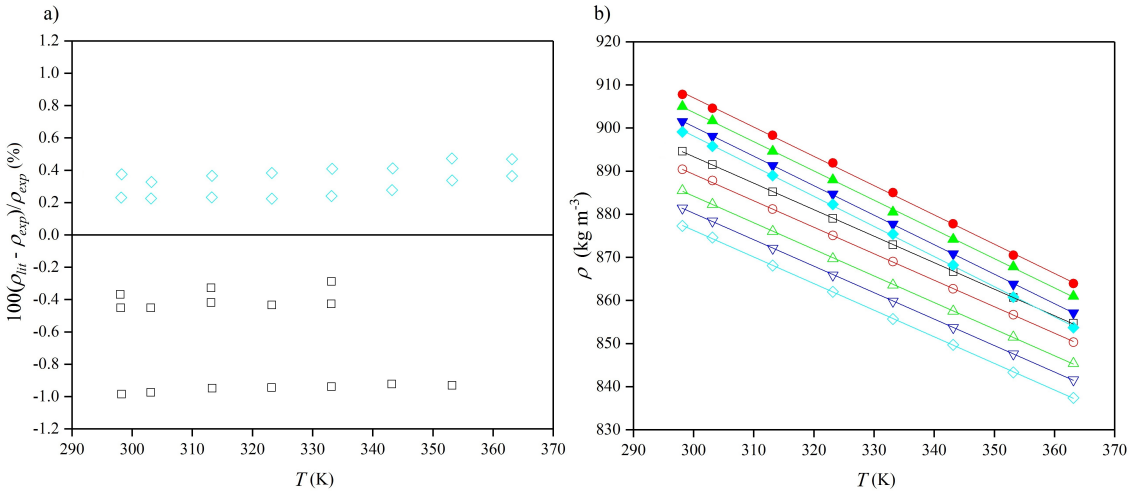

Figure 4.2.1. a) Density deviations, $100(\rho_{lit} - \rho_{exp})/\rho_{exp}$, between data in this work, ρ_{exp}, and literature, ρ_{lit}, as a function of the temperature, T; **b)** density, ρ, as a function of the temperature, T, for $[P_{14,6,6,6}][AcO]$, □ [3–5], $[P_{14,6,6,6}][ButO]$, ○, $[P_{14,6,6,6}][HexO]$, △, $[P_{14,6,6,6}][OctO]$, ▽, $[P_{14,6,6,6}][DecO]$, ◇ [2], $[P_{14,6,6,6}][ButO]$ + 16.680 H_2O wt%, ●, $[P_{14,6,6,6}][HexO]$ + 15.825 H_2O wt%, ▲, $[P_{14,6,6,6}][OctO]$ + 14.783 H_2O wt%, ▼, $[P_{14,6,6,6}][DecO]$ + 14.150 H_2O wt%, ◆ [2].

Table 4.2.1. Coefficients and their standard uncertainties, a_0, a_1, δa_0 and δa_1, of equation (2.2.42), $\rho(T)$, for pure ILs and mixtures with water, including coefficient of determination, R^2.

	$-(a_1 \pm \delta a_1) \times 10^3$ (kg m^{-3} K^{-1})	$a_0 \pm \delta a_0$ (kg m^{-3})	R^2
$[P_{14,6,6,6}][AcO]$	615 ± 2	1077.8 ± 0.5	0.99995
$[P_{14,6,6,6}][ButO]$	614 ± 4	1073.6 ± 0.1	0.99997
$[P_{14,6,6,6}][HexO]$	617 ± 2	1069.3 ± 0.7	0.99991
$[P_{14,6,6,6}][OctO]$	614 ± 1	1064.4 ± 0.4	0.99996
$[P_{14,6,6,6}][DecO]$	617 ± 2	1061.4 ± 0.7	0.99991
$[P_{14,6,6,6}][ButO]$ + 16.680 H_2O wt%	679 ± 7	1111 ± 2	0.99922
$[P_{14,6,6,6}][HexO]$ + 15.825 H_2O wt%	678 ± 5	1107 ± 2	0.99960
$[P_{14,6,6,6}][OctO]$ + 14.783 H_2O wt%	684 ± 2	1106 ± 1	0.99994
$[P_{14,6,6,6}][DecO]$ + 14.150 H_2O wt%	699 ± 5	1108 ± 2	0.99962

tris(pentafluoroethyl)trifluorophosphate [13] at 298.15 K, while the values in this work are (894.6, 890.4, 885.5, 881.4 and 877.3) kg m^{-3} for $[P_{14,6,6,6}][AcO]$, $[P_{14,6,6,6}][ButO]$, $[P_{14,6,6,6}][HexO]$, $[P_{14,6,6,6}][OctO]$ and $[P_{14,6,6,6}][DecO]$ at 298.15 K, respectively. In terms of commercial HTFs, the comparison depends on the type of material, for example the values in this work are similar to synthetic aromatic hydrocarbon mixtures (*i.e.* Therminol ADX10 or Dynalene SF), slightly lower than water, or significantly lower than glycol-

based HTFs (for example Dowtherm 4000 or Dynalene EG series).

As expected, density depends on the anion chain length with the following sequence: $[AcO]^-$ > $[ButO]^-$ > $[HexO]^-$ > $[OctO]^-$ > $[DecO]^-$, and the same sequence was found for mixtures with water. The densities for pure ILs are lower than the density of water, (10-13) %, and mixtures with water of 2%. Thus, the density for mixtures with water was higher than for pure ILs, as expected. The extent of the increase for the mixtures with water density in comparison to their pure analogues is shown in **Figure 4.2.2**.

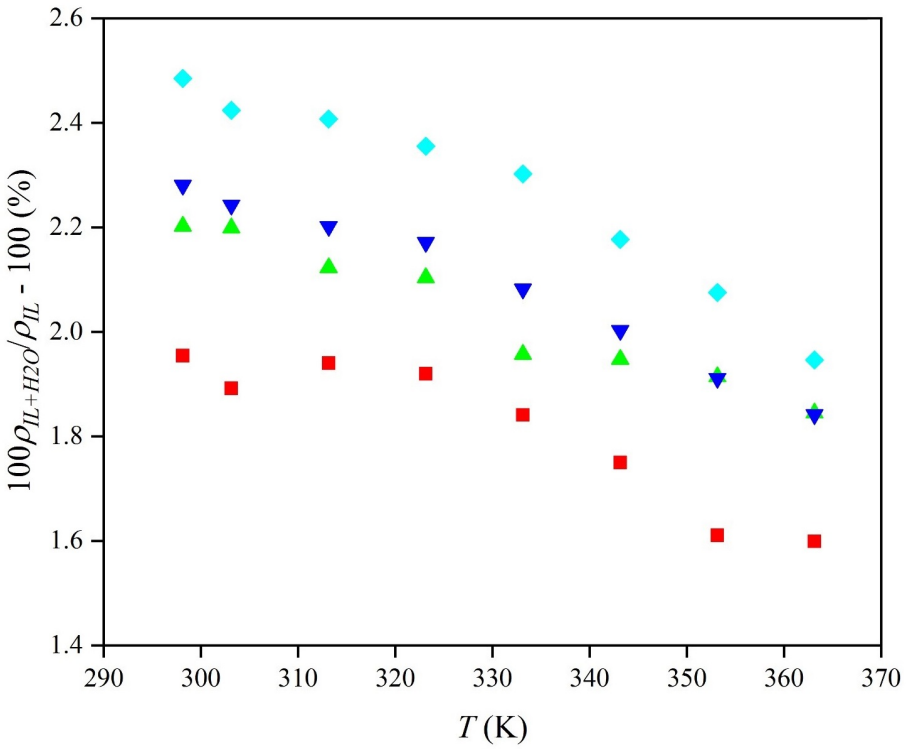

Figure 4.2.2. Density enhancement of ILs + H_2O, ρ_{IL+H_2O}/ρ_{IL}, in comparison to pure ILs, as a function of the temperature, T, for $[P_{14,6,6,6}][ButO]$ + 16.680 H_2O wt%, ●, $[P_{14,6,6,6}][HexO]$ + 15.825 H_2O wt%, ▲, $[P_{14,6,6,6}][OctO]$ + 14.783 H_2O wt%, ▼, $[P_{14,6,6,6}][DecO]$ + 14.150 H_2O wt%, ♦.

All values were approximately (1.6-2.5) % higher, while a maximum was found for $[P_{14,6,6,6}][DecO]$ as 2.48% (at 298.15 K). Jacquemin *et al.* (**2006**) [8] investigated 1-alkyl-3-methylimidazolium-based ILs and reported the decreasing of the density by 1.3%, while the pure ILs were denser than water. Trihexyl(tetradecyl)phosphonium-based mixtures with water were also investigated by Neves *et al.* (**2011**) [2] The deviations between neat ILs and mixtures with water were reported as (0-2) %. For practical industrial

heat transfer processes, materials with higher densities are desired due to their influence on the volumetric heat capacity, and thus achieving better performance in heat storage.

From the density data, the thermal expansion coefficients were calculated (equation (2.2.37)), and reported in **Table CD4.2** (Appendix CD4). The relative deviation between the values in this work and Neves *et al.* (**2011**) [2] are 1.68% and 0.29%, for the pure $[P_{14,6,6,6}]$[DecO] and mixture with water, respectively. However, it must be noted that, for mixtures with water, the behavior of water in thermal expansion coefficient becomes dominant, thus the relative deviation is smaller. Furthermore, these values are calculated based on the differentiation of $\rho(T)$, which means that the uncertainties are propagated and that numerical artifacts can appear, as indicated by Troncoso *et al.* (**2009**). [14] **Figure 4.2.3a** shows the thermal expansion coefficient as a function of temperature for all the pure ILs and mixtures with water studied, herein. The thermal expansion coefficient increases with temperature for pure ILs mixtures with water. For the pure ILs the differences between each IL studied are increasing with the anion chain length, however, the changes are very small, so it can be assumed (based on standard uncertainty) that they have the same value of isobaric thermal expansion coefficient. For the mixtures with water, the water enhances the thermal expansion of ILs. The values of isobaric thermal expansion coefficient reported in many other reports exhibit values of (5-7) $\times 10^{-4}$ K^{-1}. For example, Martins *et al.* (**2016**) [15] studied the symmetric and asymmetric pure imidazolium-based ILs mixtures with water with a bis[(trifluoromethyl)sulfonyl]imide anion. Therein, very small deviations up to 4.44% were reported comparing the pure ILs and mixtures with water with values of (6.63-7.003) $\times 10^{-4}$ K^{-1}.

The excess molar volumes of the mixtures with water were also investigated as a function of the temperature (**Figure 4.2.3b** and **Table CD4.3** in Appendix CD4). At lower temperatures, the excess molar volume is negative. The negative values may be caused by hydrogen bonding created between the carboxylate anion and water. It may also be caused by stronger attraction forces between the cation and the anion. It has also been previously reported that the negative excess volumes can indicate an amphiphilic and/or more polar character of binary mixture [47]. However, when temperature is increased, the excess molar volume becomes less negative, which indicates a weaker attraction between cation and anion. At (318.9, 332.4, 352.2 and ~367.8) K for $[P_{14,6,6,6}]$[ButO], $[P_{14,6,6,6}]$[HexO], $[P_{14,6,6,6}]$[OctO] and $[P_{14,6,6,6}]$[DecO] (value extrapolated), respectively, the excess molar

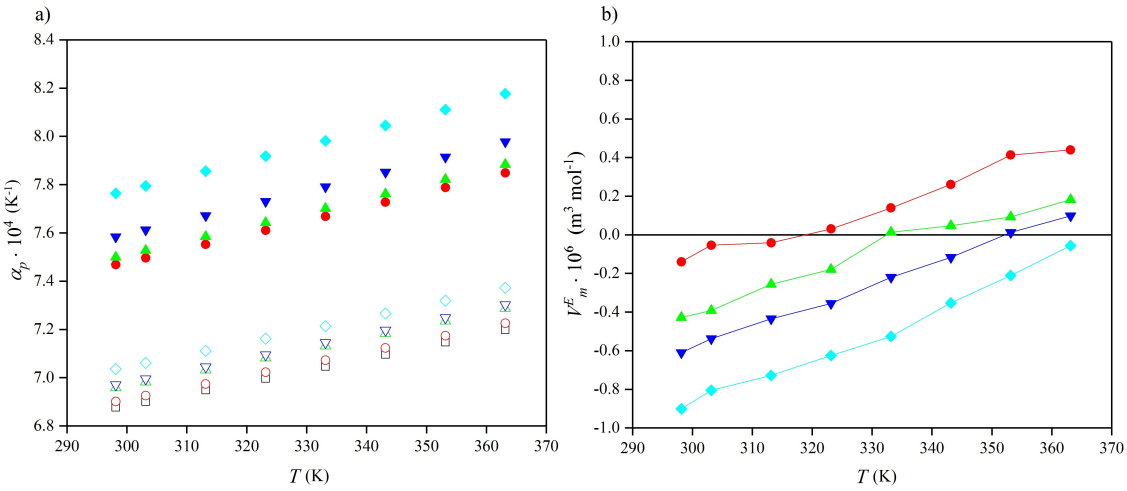

Figure 4.2.3. a) Thermal expansion coefficient, α_p, as a function of the temperature, T; **b)** excess molar volume, V_m^E, of ILs + H_2O in comparison to pure ILs, as a function of the temperature, T, for $[P_{14,6,6,6}][AcO]$, □, $[P_{14,6,6,6}][ButO]$, ○, $[P_{14,6,6,6}][HexO]$, △, $[P_{14,6,6,6}][OctO]$, ▽, $[P_{14,6,6,6}][DecO]$, ◇, $[P_{14,6,6,6}][ButO]$ + 16.680 H_2O wt%, ●, $[P_{14,6,6,6}][HexO]$ + 15.825 H_2O wt%, ▲, $[P_{14,6,6,6}][OctO]$ + 14.783 H_2O wt%, ▼, $[P_{14,6,6,6}][DecO]$ + 14.150 H_2O wt%, ♦.

volume values are 0 (m^3 mol^{-1}). At this point, the repulsion and attraction are comparable and further temperature increases cause the repulsive forces to dominate. It has also been reported previously that negative excess volumes can indicate an amphiphilic and/or polar character of solute. [16]

4.3 Isobaric Heat Capacity

To the best of our knowledge, there are no published data on the isobaric heat capacity of investigated systems. The experimental values are summarized in **Table CD4.4** (Appendix CD4). The fitting parameters of second-order equation (2.2.30), $c_p(T)$, are reported in **Table 4.3.1**. The heat capacity is increasing with temperature, as expected, the effect from 298.15 K to 363.15 K was (6.87, 7.49, 8.18, 8.39 and 8.80) % for $[P_{14,6,6,6}][AcO]$, $[P_{14,6,6,6}][ButO]$, $[P_{14,6,6,6}][HexO]$, $[P_{14,6,6,6}][OctO]$ and $[P_{14,6,6,6}][DecO]$, respectively. As can be seen, the temperature effect is increasing with the anion chain length. Heat capacity acts as a representation of the bonds energy in the molecules (spring-like), therefore, increasing the anion chain length should result in a larger effect with temperature. The heat capacity found in this work was decreasing with anion chain elongation, due to increasing molecular volume of anions.

Table 4.3.1. Coefficients and their standard uncertainties, a_0, a_1 and a_2, δa_0, δa_1 and δa_2, of equation (2.2.30), $c_p(T)$, for pure ILs and mixtures with water, including coefficient of determination, R^2.

	$(a_2 \pm \delta a_2)\times 10^3$ (J kg^{-1} K^{-3})	$a_1 \pm \delta a_1$ (J kg^{-1} K^{-2})	$a_0 \pm \delta a_0$ (J kg^{-1} K^{-1})	R^2
$[P_{14,6,6,6}][AcO]$	9 ± 1	-3.7 ± 0.7	2340 ± 110	0.99880
$[P_{14,6,6,6}][ButO]$	4.7 ± 0.2	-0.87 ± 0.15	1788 ± 45	0.99994
$[P_{14,6,6,6}][HexO]$	2.2 ± 1.1	0.90 ± 0.73	1439 ± 122	0.99885
$[P_{14,6,6,6}][OctO]$	-8.6 ± 1.5	8 ± 1	195 ± 164	0.99792
$[P_{14,6,6,6}][DecO]$	0.86 ± 0.17	1.8 ± 1.1	1190 ± 190	0.99736
$[P_{14,6,6,6}][ButO]$ + 16.680 H_2O wt%	36 ± 2	-17 ± 2	5190 ± 240	0.99961
$[P_{14,6,6,6}][HexO]$ + 15.825 H_2O wt%	38 ± 5	-18 ± 4	5160 ± 580	0.99780
$[P_{14,6,6,6}][OctO]$ + 14.783 H_2O wt%	24 ± 5	-11 ± 3	4080 ± 520	0.99691
$[P_{14,6,6,6}][DecO]$ + 14.150 H_2O wt%	6.1 ± 7.0	3.1 ± 4.6	1724 ± 360	0.99458

The measured heat capacities for the pure ILs are lower than the heat capacity of water (4181 J kg^{-1} K^{-1} at 298.15 K), [17] so as a result, mixtures with water should have higher heat capacity in comparison to their pure analogues (**Figure 4.3.1a**).

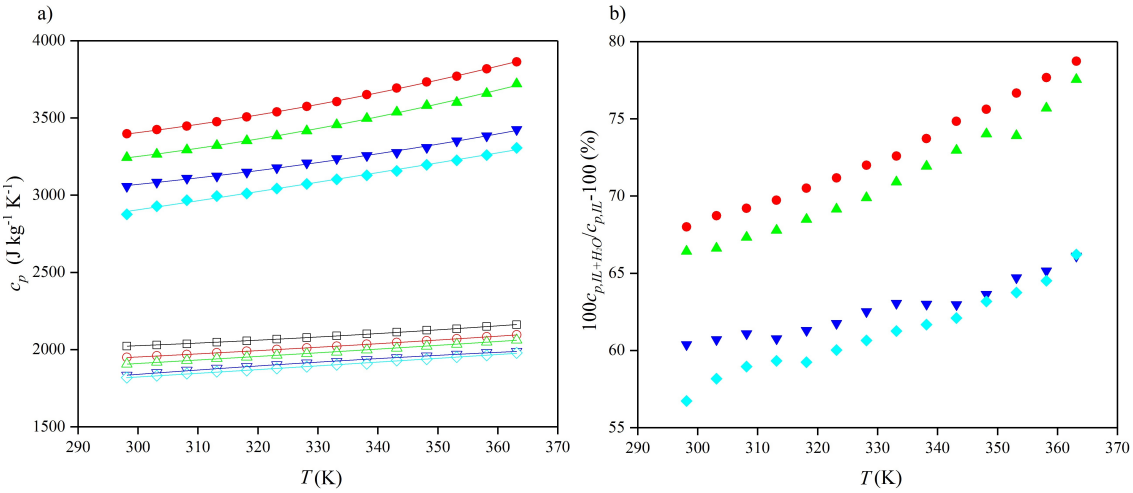

Figure 4.3.1. a) Specific isobaric heat capacity, c_p, as a function of the temperature, T; **b)** specific isobaric heat capacity enhancement, $c_{p,IL+H_2O}/c_{p,IL}$, of ILs + H_2O in comparison to pure ILs, as a function of the temperature, T, for $[P_{14,6,6,6}][AcO]$, □, $[P_{14,6,6,6}][ButO]$, ○, $[P_{14,6,6,6}][HexO]$, △, $[P_{14,6,6,6}][OctO]$, ▽, $[P_{14,6,6,6}][DecO]$, ◇, $[P_{14,6,6,6}][ButO]$ + 16.680 H_2O wt%, ●, $[P_{14,6,6,6}][HexO]$ + 15.825 H_2O wt%, ▲, $[P_{14,6,6,6}][OctO]$ + 14.783 H_2O wt%, ▼, $[P_{14,6,6,6}][DecO]$ + 14.150 H_2O wt%, ◆.

The values of isobaric heat capacity in comparison to other ILs are relatively high (2.02, 1.95, 1.91, 1.84 and 1.82) kJ kg^{-1} K^{-1} at 298.15 K for $[P_{14,6,6,6}][AcO]$, $[P_{14,6,6,6}][ButO]$, $[P_{14,6,6,6}][HexO]$, $[P_{14,6,6,6}][OctO]$ and $[P_{14,6,6,6}][DecO]$, respectively, in comparison to other ILs, for example (1.62, 1.34 or 1.61) kg^{-1} K^{-1} for 1-butyl-3-methylimidazolium tetrafluoroborate at 297.95 K, [18] 1-methyl-1-octylpyrrolidinium bis[(trifluoromethyl)sulfonyl]imide at 295.04 K, [19] or trihexyl(decyl)ammonium bis[(tri fluoromethyl)sulfonyl]imide at 298.15 K. [20]

The specific heat capacity of pure ILs in this study depends on the anion chain length in the following sequence: $[AcO]^-$ > $[ButO]^-$ > $[HexO]^-$ > $[OctO]^-$ > $[DecO]^-$, and as expected based on other reports devoted to similar dependencies and the increasing molecular volume of ILs. [21] The same dependence was found for mixtures with water. Interestingly, the addition of water did not change this behavior. The impact of water on the heat capacity of the ILs was investigated and found to be (56.73-78.32) %, with the maximum found for $[P_{14,6,6,6}][ButO]$ (**Figure 4.3.1b**).

The molar excess heat capacity data are shown in **Figure 4.3.2** and reported in

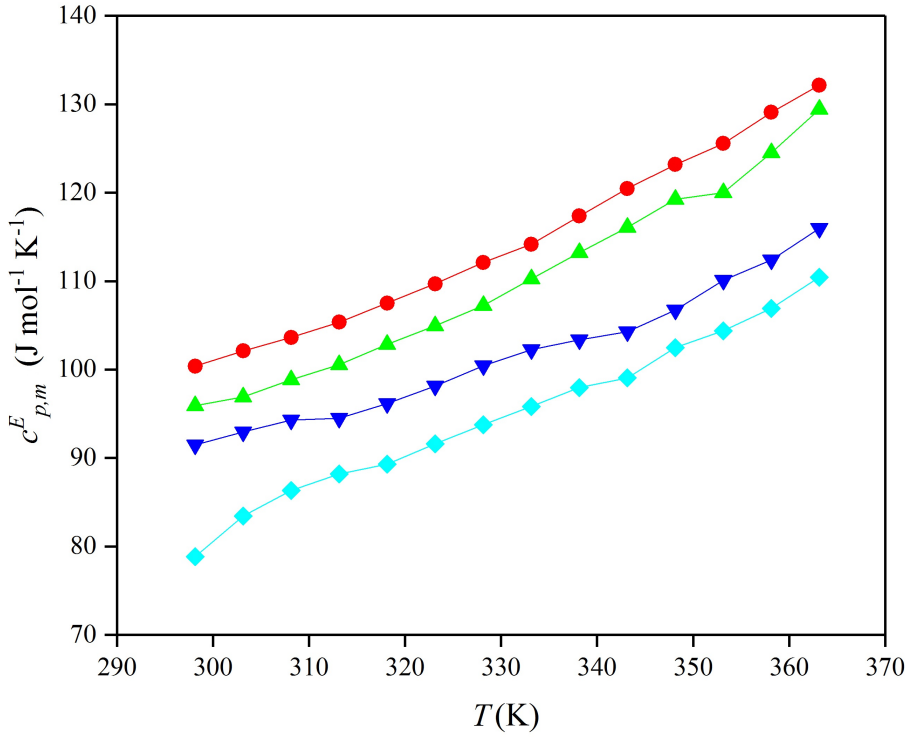

Figure 4.3.2. Excess molar heat capacity, $C^E_{p,m}$, of ILs + H_2O in comparison to pure ILs, as a function of the temperature, T, for $[P_{14,6,6,6}][ButO]$ + 16.680 H_2O wt%, ●, $[P_{14,6,6,6}][HexO]$ + 15.825 H_2O wt%, ▲, $[P_{14,6,6,6}][OctO]$ + 14.783 H_2O wt%, ▼, $[P_{14,6,6,6}][DecO]$ + 14.150 H_2O wt%, ♦.

Table CD4.5 (Appendix CD4). Negative molar excess heat capacities indicate differences in non-specific interactions between ILs and solvent (water), while positive values are explained by heteromolecular association of IL-water complexes. [22] With an increase of temperature, hydrogen bonds between ILs and water become weaker, resulting in the dehydration of carboxylic group oxygen and the release of the water, in agreement with the changes observed in the excess molar volume. Similar effects have been observed in ethylene glycol + water systems. [16] Furthermore, the van der Waals and Coulombic interactions also become weaker with the temperature increase. The excess molar heat capacity is changing in the following sequence: $[ButO]^-$ > $[HexO]^-$ > $[OctO]^-$ > $[DecO]^-$. As can be seen, the dependencies of anion carbon chain length for heat capacity, its enhancement and excess molar heat capacity are similar.

4.4 Ionic Conductivity and Viscosity

The experimental data of ionic conductivity and viscosity are summarized in **Tables CD4.6-CD4.7** (Appendix CD4), respectively, and the fitting coefficients of equation (2.2.45), $\eta(T)$, and equation (2.2.46), $\sigma(T)$ are reported in **Table 4.4.1** and **Table 4.4.2**.

Table 4.4.1. Coefficients and their standard uncertainties, η_0, B, T_0, $\delta\eta_0$, δB, δT_0, of equation equation (2.2.45), $\eta(T)$, for pure ILs and mixtures with water, including coefficient of determination, R^2.

	$(\eta_0 \pm \delta\eta_0) \times 10^2$ (Pa s)	$B \pm \delta B$ (K)	$T_0 \pm \delta T_0$ (K)	R^2
$[P_{14,6,6,6}][AcO]$	6.32 ± 0.48	1142 ± 2	156 ± 4	0.99991
$[P_{14,6,6,6}][ButO]$	5.20 ± 0.35	1252 ± 9	151 ± 1	0.99985
$[P_{14,6,6,6}][HexO]$	5.74 ± 0.11	1314 ± 3	147 ± 6	0.99984
$[P_{14,6,6,6}][OctO]$	4.16 ± 0.43	1477 ± 6	136 ± 5	0.99965
$[P_{14,6,6,6}][DecO]$	4.02 ± 0.88	1554 ± 5	130 ± 10	0.99989
$[P_{14,6,6,6}][ButO]$ + 16.680 H_2O wt%	6.03 ± 0.67	1014 ± 7	152 ± 4	0.99862
$[P_{14,6,6,6}][HexO]$ + 15.825 H_2O wt%	4.59 ± 0.99	1173 ± 4	141 ± 8	0.99941
$[P_{14,6,6,6}][OctO]$ + 14.783 H_2O wt%	5.14 ± 0.58	1345 ± 1	117 ± 2	0.99938
$[P_{14,6,6,6}][DecO]$ + 14.150 H_2O wt%	4.32 ± 0.39	1489 ± 7	104 ± 3	0.99813

Table 4.4.2. Coefficients and their standard uncertainties, σ_0, B, T_0, $\delta\sigma_0$, δB, δT_0, of equation (2.2.46), $\sigma(T)$, for pure ILs and mixtures with water, including coefficient of determination, R^2.

	$\sigma_0 \pm \delta\sigma_0$ (S m^{-1})	$B \pm \delta B$ (K)	$T_0 \pm \delta T_0$ (K)	R^2
$[P_{14,6,6,6}][AcO]$	23 ± 2	1116 ± 2	164 ± 2	0.99982
$[P_{14,6,6,6}][ButO]$	22 ± 2	1175 ± 6	160 ± 3	0.99997
$[P_{14,6,6,6}][HexO]$	22 ± 2	1276 ± 3	154 ± 6	0.99948
$[P_{14,6,6,6}][OctO]$	22 ± 6	1375 ± 5	147 ± 4	0.99934
$[P_{14,6,6,6}][DecO]$	22 ± 4	1517 ± 6	138 ± 2	0.99984
$[P_{14,6,6,6}][ButO]$ + 16.680 H_2O wt%	55 ± 5	914 ± 3	156 ± 5	0.99899
$[P_{14,6,6,6}][HexO]$ + 15.825 H_2O wt%	53 ± 7	980 ± 3	150 ± 6	0.99945
$[P_{14,6,6,6}][OctO]$ + 14.783 H_2O wt%	47 ± 4	1156 ± 5	135 ± 7	0.99983
$[P_{14,6,6,6}][DecO]$ + 14.150 H_2O wt%	36 ± 2	1179 ± 6	133 ± 9	0.99992

The only data available in the literature up to date are those reported by Fillion *et al.* (**2016**) [5] for pure $[P_{14,6,6,6}][AcO]$, and by Neves *et al.* (**2011**) [2] for pure $[P_{14,6,6,6}][DecO]$ and mixtures with water. The viscosity is thought to be the most sensitive physicochemical parameter to the presence of water and halide. [6] As described above,

Neves *et al.* (**2011**) [2] did not report the halide content of the studied ILs and the values of viscosity for pure $[P_{14,6,6,6}][DecO]$ are 0.472 Pa s (at 293.2 K, Neves *et al.* (**2011**) [2]) and 0.4098 Pa s (at 293.2 K, this study) with a relative deviation of 15.18%. Whereas, in case of pure $[P_{14,6,6,6}][AcO]$, the values are 0.406 Pa s (at 293.2 K, Fillion *et al.* (**2016**) [5]) and 0.1962 Pa s (at 293.2 K, this study) with a relative deviation close to 106.93% as shown in **Figure 4.4.1**.

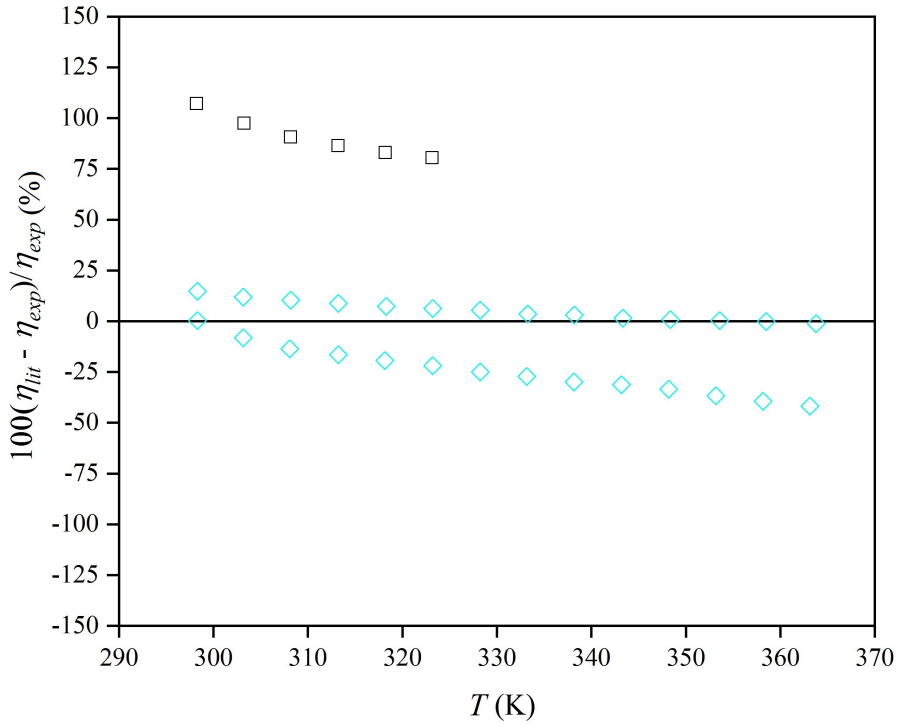

Figure 4.4.1. Dynamic viscosity deviations, $100(\eta_{lit} - \eta_{exp})/\eta_{exp}$, between data in this work, η_{exp}, and literature, η_{lit}, as a function of the temperature, T, for $[P_{14,6,6,6}][AcO]$, □ [5], $[P_{14,6,6,6}][DecO]$, ◇ [2], $[P_{14,6,6,6}][DecO]$ + 14.150 H_2O wt%, ♦ [2].

Due to the sensitivity of the measurement on the impurities, this deviation may be associated with differences in the halide content between the samples, as discussed before. The water content cannot be the sole cause of the difference as the previously reported sample had a higher water content than the sample reported, herein, Neves *et al.* (**2011**) [2] is 0.714 wt% and 0.030 wt% in this work. The technique used in this work (rheometer) is related to extremely high accuracy, unlike the Stabinger Viscometer. Also, the calibration procedure was not described in work of Neves *et al.* (**2011**) [2], therefore, a possible cause of the deviations observed may be associated with differences in the

measurement procedure. Moreover, the values for mixtures with water are (0.09095 and 0.9187) Pa s at 298.2 K, for literature and this work, respectively. If the samples contain different impurity levels, the water solubility may be related to a sample presenting a higher halide content leading to the difference in the viscosity reported. At the saturation point, if the water content is higher (due to the presence of halide) we can expect to have lower viscosity than that reported, herein (with lower halide content).

The ionic conductivity increases with temperature (**Figure 4.4.2a** and **Figure 4.4.2b** for pure ILs and mixtures with water, respectively), while the viscosity decreases with temperature exponentially (**Figure 4.4.3a** and **Figure 4.4.3b** for ILs and mixtures with water, respectively).

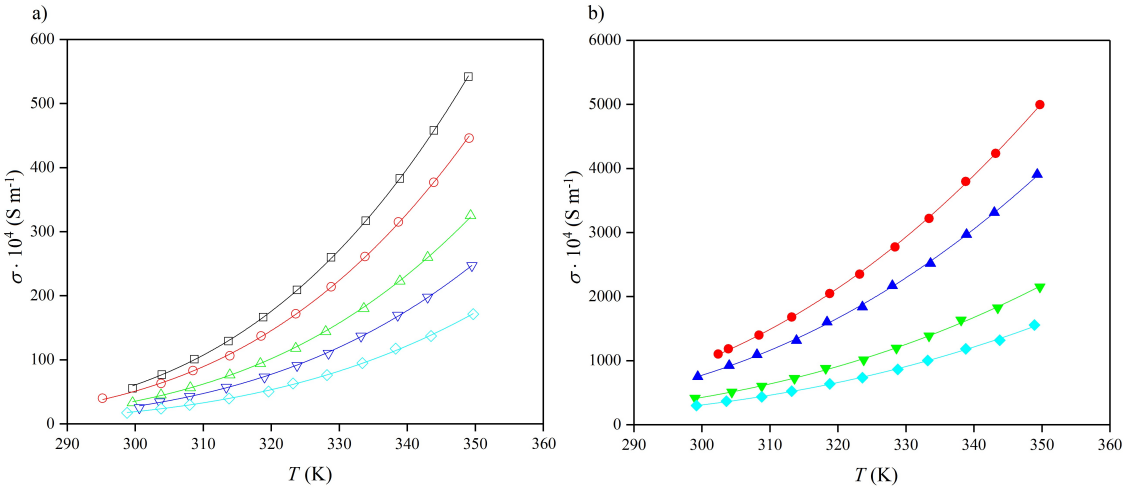

Figure 4.4.2. Ionic conductivity, σ, as a function of the temperature, T, for **a)** pure ILs; **b)** ILs + H_2O, for $[P_{14,6,6,6}][AcO]$, □, $[P_{14,6,6,6}][ButO]$, ○, $[P_{14,6,6,6}][HexO]$, △, $[P_{14,6,6,6}][OctO]$, ▽, $[P_{14,6,6,6}][DecO]$, ◇, $[P_{14,6,6,6}][ButO]$ + 16.680 H_2O wt%, ●, $[P_{14,6,6,6}][HexO]$ + 15.825 H_2O wt%, ▲, $[P_{14,6,6,6}][OctO]$ + 14.783 H_2O wt%, ▼, $[P_{14,6,6,6}][DecO]$ + 14.150 H_2O wt%, ♦.

The ionic conductivity and viscosity for pure ILs depend on the anion chain length in the following sequences: $[AcO]^-$ > $[ButO]^-$ > $[HexO]^-$ > $[OctO]^-$ > $[DecO]^-$ and $[DecO]^-$ > $[OctO]^-$ > $[HexO]^-$ > $[ButO]^-$ > $[AcO]^-$, respectively. Similar trends have been also observed for other mixtures with water for both the ionic conductivity and viscosity. Water has much lower viscosity than the ILs studied, therefore, as expected, the addition of water decreases the viscosity of 1.9-5.6 times. In comparison to other ILs,

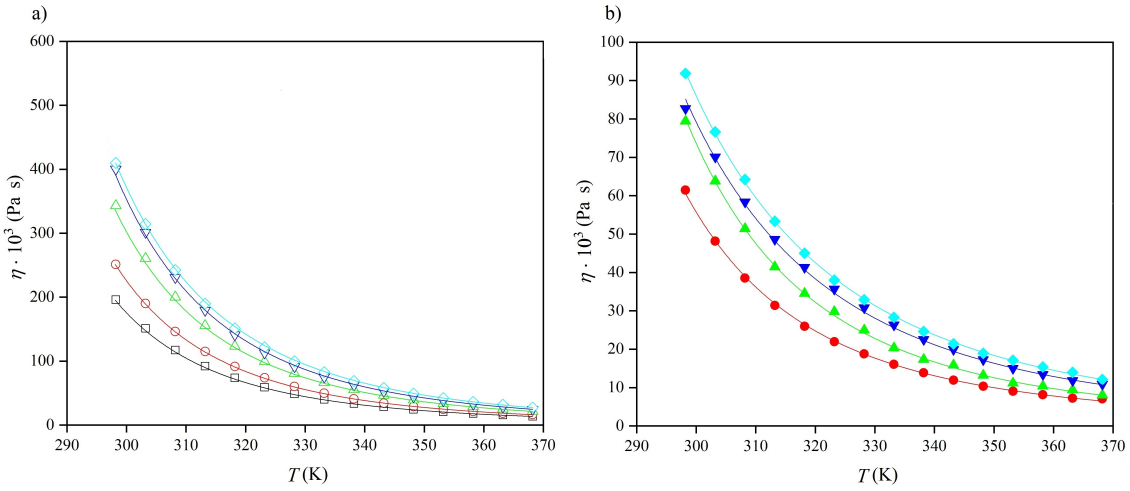

Figure 4.4.3. Dynamic viscosity, η, as a function of the temperature, T; for **a)** pure ILs; **b)** ILs + H_2O, for $[P_{14,6,6,6}][AcO]$, □, $[P_{14,6,6,6}][ButO]$, ○, $[P_{14,6,6,6}][HexO]$, △, $[P_{14,6,6,6}][OctO]$, ▽, $[P_{14,6,6,6}][DecO]$, ◇, $[P_{14,6,6,6}][ButO]$ + 16.680 H_2O wt%, ●, $[P_{14,6,6,6}][HexO]$ + 15.825 H_2O wt%, ▲, $[P_{14,6,6,6}][OctO]$ + 14.783 H_2O wt%, ▼, $[P_{14,6,6,6}][DecO]$ + 14.150 H_2O wt%, ♦.

those in this work exhibit relatively high values of viscosity, *i.e.* (430, 125.5 or 234.5) mPa s at 293.15 K for 1-butyl-3-methylimidazolium acetate, 1-butyl-3-methylimidazolium tetrafluoroborate or triethylhexylammonium bis[(trifluoromethyl)sulfonyl]imide, respectively, while the lowest viscosity in this work was found for $[P_{14,6,6,6}]$ as 254.0 mPa s at 293.15 K and the highest for $[P_{14,6,6,6}][DecO]$ as 546.3 mPa s at 293.15 K. [23–25]

The ionic conductivities for selected ILs in this work are low, (0.049, 0.039, 0.029, 0.019, 0.017) mS cm^{-1} at 298.15 K for $[P_{14,6,6,6}][AcO]$, $[P_{14,6,6,6}][ButO]$, $[P_{14,6,6,6}][HexO]$, $[P_{14,6,6,6}][OctO]$ and $[P_{14,6,6,6}][DecO]$, respectively. This behavior reflects the large size of the common cation, and increasing size of anion. However, such values are low in comparison to values reported for other ILs, *i.e.* 1-butyl-3-methylimidazolium dicyanamide, N-hexyl N-methylpyrrolidinium hexafluorophosphate or 1-ethyl-3-methylimidazolium trifluoromethanesulfonate, (1.052, 0.037 or 0.979) mS cm^{-1} at 298.15 K, respectively. [26–28]

The viscosity was correlated with temperature by the exponential VFT equation (2.2.45) of which parameters can be found in **Table 4.4.1**. The effect of temperature on viscosity is enormous (decrease of above 1000 % from 298.15 K to 363.15 K) for all ILs. The analysis of VFT equation leads to the most recognized parameter of so-called glass transition, T_0. Mauro *et al.* (**2009**) discussed the meaning of T_0, as described the rise in

viscosity when it is cooled toward the glass transition, where the sharp (super-Arrhenius) increase occurs, accompanied with very little structural change. As a further consequence, below the glass transition temperature the long structural relaxation times can be found caused by lower mobility. With above described features of T_0, after the analysis of results summarized in **Table 4.4.1**, it can be observed that increasing the anion chain length of ILs results in decreasing T_0. Increasing the anion chain length (from acetate to decanoate) decreases the mobility of anion (as a constituent of IL), therefore the T_0 was expected to decrease.

4.5 Thermogravimetric Analysis

The thermal decomposition of ILs is still subject of intensive investigations, in particular the mechanistic aspects. Many studies have been performed, to date, and have been reviewed briefly by Maton *et al* (**2013**). [29] This is important in many applications, for example the decomposition of ILs as electrolytes for lithium metal batteries has been studied by Lin *et al.* (**2015**) [30] The thermal stability of basic quaternary phosphonium ILs has been reported by Ferreira *et al.* (**2012**) [31] and detailed studies on the thermal decomposition and its mechanism has been studied using imidazolium-based carboxylate ILs by Clough *et al.* (**2013**). [32] However, to the best of our knowledge, there are no studies on quaternary phosphonium carboxylate ILs. Following the work of *Maton et al.* (**2013**), [29] the thermal decomposition temperature has been reported as the onset temperature, T_{on} (from differential thermogravimetric curves, **Figures CD4.1-CD4.2** in Appendix CD4), and temperature of 10% weight loss, $T_{10\%}$ (from the thermogravimetric curves).

These results are summarized in **Table 4.5.1**, and the TGA curves of decomposition for pure ILs and mixtures with water are presented in **Figure 4.5.1** and **Figure 4.5.2**, respectively.

Table 4.5.1. Thermogravimetric analysis results for pure ILs and mixtures with water, including the decomposition onset temperature, T_{on}, with corresponding total weight loss, and temperature at 10% weight loss, $T_{10\%}$; the standard uncertainty u are $u(T)$ = 0.5 K for T_{on} and $T_{10\%}$, and p = 101 kPa with $u(p)$ = 2 kPa.

	T_{on} (total weight loss) K (%)	$T_{10\%}$ K
$[P_{14,6,6,6}][AcO]$	549.0	532.5
$[P_{14,6,6,6}][ButO]$	543.8	521.5
$[P_{14,6,6,6}][HexO]$	529.0	507.1
$[P_{14,6,6,6}][OctO]$	516.0	492.8
$[P_{14,6,6,6}][DecO]$	542.2	533.6
$[P_{14,6,6,6}][ButO]$ + 16.680% H_2O wt%	524.0 (92.37)	511.2
$[P_{14,6,6,6}][HexO]$ + 15.825% H_2O wt%	519.1 (90.78)	498.2
$[P_{14,6,6,6}][OctO]$+ 14.783% H_2O wt%	511.4 (97.29)	490.4
$[P_{14,6,6,6}][DecO]$+ 14.150% H_2O wt%	524.7 (96.31)	513.1

As can be seen, T_{on} decreases with the anion chain length, until $[P_{14,6,6,6}][DecO]$

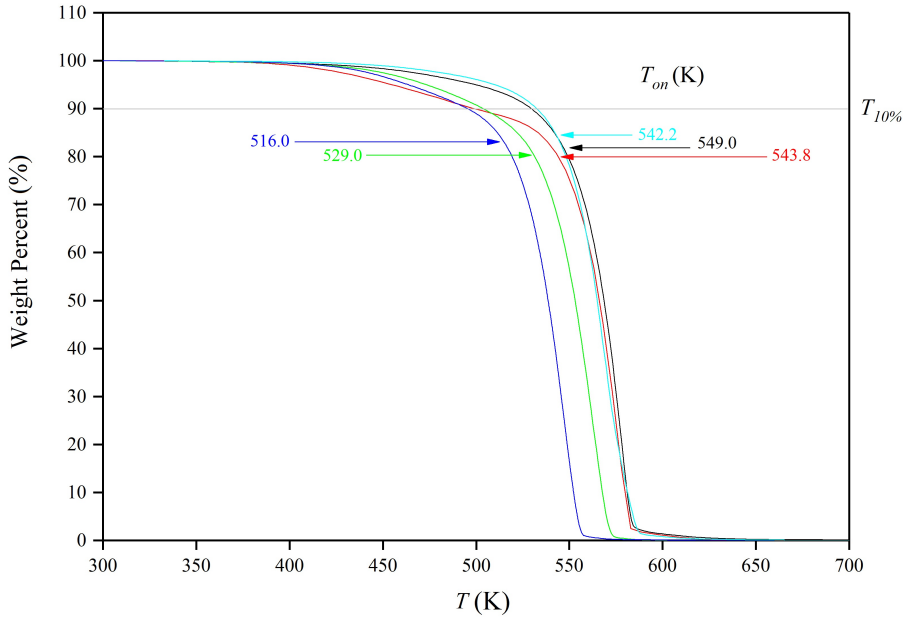

Figure 4.5.1. TGA curves for the thermal decomposition of pure ILs, with onset decomposition temperature, T_{on}, for $[P_{14,6,6,6}][AcO]$, black, $[P_{14,6,6,6}][ButO]$, red, $[P_{14,6,6,6}][HexO]$, green, $[P_{14,6,6,6}][OctO]$, blue, $[P_{14,6,6,6}][DecO]$, cyan.

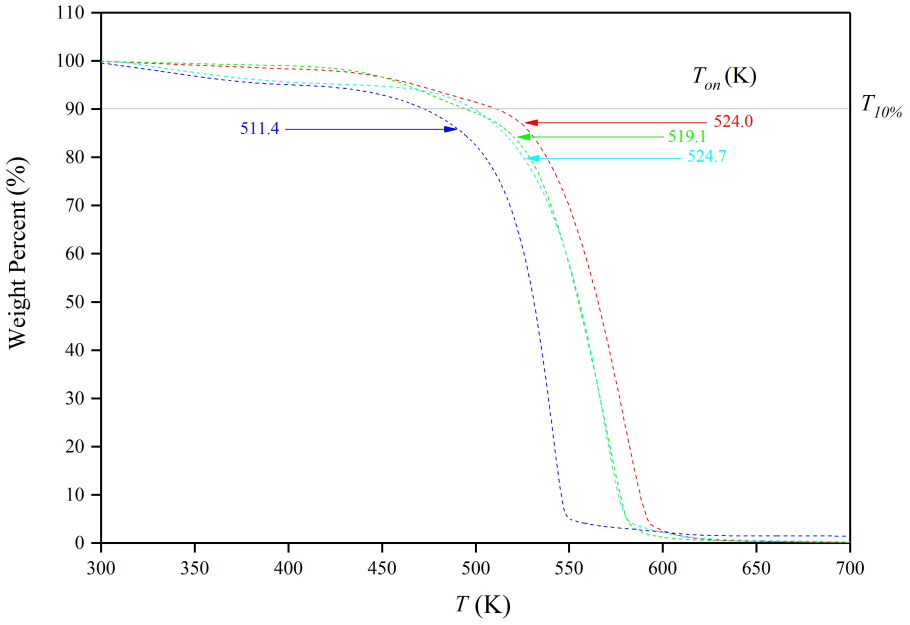

Figure 4.5.2. TGA curves for the thermal decomposition of water-saturated ILs, with onset decomposition temperature, T_{on}, for $[P_{14,6,6,6}][ButO]$ + 16.680 H_2O wt%, red, $[P_{14,6,6,6}][HexO]$ + 15.825 H_2O wt%, green, $[P_{14,6,6,6}][OctO]$ + 14.783 H_2O wt%, blue, $[P_{14,6,6,6}][DecO]$ + 14.150 H_2O wt%, cyan.

which exhibits much higher thermal stability than $[P_{14,6,6,6}]$[HexO] but lower than $[P_{14,6,6,6}]$[ButO]. Similar dependence was found for mixtures with water, however, the changes between each ILs are smaller than for the pure analogues. In case of $T_{10\%}$, a similar sequence was established for pure ILs, and $[DecO]^- > [ButO]^- > [OctO]^- > [HexO]^-$ for the mixtures with water. As can be seen, there is no dependence of $T_{10\%}$ on the anion chain length in the case of the mixtures with water. Furthermore, as indicated by Maton *et al.* (**2013**), [29] T_{on} is determined by the derivative function (dm/dT *vs.* T) which has been recognized as a sufficiently accurate parameter of thermal stability, and this is commonly used to describe the thermal decomposition. [33, 34] Moreover, the overestimation of the onset temperature is reduced.

Valor *et al.* (**2002**) [35] studied extensively the thermal decomposition of calcium salts of several carboxylic acids by TGA, IR, XRD and DSC. Therein, a decreasing thermal stability with increasing the chain length was reported because this process mainly involves the decomposition of the aliphatic chain (as shown by IR results) resulting in the formation of a carbonate species, however, no decomposition reaction was proposed. T_{on} values for such compounds were found to be (547.15, 517.15, 485.15 and 458.15) K for calcium butanoate, calcium hexanoate, calcium octanoate and calcium decanoate, respectively. Although, the results of Valor *et al.* (**2002**) [35] and herein are in a good agreement, the conditions of the previously reported data must be taken into account. Valor *et al.* (**2002**) used air as a flowing gas compared with nitrogen which was used, herein and the results of Salgado *et al.* (**2013**) [36] and Goetz *et al.* (**2015**) [37] showed that the thermal stability of ILs is commonly dependent on the atmosphere. This was also observed for the ILs investigated, herein, with the exception of $[P_{14,6,6,6}]$[DecO]. In contrast, Clough *et al.* (**2013**) [32] did not find any correlation between carboxylate anions carbon chain length (based on imidazolium ILs) and the thermal decomposition temperature. It is also worth noting that, for the mixtures with water of $[P_{14,6,6,6}]$[ButO] and $[P_{14,6,6,6}]$[HexO] higher water evaporation is observed, 7.62% and 9.81%, respectively, based on differential thermogravimetric curves, while the water contents are 16.680 wt% and 15.825 wt%, respectively; however, no water loss is found for the mixtures with water of $[P_{14,6,6,6}]$[OctO] and $[P_{14,6,6,6}]$[DecO] (the water contents are 14.783 wt% and 14.150 wt%, respectively). Thus, after the water evaporation process for these systems, there was less than 10% water remaining in the sample; however, not all the water was completely

removed. It can be assumed that it is caused by strong interactions between water and ILs constituents, and the solvated water molecules are stabilised by the IL, for example *via* strong hydrogen bonding with the anion.

The possible decomposition of quaternary phosphonium salts in the presence of hydroxide anion (originating from acid-base equilibrium between carboxylate anion and water) was described above, and presented in **Figure 2.1.2** (Section 2.1.1). However, the alkyl chain can also decompose by weakening the ionic interaction in the polar group, as shown by Valor *et al.* (**2002**) [35] The real decomposition process occurring in the investigated ILs is probably the combination of these two mechanisms. The decreasing onset temperature for the pure ILs is consistent with the decomposition based on the alkyl chain and this dominates the trend. It is expected, due to the increased hydrophobicity of the anion with increasing chain length, that the hydroxide catalyzed decomposition would decrease due to the lower hydroxide concentration which is likely to be present. These opposite effects are consistent with the minimum in the thermal stability occurring at octanoate with the decanoate based IL being stabilized possibly due to the reduced effect of hydroxide. For the mixtures with water, the thermal decomposition temperature values were found to be significant less dependent on the alkyl chain length, although the sequence remains unchanged. Very similar thermal stabilities were observed in these cases which may indicate a common mechanism, for example, promotion of the decomposition by the presence of OH^-.

Further discussion on decomposition phenomena, including isothermal thermogravimetric studies and comparison to common HTFs is presented in Section 6.7.

4.6 Thermal Conductivity

Thermal conductivity of ILs is one of the least investigated property, but is one of the most important when considering materials as HTFs. From the elementary theory of heat transfer, it is expected that with increasing the molecular size of compounds, the thermal conductivity should decrease (this behavior is true for many molecular solvents, such as simple linear alcohols). [17] ILs have interesting thermal conductivity property trends, for example Ge *et al.* (**2007**) [38] showed that the thermal conductivity of imidazolium-based ILs is not dependent on the cation chain length. The experimental thermal conductivity data are reported in **Table CD4.8** (Appendix CD4) and **Table 4.6.1** for pure ILs and mixtures with water equation (2.2.18) coefficients, $\lambda(T)$, and shown in **Figure 4.6.1a**.

Table 4.6.1. Coefficients and their standard uncertainties, a_1, a_0, δa_1, δa_0, of equation (2.2.18), $\lambda(T)$, for pure ILs and mixtures with water, including the coefficient of determination, R^2.

	$-(a_1 \pm \delta a_1) \times 10^6$ (W m^{-1} K^{-2})	$-(a_0 \pm \delta a_0) \times 10^3$ (W m^{-1} K^{-1})	R^2
[$P_{14,6,6,6}$][AcO]	111 ± 5	194 ± 2	0.98514
[$P_{14,6,6,6}$][ButO]	140 ± 6	199 ± 2	0.98754
[$P_{14,6,6,6}$][HexO]	142 ± 6	198 ± 2	0.98679
[$P_{14,6,6,6}$][OctO]	146 ± 6	202 ± 2	0.98882
[$P_{14,6,6,6}$][DecO]	138 ± 8	198 ± 2	0.97462
[$P_{14,6,6,6}$][ButO] + 16.680 H_2O wt%	144 ± 6	232 ± 2	0.99008
[$P_{14,6,6,6}$][HexO] + 15.825 H_2O wt%	162 ± 6	235 ± 2	0.99077
[$P_{14,6,6,6}$][OctO]+ 14.783 H_2O wt%	164 ± 7	236 ± 2	0.98970
[$P_{14,6,6,6}$][DecO]+ 14.150 H_2O wt%	166 ± 7	236 ± 2	0.99001

The thermal conductivity remains moderate values in comparison to other ILs, for example (0.1228, 0.161, or 0.199) W m^{-1} K^{-1} for 1-hexyl-3-methylimidazolium bis[(trifluoromethyl)sulfonyl]imide, [39] tetrabutylphosphonium L-serinate, [12] or 1-ethyl-3-methylimidazolium tetrafluoroborate at 298.15 K, [40] while the values in this work are (0.1602, 0.1566, 0.1560, 0.1581 and 0.1571) W m^{-1} K^{-1} for [$P_{14,6,6,6}$][AcO], [$P_{14,6,6,6}$][ButO], [$P_{14,6,6,6}$][HexO], [$P_{14,6,6,6}$][OctO] and [$P_{14,6,6,6}$][DecO] at 298.15, respectively.

The thermal conductivity is decreasing with increasing the temperature linearly,

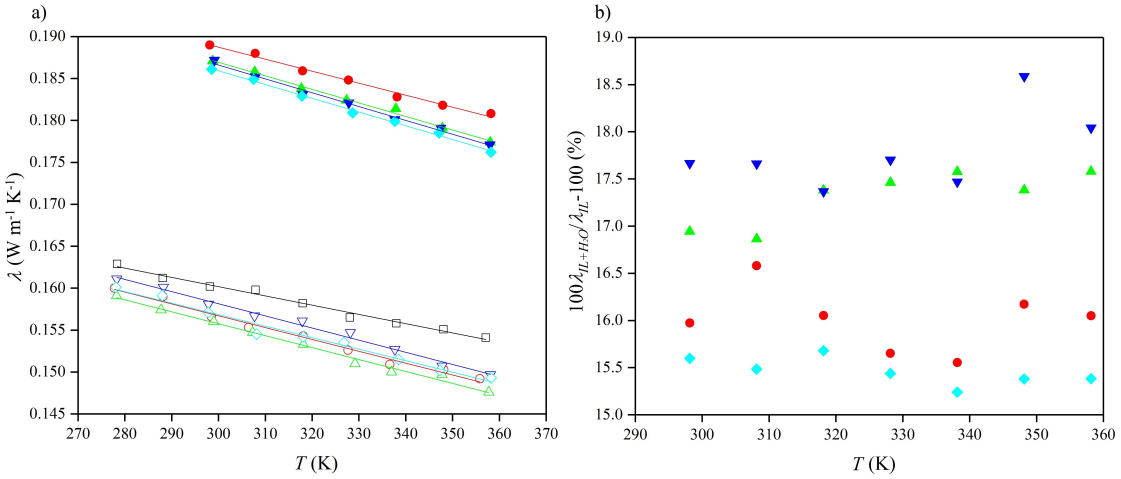

Figure 4.6.1. a) Thermal conductivity, λ, as a function of the temperature, T; **b)** thermal conductivity enhancement, $\lambda_{IL+H_2O}/\lambda_{IL}$ of ILs + H_2O in comparison to pure ILs, as a function of the temperature, T, for $[P_{14,6,6,6}][AcO]$, □, $[P_{14,6,6,6}][ButO]$, ○, $[P_{14,6,6,6}][HexO]$, △, $[P_{14,6,6,6}][OctO]$, ▽, $[P_{14,6,6,6}][DecO]$, ◇, $[P_{14,6,6,6}][ButO]$ + 16.680 H_2O wt%, ●, $[P_{14,6,6,6}][HexO]$ + 15.825 H_2O wt%, ▲, $[P_{14,6,6,6}][OctO]$ + 14.783 H_2O wt%, ▼, $[P_{14,6,6,6}][DecO]$ + 14.150 H_2O wt%, ◆.

while the slopes for all ILs remain similar values. The differences between the lowest and highest temperature are (6.71, 7.24, 7.79, 7.62 and 7.23) % for $[P_{14,6,6,6}][AcO]$, $[P_{14,6,6,6}][ButO]$, $[P_{14,6,6,6}][HexO]$, $[P_{14,6,6,6}][OctO]$ and $[P_{14,6,6,6}][DecO]$, respectively.

As can be seen, there is no dependence on the anion chain length. The thermal conductivity decreases to $[P_{14,6,6,6}][HexO]$, and then increases with alkyl chain length. It can be also seen that the values of thermal conductivity data for all pure ILs are similar, or even the same. The difference between the largest and smallest anions thermal conductivity appeared to be 2.41% which is well below the standard uncertainty of the measurement (3.44%). A similar dependence was found for imidazolium-based ILs where the thermal conductivity decreased for the cation chain lengths of up to 6 carbons, and then increased for alkyl chain lengths of 6 to 10 carbons Ge *et al.* (**2007**). [38] Furthermore, it can be seen in **Table 4.6.1** that the errors of a_1 parameters are smaller than the values of a_1 for carboxylate ILs which indicates that they are truly temperature dependent, in contrast to $[C_8C_1Im][NTf_2]$. The thermal conductivity coefficient of water (~0.6 W m^{-1} K^{-1}) is much higher than all ILs reported in this study as well as other previously reported studies. Therefore, it is expected that addition of water to ILs will enhance the thermal

conductivity, in comparison to pure ILs. To investigate this behavior, the thermal conductivity enhancement in comparison to pure ILs was calculated and shown in **Figure 4.6.1b**. The enhancement was between (15.24 – 18.59) %, with maximum for $[P_{14,6,6,6}][OctO]$ + 14.783 wt% at ~348.15 K.

4.7 Walden Plot

A Walden plot is a useful analytical tool to assess the degree of ionicity, however, it must be noted that this approach is only based on viscosity and ionic conductivity. The most accurate results may be obtained by pulsed-gradient spin-echo diffusion NMR studies. [41, 42] The Walden plot is shown in **Figure 4.7.1** for the pure ILs and mixtures with water.

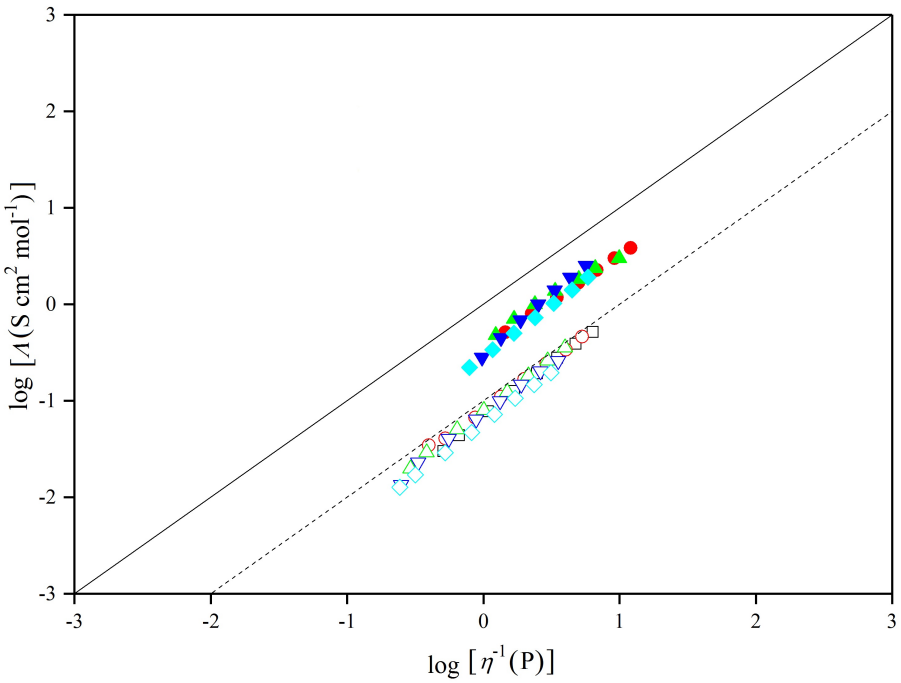

Figure 4.7.1. Walden plot for pure ILs and mixtures with water, in the meaning of molar ionic conductivity logarithm, log(Λ), as a function of inversed viscosity logarithm, log(η^{-1}), for [$P_{14,6,6,6}$][AcO], □, [$P_{14,6,6,6}$][ButO], ○, [$P_{14,6,6,6}$][HexO], △, [$P_{14,6,6,6}$][OctO], ▽, [$P_{14,6,6,6}$][DecO], ◇, [$P_{14,6,6,6}$][ButO] + 16.680 H_2O wt%, ●, [$P_{14,6,6,6}$][HexO] + 15.825 H_2O wt%, ▲, [$P_{14,6,6,6}$][OctO] + 14.783 H_2O wt%, ▼, [$P_{14,6,6,6}$][DecO] + 14.150 H_2O wt%, ♦.

In this work, the fractional Walden rule, described by Schreiner *et al.* (**2009**), [43] has also been applied. To establish the degree of ionicity, two quantities are compared (C' and ΔW) and summarized in **Table 4.7.1**.

Table 4.7.1. Walden plot results, logarithm of Walden product and its standard uncertainty, logC' and δlogC', fractional factor and its standard uncertainty, α and $\delta\alpha$, and ΔW factor, for pure ILs and mixtures with water

	-log$C' \pm \delta$logC'	$\alpha \pm \delta\alpha$	ΔW
$[P_{14,6,6,6}]$[AcO]	1.1658 ± 0.0076	1.116 ± 0.016	1.23
$[P_{14,6,6,6}]$[ButO]	1.119 ± 0.010	1.090 ± 0.024	1.20
$[P_{14,6,6,6}]$[HexO]	1.0999 ± 0.0044	1.088 ± 0.011	1.17
$[P_{14,6,6,6}]$[OctO]	1.150 ± 0.013	1.089 ± 0.034	1.27
$[P_{14,6,6,6}]$[DecO]	1.2363 ± 0.0023	1.076 ± 0.060	1.29
$[P_{14,6,6,6}]$[ButO] + 16.680 H_2O wt%	0.3654 ± 0.0036	0.936 ± 0.047	0.38
$[P_{14,6,6,6}]$[HexO] + 15.825 H_2O wt%	0.3409 ± 0.0088	0.934 ± 0.013	0.35
$[P_{14,6,6,6}]$[OctO]+ 14.783 H_2O wt%	0.553 ± 0.013	1.015 ± 0.022	0.57
$[P_{14,6,6,6}]$[DecO]+ 14.150 H_2O wt%	0.651 ± 0.010	1.074 ± 0.019	0.64

It can be seen qualitatively that pure ILs show rather poor ionic character and they lie well below the 10% ionicity line for 0.01 mol dm^{-3} KCl (**Figure 4.7.1**). While the mixtures with water lie very close to the ideal ionicity line. This is probably due to the solvation of carboxylate anion with smaller water molecules freeing the ion pair aggregates present in the neat ILs. The ionicity based on the fractional Walden product, C', was found to be in the following sequences: $[HexO]^- > [ButO]^- > [OctO]^- > [AcO]^- > [DecO]^-$ and $[HexO]^- > [ButO]^- > [OctO]^- > [DecO]^-$ for pure ILs and mixtures with water, respectively. Another Walden product, ΔW, was found to be in the following sequences: $[DecO]^- > [OctO]^- > [HexO]^- > [AcO]^- > [ButO]^-$ and $[DecO]^- > [OctO]^- > [ButO]^- > [HexO]^-$ for pure ILs and mixtures with water, respectively. It can be seen that $[P_{14,6,6,6}]$[HexO] remains the most ionic, while $[P_{14,6,6,6}]$[DecO] the least ionic (as expected). This behaviour is related to the ability of COO^- to interact with the P^+ centre (the easiest for acetate and the hardest for decanoate) and the van der Waals interactions (the weakest for acetate and the strongest for decanoate). Therefore, the ion pair is likely to be weakest for hexanoate (as the balance between Coulombic and van der Waals interactions) which results in the highest ionicity among the investigated ILs. Schreiner *et al.* (**2009**) [43] analyzed 1-alkyl-3-methylimidazolium ILs with tetrafluoroborate and dicyanamide anions. The authors showed that these ILs have relatively high ionicity in the meaning of Walden Rule (fractional parameters 0.90 – 0.94). An extensive investigation was done by MacFarlane *et al.* (**2009**) [44] where different classes of ILs were studied. It was found that 1-methyl-1-propylpyrrolidinium dicyanamide is almost the ideally ionic, while quaternary phosphonium-based ILs are poorly ionic.

4.8 Conclusions

The density, isobaric heat capacity, ionic conductivity, thermal stability, thermal conductivity, viscosity data as well as the excess molar properties and Walden rule have been measured for trihexyl(tetradecyl)phosphonium based ILs as a function of the alkyl chain length on a series of carboxylate anions (acetate, butanoate, hexanoate, octanoate and decanoate) and compared with commonly used HTFs. These measurements have also been performed on the mixtures with water.

The ILs studied in this work exhibit properties which enable them to be applied successfully as HTFs including heat capacity, thermal conductivity and thermal stability which are comparable or better than those of commonly used heat transfer materials. This is particularly true for the mixtures with water. It is justified based on the thermophysical properties reported in this work, it means that many of them are enhanced or improved in the meaning of ideal HTFs (low viscosity, high density, high heat capacity, high thermal conductivity, high thermal stability).

Bibliography

[1] M. G. Freire, P. J. Carvalho, R. L. Gardas, L. M. Santos, I. M. Marrucho, and J. A. P. Coutinho, *Journal of Chemical & Engineering Data* **53**, 2378 (2008).

[2] C. M. S. S. Neves, P. J. Carvalho, M. G. Freire, and J. A. P. Coutinho, *The Journal of Chemical Thermodynamics* **43**, 948 (2011).

[3] M. Tariq, P. A. S. Forte, M. F. C. Gomes, J. N. C. Lopes, and L. P. N. Rebelo, *The Journal of Chemical Thermodynamics* **41**, 790 (2009).

[4] J. M. S. S. Esperança, H. J. R. Guedes, M. Blesic, and L. P. N. Rebelo, *Journal of Chemical & Engineering Data* **51**, 237 (2006).

[5] J. J. Fillion, H. Xia, M. A. Desilva, M. Quiroz-Guzman, and J. F. Brennecke, *Journal of Chemical & Engineering Data* **61**, 2897 (2016).

[6] K. R. Seddon, A. Stark, and M.-J. Torres, *Pure and Applied Chemistry* **72**, 2275 (2000).

[7] F. J. Deive, M. A. Rivas, and A. Rodríguez, *The Journal of Chemical Thermodynamics* **62**, 98 (2013).

[8] J. Jacquemin, P. Husson, A. A. H. Padua, and V. Majer, *Green Chemistry* **8**, 172 (2006).

[9] A. Muhammad, M. I. A. Mutalib, C. D. Wilfred, T. Murugesan, and A. Shafeeq, *The Journal of Chemical Thermodynamics* **40**, 1433 (2008).

[10] J. Jacquemin, R. Ge, P. Nancarrow, D. W. Rooney, M. F. Costa Gomes, A. A. H. Pádua, and C. Hardacre, *Journal of Chemical & Engineering Data* **53**, 716 (2008).

[11] F. M. Gaciño, T. Regueira, A. V. Bolotov, A. Sharipov, L. Lugo, M. J. P. Comuñas, and J. Fernández, *The Journal of Chemical Thermodynamics* **93**, 24 (2016).

[12] R. L. Gardas, R. Ge, P. Goodrich, C. Hardacre, A. Hussain, and D. W. Rooney, *Journal of Chemical & Engineering Data* **55**, 1505 (2009).

[13] C. E. Ferreira, N. M. C. Talavera-Prieto, I. M. A. Fonseca, A. T. G. Portugal, and A. G. M. Ferreira, *The Journal of Chemical Thermodynamics* **47**, 183 (2012).

[14] J. Troncoso, C. A. Cerdeirina, P. Navia, Y. A. Sanmamed, D. González-Salgado, and L. Romaní, *The Journal of Physical Chemistry Letters* **1**, 211 (2009).

[15] M. A. R. Martins, C. M. S. S. Neves, K. A. Kurnia, P. J. Carvalho, M. A. A. Rocha, L. M. Santos, S. P. Pinho, and M. G. Freire, *Fluid Phase Equilibria* **407**, 188 (2016).

[16] C. Aucouturier, G. Roux-Desgranges, and A. H. Roux, *The Journal of Chemical Thermodynamics* **31**, 289 (1999).

[17] J. R. Rumble, *CRC Handbook of Chemistry and Physics*, CRC Press Taylor & Francis Group, Boca Raton, Florida, USA, 2017.

[18] Y. U. Paulechka, A. V. Blokhin, and G. J. Kabo, *Thermochimica Acta* **604**, 122 (2015).

[19] G. Chatel, L. Leclerc, E. Naffrechoux, C. Bas, N. Kardos, C. Goux-Henry, B. Andrioletti, and M. Draye, *Journal of Chemical & Engineering Data* **57**, 3385 (2012).

[20] K. Machanová, Z. Wagner, A. Andresová, J. Rotrekl, A. Boisset, J. Jacquemin, and M. Bendová, *Journal of Solution Chemistry* **44**, 790 (2015).

[21] A. Diedrichs and J. Gmehling, *Fluid Phase Equilibria* **244**, 68 (2006).

[22] S. ZHANG and K. DONG, *Structures and Interactions of Ionic Liquids*, Springer-Verlag, Berlin, Germany, 2013.

[23] H. F. D. ALMEIDA, H. PASSOS, J. A. LOPES-DA SILVA, A. M. FERNANDES, M. G. FREIRE, and J. A. P. COUTINHO, *Journal of Chemical & Engineering Data* **57**, 3005 (2012).

[24] K. MACHANOVÁ, A. BOISSET, Z. SEDLÁKOVÁ, M. ANOUTI, M. BENDOVÁ, and J. JACQUEMIN, *Journal of Chemical & Engineering Data* **57**, 2227 (2012).

[25] G. VAKILI-NEZHAAD, M. VATANI, M. ASGHARI, and I. ASHOUR, *The Journal of Chemical Thermodynamics* **54**, 148 (2012).

[26] Y.-H. YU, A. N. SORIANO, and M.-H. LI, *The Journal of Chemical Thermodynamics* **41**, 103 (2009).

[27] R. ZARROUGUI, N. RAOUAFI, and D. LEMORDANT, *Journal of Chemical & Engineering Data* **59**, 1193 (2014).

[28] O. ZECH, A. STOPPA, R. BUCHNER, and W. KUNZ, *Journal of Chemical & Engineering Data* **55**, 1774 (2010).

[29] C. MATON, N. DE VOS, and C. V. STEVENS, *Chemical Society Reviews* **42**, 5963 (2013).

[30] X. LIN, R. KAVIAN, Y. LU, Q. HU, Y. SHAO-HORN, and M. W. GRINSTAFF, *Chemical Science* **6**, 6601 (2015).

[31] A. F. FERREIRA, P. N. SIMÕES, and A. G. M. FERREIRA, *The Journal of Chemical Thermodynamics* **45**, 16 (2012).

[32] M. T. CLOUGH, K. GEYER, P. A. HUNT, J. MERTES, and T. WELTON, *Physical Chemistry Chemical Physics* **15**, 20480 (2013).

[33] H. L. NGO, K. LECOMPTE, L. HARGENS, and A. B. MCEWEN, *Thermochimica Acta* **357**, 97 (2000).

[34] J. G. HUDDLESTON, A. E. VISSER, W. M. REICHERT, H. D. WILLAUER, G. A. BROKER, and R. D. ROGERS, *Green Chemistry* **3**, 156 (2001).

[35] A. VALOR, E. REGUERA, E. TORRES-GARCÍA, S. MENDOZA, and F. SANCHEZ-SINENCIO, *Thermochimica Acta* **389**, 133 (2002).

[36] J. SALGADO, M. VILLANUEVA, J. J. PARAJÓ, and J. FERNÁNDEZ, *The Journal of Chemical Thermodynamics* **65**, 184 (2013).

[37] M. GOETZ, R. REIMERT, S. BAJOHR, H. SCHNETZER, J. WIMBERG, and T. J. S. SCHUBERT, *Thermochimica Acta* **600**, 82 (2015).

[38] R. GE, C. HARDACRE, P. NANCARROW, and D. W. ROONEY, *Journal of Chemical & Engineering Data* **52**, 1819 (2007).

[39] A. P. FRÖBA, M. H. RAUSCH, K. KRZEMINSKI, D. ASSENBAUM, P. WASSERSCHEID, and A. LEIPERTZ, *International Journal of Thermophysics* **31**, 2059 (2010).

[40] M. E. VAN VALKENBURG, R. L. VAUGHN, M. WILLIAMS, and J. S. WILKES, *Thermochimica Acta* **425**, 181 (2005).

[41] A. NODA, K. HAYAMIZU, and M. WATANABE, *The Journal of Physical Chemistry B* **105**, 4603 (2001).

[42] T. UMECKY, Y. SAITO, and H. MATSUMOTO, *The Journal of Physical Chemistry B* **113**, 8466 (2009).

[43] C. SCHREINER, S. ZUGMANN, R. HARTL, and H. J. GORES, *Journal of Chemical & Engineering Data* **55**, 1784 (2009).

[44] D. R. MACFARLANE, M. FORSYTH, E. I. IZGORODINA, A. P. ABBOTT, G. ANNAT, and K. FRASER, *Physical Chemistry Chemical Physics* **11**, 4962 (2009).

Chapter 5

Modelling of Pure Ionic Liquids Physical Properties

5.1 Quantum chemical Calculations

To fully reflect the group contribution methodology, the exact structure of investigated compounds must be known. In the case of simple organic compounds (*i.e.* carbohydrates, alcohols, organic acids, *etc.*), the charge can be successfully neglected as its impact is negligible, [1–4] as a result of them acting as van der Waals liquids. However, ILs are known for the many types of interactions occurring between the constituents. [5,6] For this reason, the charge distribution is an important factor which must be considered when developing the group contribution methods. Wu *et al.* (**2013**) have already included this effect by dividing the parameters in terms of cation type. [7] Furthermore, following the works of Benson and Buss (**1958**), [8] and Joback (**1984**) [9] in which the group contribution methodology was proposed to be used for heat capacity predictions of molecular solvents, Ge *et al.* (**2008**) used this model to predict the heat capacity of ILs, [10] Nancarrow *et al.* (**2015**) added reoptimized and new groups to the model. [11] As can be noted, none of the models for heat capacity included the charge localization on the molecule, nor the type of cation/anion. It seems to be essential to reconsider this model in order to introduce additional parameters describing the charge distribution on charged species like IL ions.

For this purpose, the Mulliken charges on each atom were used for all selected ions. The comparison of the IL cations and anions with a van der Waals molecule, hexane, was undertaken due to its entire neutral charge character. It can be seen that hexane can be divided into two regions (**Figure 5.1.1**); the first consists of -CH_3 groups with the Mulliken charge of ~-0.634 and ~0.206, for carbon and hydrogen, respectively. The other

region consists of -CH_2- groups with the charge of ~-0.381 and ~0.194, for carbon and hydrogen, respectively.

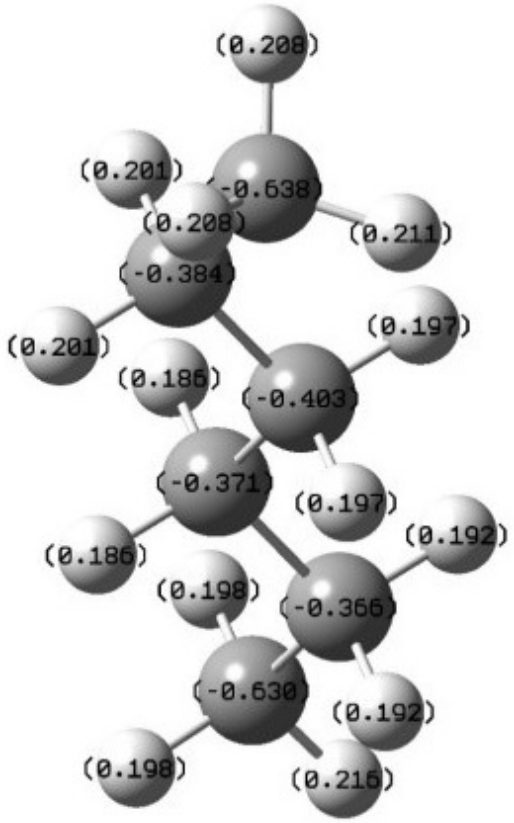

Figure 5.1.1. The structure of hexane with calculated Mulliken charges.

The structures of all the considered cations are shown in **Figure 5.1.2**, and values collected in **Table D1**. It can be observed that all nitrogen-based cations (imidazolium, pyridinium, tetraalkyl ammonium, pyrrolidinium and quinolinium) have similar charge distributions with a slightly negative N-centre with charge of *ca.* -0.090. This can be explained as charge transfer to groups bonded to the positive N-centre, particularly the first one, which exhibits higher charge than in comparison to other groups. It can be also observed that the following 3 groups from N^+ centre are affected, and their behaviour deviated from typically van der Waals-like behaviour, in particular the charge located on hydrogen atoms. It seems reasonable that these should be considered separately from the neutral chains (such as these in hexane). In case of phosphonium cation, the positive charge is located on P^+ centre, as close to +0.928, in contrast to N-based. Moreover, the first 3 groups bonded to P^+ centre are affected, similarly to those of N-based cations.

trimethyl(tetradecyl)ammonium cation

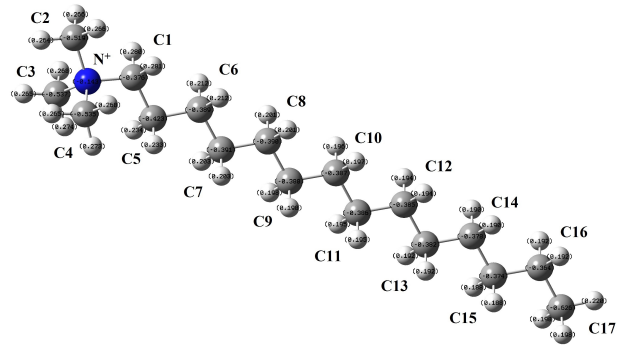

trihexyl(tetradecyl)phosphonium cation

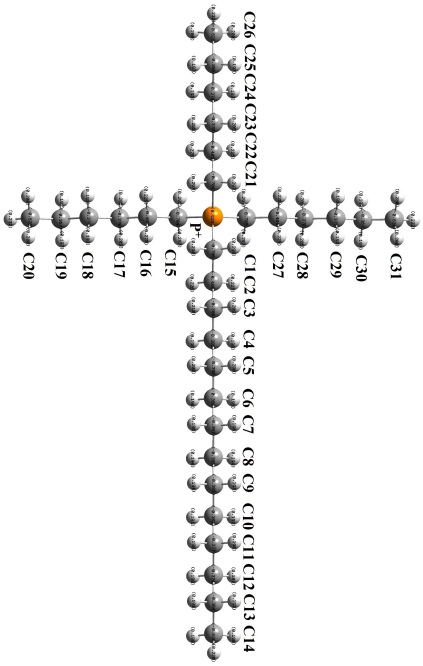

1-octyl-1-methylpyrrolidinium cation

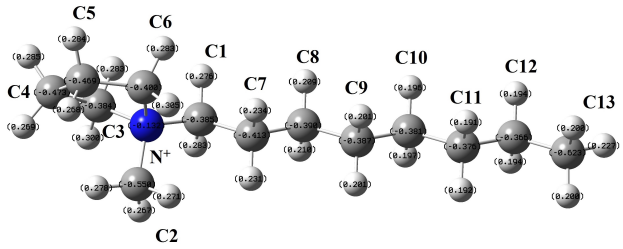

1-hexylquinolinium cation

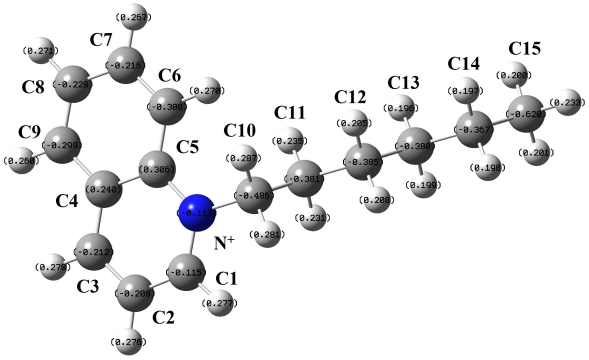

1-octyl-3-methylpyridinium cation

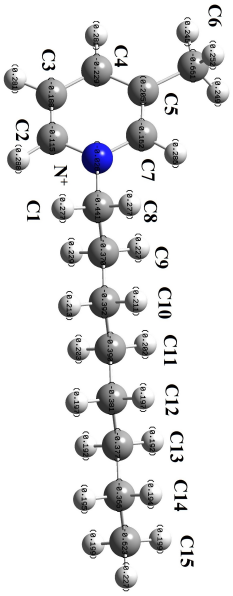

1-methyl-3-tetradecylimidazolium cation

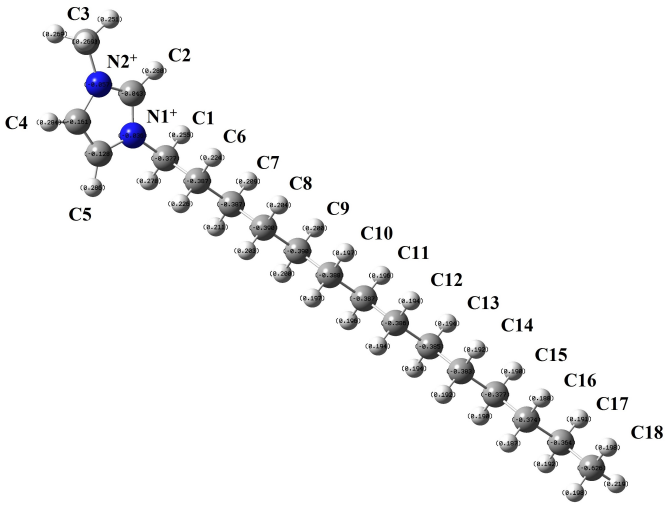

Figure 5.1.2. The structures of considered cations with calculated Mulliken charges.

A similar approach was applied to the anions (**Figure 5.1.3**, and values collected in **Table D2**). Moreover, to distinguish the differences between cations and anions that are N- or P-based, bis[(trifluoromethyl)sulfonyl]imide and hexafluorophosphate anions were considered. It can be seen that the effect of the negative charged group pertains up to the third carbon in the alkyl chain length in the carboxylate anions as found for the cations. Moreover, the nitrogen atom in bis[(trifluoromethyl)sulfonyl]imide anion is highly negative, as expected. It can be also observed that the phosphorus atom in hexafluorophosphate anion is highly positive which is caused by the highly electronegative fluorine atoms attached to the central phosphorus.

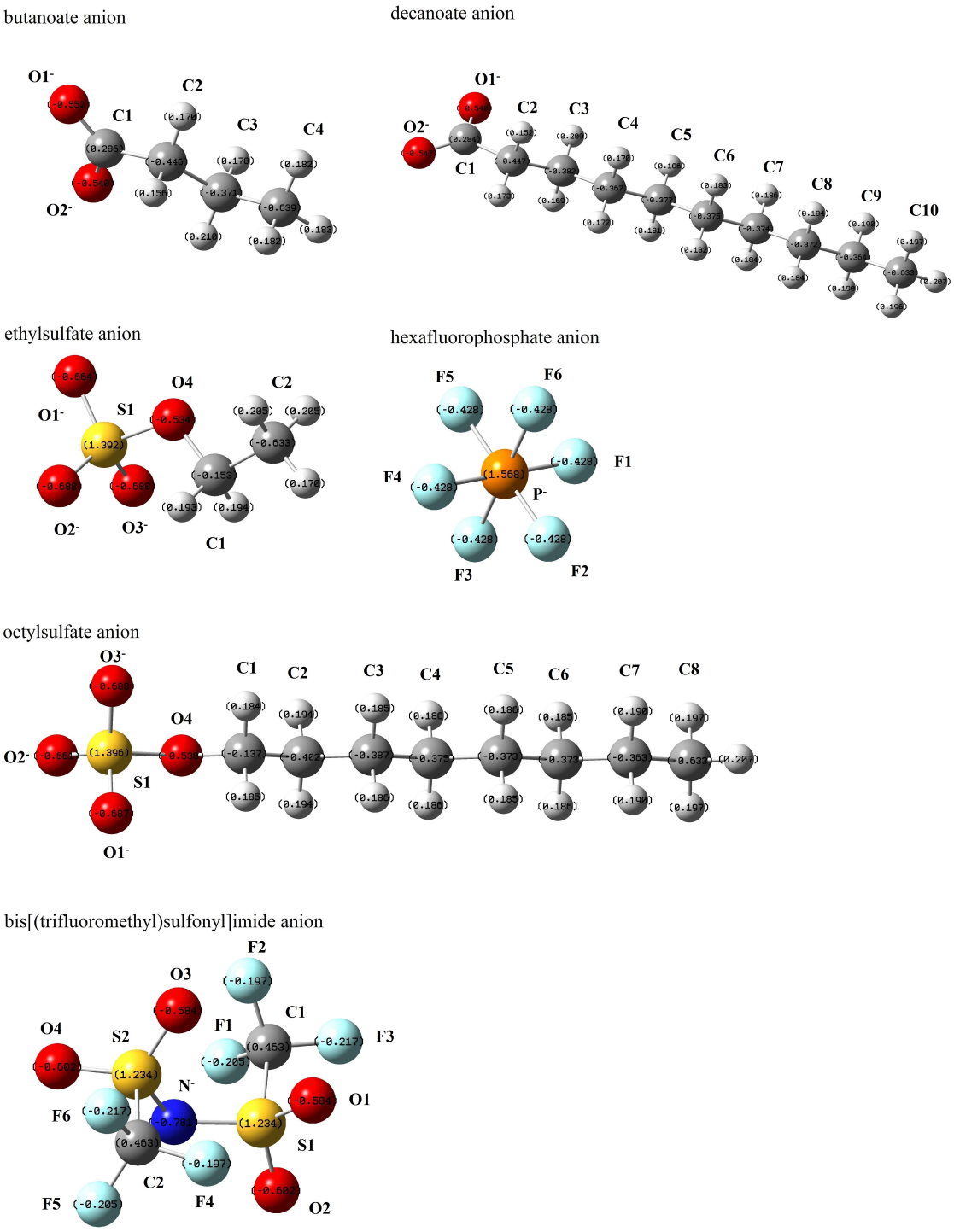

Figure 5.1.3. The structures of considered anions with calculated Mulliken charges.

The above considerations allow new groups to be defined which include the charge distribution. These can be characterised as **a)** van der Waals-like, N-based, P-based and anion-based CH_3 group; **b)** van der Waals-like, N-based, P-based and anion-based CH_2 group; **c)** neutral, cation-based and anion-based >N- group; **d)** cation-based and anion-

based -P group. The first 3 bound carbon groups to the charged centre (both positively and negatively) are divided in terms of N-based, P-based cations, and anions.

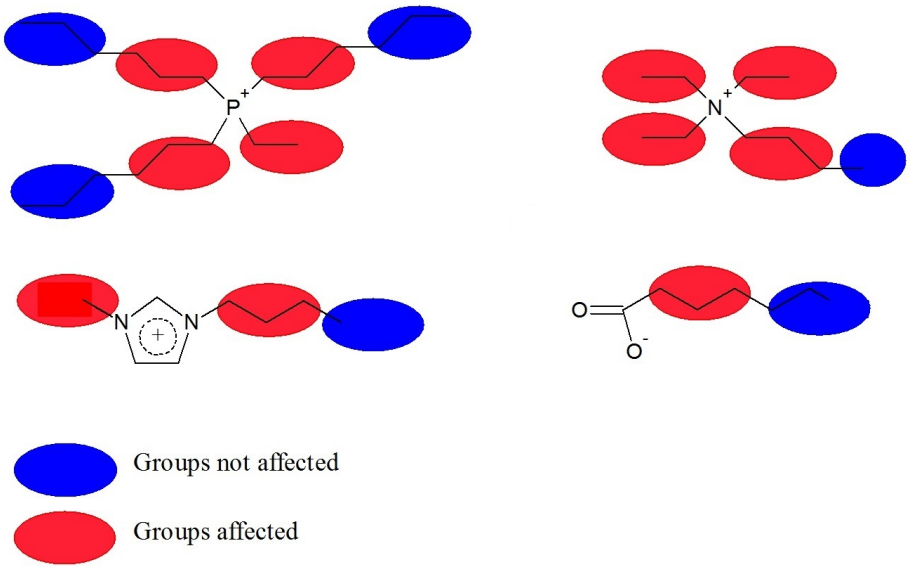

Figure 5.1.4. The examples of phosphonium-, ammonium- and imidazolium-based cations, and carboxylate anions, for heat capacity predictions.

Following this approach, the examples can be given (for cations and anion in **Figure 5.1.4**; red are affected by charge, and blue are not affected): **a)** for ethyltri-hexylphosphonium cation (upper left) – (red: $10 \times –CH_2–_{P-based} + 1 \times –CH_{3,P-based}$) + (blue: $6 \times –CH_2–_{neutral} + 3 \times –CH_{3,neutral}$); **b)** for butyltrimethylammonium cation (upper right) – (red: $6 \times –CH_2–_{N-based} + 3 \times –CH_{3,N-based}$) + (blue: $1 \times –CH_{3,neutral}$); **c)** for 1-butyl-3-methylimidazolium cation (lower left) – (red: $3 \times –CH_2–_{N-based} + 1 \times –CH_{3,N-based}$) + (blue: $1 \times –CH_{3,neutral}$); **d)** for heptanoate anion (lower right) – (red: $3 \times –CH_2–_{anion-based}$) + ($2 \times –CH_2–_{neutral} + 1 \times –CH_{3,neutral}$).

5.2 Thermal Conductivity

As an input to test the available models predictive capabilities, a series of trihexyl(tetredacyl)phosphonium acetate [$P_{14,6,6,6}$][AcO], butanoate [$P_{14,6,6,6}$][ButO], hexanoate [$P_{14,6,6,6}$][HexO], octanoate [$P_{14,6,6,6}$][OctO], and decanoate [$P_{14,6,6,6}$][DecO] ILs were used. This is since this class of ILs (tetraalkylphosphonium cation combined with carboxylate anions) has not been used to establish any of the existing models reported and tested, up to date. It has been previously reported that the thermal conductivity coefficient was not dependent on the anion chain length for investigated [$P_{14,6,6,6}$][*R*O] ILs (Section 4.6), and similar relationships were found for 1-alkyl-3-methylimidazolium-based ILs with different alkyl chain lengths of cation. [12] Regarding the elementary relationship between molar mass of compounds and thermal conductivity, [13] the discrepancy which can be found in ILs influences significantly the ability to predict the thermal conductivity coefficient. This error may be the result of strong cation-anion Coulombic interactions. [5, 7, 14] Moreover, the contribution of hydrogen bonding, as well as van der Waals interactions are not negligible as ILs can form a large variety of these interactions as reported by Hunt *et al.* (**2015**). [5] On the other hand, it was shown in other reports devoted to the predictions that ILs with high molecular mass can deviate from theoretical properties and correction factors are necessary. [15]

The predicted values of thermal conductivity for all the ILs studied are summarised in **Table CD5.1** (Appendix CD5). **Figure 5.2.1a** shows the experimental data as well as the modelled data as a function of temperature, before and after the optimization. To assess the quality of predictions (in comparison to experimental data), relative deviation (RD) were calculated (**Figure 5.2.1b**). Their values were collected in **Table CD5.1** (Appendix CD5), and average absolute relative deviation (AARD) in **Table 5.2.1**.

The deviations using the Wu model before optimization are negative values which may be caused by insufficient anions with a range of carbon chain length being used to derive the model (**Figure 5.2.1b**, **Table CD5.1** in Appendix CD5). After the optimization, the deviations are close to 0%, ranging from positive to negative values. However, to compare the model, overall AARD was calculated as 16.31% for Wu model before optimization. [7, 16, 17]

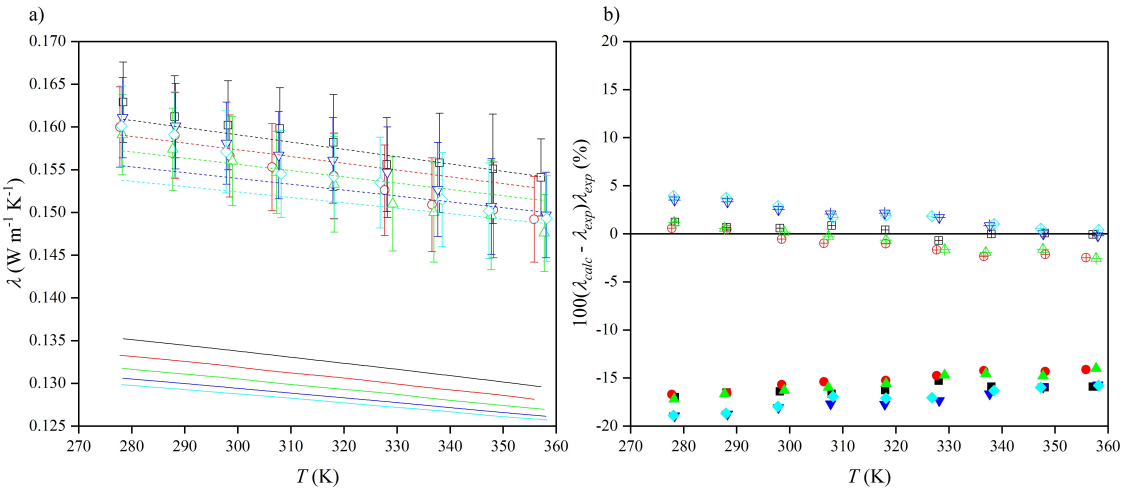

Figure 5.2.1. a) Thermal conductivity, λ, as a function of the temperature, T, for: experimental data, symbols, Wu model before optimization, solid lines, Wu model after optimization, dash lines, $[P_{14,6,6,6}][AcO]$, black, $[P_{14,6,6,6}][ButO]$, red, $[P_{14,6,6,6}][HexO]$, green, $[P_{14,6,6,6}][OctO]$, blue, $[P_{14,6,6,6}][DecO]$, cyan; **b)** relative deviations, $100(\lambda_{calc} - \lambda_{exp})/\lambda_{exp}$, for thermal conductivity prediction in case of Wu model before optimization, full symbols ■, Wu model after optimization, symbols with plus ⊞.

Table 5.2.1. Average absolute relative deviation (AARD) values of investigated ionic liquids thermal conductivity predictions, T = (278-358) K, at atmospheric pressure.

	AARD (%)	
	Wu model before optimization	Wu model after optimization
$[P_{14,6,6,6}][AcO]$	16.20	0.52
$[P_{14,6,6,6}][ButO]$	15.22	1.36
$[P_{14,6,6,6}][HexO]$	15.52	1.18
$[P_{14,6,6,6}][OctO]$	17.42	1.81
$[P_{14,6,6,6}][DecO]$	17.18	2.00

The uncertainty of the measurement determined by the calibration procedure, $K \pm \delta K$, was 0.9932 ± 0.0075 (where K is the calibration constant), what remains 1.50% deviation in case of the calibration constant, and mean 3.44% in case of measurement of $[P_{14,6,6,6}][RO]$ ILs. Nevertheless, the measurement uncertainty reported in the literature was observed to reach values up to 9%. [12, 18] As can be seen, the AARD are highly deviated when compared to the uncertainty of the measurement (before optimization). The maximum RD was found as -18.93% for $[P_{14,6,6,6}][OctO]$ at 278.28 K (**Figure 5.2.1b**, **Table CD5.1** in Appendix CD5). The smallest RD was found as -13.99% for $[P_{14,6,6,6}][HexO]$ at 357.74 K for the Wu model. As can be seen, the maximum RD was

found for the lowest temperature (~278 K), however, the model included no data at these temperatures.

Another important relationship can be found for deviations between calculated and experimental results as a function of temperature (**Figure 5.2.1b**) where for the Wu model before optimization the deviations for all ILs are similar. It may be caused by not accurate enough parametrization of $–CH_2–$ group model which is the only one factor changing in investigated ILs. It can be observed also in **Figure 5.2.2** where the results of thermal conductivity coefficient as a function of anion chain length are presented. Experimental data and values calculated with Wu model exhibited similar gradients which indicates that the prediction can be reliable (in the meaning of anion chain length dependence) while the re-optimization may solve this problem. The slight shifts with consistent slope in the dependence of anion chain length were achieved due to previously mentioned characterization of different $–CH_2–$ group, in the meaning of ILs type (ammonium, phosphonium or others). [7]

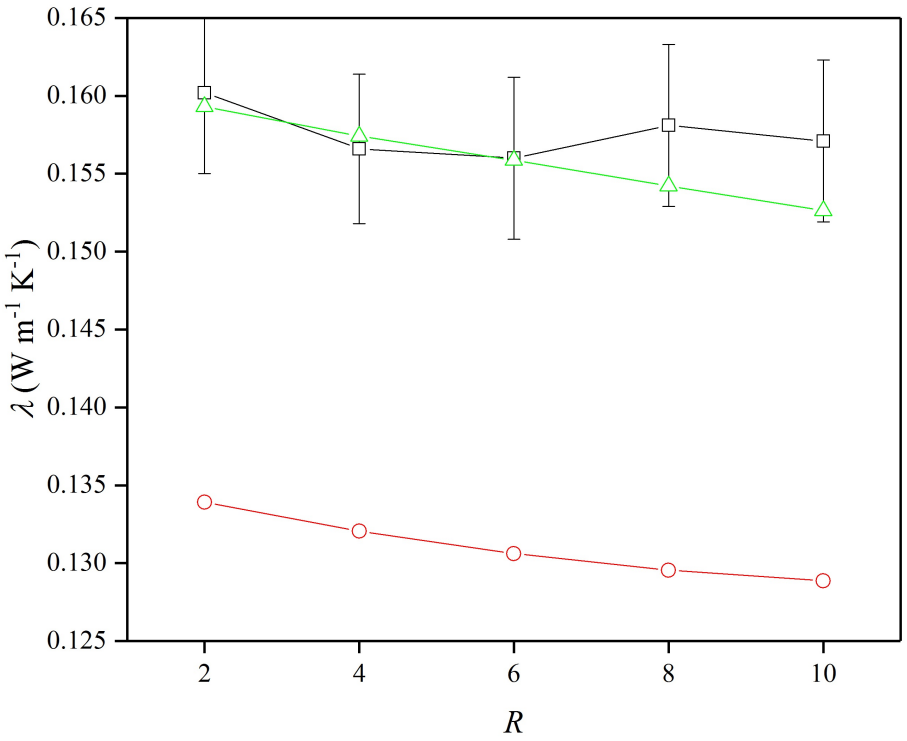

Figure 5.2.2. Thermal conductivity, λ, as a function of $[P_{14,6,6,6}][RO]$ anion chain length, R, at 298.15 K for experimental data, □, Wu model before optimization, ○, Wu model after optimization, △.

The primary Wu model included only a few data points using quaternary phosphonium based ILs (8 ILs with overall 54 data points). In general, the model showed a linear decrease in the thermal conductivity with increasing the chain length. As mentioned above, ILs with high molecular mass are very specific in the meaning of their critical properties due to their deviations from molecular solvents. As was shown by Valderrama *et al.* (**2015**) these properties exhibit deviations from linearity of critical parameters as function of molecular mass when compared to simple molecular solvents. This problem was solved by the introduction of mass connectivity index as a correction factor. [15]

Group contribution methods are known for their simplicity to improve them and implement more data. [19, 20] The only model that was discussed and fully based on this approach is Wu model. All data used to improve the Wu model are summarized in **Table 5.2.2**. 55 ILs were used including those based on imidazolium, pyrrolidinium, pyridinium, phosphonium and ammonium cations. Overall 399 data points were used in the temperature range of (273.15-390) K. Moreover, 9 ILs with molecular mass higher than 500 g mol^{-1} were used, and their critical parameters were calculated based on the methods proposed by Valderrama *et al.* (**2015**). [15] As the thermal conductivity is a transport property, it seems to be reasonable to include the mass connectivity index and describe the connection between cation and anion. The availability of experimental data points for thermal conductivity is still very limited in the literature, thus, it affects the predictive models directly. Moreover, there is significant scatter for the values reported, *e.g.* for $[C_2C_1Im][NTf_2]$ the thermal conductivity has been reported as 0.130 W m^{-1} K^{-1} (298 K) [12] and 0.1202 W m^{-1} K^{-1} (298 K). [21] Therefore, in order to select the data used for the model improvement/development a number of factors were considered including **a)** the sample source, purification, purity and water content, treatment; **b)** the method used to determine the thermal conductivity (transient-hot wire *vs.* parallel plate), and the associated uncertainties; **c)** the experimental data treatment and analysis including calibration, systematic errors reduction and statistical analysis. These three points are not negligible and must be always considered. For example, as was mentioned by Tomida *et al.* (**2007**) [22] and additionally highlighted by Wu *et al.* (**2013**), [7] the data in work of van Valkenburg *et al.* (**2005**) [23] cannot be reliable due to technique that was used which was a transient hot-wire measurement with a tantalum wire having a diameter of 0.052 mm and length of 25.3 mm and a heating rate of 30 K s^{-1}.

The optimization was performed (as explained in Section 2.3) and the AARD values of the model for investigated ILs can be found in **Table 5.2.1**, and whole database in **Table 5.2.2**. As can be seen, after the optimization, the values are below the measurement uncertainty (3.44%), with maximum for $[P_{14,6,6,6}][DecO]$, RD of 3.95 %. The overall AARD for all data sets used is 1.66 %, with maximum AARD of 7.16 % for 1,3-dibutylimidazolium bis[(trifluoromethyl)sulfonyl]imide (**Table 5.2.2**). Wu *et al.* (**2013**) reported the same value of overall AARD, 1.66 %, while the maximum AARD was 11.0 %. [7] Using the extended database in this work, the AARD of the model is 6.80 % (before optimization). The results were also shown in **Figure 5.2.3**, including models before and after optimization. When the uncertainty of the method is taken into account, it can be assumed that the values produced by this method after optimization are satisfactory. Only eight points were out of this range which is only 2% of the whole database. The new group contribution model coefficients are reported in **Table 5.2.3**. The database used together with the calculations applied is included in **Table CD5.2** (Appendix CD5).

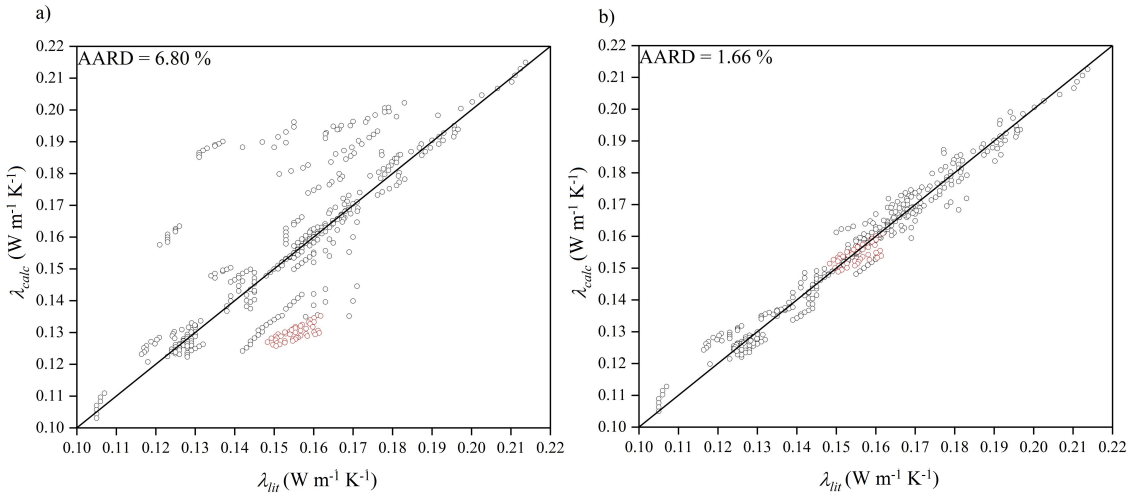

Figure 5.2.3. Linear relationship between experimental, λ_{exp}, and calculated, λ_{calc}, thermal conductivites for all sets of ionic liquids, **a)** before optimization; **b)** after optimization, for training set, ○, testing set (trihexyl(tetradecyl)phosphonium carboxylate ILs, ○.

Table 5.2.2. Summary of ILs data used for the thermal conductivity model improvement.

Name	T (K)	Amount of data	M (g mol^{-1})	AARD (%)
1,2-dimethyl-3-propylimidazolium bis[(trifluoromethyl)sulfonyl]imide [23]	300 – 390	10	419.36	2.22
1,3-dibutyl-imidazolium bis[(trifluoromethyl)sulfonyl]imide [21]	293.15 –353.15	9	461.44	-7.16
1-butyl-1-methylpyrrolidinium bis[(trifluoromethyl)sulfonyl]imide [12]	293 – 323	4	422.41	-0.69
1-butyl-1-methylpyrrolidinium dicyanamide [24]	293.5 – 343.4	6	208.30	-0.79
1-butyl-1-methylpyrrolidinium tris(pentafluoroethyl)trifluorophosphate [12]	293 – 353	7	587.27	-3.14
1-butyl-3-methylimidazolium bis[(trifluoromethyl)sulfonyl]imide [12]	293 – 353	7	419.36	-0.79
1-butyl-3-methylimidazolium dicyanamide [24]	293.6 – 344.2	6	205.26	-2.53
1-butyl-3-methylimidazolium hexafluorophosphate [18]	293 – 353	7	284.18	1.47
1-butyl-3-methylimidazolium tetracyanoborate [25]	283.15 – 353.15	8	254.10	-1.76
1-butyl-3-methylimidazolium tetrafluoroborate [22]	294.2 – 334.3	3	226.02	1.97
1-butyl-3-methylimidazolium tricyanomethane [25]	283.15 – 353.15	8	229.28	-3.17
1-butyl-3-methylimidazolium trifluoromethanesulfonate [12]	293 – 353	7	288.29	0.51
1-butylpyridinium tetrafluoroborate [26]	294.2 – 334.3	3	223.02	3.04
1-decyl-3-methylimidazolium bis[(trifluoromethyl)sulfonyl]imide [12]	293 – 353	7	503.52	3.00
1-decyl-3-methylimidazolium tetracyanoborate [25]	283.15 – 353.15	8	338.26	1.79
1-ethyl-3-methylimidazolium acetate [21]	273.15 – 353.15	9	170.21	0.95
1-ethyl-3-methylimidazolium bis[(trifluoromethyl)sulfonyl]imide [12]	293 – 353	7	391.31	1.04
1-ethyl-3-methylimidazolium dicyanamide [24]	293.4 – 343.4	6	177.21	4.10
1-ethyl-3-methylimidazolium ethylsulfate [12]	293 – 353	7	236.29	0.45
1-ethyl-3-methylimidazolium methylphosphonate [21]	273.15 – 353.15	9	205.18	1.77
1-ethyl-3-methylimidazolium octylsulfate [21]	273.15 – 353.15	9	320.45	0.67
1-ethyl-3-methylimidazolium tricyanomethanide [21, 25]	273.15 – 353.15	17	201.23	1.05
1-hexyl-3-methylimidazolium bis[(trifluoromethyl)sulfonyl]imide [12]	293 – 353	7	447.42	0.41
1-hexyl-3-methylimidazolium hexafluorophosphate [18, 27]	293 – 353	13	312.24	1.80
1-hexyl-3-methylimidazolium tetracyanoborate [25]	283.15 – 353.15	8	282.15	1.05
1-hexyl-3-methylimidazolium tetrafluoroborate [28]	294.2 – 334.4	3	226.02	1.50
1-hexyl-3-methylimidazolium tricyanomethanide [25]	283.15 – 353.15	8	257.33	1.38
1-hexylpyridinium tetrafluoroborate [26]	294.2 – 334.3	3	251.07	1.80
1-octyl-3-methylimidazolium bis[(trifluoromethyl)sulfonyl]imide [12]	293 – 353	7	475.47	0.46
1-octyl-3-methylimidazolium hexafluorophosphate [27]	295.1 – 335.2	3	340.29	2.20
1-octyl-3-methylimidazolium tetracyanoborate [25]	283.15 – 353.15	8	310.21	3.18
1-octyl-3-methylimidazolium tetrafluoroborate [28]	294.2 – 334.3	3	282.13	0.86

1-octyl-3-methylimidazolium tricyanomethanide [25]	283.15 – 353.15	8	285.39	3.01
1-octylpyridinium tetrafluoroborate [26]	294.2 – 334.3	3	279.13	2.25
3-decyl-1-methylimidazolium tricyanomethanide [25]	283.15 – 353.15	8	313.44	1.00
butyltrimethylammonium bis[(trifluoromethyl)sulfonyl]imide [29]	296.69 – 332.21	3	396.38	1.52
methyltrioctylammonium bis[(trifluoromethyl)sulfonyl]imide [21]	273.15 – 353.15	9	648.85	0.83
tetrabutylphosphonium 2-aminoethanesulfonate [30]	298.15 – 353.15	7	383.57	4.43
tetrabutylphosphonium L-cysteinate [30]	298.15 – 353.15	7	379.58	0.14
tetrabutylphosphonium L-lysinate [30]	298.15 – 353.15	7	404.61	0.05
tetrabutylphosphonium L-prolinate [30]	298.15 – 353.15	7	373.55	0.08
tetrabutylphosphonium L-serinate [30]	298.15 – 353.15	7	363.52	1.31
tetrabutylphosphonium L-threoninate [30]	298.15 – 353.15	7	377.54	0.25
tetrabutylphosphonium L-valinate [30]	313.15 – 353.15	5	375.57	0.20
tributylmethylammonium 2-aminoethanesulfonate [30]	298.15 – 353.15	7	324.52	0.28
tributylmethylammonium L-lysinate [30]	298.15 – 353.15	7	345.56	1.89
tributylmethylammonium L-serinate [30]	298.15 – 353.15	7	304.47	0.21
tributylmethylammonium L-threoninate [30]	298.15 – 353.15	7	318.50	0.13
tributylmethylphosphonium methyl sulfate [31]	283.34 – 353.51	9	328.45	1.84
trihexyl(tetradecyl)phosphonium acetate	278.37 – 357.10	9	542.92	0.52
trihexyl(tetradecyl)phosphonium bis[(trifluoromethyl)sulfonyl]imide [12, 31]	285.65 – 353	14	764.00	2.36
trihexyl(tetradecyl)phosphonium chloride [12]	293 – 353	7	519.31	0.15
trihexyl(tetradecyl)phosphonium decanoate	278.09 – 358.21	9	655.13	2.00
trihexyl(tetradecyl)phosphonium tris(pentafluoroethyl)trifluorophosphate [31]	282.19 – 355.07	9	928.87	4.72
trihexyltetradecylphosphonium bis(2,4,4-trimethylpentyl)phosphinate [31]	282.47 – 353.62	9	773.27	1.85
55 unique ILs	**273.15 – 390**	**399**	**170.21 – 928.87**	**1.66**

Table 5.2.3. New parameters for equation (2.3.35) in the Wu model (thermal conductivity).

Group Without rings	$\Delta\lambda_{0,j}$	Amount of data points
-CH_3	0.5929	396
-CH_2- (ammonium-based)	0.101	40
-CH_2- (phosphonium-based)	0.407	113
-CH_2- (with others)	0.701	237
>C<	-0.467	165
>CH-	1.927	63
-CN	2.563	99
-COO-	1.029	88
>N-/>N<$^+$/-N-$^-$	5.28	130
-NH_2	0.929	63
-SO_2-	7.54	130
-O-/[-O]$^-$	-0.208	64
-OH	1.925	28
=O	0.323	18
-F	1.3166	145
-Cl	0.841	7
-B	-1.04	50
-P	3.2939	149
-S-	5.37	7
With rings		
=CH-	-0.022	226
-CH_2-	1.5145	24
>CH-	2.055	7
-NH-	0.547	7
-N=	1.835	226
>N-/>N<$^+$	0.042	234
Coefficients		
k_0	372.98×10^{-2}	
a_0	646.97×10^{-4}	
a_1	-1871.59×10^{-6}	
a_2	25.85×10^{-6}	

5.3 Heat Capacity

As discussed above, the P^+/N^+ centres lead to significant differences in the charge distribution on the bound alkyl chain. For this reason, the charge effect was included in the structure characterization for heat capacity prediction to correctly reproduce the group contribution methodology (as explained in Section 5.1).

The results of heat capacity prediction are summarised in **Table CD5.3** (Appendix CD5), and presented in **Figure 5.3.1a**. The Ge-Nancarrow model does not include any information about connections but divides the structure into characteristic groups (as group contribution methods) for both cation and anion without distinction on the charge type or place on the molecule, [10, 11] as in Joback method. [9] As can be seen, the predicted values have increasingly large deviations from the experimental data with increasing the anion chain length using the model. It is expected that the heat capacity increases with anion chain length which is observed in the experimental and predicted data. The calculated overall AARD is 3.76% before optimization. The maximum determined RD is -7.70% for $[P_{14,6,6,6}]$[DecO] at 298.15 K. While the minimum RD is -0.99% for $[P_{14,6,6,6}]$[OctO] at 363.15 K, as shown in **Figure 5.3.1b**. The AARD values are reported in **Table 5.3.1**. As can be seen, the Ge-Nancarrow model estimated the AARD values of heat capacity below 5% (except $[P_{14,6,6,6}]$[DecO] which was close to this value) for all ILs. The uncertainty of the experimental measurements of heat capacity have been reported to be higher than 10% in some works but, [32–34] more commonly, are up to 3%. [35–37] Thus, the capability of a model that works well is assessed as the AARD below 3%.

Table 5.3.1. Average absolute relative deviation (AARD) values of investigated ionic liquids and models (heat capacity), T = (298.15-363.15) K, at atmospheric pressure.

	AARD (%)	
	Ge-Nancarrow model before optimization	Ge-Nancarrow model after optimization
$[P_{14,6,6,6}]$[AcO]	3.65	2.86
$[P_{14,6,6,6}]$[ButO]	2.95	2.96
$[P_{14,6,6,6}]$[HexO]	3.82	2.28
$[P_{14,6,6,6}]$[OctO]	3.33	1.79
$[P_{14,6,6,6}]$[DecO]	5.05	3.04

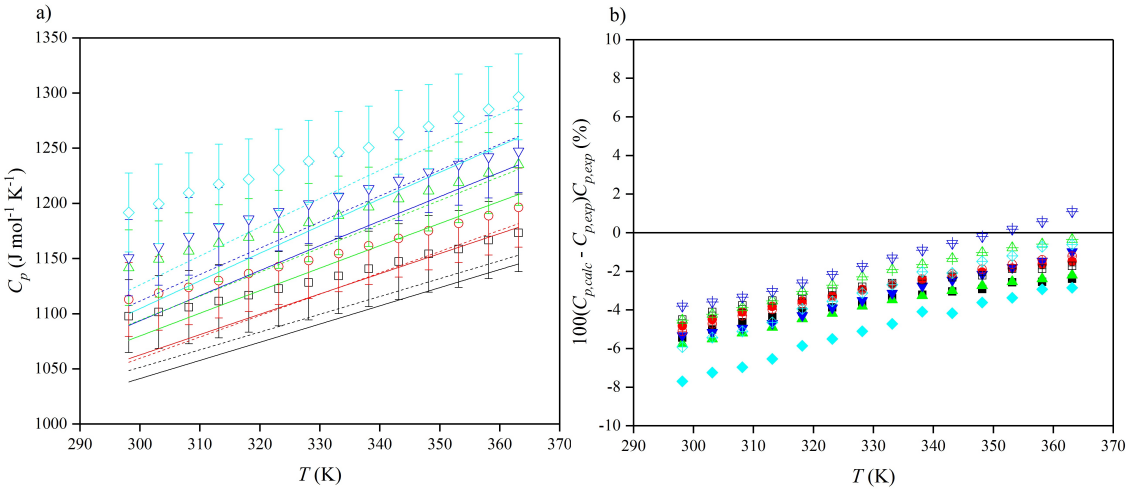

Figure 5.3.1. a) Isobaric heat capacity, C_p, as a function of the temperature, T, for experimental data, symbols, Ge-Nancarrow model before optimization, solid lines, Ge-Nancarrow model after optimization, dash lines [$P_{14,6,6,6}$][AcO], black, [$P_{14,6,6,6}$][ButO], red, [$P_{14,6,6,6}$][HexO], green, [$P_{14,6,6,6}$][OctO], blue, [$P_{14,6,6,6}$][DecO], cyan; **b)** relative deviations, $100(C_{p,calc} - C_{p,exp})/C_{p,exp}$, for isobaric heat capacity prediction in case of Ge-Nancarrow model before optimization, full symbols ■, Wu model after optimization, symbols with plus ⊞.

The deviations for the Ge-Nancarrow model remain similar what may indicate the propagation of the same error, *e.g.* the -CH_2- group characterization, with [$P_{14,6,6,6}$][DecO] as an exception. The heat capacity as a function of anion chain length is presented in **Figure 5.3.2**. The heat capacity depends almost linearly with the anion chain length and a similar dependence was found for the model before and after optimization. Otherwise, a deviation can be easily observed and may be originated from small amount of data for carboxylate anions used to establish the parameters.

The summary of data sets used for the improvement are reported in **Table 5.3.2**. 3646 data points from 103 ILs were used in the temperature range of (190 – 520) K, including those based on imidazolium, pyrrolidinium, pyridinium, phosphonium, ammonium cations. While in the original Ge-Nancarrow model 2642 data points from 96 ILs were used. The described method including the charge distribution was applied in the present work. The availability of heat capacity data in the literature is relatively well-developed, however, different qualities can be observed with very distinctive deviations. The purity

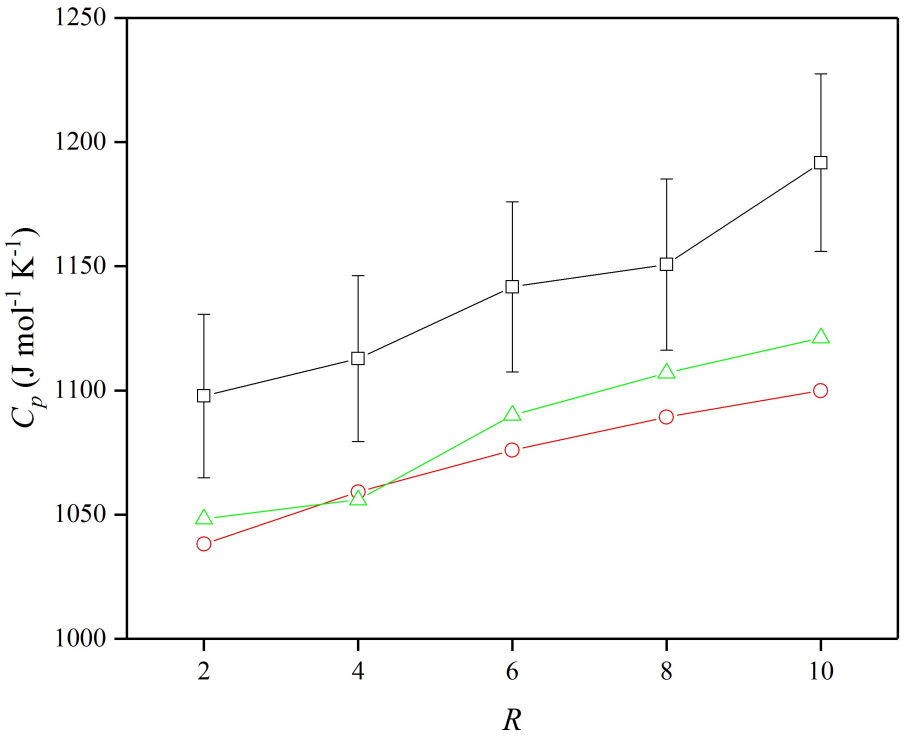

Figure 5.3.2. Isobaric heat capacity, C_p, as a function of $[P_{14,6,6,6}][RO]$ anion chain length, R, at 298.15 K for experimental, □, Ge-Nancarrow model before optimization, ○, Ge-Nancarrow after optimization, △.

(particularly the water content), purity assessment, measurement methodology or measurement uncertainty were taken into account. Similar approach was used as in Nancarrow *et al.* (**2015**) to reduce the impact of one IL's data into the modelling. [11] For example, a large number of data points for $[C_4C_1Im][PF_6]$ originated from one source. [38] Thus, the data sets were selected to consist of no more than 5% of the total number of data points utilised. Similar data discrimination process was used as for the thermal conductivity model optimisation, herein, and in the study by Nancarrow *et al.* (**2015**).

AARD values of the model after optimization are reported in **Table 5.3.1**. It was possible to achieve AARD lower than 3%, with a maximum of 3.04% for $[P_{14,6,6,6}][DecO]$. The overall AARD including all data points is 4.28% which indicates a high prediction ability, in comparison to the measurement uncertainty. Ge-Nancarrow *et al.* (**2015**) reported an overall AARD of 6.27% (using the original database) or 12.57% using the database in this work. Significantly high deviations were observed for 1-ethyl-3-methylimidazolium thiocyanate, [39] 1-methyl-3-propylpyrrolidinium bis[(trifluoromethyl)sulfonyl]imide, [40] 1-butyl-3-methylimidazolium thiocyanate, [39] 1-hexylquinolinium bis[(trifluoromethyl)sulf-

onyl]imide, [41] tributylmethylammonium L-lysinate. [30] This may be caused by the measurement error. The results of the Ge-Nancarrow model before (using the dataset in this work) and after optimization are shown in **Figure 5.3.3**. The original and new model parameters are reported in **Table 5.3.3**. Nevertheless, the prediction for $[P_{14,6,6,6}][RO]$ is better after re-optimization (**Figure 5.3.2**), it is still out of the uncertainty range. However, the general prediction capability is better for all data. A whole database used for the predictions and development can be found in Table CD5.4 (Appendix CD5)

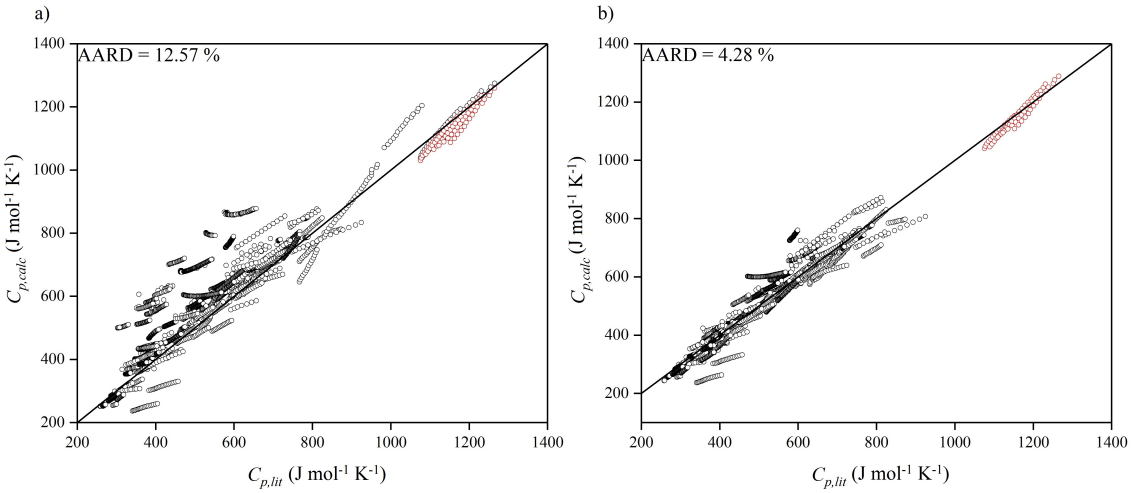

Figure 5.3.3. Linear relationship between experimental, $C_{p,exp}$, and calculated, $C_{p,calc}$, heat capacities for all sets of ionic liquids, **a)** before; **b)** after optimization, for training set, ○, testing set (trihexyl(tetradecyl)phosphonium carboxylate ILs, ○.

Table 5.3.2. Summary of ILs data used for the heat capacity model improvement.

Name	T (K)	Amount of data	M (g mol^{-1})	AARD (%)
2-hydroxy-N-methylethanaminium propionate [42]	287.15-326.15	111	148.2	0.35
1-(2-hydroxyethyl)-3-methylimidazolium 2,2,2-trifluoroacetate [43]	283.15 – 343.15	7	240.2	11.24
1,3-dimethylimidazolium methylsulfate [44]	318.15 – 368.15	6	208.2	5.68
1-butyl-1-methylpyrrolidinium bis[(trifluoromethyl)sulfonyl]imide [10,45]	237.44 – 368.4	85	422.4	2.55
1-butyl-1-methylpyrrolidinium trifluoromethanesulfonate [46]	288.15 – 308.15	3	277.3	9.95
1-butyl-1-methylpyrrolidinium tris(pentafluoroethyl)trifluorophosphate [10]	293 – 358	14	573.3	12.63
1-butyl-2,3-dimethylimidazolium tetrafluoroborate [47,48]	313.2 – 383.2	17	240.1	5.54
1-butyl-2-methylpyridinium tetrafluoroborate [49]	288.15 – 338.15	21	237.1	1.01
1-butyl-3-cyanopyridinium bis[(trifluoromethyl)sulfonyl]imide [50]	298.15 – 353.15	3	441.4	7.22
1-butyl-3-methylimidazolium acetate [51,52]	210 – 413.15	32	198.3	5.43
1-butyl-3-methylimidazolium bis(oxalato)borate [53]	244.30 – 292.74	50	326.1	9.87
1-butyl-3-methylimidazolium bis[(trifluoromethyl)sulfonyl]imide [54–56]	190 – 328.15	32	419.4	0.65
1-butyl-3-methylimidazolium bromide [48,54,57–59]	225.62 – 403.2	57	219.1	5.56
1-butyl-3-methylimidazolium dicyanamide [45,54,60–62]	235.8 – 372.2	156	205.3	4.40
1-butyl-3-methylimidazolium hexafluorophosphate [54,56]	283.15 – 323.15	10	284.2	8.55
1-butyl-3-methylimidazolium iodide [63,64]	209.86 – 370	134	266.1	1.56
1-butyl-3-methylimidazolium methylsulfate [36,65,66]	293.15 – 318.15	18	250.3	0.57
1-butyl-3-methylimidazolium octylsulfate [67]	298.15 – 343.15	46	348.5	2.06
1-butyl-3-methylimidazolium phenolate [68]	303.15 – 353.15	11	220.3	6.38
1-butyl-3-methylimidazolium tetrafluoroborate [40,54,57,69]	278.15 – 358.15	40	226.0	2.44
1-butyl-3-methylimidazolium thiocyanate [39]	296.2 – 372.2	20	197.3	24.19
1-butyl-3-methylimidazolium trifluoroacetate [52]	190 – 370	21	252.2	1.00
1-butyl-3-methylimidazolium trifluoromethanesulfonate [10,32,36,45,54,65,66,70]	292.86 – 425.15	162	288.3	2.18
1-butyl-3-methylpyridinium bis[(trifluoromethyl)sulfonyl]imide [32]	293.1 – 333.1	41	430.4	7.12
1-butyl-3-methylpyridinium trifluoromethanesulfonate [71]	323.1 – 353.1	31	299.3	1.06
1-butyl-4-methylpyridinium bis[(trifluoromethyl)sulfonyl]imide [32]	296.2 – 372.2	20	430.4	8.04
1-butylpyridinium bis[(trifluoromethyl)sulfonyl]imide [70]	323.18 – 423.15	21	416.4	3.19
1-butylpyridinium tetrafluoroborate [72]	284.33	41	223	8.63
1-butylpyridinium trifluoromethanesulfonate [49]	298.15 – 338.15	17	285.3	9.02
1-decyl-3-methylimidazolium phenolate [68]	303.15 – 353.15	11	304.5	1.78
1-ethyl-2,3-dimethylimidazolium bis[(trifluoromethyl)sulfonyl]imide [54]	309.15 – 323.15	4	405.4	12.53
1-ethyl-3-methylimidazolium acetate [73]	298.15	1	170.2	6.22

1-ethyl-3-methylimidazolium bis[(trifluoromethyl)sulfonyl]imide [34, 40, 54, 59, 74]	256.91 – 463.15	72	391.3	1.68
1-ethyl-3-methylimidazolium bromide [59]	347.66 – 367.5	16	191.1	4.37
1-ethyl-3-methylimidazolium dicyanamide [73, 75]	298.15 – 358.2	13	177.2	1.65
1-ethyl-3-methylimidazolium ethylsulfate [36, 65, 66, 76]	190 – 389.95	208	236.3	1.79
1-ethyl-3-methylimidazolium methylsulfate [43, 73, 77]	288.15 – 343.15	11	222.3	6.05
1-ethyl-3-methylimidazolium tetrafluoroborate [40, 78–80]	283.15 – 358.15	28	198.0	1.09
1-ethyl-3-methylimidazolium thiocyanate [39]	296.2 – 372.2	20	169.3	32.42
1-ethyl-3-methylimidazolium trifluoromethanesulfonate [36, 43, 66, 70]	283.15 – 425.15	77	260.2	1.19
1-ethyl-3-methylpyridinium bis[(trifluoromethyl)sulfonyl]imide [32]	293.1 – 333.1	82	402.3	6.99
1-ethyl-3-methylpyridinium ethylsulfate [71]	298 – 323	2	247.3	4.74
1-ethylpyridinium bis[(trifluoromethyl)sulfonyl]imide [81]	288.15 – 338.15	21	388.3	6.77
1-ethylpyridinium bromide [82]	397.31 – 409.65	5	188.1	12.68
1-heptyl-3-methylimidazolium bis[(trifluoromethyl)sulfonyl]imide [83]	298.15	1	461.5	2.65
1-hexyl-2,3-dimethylimidazolium bis[(trifluoromethyl)sulfonyl]imide [71]	298 – 323	2	461.5	0.32
1-hexyl-3,5-dimethylpyridinium bis[(trifluoromethyl)sulfonyl]imide [71]	298 – 323	2	472.5	13.71
1-hexyl-3-methylimidazolium bis(oxalato)borate [53]	239.33 – 397.44	80	354.1	10.55
1-hexyl-3-methylimidazolium bis[(trifluoromethyl)sulfonyl]imide [70, 71, 84, 85]	190 – 425.15	250	447.4	1.46
1-hexyl-3-methylimidazolium bromide [71]	298 – 323	2	247.2	5.81
1-hexyl-3-methylimidazolium hexafluorophosphate [86]	293.15 – 343.15	51	312.2	1.86
1-hexyl-3-methylimidazolium phenolate [68]	303.15 – 353.15	11	248.4	4.96
1-hexyl-3-methylimidazolium tetrafluoroborate [36, 66, 71, 87, 88]	283.15 – 323.15	24	254.1	0.71
1-hexyl-3-methylimidazolium trifluoromethanesulfonate [70]	313.14 – 425.15	64	330.4	1.03
1-hexyl-3-methylimidazolium tris(pentafluoroethyl)trifluorophosphate [86]	293.15 – 343.15	51	612.3	2.31
1-hexyl-3-methylpyridinium bis[(trifluoromethyl)sulfonyl]imide [71, 89]	298 – 323	2	458.5	6.37
1-hexyl-4-cyanopyridinium bis[(trifluoromethyl)sulfonyl]imide [50]	298.15 – 353.15	3	469.4	11.26
1-hexylpyridinium bis[(trifluoromethyl)sulfonyl]imide [71]	298 – 323	2	444.4	1.42
1-hexylquinolinium bis[(trifluoromethyl)sulfonyl]imide [41]	321.52 – 370.13	79	494.5	25.58
1-methyl-1-octylpyrrolidinium bis[(trifluoromethyl)sulfonyl]imide [33]	265.06 – 385.14	13	478.5	11.75
1-methyl-1-propylpiperidinium bis[(trifluoromethyl)sulfonyl]imide [90]	298 – 520	24	422.4	1.84
1-methyl-3-octylimidazolium phenolate [68]	303.15 – 353.15	11	276.4	5.86
1-methyl-3-octylimidazolium tetrafluoroborate [71, 76, 88, 91]	192.85 – 370	132	282.1	0.22
1-methyl-3-pentylimidazolium bis[(trifluoromethyl)sulfonyl]imide [83]	298.15	1	433.4	1.39
1-methyl-3-propylimidazolium bis[(trifluoromethyl)sulfonyl]imide [92]	283.15 – 358.15	41	405.4	7.29
1-methyl-3-propylimidazolium bromide [64]	218.48 – 367.18	39	205.1	5.13
1-octyl-3-methylimidazolium bis[(trifluoromethyl)sulfonyl]imide [71]	298 – 323	2	475.5	8.54

1-octyl-3-methylimidazolium trifluoromethanesulfonate [70]	313.17 – 425.15	64	344.4	1.59
1-octyl-3-methylpydridinium bis[(trifluoromethyl)sulfonyl]imide [71]	298 – 323	2	486.5	9.98
1-octylpyridinium bis[(trifluoromethyl)sulfonyl]imide [33]	265.04 – 385.13	13	472.5	7.63
1-pentylpyridinium hexafluorophosphate [93]	330.91 – 400	50	295.2	1.02
1-propylpyridinium bromide [82]	351.39 – 397.71	16	202.1	9.91
1-propylpyridinium tetrafluoroborate [94]	278.15 – 338.15	25	209	11.54
2-hydroxy-N,N,N-trimethyl-ethanaminium 1-butylsulfate [95]	360.15 – 400.15	9	241.4	1.33
2-hydroxy-N-methylethanaminium butanoate [42]	286.15 – 336.15	92	162.2	3.26
2-hydroxy-N-methylethanaminium pentanoate [42]	283.15 – 333.15	107	176.2	0.34
2-methyl-1-propylpyridinium bis[(trifluoromethyl)sulfonyl]imide [96]	278.15 – 338.15	25	416.4	1.00
2-octylisoquinolinium thiocyanate [97]	278.15 – 343.15	14	300.5	1.15
3-cyano-1-octylpyridinium bis[(trifluoromethyl)sulfonyl]imide [50]	298.15 – 353.15	3	469.4	0.74
3-methyl-1-propylimidazolium (S)-2-amino-4-carboxybutanoate [98]	244.24 – 357.68	58	271.3	16.94
3-methyl-1-propylpyridinium bis[(trifluoromethyl)sulfonyl]imide [32]	293.1 – 333.1	41	416.4	6.61
4-(dimethylamino)-1-hexyl-pyridinium bis[(trifluoromethyl)sulfonyl]imide [70]	315.15 – 425.15	23	487.5	0.69
4,6-dimethyl-N-phenylpyrimidin-2-amine dodecanoate [99]	323.46 – 339.26	10	398.6	7.28
butylethyldimethylammonium ethylsulfate [95]	360.15 – 390.15	7	255.4	2.21
butyltrimethylammonium bis[(trifluoromethyl)sulfonyl]imide [45]	278.32 – 367.93	48	396.4	3.68
N-(2-hydroxyethyl)-N,N-dimethylbutanaminium bromide [35]	409.71 – 438.26	19	226.2	7.33
N-(2-hydroxyethyl)-N,N-dimethylhexan-1-aminium bromide [35]	386.41 – 403.35	13	254.2	1.86
N-(2-hydroxyethyl)-N,N-dimethylpropanaminium bromide [35]	382.50 – 429.98	48	212.1	0.80
n-butyl-4-(n',n'-dimethylammonium)pyridinium bis[(trifluoromethyl)sulfonyl]imide [70]	313.13 – 425.15	64	459.4	4.02
N-ethyl-2-hydroxy-N,N-dimethylethanaminium octylsulfate [95]	355.15 – 395.15	9	311.5	2.83
n-ethyl-4-(n',n'-dimethylammonium)pyridinium bis[(trifluoromethyl)sulfonyl]imide [70]	313.12 – 423.17	23	431.4	1.54
N-ethyl-N-(2-hydroxyethyl)-N,N-dimethylammonium ethylsulfate [95]	300.15 – 375.15	16	243.3	3.03
N-octyl-3-methylpyridinium tetrafluoroborate [49]	278.15 – 328.15	21	293.2	14.50
tetrabutylphosphonium L-serinate [30]	293.15 – 363.15	9	363.5	7.64
tetrabutylphosphonium L-valinate [30]	293.15 – 363.15	9	375.6	9.22
tributylmethylammonium L-lysinate [30]	293.15 – 363.15	9	345.6	10.94
tributylmethylammonium L-serinate [30]	293.15 – 363.15	9	304.5	0.16
tributylmethylammonium L-threoninate [30]	293.15 – 363.15	9	318.5	7.21
tributylmethylphosphonium methylsulfate [34]	343.15 – 463.15	50	328.5	0.47
triethylhexylammonium bis[(trifluoromethyl)sulfonyl]imide [100]	298.15 – 305.15	8	466.5	2.08
triethyloctylammonium bis[(trifluoromethyl)sulfonyl]imide [100]	298.15 – 305.15	8	494.6	1.35
trihexyl(tetradecyl)phosphonium acetate	298.15 – 363.15	14	542.9	2.86

trihexyl(tetradecyl)phosphonium decanoate	298.15 – 363.15	14	655.1	3.04
103 unique ILs	**190 – 520**	**3646**	**148.18 – 655.12**	**4.28**

Table 5.3.3. Original and new parameters for equation (2.3.40) in the Ge-Nancarrow model for heat capacity.

Group	$A_{Cp,i}$ (J mol^{-1} K^{-1})	$B_{Cp,i} \times 10^{-3}$ (J mol^{-1} K^{-2})	$C_{Cp,i} \times 10^{-5}$ (J mol^{-1} K^{-3})	$D_{Cp,i} \times 10^{-8}$ (J mol^{-1} K^{-4})	Amount of data points
Without rings					
-$CH_{3,neutral}$	42.22	-57.25	15.22	-9.67	2676
-$CH_{3,P-based}$	16.25	-74.10	15.24	-9.67	50
-$CH_{3,N-based}$	16.84	6.18	15.22	-9.67	3217
-$CH_{3,anion-based}$	11.51	-29.01	15.40	-9.67	583
-CH_2-$_{neutral}$	1.62	92.40	-5.54	1.19	1385
-CH_2-$_{P-based}$	-6.86	58.95	-5.47	1.19	98
-CH_2-$_{N-based}$	-9.15	111.90	-5.28	1.19	3534
-CH_2-$_{anion-based}$	-28.24	163.54	-5.41	1.19	622
>CH-	-23.00	204.00	-26.50	12.00	124
>C<	-66.20	427.00	-64.10	30.10	1638
-OH	25.70	-69.10	17.70	-9.88	465
-O-	25.50	-63.20	11.10	-5.48	794
-COOH	24.10	42.70	8.04	-6.87	58
-COO-	24.50	40.20	4.02	-4.52	665
-NH_2	26.90	-41.20	16.40	-9.76	124
-NH-	-1.21	76.20	-4.86	1.05	310
>N-$_{cation-based}$	-132.83	419.70	-32.03	14.60	639
>N-$_{anion-based}$	-9.42	143.76	-31.84	14.60	1034
>N-$_{neutral}$	11.86	160.74	-32.44	14.60	46
-CN	36.50	-73.30	18.40	-10.30	275
-F	26.50	-91.30	19.10	-10.30	2053
-Br	28.60	-64.90	13.60	-7.45	215
-I	32.10	-64.10	12.60	-6.87	134
-$P_{cation-based}$	22.58	596.68	0.52		98
-$P_{anion-based}$	51.30	-253.86	0.01		176
-B	-71.24	211.46			481
-S-	-38.23	59.90			54
-SO_2	90.18	7.53			1880
With rings					
=CH-	-2.14	57.40	-0.16	-1.59	2953
=C<	-8.25	101.00	-14.20	6.78	541
-O-	12.20	-12.60	6.03	-3.86	50
=N-	8.83	-3.84	4.35	-2.60	2953

5.4 Conclusions

The prediction of thermophysical properties can lead to a significant reduction in the time and efficiency for designing heat transfer processes using ILs as HTFs. However, robust models must be developed, for of accurate prediction in case of all type of ILs. Together with the development of these models, they should be checked with experimental data not included in the original model formulation. As presented, herein, very low deviations reported by the authors of models do not necessarily lead to good prediction for ILs. This may be due to the range of interactions which are present in the ILs. Unfortunately, it was found in this study that there is no reliable existing models for thermal conductivity and heat capacity which are able to predict these values with high accuracy or in good correlation to the experimental data for a range of tetraalkyl phosphonium carboxylate ILs. Thus, the models for heat capacity and thermal conductivity were improved and the achieved results provide a better predictive capability for ILs. This model development included a novel approach to include the impact of cation/anion core atom on the structure and physical properties of the ILs and was included in the model with proper corrections.

Bibliography

[1] A. FREDENSLUND, R. L. JONES, and J. M. PRAUSNITZ, *AIChE Journal* **21**, 1086 (1975).

[2] K. G. JOBACK and R. C. REID, *Chemical Engineering Communications* **57**, 233 (1987).

[3] R. KÜHNE, R.-U. EBERT, F. KLEINT, G. SCHMIDT, and G. SCHÜÜRMANN, *Chemosphere* **30**, 2061 (1995).

[4] D. T. WU, *Fluid Phase Equilibria* **30**, 149 (1986).

[5] P. A. HUNT, C. R. ASHWORTH, and R. P. MATTHEWS, *Chemical Society Reviews* **44**, 1257 (2015).

[6] R. P. MATTHEWS, T. WELTON, and P. A. HUNT, *Physical Chemistry Chemical Physics* **16**, 3238 (2014).

[7] K.-J. WU, C.-X. ZHAO, and C.-H. HE, *Fluid Phase Equilibria* **339**, 10 (2013).

[8] S. W. BENSON and J. H. BUSS, *The Journal of Chemical Physics* **29**, 546 (1958).

[9] K. G. JOBACK, *A Unified Approach to Physical Property Estimation Using Multivariate Statistical Techniques*, PhD Thesis, Massachusetts Institute of Technology, Cambridge, Massachusetts, USA, 1984.

[10] R. GE, C. HARDACRE, J. JACQUEMIN, P. NANCARROW, and D. W. ROONEY, *Journal of Chemical & Engineering Data* **53**, 2148 (2008).

[11] P. NANCARROW, M. LEWIS, and L. ABOUCHACRA, *Chemical Engineering & Technology* **38**, 632 (2015).

[12] R. GE, C. HARDACRE, P. NANCARROW, and D. W. ROONEY, *Journal of Chemical & Engineering Data* **52**, 1819 (2007).

[13] M. J. ASSAEL, E. CHARITIDOU, and W. A. WAKEHAM, *International Journal of Thermophysics* **10**, 793 (1989).

[14] P. A. HUNT, B. KIRCHNER, and T. WELTON, *Chemistry–A European Journal* **12**, 6762 (2006).

[15] J. O. VALDERRAMA, L. A. FORERO, and R. E. ROJAS, *Industrial & Engineering Chemistry Research* **54**, 3480 (2015).

[16] S. ATASHROUZ, M. MOZAFFARIAN, and G. PAZUKI, *Industrial & Engineering Chemistry Research* **54**, 8600 (2015).

[17] J. A. LAZZÚS, *Fluid Phase Equilibria* **405**, 141 (2015).

[18] C. A. NIETO DE CASTRO, M. J. V. LOURENÇO, A. P. C. RIBEIRO, E. LANGA, S. I. C. VIEIRA, P. GOODRICH, and C. HARDACRE, *Journal of Chemical & Engineering Data* **55**, 653 (2009).

[19] L. CONSTANTINOU and R. GANI, *AIChE Journal* **40**, 1697 (1994).

[20] H. S. ELBRO, A. FREDENSLUND, and P. RASMUSSEN, *Industrial & Engineering Chemistry Research* **30**, 2576 (1991).

[21] A. P. FRÖBA, M. H. RAUSCH, K. KRZEMINSKI, D. ASSENBAUM, P. WASSERSCHEID, and A. LEIPERTZ, *International Journal of Thermophysics* **31**, 2059 (2010).

[22] D. TOMIDA, S. KENMOCHI, T. TSUKADA, and C. YOKOYAMA, *Heat Transfer—Asian Research* **36**, 361 (2007).

[23] M. E. VAN VALKENBURG, R. L. VAUGHN, M. WILLIAMS, and J. S. WILKES, *Thermochimica Acta* **425**, 181 (2005).

[24] J. M. P. FRANÇA, S. I. C. VIEIRA, M. J. V. LOURENÇO, S. M. S. MURSHED, and C. A. NIETO DE CASTRO, *Journal of Chemical & Engineering Data* **58**, 467 (2013).

[25] T. M. KOLLER, S. R. SCHMID, S. J. SACHNOV, M. H. RAUSCH, P. WASSERSCHEID, and A. P. FRÖBA, *International Journal of Thermophysics* **35**, 195 (2014).

[26] D. TOMIDA, S. KENMOCHI, K. QIAO, T. TSUKADA, and C. YOKOYAMA, *Fluid Phase Equilibria* **340**, 31 (2013).

[27] D. TOMIDA, S. KENMOCHI, T. TSUKADA, K. QIAO, and C. YOKOYAMA, *International Journal of Thermophysics* **28**, 1147 (2007).

[28] D. TOMIDA, S. KENMOCHI, T. TSUKADA, K. QIAO, Q. BAO, and C. YOKOYAMA, *International Journal of Thermophysics* **33**, 959 (2012).

[29] H. LIU, E. MAGINN, A. E. VISSER, N. J. BRIDGES, and E. B. FOX, *Industrial & Engineering Chemistry Research* **51**, 7242 (2012).

[30] R. L. GARDAS, R. GE, P. GOODRICH, C. HARDACRE, A. HUSSAIN, and D. W. ROONEY, *Journal of Chemical & Engineering Data* **55**, 1505 (2009).

[31] A. G. M. FERREIRA, P. N. SIMÕES, A. F. FERREIRA, M. A. FONSECA, M. S. A. OLIVEIRA, and A. S. M. TRINO, *The Journal of Chemical Thermodynamics* **64**, 80 (2013).

[32] N. CALVAR, E. GÓMEZ, E. A. MACEDO, and Á. DOMÍNGUEZ, *Thermochimica Acta* **565**, 178 (2013).

[33] G. CHATEL, L. LECLERC, E. NAFFRECHOUX, C. BAS, N. KARDOS, C. GOUX-HENRY, B. ANDRIOLETTI, and M. DRAYE, *Journal of Chemical & Engineering Data* **57**, 3385 (2012).

[34] A. F. FERREIRA, P. N. SIMÕES, and A. G. M. FERREIRA, *The Journal of Chemical Thermodynamics* **45**, 16 (2012).

[35] U. DOMAŃSKA and R. BOGEL-ŁUKASIK, *The Journal of Physical Chemistry B* **109**, 12124 (2005).

[36] G. GARCÍA-MIAJA, J. TRONCOSO, and L. ROMANÍ, *The Journal of Chemical Thermodynamics* **41**, 161 (2009).

[37] Y. A. SANMAMED, P. NAVIA, D. GONZÁLEZ-SALGADO, J. TRONCOSO, and L. ROMANÍ, *Journal of Chemical & Engineering Data* **55**, 600 (2009).

[38] G. J. KABO, A. V. BLOKHIN, Y. U. PAULECHKA, A. G. KABO, M. P. SHYMANOVICH, and J. W. MAGEE, *Journal of Chemical & Engineering Data* **49**, 453 (2004).

[39] P. NAVARRO, M. LARRIBA, J. GARCÍA, and F. RODRÍGUEZ, *Thermochimica Acta* **588**, 22 (2014).

[40] D. WALISZEWSKI, I. STĘPNIAK, H. PIEKARSKI, and A. LEWANDOWSKI, *Thermochimica Acta* **433**, 149 (2005).

[41] U. DOMAŃSKA, M. ZAWADZKI, and M. ZWOLIŃSKA, *The Journal of Chemical Thermodynamics* **43**, 775 (2011).

[42] N. M. C. TALAVERA-PRIETO, A. G. M. FERREIRA, P. N. SIMÕES, P. J. CARVALHO, S. MATTEDI, and J. A. P. COUTINHO, *The Journal of Chemical Thermodynamics* **68**, 221 (2014).

[43] L. E. FICKE, H. RODRÍGUEZ, and J. F. BRENNECKE, *Journal of Chemical & Engineering Data* **53**, 2112 (2008).

[44] S. APARICIO, R. ALCALDE, B. GARCIA, and J. M. LEAL, *The Journal of Physical Chemistry B* **113**, 5593 (2009).

[45] Y. U. PAULECHKA, A. G. KABO, A. V. BLOKHIN, G. J. KABO, and M. P. SHEVELYOVA, *Journal of Chemical & Engineering Data* **55**, 2719 (2010).

[46] E. J. GONZÁLEZ, Á. DOMÍNGUEZ, and E. A. MACEDO, *Journal of Chemical & Engineering Data* **57**, 2165 (2012).

[47] C. P. FREDLAKE, J. M. CROSTHWAITE, D. G. HERT, S. N. V. K. AKI, and J. F. BRENNECKE, *Journal of Chemical & Engineering Data* **49**, 954 (2004).

[48] H.-C. HU, A. N. SORIANO, R. B. LERON, and M.-H. LI, *Thermochimica Acta* **519**, 44 (2011).

[49] I. BANDRES, G. PERA, S. MARTIN, M. CASTRO, and C. LAFUENTE, *The Journal of Physical Chemistry B* **113**, 11936 (2009).

[50] U. DOMAŃSKA, K. SKIBA, M. ZAWADZKI, K. PADUSZYŃSKI, and M. KRÓLIKOWSKI, *The Journal of Chemical Thermodynamics* **56**, 153 (2013).

[51] J. SAFAROV, M. GEPPERT-RYBCZYŃSKA, I. KUL, and E. HASSEL, *Fluid Phase Equilibria* **383**, 144 (2014).

[52] A. A. STRECHAN, Y. U. PAULECHKA, A. V. BLOKHIN, and G. J. KABO, *The Journal of Chemical Thermodynamics* **40**, 632 (2008).

[53] M. YANG, J.-N. ZHAO, Q.-S. LIU, L.-X. SUN, P.-F. YAN, Z.-C. TAN, and U. WELZ-BIERMANN, *Physical Chemistry Chemical Physics* **13**, 199 (2011).

[54] C. P. FREDLAKE, M. J. MULDOON, S. N. V. K. AKI, T. WELTON, and J. F. BRENNECKE, *Physical Chemistry Chemical Physics* **6**, 3280 (2004).

[55] A. V. Blokhin, Y. U. Paulechka, A. A. Strechan, and G. J. Kabo, *The Journal of Physical Chemistry B* **112**, 4357 (2008).

[56] J. Troncoso, C. A. Cerdeiriña, Y. A. Sanmamed, L. Romaní, and L. P. N. Rebelo, *Journal of Chemical & Engineering Data* **51**, 1856 (2006).

[57] K.-S. Kim, B.-K. Shin, H. Lee, and F. Ziegler, *Fluid Phase Equilibria* **218**, 215 (2004).

[58] K. S. Kim and H. Lee, *The Korean Journal of Chemical Engineering* **21**, 1010 (2004).

[59] Y. U. Paulechka, G. J. Kabo, A. V. Blokhin, A. S. Shaplov, E. I. Lozinskaya, and Y. S. Vygodskii, *The Journal of Chemical Thermodynamics* **39**, 158 (2007).

[60] N. Calvar, I. Domínguez, E. Gómez, J. Palomar, and Á. Domínguez, *The Journal of Chemical Thermodynamics* **67**, 5 (2013).

[61] C. A. N. de Castro, E. Langa, A. L. Morais, M. L. M. Lopes, M. J. V. Lourenço, F. J. V. Santos, M. S. C. S. Santos, J. N. C. Lopes, H. I. M. Veiga, and M. Macatrão, *Fluid Phase Equilibria* **294**, 157 (2010).

[62] P. Navarro, M. Larriba, E. Rojo, J. García, and F. Rodríguez, *Journal of Chemical & Engineering Data* **58**, 2187 (2013).

[63] G. J. Kabo, Y. U. Paulechka, A. G. Kabo, and A. V. Blokhin, *The Journal of Chemical Thermodynamics* **42**, 1292 (2010).

[64] Y. U. Paulechka and A. V. Blokhin, *The Journal of Chemical Thermodynamics* **79**, 94 (2014).

[65] G. García-Miaja, J. Troncoso, and L. Romaní, *Fluid Phase Equilibria* **274**, 59 (2008).

[66] G. García-Miaja, J. Troncoso, and L. Romaní, *The Journal of Chemical Thermodynamics* **41**, 334 (2009).

[67] M. J. Dávila, S. Aparicio, R. Alcalde, B. García, and J. M. Leal, *Green Chemistry* **9**, 221 (2007).

[68] S. N. Shah, K. C. Lethesh, M. I. A. Mutalib, and R. B. M. Pilus, *Industrial & Engineering Chemistry Research* **54**, 3697 (2015).

[69] L. P. N. Rebelo, V. Najdanovic-Visak, Z. P. Visak, M. N. Da Ponte, J. Szydlowski, C. A. Cerdeirina, J. Troncoso, L. Romani, J. Esperanca, and H. J. R. Guedes, *Green Chemistry* **6**, 369 (2004).

[70] A. Diedrichs and J. Gmehling, *Fluid Phase Equilibria* **244**, 68 (2006).

[71] J. M. Crosthwaite, M. J. Muldoon, J. K. Dixon, J. L. Anderson, and J. F. Brennecke, *The Journal of Chemical Thermodynamics* **37**, 559 (2005).

[72] Z.-H. Zhang, Z.-C. Tan, L.-X. Sun, Y. Jia-Zhen, X.-C. Lv, and Q. Shi, *Thermochimica Acta* **447**, 141 (2006).

[73] M. G. Freire, A. R. R. Teles, M. A. A. Rocha, B. Schröder, C. M. S. S. Neves, P. J. Carvalho, D. V. Evtuguin, L. M. Santos, and J. A. P. Coutinho, *Journal of Chemical & Engineering Data* **56**, 4813 (2011).

[74] M. Dzida, M. Chorążewski, M. Geppert-Rybczyńska, E. Zorębski, M. Zorębski, M. Zarska, and B. Czech, *Journal of Chemical & Engineering Data* **58**, 1571 (2013).

[75] Y.-H. Yu, A. N. Soriano, and M.-H. Li, *The Journal of Chemical Thermodynamics* **41**, 103 (2009).

[76] Y. U. Paulechka, A. V. Blokhin, and G. J. Kabo, *Thermochimica Acta* **604**, 122 (2015).

[77] P. F. Requejo, E. J. González, E. A. Macedo, and Á. Domínguez, *The Journal of Chemical Thermodynamics* **74**, 193 (2014).

[78] V. K. Sharma, S. Bhagour, S. Solanki, and D. Sharma, *The Journal of Chemical Thermodynamics* **79**, 19 (2014).

[79] V. K. Sharma, S. Solanki, and S. Bhagour, *Journal of Chemical & Engineering Data* **59**, 1140 (2014).

[80] V. K. Sharma, S. Solanki, and S. Bhagour, *Journal of Chemical & Engineering Data* **59**, 1852 (2014).

[81] J. Benito, M. García-Mardones, V. Pérez-Gregorio, I. Gascón, and C. Lafuente, *Journal of Solution Chemistry* **43**, 696 (2014).

[82] B. Tong, Q.-S. Liu, Z.-C. Tan, and U. Welz-Biermann, *The Journal of Physical Chemistry A* **114**, 3782 (2009).

[83] M. A. A. Rocha, M. Bastos, J. A. P. Coutinho, and L. M. Santos, *The Journal of Chemical Thermodynamics* **53**, 140 (2012).

[84] D. G. ARCHER, *Thermodynamic Properties of 1-Hexyl-3-methylimidazolium Bis(trifluoromethylsulfonyl)imide*, US Department of Commerce, Technology Administration, National Institute of Standards and Technology, Gaithersburg, Maryland, USA, 2006.

[85] A. V. BLOKHIN, Y. U. PAULECHKA, and G. J. KABO, *Journal of Chemical & Engineering Data* **51**, 1377 (2006).

[86] J.-G. LI, Y.-F. HU, S. LING, and J.-Z. ZHANG, *Journal of Chemical & Engineering Data* **56**, 3068 (2011).

[87] G. GARCÍA-MIAJA, J. TRONCOSO, and L. ROMANÍ, *The Journal of Chemical Thermodynamics* **41**, 161 (2009).

[88] D. WALISZEWSKI, *The Journal of Chemical Thermodynamics* **40**, 203 (2008).

[89] G. W. MEINDERSMA, B. T. J. SIMONS, and A. B. DE HAAN, *The Journal of Chemical Thermodynamics* **43**, 1628 (2011).

[90] C. J. RAO, R. V. KRISHNAN, K. A. VENKATESAN, K. NAGARAJAN, and T. G. SRINIVASAN, *Journal of Thermal Analysis and Calorimetry* **97**, 937 (2009).

[91] D. WALISZEWSKI and H. PIEKARSKI, *The Journal of Chemical Thermodynamics* **42**, 189 (2010).

[92] E. GÓMEZ, N. CALVAR, Á. DOMÍNGUEZ, and E. A. MACEDO, *Industrial & Engineering Chemistry Research* **52**, 2103 (2013).

[93] Q.-S. LIU, Z.-C. TAN, U. WELZ-BIERMANN, and X.-X. LIU, *The Journal of Chemical Thermodynamics* **68**, 82 (2014).

[94] I. BANDRÉS, M. C. LÓPEZ, M. CASTRO, J. BARBERÁ, and C. LAFUENTE, *The Journal of Chemical Thermodynamics* **44**, 148 (2012).

[95] M. MAHROVA, M. VILAS, A. DOMINGUEZ, E. GÓMEZ, N. CALVAR, and E. TOJO, *Journal of Chemical & Engineering Data* **57**, 241 (2012).

[96] M. GARCÍA-MARDONES, I. BANDRÉS, M. C. LÓPEZ, I. GASCÓN, and C. LAFUENTE, *Journal of Solution Chemistry* **41**, 1836 (2012).

[97] M. KRÓLIKOWSKA, K. PADUSZYŃSKI, and M. ZAWADZKI, *Journal of Chemical & Engineering Data* **58**, 285 (2013).

[98] Q.-S. LIU, J.-N. ZHAO, J. TONG, L.-X. SUN, Z.-C. TAN, and U. WELZ-BIERMANN, *Journal of Chemical & Engineering Data* **55**, 4036 (2010).

[99] X.-H. SUN, Y.-F. LIU, Z.-C. TAN, Y.-Y. DI, H.-F. WANG, and M.-H. WANG, *The Journal of Chemical Thermodynamics* **36**, 895 (2004).

[100] K. MACHANOVÁ, Z. WAGNER, A. ANDRESOVÁ, J. ROTREKL, A. BOISSET, J. JACQUEMIN, and M. BENDOVÁ, *Journal of Solution Chemistry* **44**, 790 (2015).

Chapter 6

Trihexyl(tetradecyl)phosphonium Carboxylate - Based Ionanofluids

6.1 Density

ILs containing nanoparticles were also measured in terms of density (data can be found in **Figure CD6a.1-CD6a.5**, Appendix CD6a, and **Table CD6b.1**, Appendix CD6b). The parameters of linear equation (2.2.42), $\rho(T)$, as a function of the temperature can be found in **Table CD6a.1** (Appendix CD6a). The values of the slope for all systems are very similar, therefore, the changes within the whole temperature range are similar to those of pure ILs (~4.7% of decrease from the lowest to the highest temperature, as in Section 4.2).

Solids usually have a higher density than liquids, particularly the investigated nanoparticles, as investigated in Section 3.2.1, (1626.34, 1911.89 and 1711.99) kg m^{-3} for carbon nanotubes, boron nitride and graphite at 298.15 K, respectively, therefore, the density of IL and nanoparticle mixtures have higher values than these of pure IL. Unfortunately, at the stage of studies carried out in Section 3.2.1, mesoporous carbon was not considered, thus the values of density for this materials were not characterized, therein, as explained later.

The enhancement can be onserved in **Figure 6.1.1** (for 298.15 K) and **Figure 6.1.2** (for 363.15 K), with enhancements values listed in **Table C1** (Appendix C). It can be seen that the density is depending on the nanoparticle concentration almost linearly.

The differences between enhancements at these temperatures are very small, usually only slightly increasing with temperature, more specifically the maximum range of enhancement was found as (2.40-1.99, 2.58-2.22, 3.15-2.87 and 2.32-1.56) % for

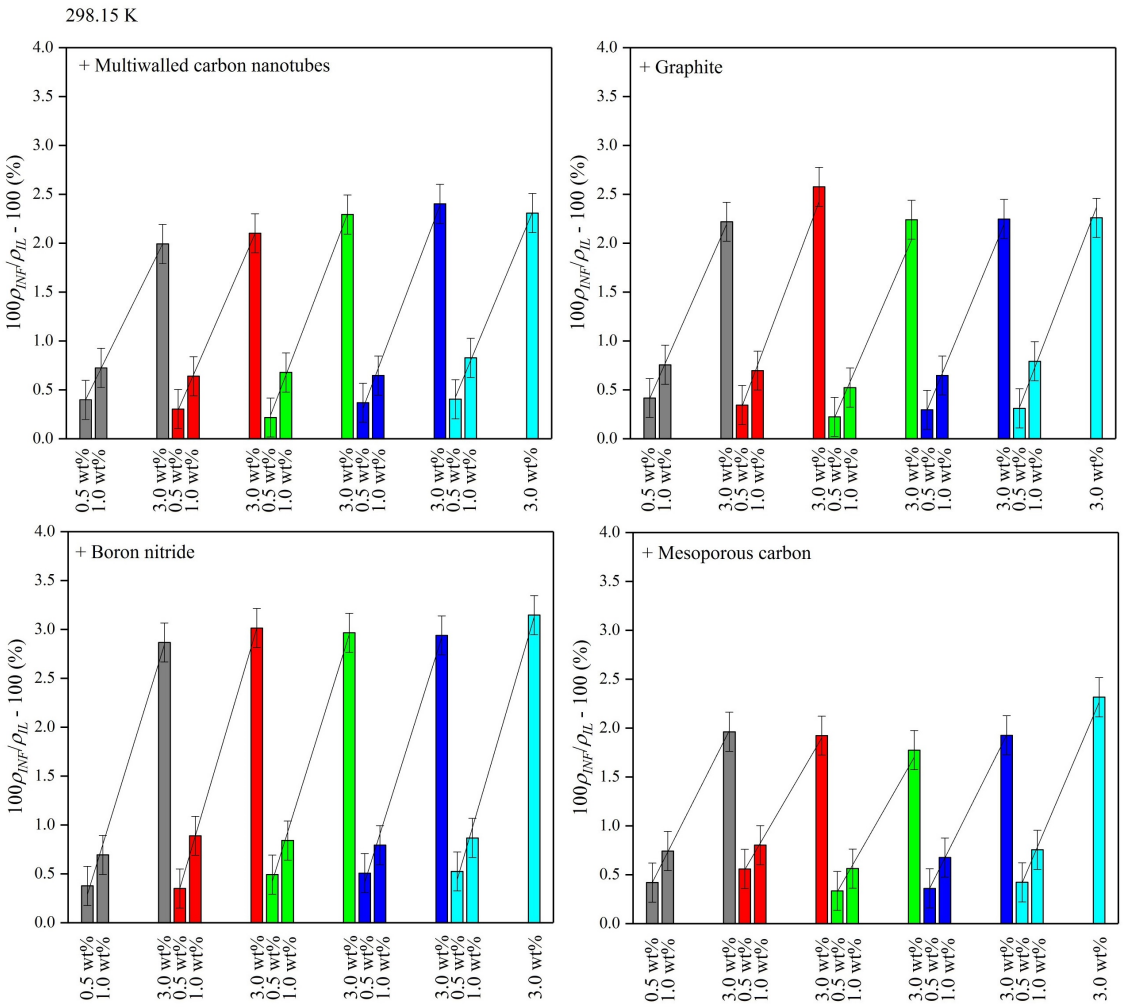

Figure 6.1.1. Density enhancement of ionanofluids, ($100\rho_{INF}/\rho_{IL}$-100), in comparison to pure ionic liquids, over the nanoparticles mass fraction, for $[P_{14,6,6,6}]$[AcO] INF, grey, $[P_{14,6,6,6}]$[ButO] INF, red, $[P_{14,6,6,6}]$[HexO] INF, green, $[P_{14,6,6,6}]$[OctO] INF, blue, $[P_{14,6,6,6}]$[DecO] INF, cyan, at 298.15 K.

MWCNT, G, BN and MC at 298.15 K, respectively, and (2.45-2.05, 2.70-2.32, 3.33-3.00 and 2.42-1.56) % for MWCNT, G, BN and MC at 363.15 K, respectively. While the average enhancement error is similar for all samples and equals to about ± 0.20 %.

The influence of IL structure on the intermolecular interactions has been widely investigated in the literature. [1–3] Particularly for ILs with various anion chain length. The breakthrough of intermolecular interactions occurs at about 6 hydrocarbon chain segments where the pure Coulombic driven forces are significantly affected by van der Waals interactions and/or the volume of anions starts to be an influencing factor (as explained in Section 4.7). The effect of anion on the enhancement can be studied in this work, as

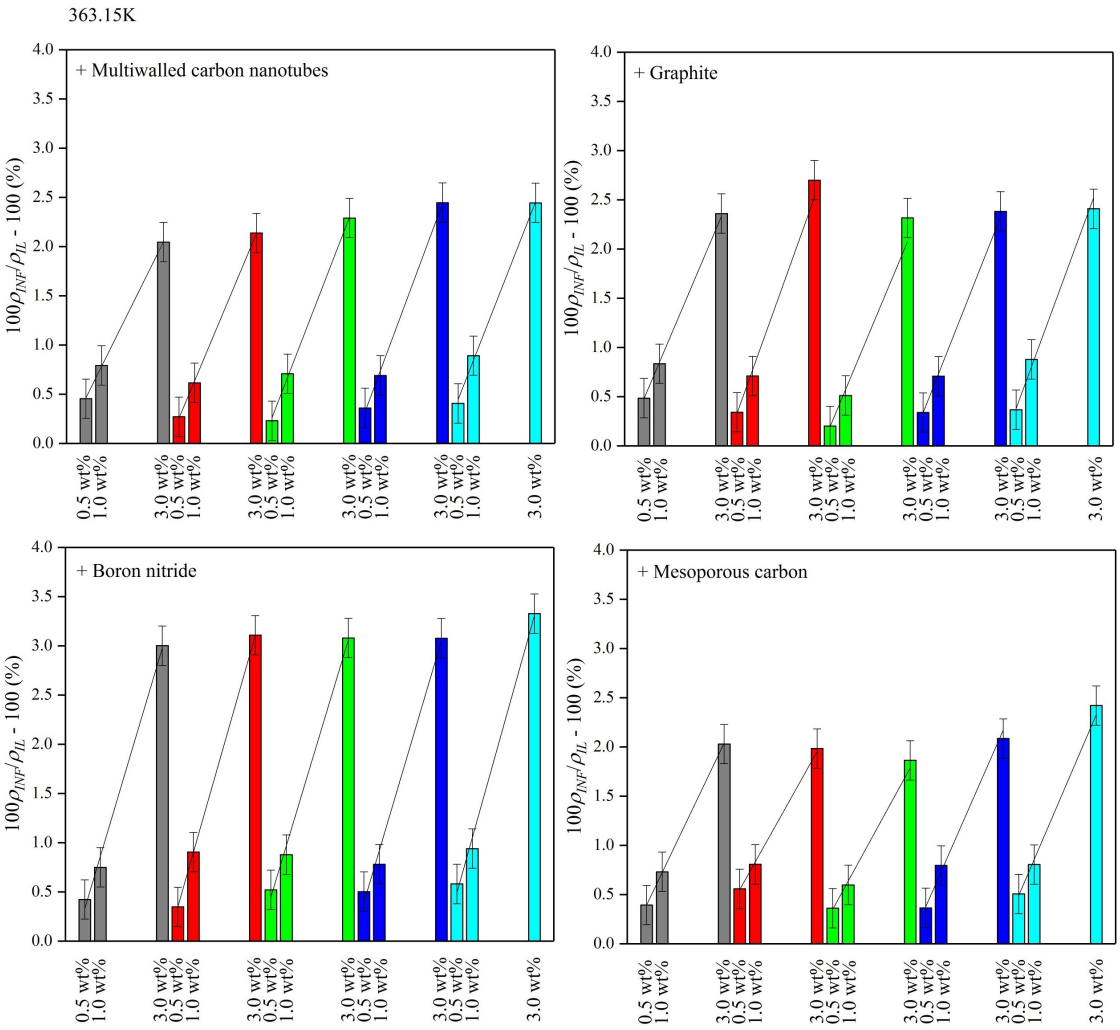

Figure 6.1.2. Density enhancement of ionanofluids, ($100\rho_{INF}/\rho_{IL}$-100), in comparison to pure ionic liquids, over the nanoparticles mass fraction, for $[P_{14,6,6,6}]$[AcO] INF, grey, $[P_{14,6,6,6}]$[ButO] INF, red, $[P_{14,6,6,6}]$[HexO] INF, green, $[P_{14,6,6,6}]$[OctO] INF, blue, $[P_{14,6,6,6}]$[DecO] INF, cyan, at 363.15 K.

several anions with various chain lengths were studied. In most cases the enhancement decreases with anion chain length to hexanoate anion (negligible effect of anion chain length size but caused by the bulkier properties so as a result less possibilities to adsorb on the surface of nanoparticles), and then increasing again (driven by decreasing the electrostatic forces between cations and anions, therefore, more favoured adsorption onto the surface of nanoparticles).

The density of ionanofluids was also extensively investigated for different classes of ILs, 1-butyl-3-methylimidazolium dicyanamide, 1-butyl-3-methylimidazolium bis[(trifluo romethyl)sulfonyl]imide, 1-butyl-1-methylpyrrolidinium bis[(trifluoromethyl)sulfonyl]imi

de, 1-hexyl-3-methylimidazolium hexafluorophosphate, 1-ethyl-3-methylimidazolium ethylsulfate, with multiwalled carbon nanotubes, boron nitride and graphite in Section 3.2.1. However, no dependence was found therein. The enhancement, as presented above, can be found to be dependent on the nanoparticle and size: MWCNT < MC < BN < G.

The highest value of density in this work, 920.24 kg m^{-3} for $[P_{14,6,6,6}][AcO]$ + 3 wt% BN at 298.15 K (from 894.6 kg m^{-3} for pure IL), is still moderate in comparison to commonly used HTFs. To remind, this depends on the type of compound used in the HTFs, for example the values in this work are similar to synthetic aromatic hydrocarbon mixtures (*i.e.* Therminol ADX10 or Dynalene SF), slightly lower than water, or significantly lower than glycol-based HTFs (for example Dowtherm 4000 or Dynalene EG series).

The density of ionanofluids was calculated by using the additivity model, described by equation (2.3.52). As discussed in Section 3.2.1, this approach was successfully used for ionanofluids with imidazolium- and pyrrolidinium-based ILs and carbon nanotubes, boron nitride and graphite. The input parameters for the prediction of ionanofluids density are density of nanoparticles, density of ILs and concentration of nanoparticles. Unfortunately, studies carried out for imidazolium- and pyrrolidinium-based ILs included only carbon nanotubes, boron nitride and graphite, without mesoporous carbon (at the stage of this experiment, mesoporous carbon was not considered). Therefore, the data for mesoporous carbon density are not available and similar calculations to those in Section 3.2.1 were needed to be performed. The results of calculations can be found in **Table CD6b.1**, Appendix CD6b), and the density for mesoporous carbon is 1477.50 kg m^{-3} at 298.15. This is also in a good agreement with above conclusion about the general enhancement of density occurring in ionanofluids in comparison to the density of nanoparticles. While those for carbon nanotubes, boron nitride and graphite are (1626.34, 1911.89 and 1711.99) kg m^{-3} at 298.15 K, respectively.

The results of all calculations were shown in **Figure 6.1.3a**. It can be observed that the experimental *vs.* calculated densities are almost linear which represents good prediction ability. The deviations between experimental and calculated values can be found in **Figure 6.1.3b** (note that the data of those ionanofluids containing mesoporous carbon were calculated based on the determined density in this chapter). The average absolute relative deviations of (0.21, 0.31, 0.32 and 0.10) % were achieved for MWCNT, G, BN and MC, respectively. While the maximum deviations were (0.66, 0.67, 0.58 and

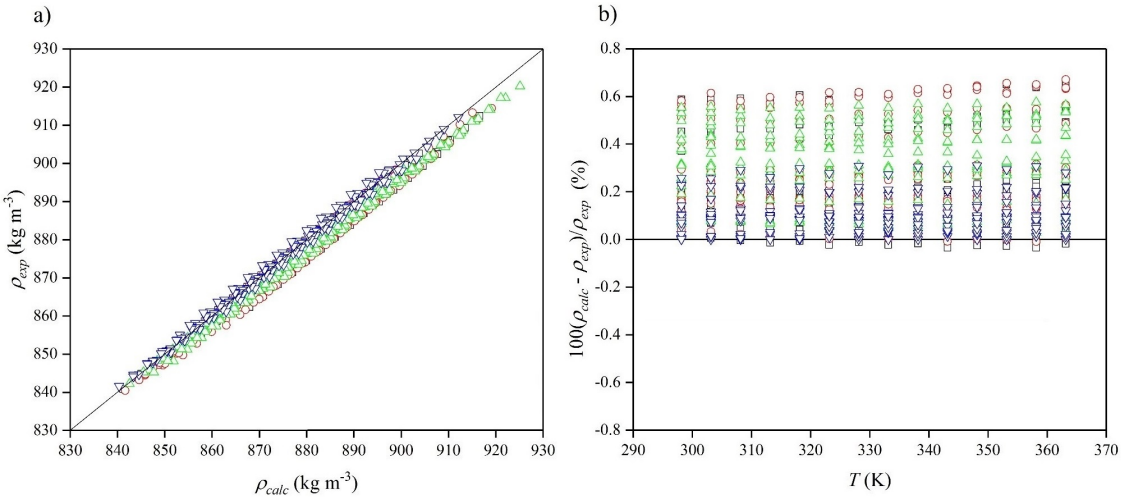

Figure 6.1.3. a) Experimental, ρ_{exp}, *vs.* calculated, ρ_{calc}, density of ionanofluids; **b)** relative deviations between calculated and experimental values of ionanofluids density, $100(\rho_{calc} - \rho_{exp})/\rho_{exp}$, against the temperature, T, for $[P_{14,6,6,6}][RO]$ + MWCNT, □, $[P_{14,6,6,6}][RO]$ + G, ○, $[P_{14,6,6,6}][RO]$ + BN, △, $[P_{14,6,6,6}][RO]$ + MC, ▽.

0.31) % for $[P_{14,6,6,6}]$[HexO] + 3 wt% MWCNT at 363.15 K, $[P_{14,6,6,6}]$[HexO] + 3 wt% G at 363.15 K, $[P_{14,6,6,6}]$[OctO] + 3 wt% BN at 358.15 K and $[P_{14,6,6,6}]$[DecO] + 3 wt% MC at 348.15 K, respectively.

Interestingly, all relative deviations between experimental and calculated values are positive. It indicates that the calculated values are higher than experimental. The reason for that might originate from the existing interfacial nanolayering of higher density values (which shifts the calculated results to higher values region). For the future work, additional parameter including the structure of IL used could be possibly included as an implicit function.

Such deviations illustrate that we are able to calculate the density of ionanofluids with high accuracy, well below 1%, considering that it is a sophisticated system of two phases mixture (nano-solid + liquid). It should be also noted that the calculations for just pure ILs densities with the most accurate approach, the fluctuation theory-based Tait-like equation of state (FT-EoS), reach the deviations of up to 6%. [4]

6.2 Dynamic Viscosity

The viscosity was also measured for ILs with nanoparticles (results can be seen in **Figure CD6a.6-CD6a.10**, Appendix CD6a and data are reported in **Table CD6b.2**, Appendix CD6b). It is well-known that the viscosity is increasing with adding the nanoparticles. [5, 6] This can be also seen in **Figure 6.2.1** for 298.15 K and **Figure 6.2.2** for 363.15 K, whereas the values were listed in **Table C1** (Appendix C), as enhancements of ionanofluids viscosity in comparison to their pure analogues. Unfortunately, the relation between viscosity and nanoparticles concentration is still not clear. However, for most cases the linear correlation can be seen accurate enough, with few exceptions (for example $[P_{14,6,6,6}]$[AcO] + MWCNT at 298.15 K, $[P_{14,6,6,6}]$[DecO] + G at 298.15 K, $[P_{14,6,6,6}]$[ButO] + BN at 363.15 K or $[P_{14,6,6,6}]$[OctO] + MC at 363.15 K).

To screen the viscosity enhancements dependence upon the temperature, those are presented at 298.15 K and 363.15 K. Generally, the enhancement is increasing with temperature in the ranges of (17.8-28.8, 16.4-23.0, 12.8-26.1, 13.5-32.6) % for 0.5 wt% at 298.15 K, respectively, and (36.8-62.1, 28.5-60.9, 28.5-66.0, 33.1-57.9) % for 1.0 wt% at 298.15 K, respectively, (20.2-31.5, 20.1-31.3, 14.7-38.8, 17.2-38.9) % for 0.5 wt% at 363.15 K, respectively, (40.1-66.9, 38.9-63.6, 31.0-60.7, 40.7-69.0) % for 1.0 wt% at 363.15 K, respectively. The enhancements for nanoparticles concentration of 3.0 wt% are much higher (92.9-156.7, 121.0-143.6, 78.2-119.5, 97.4-144.0) % at 298.15 K and (98.5-154.0, 135.0-159.3, 93.4-119.5, 92.6-153.1) % at 363.15 K. While the average enhancements errors are (2.4, 9.0, 13.3) % for systems with 0.5 wt%, 1.0 wt% and 3.0 wt% loading of nanoparticles, respectively.

The VFT equation (2.2.45), $\eta(T)$, can give an insight into the dependence of the IL structure onto the viscosity (**Table CD6a.1**, Appendix CD6a). The influence of IL structure was discussed in Section 4.4. To remind, the rise in viscosity when it is cooled toward the glass transition (where the sharp super-Arrhenius increase occurs) is accompanied with very little structural change so increasing the anion chain length of ILs results in decreasing T_0. The addition of the nanoparticles (as well as increasing those concentration) results in further T_0 decreasing. Unfortunately, there was no dependence found for nanoparticle type and the T_0. It might be caused by specific properties of interfacial nanolayering of liquid molecules on the surface of nanoparticles, resulting in

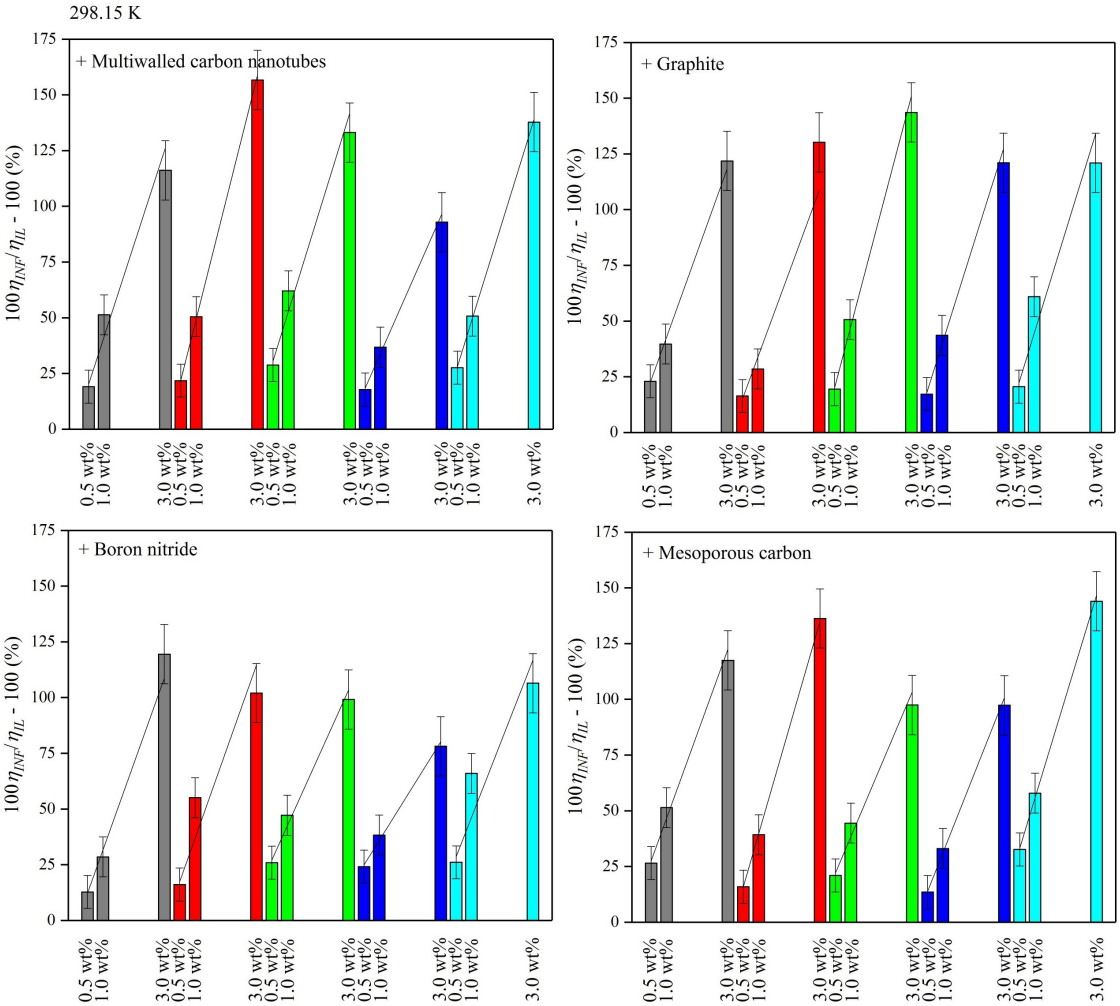

Figure 6.2.1. Dynamic viscosity enhancement of ionanofluids, (100η_{INF}/η_{IL}-100), in comparison to pure ionic liquids, over the nanoparticles mass fraction, for $[P_{14,6,6,6}]$[AcO] INF, grey, $[P_{14,6,6,6}]$[ButO] INF, red, $[P_{14,6,6,6}]$[HexO] INF, green, $[P_{14,6,6,6}]$[OctO] INF, blue, $[P_{14,6,6,6}]$[DecO] INF, cyan, at 298.15 K.

higher contribution to the decreasing of anions mobilities.

For prospective application purposes, particularly HTFs, the viscosity is expected to be as low as possible. It is widely known that ILs exhibit higher values than simple molecular solvents (with some exceptions, *i.e.* ethylene glycol) or other commercially available HTFs. This is the main disadvantage of ILs. For example (16.9, 6.19 or 3.71) mPa s for Dowtherm MX, Dynalene PG60 or Dowtherm A at 298.15 K, respectively. On the other hand, the temperature has an enormous impact on the viscosity (above 1000 % from 298.15 K to 363.15 K). Therefore, at high temperature the viscosity of ILs and commercial HTFs become similar with no significant differences.

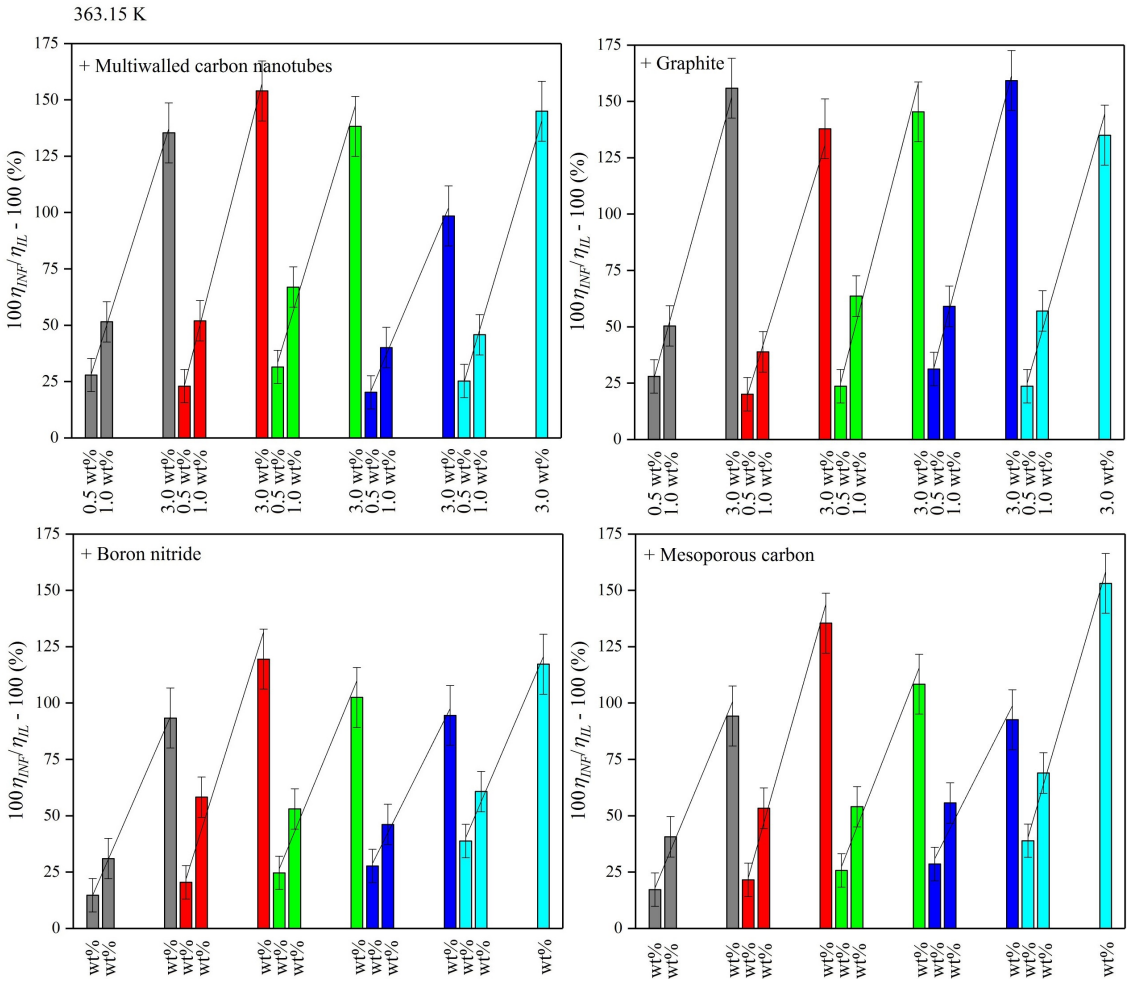

Figure 6.2.2. Dynamic viscosity enhancement of ionanofluids, ($100\eta_{INF}/\eta_{IL}$-100), in comparison to pure ionic liquids, over the nanoparticles mass fraction, for $[P_{14,6,6,6}]$[AcO] INF, grey, $[P_{14,6,6,6}]$[ButO] INF, red, $[P_{14,6,6,6}]$[HexO] INF, green, $[P_{14,6,6,6}]$[OctO] INF, blue, $[P_{14,6,6,6}]$[DecO] INF, cyan, at 363.15 K.

Viscosity is very difficult property to include in theoretical descriptions. Many efforts were put to calculate the theoretical viscosity of nanofluids with various results. [7–10] However, the prediction of viscosity is dependent on many factors: viscosity of base fluid, type of nanoparticles, concentration of nanoparticles, temperature, *etc.* There are several models constructed with thermodynamics and mechanics laws. There are also some reports concerning the correlation for ionanofluids, however, they are prepared for specific ILs/nanoparticles. [11] To the best of our knowledge, there is no versatile model that could be used for every system, or for the investigated mixtures.

6.3 Kinematic Viscosity - Lubrication Properties

For industrial purposes, the lubrication properties are very important. The selection of lubricating material for a specific application is essential. Materials are classified in several groups, depending on the lubrication abilities. The property on which the classification is performed is called kinematic viscosity, ν, calculated from dynamic viscosity and density ($\nu = \eta/\rho$) at 313.15 K. [12–14] The ISO classification (ISO 3448:1992) includes a wide range of materials from kinematic viscosity of 2.2 $mm^2\ s^{-1}$ (ISO VG 2) to 1500 $mm^2\ s^{-1}$ (ISO VG 1500).

The results of kinematic viscosity calculations and assignments to lubrication properties are shown in **Figure 6.3.1**. The kinematic viscosities for pure ILs were (104.2, 130.5, 177.9, 205.6 and 218.6) $mm^2\ s^{-1}$ for $[P_{14,6,6,6}]$[AcO], $[P_{14,6,6,6}]$[ButO], $[P_{14,6,6,6}]$[HexO], $[P_{14,6,6,6}]$[OctO] and $[P_{14,6,6,6}]$[DecO], respectively. As can be seen the kinematic viscosity increases with the anion chain length (driven by the dynamic viscosity).

The addition of nanoparticles shifts the kinematic viscosity to higher values, as expected. The maximum kinematic viscosity was found as 547.5 $mm^2\ s^{-1}$, corresponding to $[P_{14,6,6,6}]$[DecO] + 3 wt% MC. The lubrication properties are also analysed based on the friction force coefficients, however, it does not relate to industrial assignment of material (in accordance to ISO classification). Nevertheless, the previous reports show that ILs have very promising lubricative properties (based on the friction coefficients). In this work, we additionally showed that ILs are very useful as lubricates (due to high variety in ISO classification), moreover, the possibility of doping the ILs with nanoparticle enables tailoring the kinematic viscosity which might be desirable for some applications (as mentioned above, the materials are selected for specific application), starting from relatively low kinematic viscosity (as for $[P_{14,6,6,6}]$[AcO]) up to higher values (as for $[P_{14,6,6,6}]$[DecO] + 3 wt% MC).

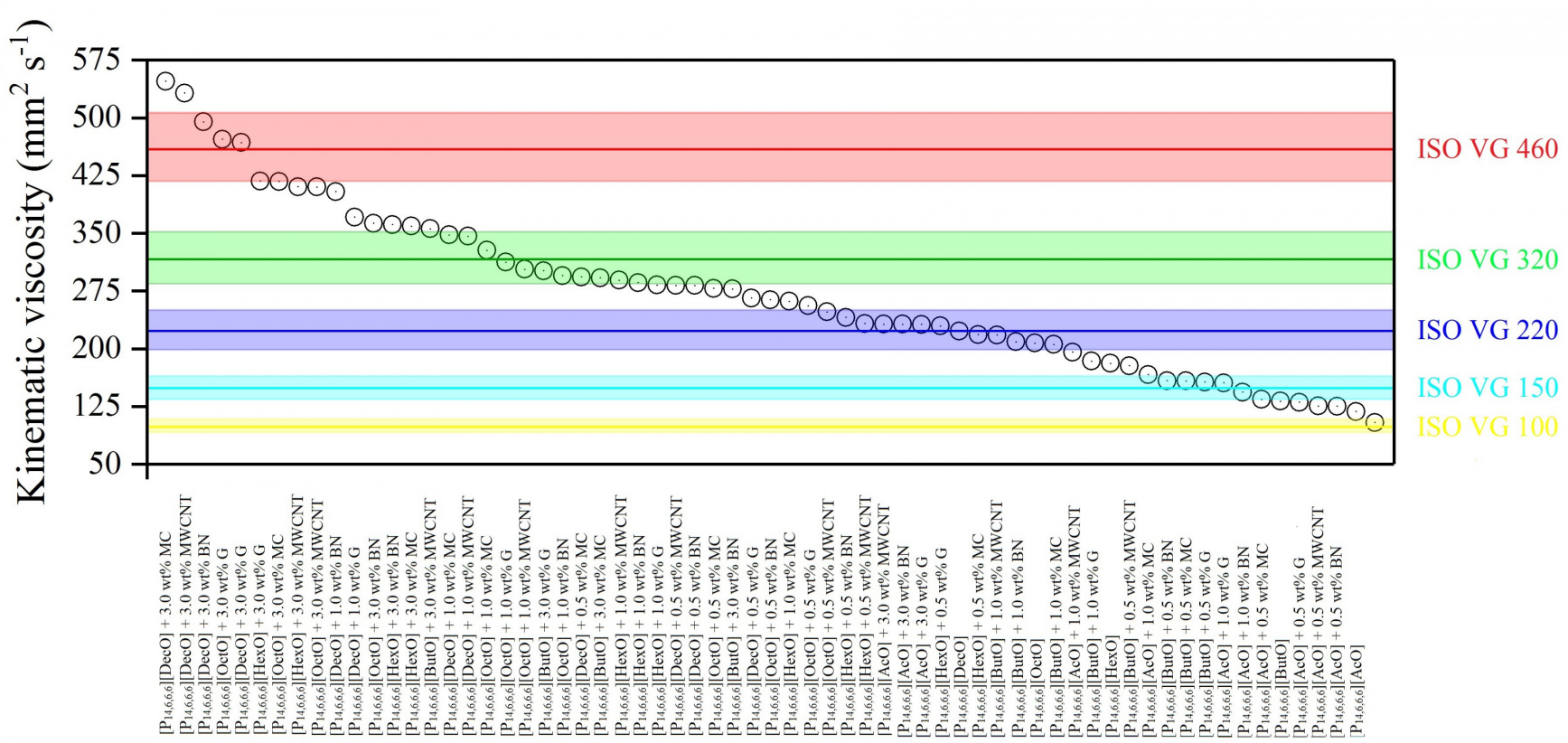

Figure 6.3.1. The ISO lubrication properties classification based on the kinematic viscosity, the bold coloured lines represent the mid-point kinematic viscosity of the class, whereas the borders of coloured field represent the minimum and maximum kinematic viscosity of the class.

6.4 Thermal Conductivity

Thermal conductivity was also measured for ionanofluids with carbon nanotubes, boron nitride, graphite and mesoporous carbon of loading up to 3 % by weight. The results were presented in **Figure CD6a.11-CD6a.15** (Appendix CD6a), reported in **Table CD6b.3** (Appendix CD6b), and the coefficients of linear equation (2.2.18), $\lambda(T)$, as a function of temperature can be found in **Table CD6a.2** (Appendix CD6a) .

The thermal conductivity was linearly decreasing with temperature for pure ILs, and the same dependence was found for nanoparticles-doped ILs, while the slope was consistently the same (~7.5% between 278 and 358 K), however, the values of thermal conductivity were shifted to higher values. For the applicable meaning, the materials can be tuned to have a specific value of thermal conductivity by addition of nanoparticles.

More specific discussion can be done by looking at the enhancements of thermal conductivity caused by the addition of nanoparticles (**Figure 6.4.1** for 278.15 K and **Figure 6.4.2** for 358.15 K). The thermal conductivity of solids is higher than liquids, and for nanoparticles particularly, in case of investigated nanoparticles the following thermal conductivity coefficients can be found as (3223.4, 874.1, 35.7 and ~12.0) W m^{-1} K^{-1} for carbon nanotubes, boron nitride, graphite and mesoporous carbon, respectively. [15–18] Therefore, because of mixing nanoparticles and ILs, the expectation is that the thermal conductivity of mixture is higher than this of pure base fluid. Moreover, increasing the amount of nanoparticles results in higher thermal conductivity. As can be seen, this dependence is represented linearly.

The range of maximum enhancements observed in this work is (19.8-22.6, 9.5-12.0, 13.2-15.1 and 7.6-11.4) % for MWCNT, G, BN and MC at 278.15 K, respectively, (18.0-21.4, 8.8-12.3, 13.0-17.3 and 7.2-10.3) % for MWCNT, G, BN and MC at 358.15 K, respectively. Generally, the enhancement is slightly decreasing with temperature, however, including the errors of enhancements, the temperature effect can be neglected. Moreover, as discussed before in Section 3.2.3, the temperature profile of thermal conductivity is originated from liquid not nanoparticles.

The thermal conductivity of ILs was found to not influence the thermal conductivity enhancements as those are very similar in terms of different types of anions (as shown above in the ranges of enhancements). However, a significant impact can be observed

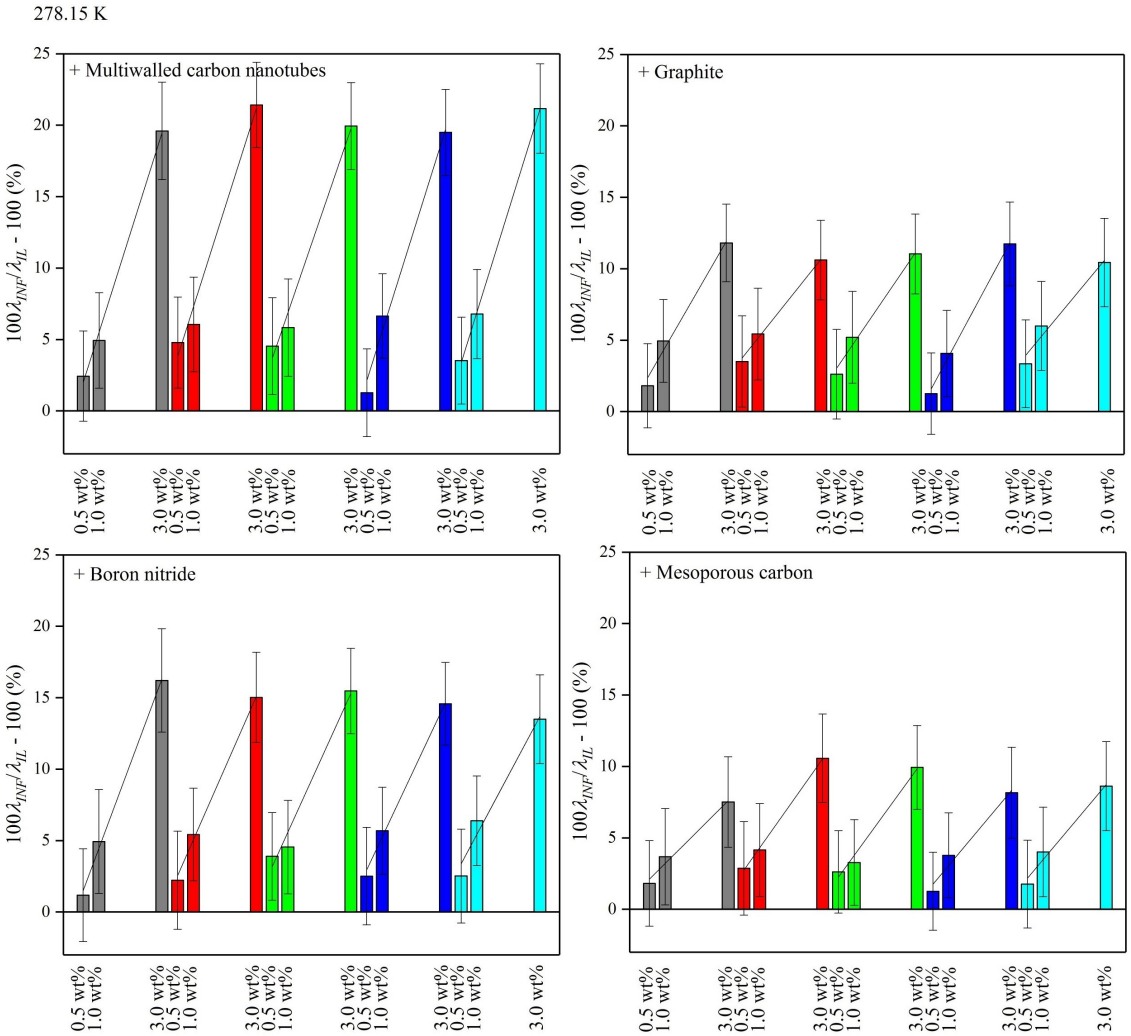

Figure 6.4.1. Thermal conductivity enhancement of ionanofluids, ($100\lambda_{INF}/\lambda_{IL}$-100), in comparison to pure ionic liquids, over the nanoparticles mass fraction, for $[P_{14,6,6,6}]$[AcO] INF, grey, $[P_{14,6,6,6}]$[ButO] INF, red, $[P_{14,6,6,6}]$[HexO] INF, green, $[P_{14,6,6,6}]$[OctO] INF, blue, $[P_{14,6,6,6}]$[DecO] INF, cyan, at 278.15 K.

for different types of nanoparticles. In this work, 4 different types of nanoparticles were used with a wide range of thermal conductivity (from a very high for carbon nanotubes to relatively low for mesoporous carbon). Carbon nanotubes were found to increase the thermal conductivity the most,as corresponding to their highest thermal conductivity, 3223.4 W m^{-1} K^{-1}), following boron nitride, 874.1 W m^{-1} K^{-1}, graphite, 35.7 W m^{-1} K^{-1}, and mesoporous carbon, ~12.0 W m^{-1} K^{-1}, as expected. [15–18]

Thermal conductivity of ionanofluids is probably the most widely investigated property of ionanofluids. Similar results were found for other systems, for example 3.71 % for 1-butyl-1-methylpyrrolidinium dicyanamide + 0.5 wt% MWCNT at 293.1 K

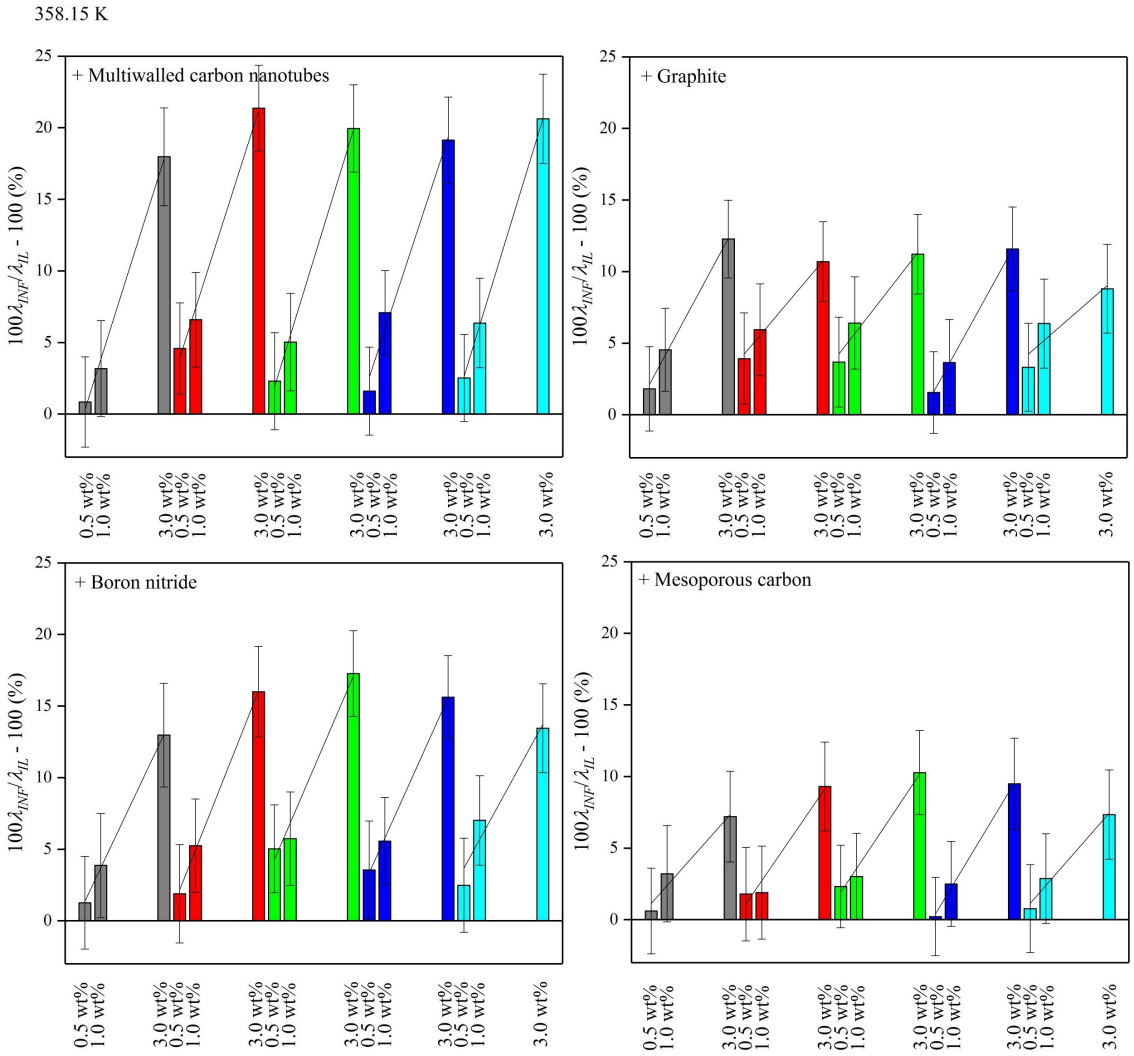

Figure 6.4.2. Thermal conductivity enhancement of ionanofluids, ($100\lambda_{INF}/\lambda_{IL}$-100), in comparison to pure ionic liquids, over the nanoparticles mass fraction, for $[P_{14,6,6,6}]$[AcO] INF, grey, $[P_{14,6,6,6}]$[ButO] INF, red, $[P_{14,6,6,6}]$[HexO] INF, green, $[P_{14,6,6,6}]$[OctO] INF, blue, $[P_{14,6,6,6}]$[DecO] INF, cyan, at 358.15 K.

(0.84-4.58 % in this work), [19] 4.8 % for 1-hexyl-3-methylimidazolium tetrafluoroborate + 1 wt% MWCNT at 293 K (3.18-7.45 % in this work), [20] or 20.46 % for 1-ethyl-3-methylimidazolium ethylsulfate + 3 wt% MWCNT at 293.77 K (17.98-22.62 % in this work). [21]

As described in Section 3.2.3, the model of Atashrouz was found to be the most reliable in terms of ionic liquid-based nanofluids thermal conductivity predictive reproducibility. Therefore, in this chapter, this model was also used to predict the thermal conductivity of ionanofluids as a function of the temperature with equation (2.3.51). Moreover, other models for nanofluids with molecular solvents as base fluids were excluded

from further consideration, as shown in Section 3.2.3.

It should be noted that this is the first work in which such studies are conducted, particularly for ILs not included the work in which the model was developed. This model is expected to reproduce the thermal conductivity with high accuracy because it is fully based on thermodynamics (modified geometry mean), and the interactions between ILs and nanoparticles are also included in its development. Liquids have lower thermal conductivity (order of 10^{-1} W m^{-1} K^{-1}) than solids, more specifically (3223.4, 874.1, 35.7 and ~12.0) W m^{-1} K^{-1} for carbon nanotubes, boron nitride, graphite and mesoporous carbon, respectively. [15–18]

The results of calculations (experimental enhancement *vs.* calculated enhancement) are presented in **Figure 6.4.3a**.

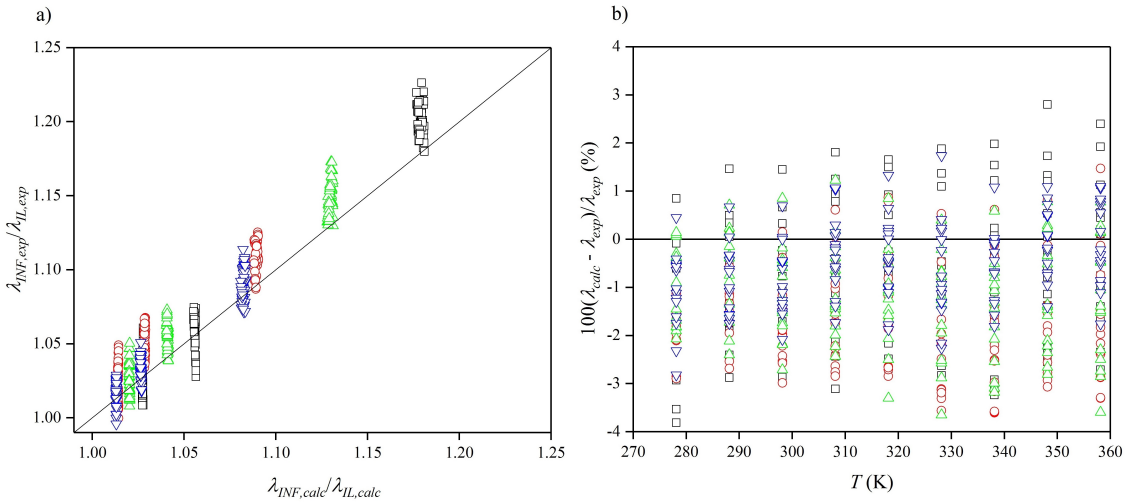

Figure 6.4.3. a) Experimental, λ_{exp}, *vs.* calculated, λ_{calc}, thermal conductivity of ionanofluids; **b)** relative deviations between calculated and experimental values, $100(\lambda_{calc} - \lambda_{exp})/\lambda_{exp}$, of ionanofluids thermal conductivity against the temperature, T, for $[P_{14,6,6,6}][RO]$ + MWCNT, □, $[P_{14,6,6,6}][RO]$ + G, ○, $[P_{14,6,6,6}][RO]$ + BN, △, $[P_{14,6,6,6}][RO]$ + MC, ▽.

The average absolute relative deviation was found as (0.66, 1.8, 1.2 and 0.54) % for MWCNT, G, BN and MC, respectively, while the maximum values of relative deviation were -(3.82, 3.61, 3.65 and 2.82) % for $[P_{14,6,6,6}]$[ButO] + 3 wt% MWCNT at 278.15 K, $[P_{14,6,6,6}]$[ButO] + 1 wt% G at 338.15 K, $[P_{14,6,6,6}]$[HexO] + 3 wt% BN at 328.15 K and $[P_{14,6,6,6}]$[ButO] + 3 wt% MC at 278.15 K, respectively. The average standard

uncertainty of determined enhancements is 4.5%. As can be clearly seen, all values are well within the linear relation (solid line in **Figure 6.4.3b**) between experimental and calculated values of enhancement. More specifically, in **Figure 6.4.3b**, the relative deviations are presented. None of the calculated values exceed the standard uncertainty of determined enhancement (all of them are below 4%). To confirm the conclusions made in Section 3.2.3, the Atashrouz model can be used to predict the thermal conductivity of ionanofluids accurately without any descriptors of molecular structure of ILs. Moreover, the only parameters needed for such calculations are thermal conductivities of ILs and nanoparticles, and nanoparticles concentration.

6.5 Isobaric Heat Capacity

The isobaric heat capacity was also studied for ILs with carbon nanotubes, boron nitride, graphite and mesoporous carbon in the concentration of up to 3 wt%, of which experimental results can be found in **Figure CD6a.16-CD6a.20** (Appendix CD6a) and **Table CD6b.4** (Appendix CD6b). A more insight into discussion can be made based on the enhancements of ionanofluids heat capacity in comparison to equivalent IL heat capacity. The heat capacity enhancement was also discussed in Section 3.2.2. In accordance to traditional mixing rules in which the resulting heat capacity is made by the contribution of mixed materials (solids - lower heat capacity, liquids - higher heat capacity), the heat capacity of ionanofluids should be lower than this of pure ILs. [22–24] In reality, for ionic liquid-based nanofluids, the heat capacity is increasing with addition of nanoparticles. This behaviour was associated with the interfacial nanolayers created by adhered liquid molecules on the surface of nanoparticles. [25, 26] The results of the enhancements were presented in **Figure 6.5.1** (for 298.15 K) and **Figure 6.5.2** (for 363.15 K). In all cases, the linear correlation was accurate enough to establish the qualitative dependence on the nanoparticles concentration.

The maximum enhancements observed were (10.3-11.7, 28.7-31.5, 20.3-21.6 and 25.1-27.4) % for MWCNT, G, BN and MC at 298.15 K, respectively, and (7.0-10.0, 32.7-36.1, 20.6-21.5 and 27.5-30.9) % for MWCNT, G, BN and MC at 363.15 K, respectively. As discussed in Section 3.2.2, the enhancements as a function of temperature depend on the properties of nanoparticles. It can be seen that for carbon nanotubes the enhancement is decreasing with temperature (related to increasing hydrophobicity, less favoured attraction of liquid molecules), [27] graphite is increasing with temperature (decreasing hydrophobicity, therefore, easier creation of nanolayers), [28] boron nitride (more or less constant with temperature, stabilized by the diversely charged surface of charge distribution between nitrogen and boron). [29] Mesoporous carbon has a relatively high hydrophobicity at room temperature as well as graphite, therefore, it is expected that this material exhibits similar properties to graphite. As can be seen the enhancement is increasing with temperature for mesoporous carbon. [30]

There was no dependence on the anion chain length found in this work. However, the type of nanoparticles, or more specifically their size, was an influencing factor for the

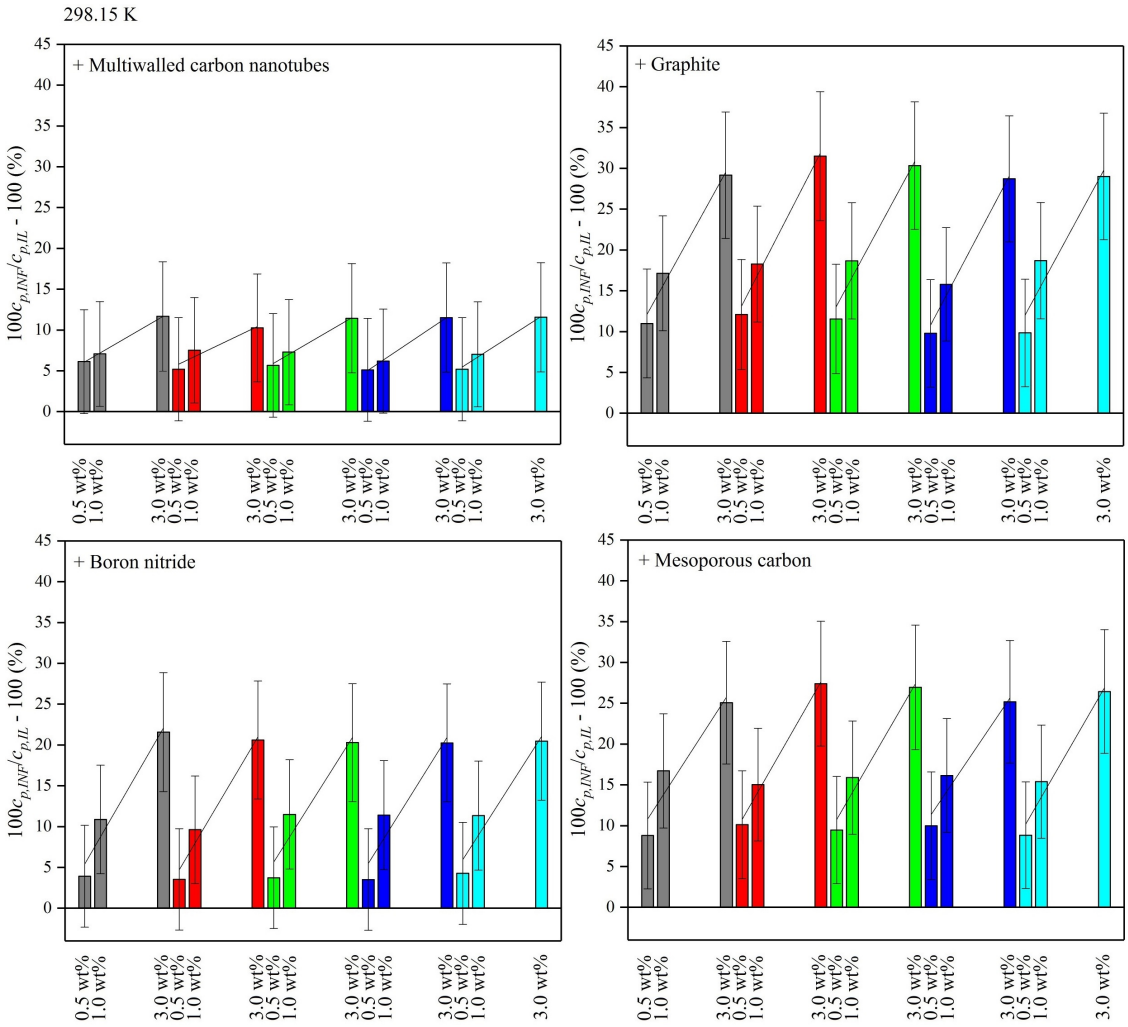

Figure 6.5.1. Isobaric heat capacity enhancement of ionanofluids, (100$c_{p,INF}/c_{p,IL}$-100), in comparison to pure ionic liquids, over the nanoparticles mass fraction, for $[P_{14,6,6,6}]$[AcO] INF, grey, $[P_{14,6,6,6}]$[ButO] INF, red, $[P_{14,6,6,6}]$[HexO] INF, green, $[P_{14,6,6,6}]$[OctO] INF, blue, $[P_{14,6,6,6}]$[DecO] INF, cyan, at 298.15 K.

enhancement. The following dependence of enhancements, MWCNT < BN < MC < G, was established. In the Section 3.2.2, it was shown that increasing the size of nanoparticles results in increasing the enhancement caused by larger number of liquid molecules adhered on the surface of nanoparticles (investigated for MWCNT, BN and G), which is in a good agreement with results in this chapter. However, in the case of mesoporous carbon, the enhancement is higher than for boron nitride but lower than graphite. This disturbance might be caused by the very high porosity of mesoporous carbon which influences the adsorption of liquid molecules, and therefore the enhancement. [31]

In comparison to commercial HTFs, the values of heat capacity presented in this

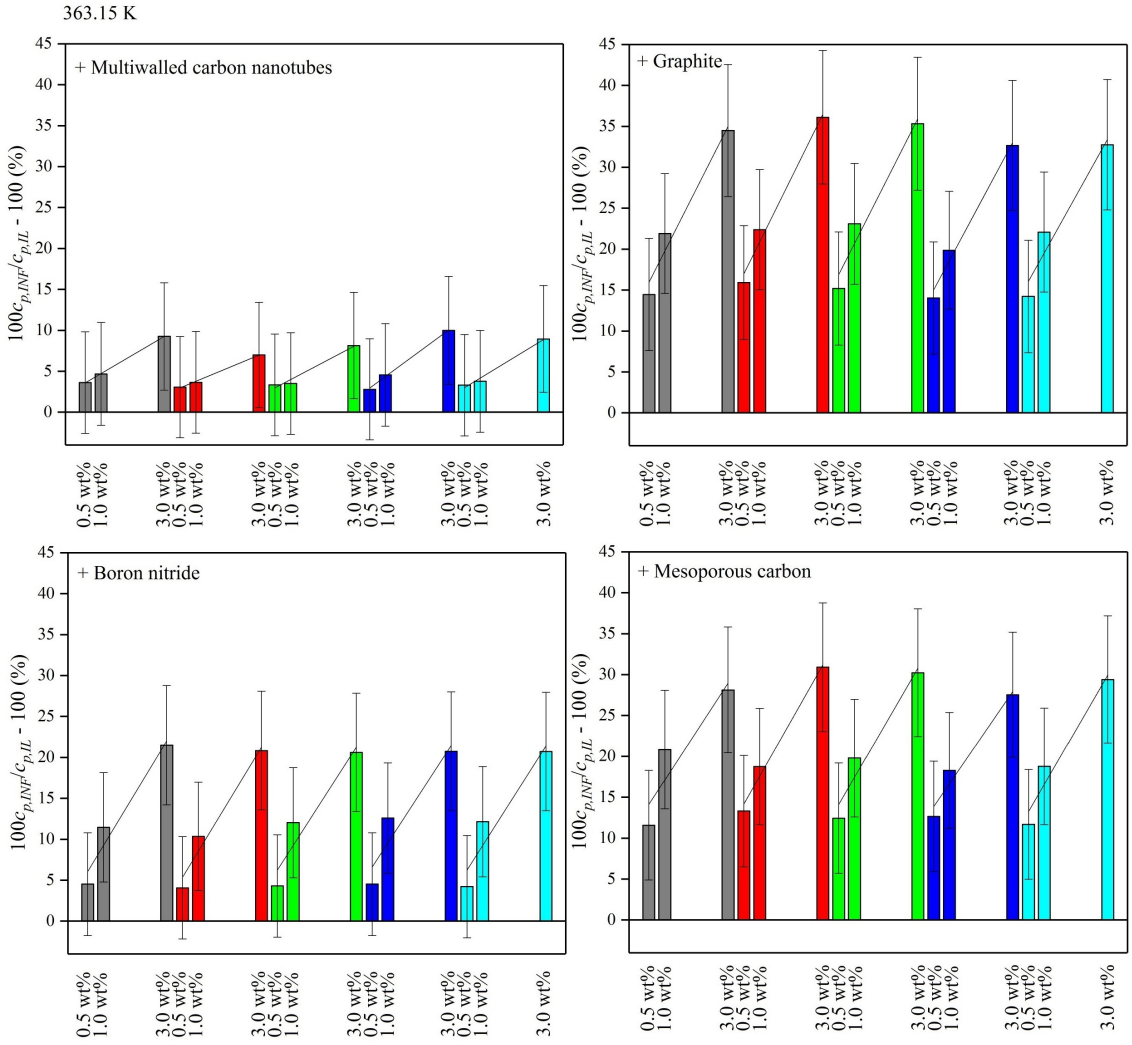

Figure 6.5.2. Isobaric heat capacity enhancement of ionanofluids, ($100c_{p,INF}/c_{p,IL}$-100), in comparison to pure ionic liquids, over the nanoparticles mass fraction, for $[P_{14,6,6,6}][AcO]$ INF, grey, $[P_{14,6,6,6}][ButO]$ INF, red, $[P_{14,6,6,6}][HexO]$ INF, green, $[P_{14,6,6,6}][OctO]$ INF, blue, $[P_{14,6,6,6}][DecO]$ INF, cyan, at 363.15 K.

work are similar to the commercial HTFs, for example (1.93, 1.90 or 1.63) kJ kg^{-1} K^{-1} Therminol ADX10, Dynalene LO-170, Dowtherm Q at 298.15 K, respectively, while the values in this work are (2.02, 1.95, 1.91, 1.84 and 1.82) kJ kg^{-1} K^{-1} for $[P_{14,6,6,6}][AcO]$, $[P_{14,6,6,6}][ButO]$, $[P_{14,6,6,6}][HexO]$, $[P_{14,6,6,6}][OctO]$ and $[P_{14,6,6,6}][DecO]$ at 298.15 K, respectively.

The heat capacity of investigated ionanofluids was also calculated by using fully empirical correlations determined in Section 3.2.2 with equations (3.2.1), (3.2.2) and (3.2.3). The models discussed in the literature are fully based on the mixing theory which was repeatedly shown to fail in case of ionanofluids, [32,33], and some nanofluids. [25,26]

Unfortunately, up to date, there is no correlation of heat capacity proposed to determine the heat capacity properly. Therefore, we proposed a fully empirical second-order correlation as a function of nanoparticles concentration and temperature. The main drawback of this approach is limited applicability for a certain type of nanoparticles. This can be done because, as shown in Section 3.2.2, the heat capacity enhancement depends on the type of nanoparticles.

Solids have lower heat capacity than liquids, which should reflect in decreasing the heat capacity when mixed with nanoparticles (as for the mixing rules). In fact, due to interfacial nanolayers of higher physical properties existence, one can observe the heat capacity enhancement in comparison to pure ILs. As for the results of density calculations, the previous work include only studies for carbon nanotubes, boron nitride and graphite, therefore, the prediction of heat capacity is possible for ionanofluids with only these nanoparticles.

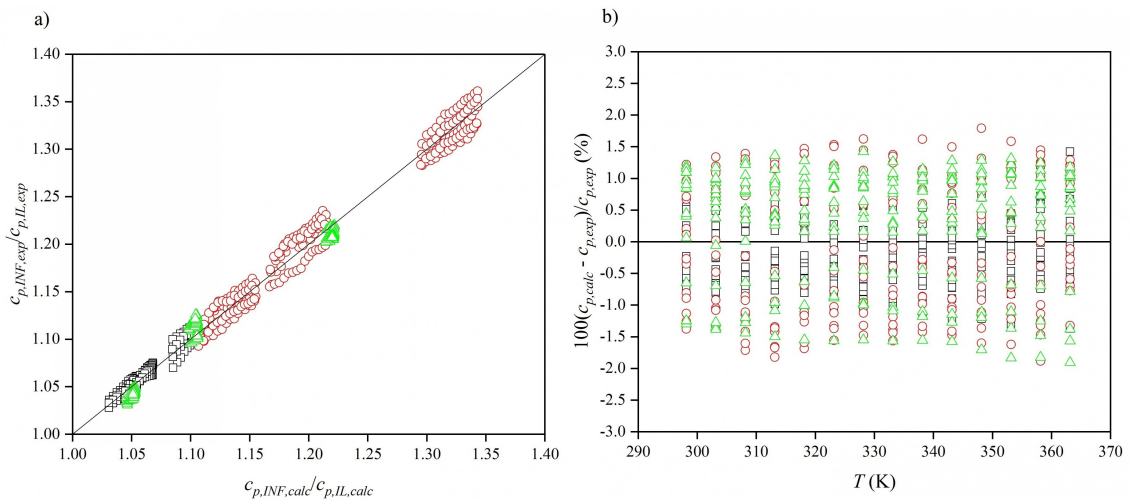

Figure 6.5.3. a) Experimental, $c_{p,exp}$, *vs.* calculated, $c_{p,calc}$, isobaric heat capacity of ionanofluids; **b)** relative deviations, $100(c_{p,calc}\text{-}c_{p,exp})/c_{p,exp}$, between calculated and experimental values of ionanofluids isobaric heat capacity against the temperature, T, for $[P_{14,6,6,6}][RO]$ + MWCNT, □, $[P_{14,6,6,6}][RO]$ + G, ○, $[P_{14,6,6,6}][RO]$ + BN, △, $[P_{14,6,6,6}][RO]$ + MC, ▽.

The representation of experimental data *versus* those calculated can be found in **Figure 6.5.3a**. More precisely, the differences can be found in **Figure 6.5.3b**. The average absolute relative deviations are (0.47, 0.96 and 0.87) % for ionanofluids with MWCNT,

G and BN, respectively, while the maximum relative deviations were found to be (-1.82, -1.91 and 1.41) % for $[P_{14,6,6,6}][OctO]$ + 3 wt% G, $[P_{14,6,6,6}][ButO]$ + 1 wt% BN and $[P_{14,6,6,6}][AcO]$ + 3 wt% MWCNT, respectively. As can be seen, all the relative deviations were well below 2 %. It should be noted that the calculated enhancements are below the heat capacity relative deviation (of 3%). Therefore, it is possible to calculate the heat capacity of ionanofluids with carbon nanotubes, boron nitride and graphite accurately.

To enable the prediction of heat capacity enhancement for mesoporous carbon, similar equation was established as for carbon nanotubes, boron nitride and graphite (Section 3.2.2):

$$\frac{c_{p,INF}}{c_{p,IL}} = (31.00 \pm 0.85) \times 10^{-2}\varphi_{MC} + (3.2 \pm 1.1) \times 10^{-3}T - (9.60 \pm 0.39) \times 10^{-2}\varphi_{MC}^2 - (4.1 \pm 1.7) \times 10^{-6}T^2 + (0.40 \pm 0.19) \quad (6.5.1)$$

with coefficient of determination, $R^2 = 0.98307$.

6.6 Volumetric Heat Capacity

The most important property in case of application as HTFs is the ability to store the energy (as heat). This can be represented with a property called volumetric heat capacity, c_V, which is calculated based on isobaric specific heat capacity, c_p, and specific density, ρ, $c_V = c_p \times \rho$. [34] One can describe it as a viability to store the heat in a volume of a material, as a change in temperature. Higher values of volumetric heat capacity result in increased ability to store the heat, therefore, these are favoured. As expected, high isobaric heat capacity and high density contribute to the high volumetric heat capacity.

The ILs investigated in this work have relatively low density (below 1000 kg m^{-3}), however, they have relatively high specific heat capacity (1.82-2.91 kJ kg^{-1} K^{-1}). The volumetric heat capacity at 298.15 K and 363.15 K is shown in **Figure 6.6.1**. The volumetric heat capacity found in this work was in the range of (1.60-2.39 and 1.66-2.54) MJ K^{-1} m^{-3} at 298.15 K and 363.15 K, respectively. The maximum was found as 2.39 MJ K^{-1} m^{-3} for $[P_{14,6,6,6}][AcO]$ + 3.0 wt% G at 298.15 K and 2.54 MJ K^{-1} m^{-3} for $[P_{14,6,6,6}][AcO]$ + 3.0 wt% G at 363.15 K, respectively. While the minimum was as 1.60 MJ K^{-1} m^{-3} for $[P_{14,6,6,6}][DecO]$ at 298.15 K and 1.66 MJ K^{-1} m^{-3} for $[P_{14,6,6,6}][DecO]$ at 363.15 K, respectively. For pure ILs, the c_V is increasing with the anion chain length, also driven by the isobaric heat capacity.

The temperature effect was found to be similar for all systems, about 4 % increase of volumetric heat capacity from 298.15 K to 363.15 K (driven by the increase of isobaric heat capacity). As can be seen the values of volumetric heat capacity of systems in this work are relatively high. The addition of nanoparticles increase the c_V, for example the minimum enhancement at 298.15 K was found as 3.16 % for $[P_{14,6,6,6}][OctO]$ + 0.5 wt% MWCNT, and maximum as 39.78 % for $[P_{14,6,6,6}][ButO]$ + 0.5 wt% G. Generally, the enhancement was observed to be strictly dependent on the isobaric heat capacity. Therefore, the enhancements were found in the following sequence: MWCNT < MC < BN < G.

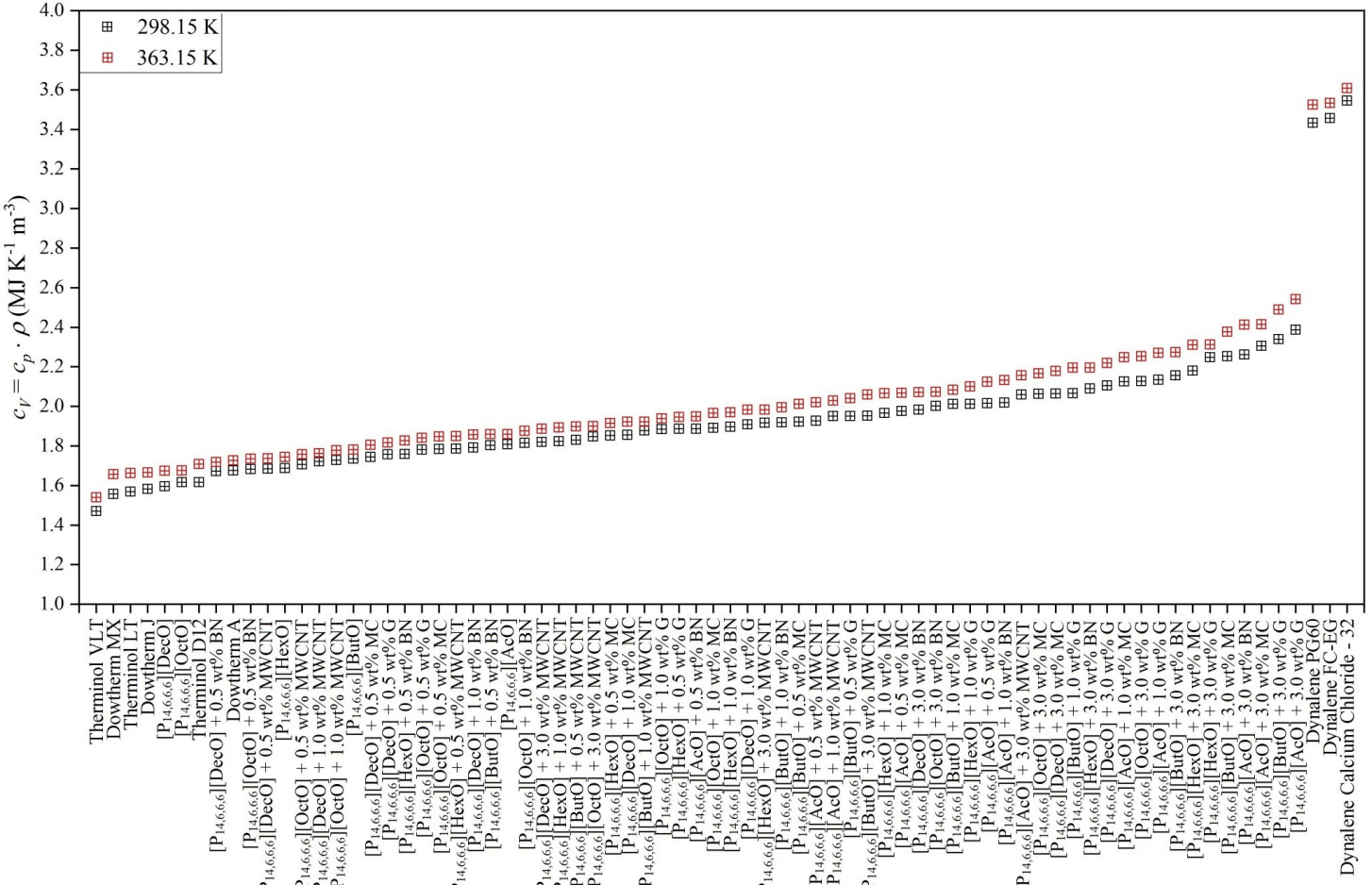

Figure 6.6.1. Volumetric heat capacity, c_V, for all investigated systems and some commercially available HTFs for the comparison, at 298.15 K and 363.15 K.

As a comparison, some commercially available HTFs were selected. There are several heat transfer of which volumetric heat capacity is lower that these in this work, for example 1.47 MJ K^{-1} m^{-3} at 298.15 K and 1.54 MJ K^{-1} m^{-3} at 363.15 for Therminol VLT, 1.56 MJ K^{-1} m^{-3} at 298.15 K and 1.68 MJ K^{-1} m^{-3} at 363.15 for Dowtherm MX, 1.57 MJ K^{-1} m^{-3} at 298.15 K and 1.66 MJ K^{-1} m^{-3} at 363.15 for Therminol LT, 1.58 MJ K^{-1} m^{-3} at 298.15 K and 1.67 MJ K^{-1} m^{-3} at 363.15 for Dowtherm J, 1.62 MJ K^{-1} m^{-3} at 298.15 K and 1.71 MJ K^{-1} m^{-3} at 363.15 for Therminol D12, or 1.68 MJ K^{-1} m^{-3} at 298.15 K and 1.78 MJ K^{-1} m^{-3} at 363.15 for Dowtherm A. These HTFs are mainly based on organic compounds (synthetic, aromatics, silicones and carbohydrates). Obviously, there are some HTFs that have higher values of volumetric heat capacity, for example 3.43 MJ K^{-1} m^{-3} at 298.15 K and 3.53 MJ K^{-1} m^{-3} at 363.15 for Dynalene PG60, 3.46 MJ K^{-1} m^{-3} at 298.15 K and 3.52 MJ K^{-1} m^{-3} at 363.15 for Dynalene FC-EG, 3.55 MJ K^{-1} m^{-3} at 298.15 K and 3.61 MJ K^{-1} m^{-3} at 363.15 for Dynalene CaCl2-32. The major impact in their high values is originated from water. Even though water has moderate density (or in comparison to other liquid quite low), the isobaric heat capacity of this material is very high (4.18 kJ kg^{-1} K^{-1} at 298.15 K), and all of those HTFs are based on water.

6.7 Thermogravimetric Analysis - Thermal Stability

The thermogravimetric analysis (TGA) was used to investigate the thermal decomposition profile of investigated systems. All pure ILs and mixtures with carbon nanotubes, boron nitride, graphite and mesoporous carbon have been studied. The results of thermogravimetric curves can be found separately in Figures **CD6a.22-CD6a.81** (Appendix CD6a). Those figures also include the derivative thermogravimetric curve (dm/dT *vs.* T). As explained in Section 2.2.2, the mostly recognized decomposition parameter is onset temperature, T_{on}. The determination of T_{on} based on derivative curve leads to the reduction of its overestimation. The determined onset temperatures were collected in **Table 6.7.1**, and these were also presented against the nanoparticles weight concentration in **Figure 6.7.1**.

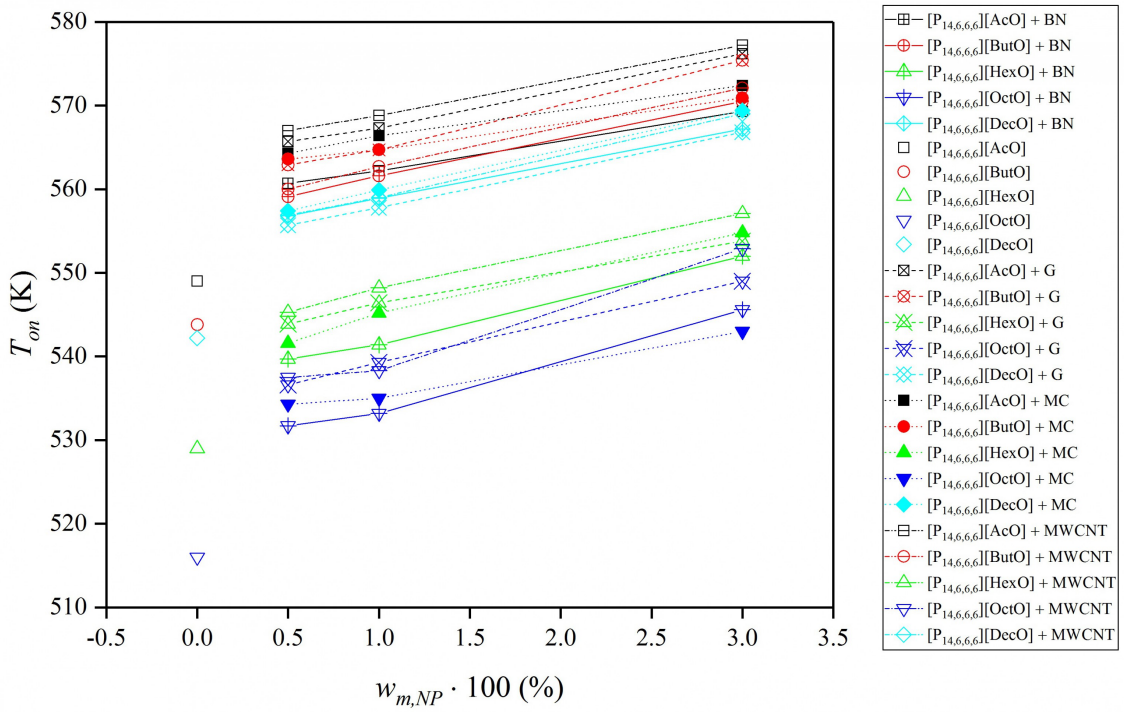

Figure 6.7.1. The onset temperature, T_{on}, determined from thermogravimetric analysis for all investigated ionic liquids and ionanofluids.

Table 6.7.1. The results of thermogravimetric analysis including determined onset temperature, T_{on} (the standard uncertainty, u, of onset temperature is $u(T_{on})$ = 0.5 K)

		T_{on} (K)			
		BN	G	MC	MWCNT
$[P_{14,6,6,6}][AcO]$	0.5%	560.7	565.7	564.3	567.0
Pure T_{on} = 549.0 K	1.0%	562.2	567.3	566.4	568.8
	3.0%	569.3	576.2	572.4	577.2
$[P_{14,6,6,6}][ButO]$	0.5%	559.1	562.9	563.6	560.0
Pure T_{on} = 543.8 K	1.0%	561.6	564.7	564.7	562.7
	3.0%	570.5	575.4	570.9	572.1
$[P_{14,6,6,6}][HexO]$	0.5%	539.7	543.9	541.6	545.3
Pure T_{on} = 529.0 K	1.0%	541.4	546.4	545.2	548.2
	3.0%	552.0	553.8	554.8	557.1
$[P_{14,6,6,6}][OctO]$	0.5%	531.7	536.6	534.3	537.5
Pure T_{on} = 516.0 K	1.0%	533.2	539.3	535.0	538.3
	3.0%	545.6	549.0	543.0	552.9
$[P_{14,6,6,6}][DecO]$	0.5%	556.8	555.7	557.4	556.9
Pure T_{on} = 542.2 K	1.0%	558.9	557.8	559.9	559.0
	3.0%	567.2	566.8	569.4	569.0

It can be seen (**Figure 6.7.1**) that the determined T_{on} increases with increasing the number of nanoparticles which is understandable as these nanomaterials have higher thermal stability than investigated ILs (or more generally all ILs), as can be shown in **Figure CD6a.21** (Appendix CD6a). The nanoparticles were significantly more stable the investigated ILs (by estimation T_{on} > 750 K). Moreover, the T_{on} exhibit more or less linear dependence upon the nanoparticles concentration. The enhancement range of onset temperature caused by the addition of nanoparticles was (2.02-5.74, 2.71-7.15, 2.49-6.40, 2.38-5.23) % for boron nitride-, carbon nanotubes-, graphite- and mesoporous carbon-doped ILs, respectively, or (2.13-5.14, 2.81-5.81, 2.02-5.31, 3.04-7.15, 2.49-5.02) % for $[P_{14,6,6,6}][AcO]$-, $[P_{14,6,6,6}][ButO]$-, $[P_{14,6,6,6}][HexO]$-, $[P_{14,6,6,6}][OctO]$- and $[P_{14,6,6,6}][DecO]$-based ionanofluids, respectively. As can be seen, all shifts of T_{on} are similar which means that the driving force for the enhancement is purely caused by the addition of more stable species (nanoparticles) into the ILs.

To the best of our knowledge, there are no published data which take into consideration the thermal stability of nanofluids with different type basefluids or nanoparticles, particularly when ILs are used as basefluids. Therefore, the analysis and comparison to previously reported results become more difficult. The linear-like dependence of T_{on} on the nanoparticles concentration shows that the thermal stability is rather dependent on the addition/type of nanoparticles instead of some more sophisticated mechanism.

Specific structure of nanofluids, particularly the surface of nanoparticles (*i.e.* solid-liquid nanolayering), remaining an apparent influence on the physical properties, might also be the cause of some shifts in thermal stability. Nevertheless, this was not observed in such studies probably because the measurements conducted are short thermal stability (with 5 K min^{-1} heating rate), unlike the long thermal stability (or so-called isothermal thermogravimetric analysis) where the investigated system is studied for a long time (several hours) at constant temperature.

Also, the thermal decomposition is dependent on the anion chain length in the following sequence: [AcO] > [ButO] > [DecO] > [HexO] > [OctO]. As can be seen, $[P_{14,6,6,6}]$[DecO] exhibits a discrepancy from the linear relationship. The possible cause of this behaviour is that decanoic acid is a solid at room temperature, therefore, it influences the molecular structure of $[P_{14,6,6,6}]$[DecO], inducing different molecular recognition than in comparison to other ILs with carboxylate anion. Moreover, similar sequences were found for ionanofluids based on these ILs which confirms the results for pure ILs.

The short-time thermogravimetric analysis provides the very important onset temperature needed for decomposition kinetics or structure-property relationships. [35, 36] The description of thermal stability by this type of analysis is rather ill-defined. The real thermal stability should be investigated based on long-term stability (*i.e.* isothermal thermogravimetric analysis). Unfortunately, this is a very long measurement of which time is the main disadvantage. However, this can be overcome by a few assumptions based on above presented results: **a)** the onset temperature for all samples is dependent on type of IL and addition of nanoparticles; **b)** the onset temperature is a point at which advanced decomposition can be observed (even up to 20% of weight change, for example $[P_{14,6,6,6}]$[AcO] + 1.0 wt% G $[P_{14,6,6,6}]$[OctO] + 0.5 wt% MWCNT or $[P_{14,6,6,6}]$[DecO] + 1.0 wt% MC; **c)** the onset temperature cannot be considered as the descriptor of sample thermal stability; **d)** the common feature of all samples is that the decomposition begins to be detectible at about 400 K. This leads to reduction of studies needed to be carried out - because all samples start to decompose at about 400 K, one sample is enough to be studied. The one with the lowest onset temperature was selected, $[P_{14,6,6,6}]$[DecO]. The isothermal TGA was conducted at 400 K, 450 K, 500 K and 550 K. The results can be found in **Figure 6.7.2**.

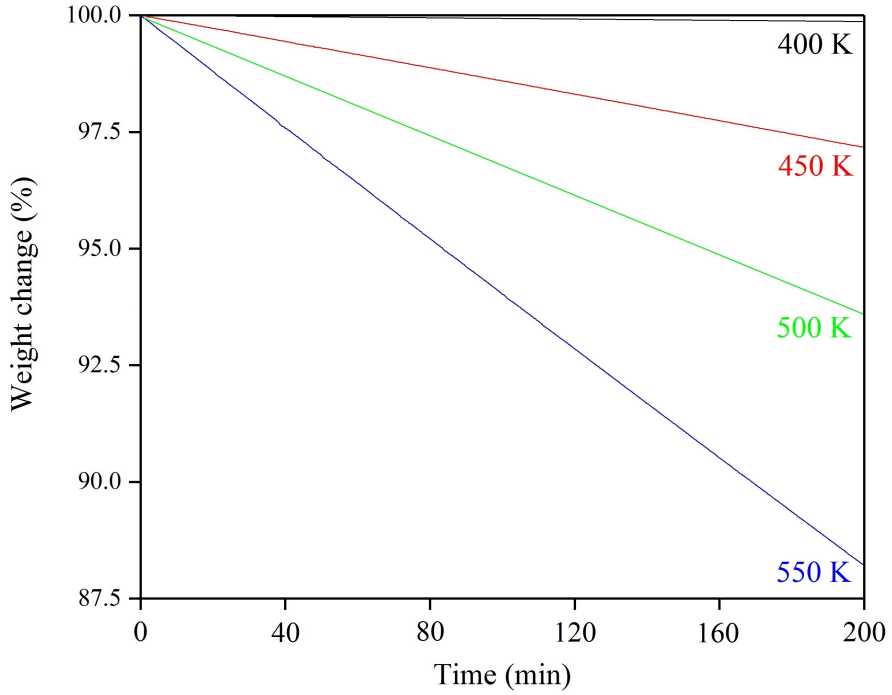

Figure 6.7.2. Isothermal thermogravimetric results as decomposition weight loss over the time at different temperatures for $[P_{14,6,6,6}][DecO]$.

The weight losses observed are (0.1, 2.9, 6.4 and 11.8) % at 400 K, 450 K, 500 K and 550 K, respectively. It can be seen that sample is stable at 400 K, and the weight loss is probably caused by some water removal (absorbed from the air during sample preparation and transportation). Further increase of temperature is causing more intensive weight loss (decomposition).

In terms of practical application of these systems, a consideration as HTFs is a viable option, as can be seen in **Table 6.7.2**. There are several different types of HTFs-based on glycols (*i.e.* Dynalene PG/EG series, Dowcal 100), alkanes (*i.e.* Therminol VLT), aromatic compounds (*i.e.* Therminol LT), water (*i.e.* Dynalene Calcium Chloride series). Some examples of commercially available HTFs with lower thermal stability can be found (as well as those with higher thermal stability), however, the presented studies show that investigated ILs can be successfully considered as a replacement. Even though the addition of nanoparticles increases the onset temperature, the maximum temperature of operation is still limited by the thermal stability of ILs.

Table 6.7.2. A comparison of maximum temperature of operation between commercially available HTFs and fluids in this work.

	Maximum temperature of operation (K)
Dynalene PG series	450
Dynalene EG series	450
Dynalene FC series (closed systems)	353
Dynalene HC series (open systems)	383
Dynalene Bioglycol	450
Dynalene Calcium Chloride Series	373
Dowtherm SR-1	393
Dowtherm A	673
Dowtherm J	588
Dowtherm MX	603
Therminol VLT	448
Therminol LT	453
Therminol D12	533
Systems studied in this work	~400

6.8 Conclusions

Comprehensive studies on ionanofluids composed of trihexyl(tetradecyl)phosphonium acetate, butanoate, hexanoate, octanoate and decanoate ILs with multiwalled carbon nanotubes, boron nitride, graphite and mesoporous carbon nanoparticles up to 3 wt% of concentration, were carried out. The experimental data of density, dynamic viscosity, thermal conductivity, isobaric heat capacity, short-range and long-range thermogravimetric analysis were presented, along with calculated kinematic viscosity and volumetric heat capacity of studied systems. The discussion presented in this chapter finalized the impact of ILs and ionic liquid–based nanofluids properties onto the HTFs design, including the molecular recognition. Most importantly, this is the first work of this kind in which ionanofluids are considered for industrial purposes from both molecular and engineering point of views.

Firstly, the limiting factor for the HTFs design in case of ILs is viscosity, remaining high values results in limited thermal performance, even though the other physical properties are very prospective. The addition of nanoparticles into the ILs results in the enhancements of all physical properties, including the limiting viscosity which negatively overpowers other enhancements. Temperature was found to affect the enhancement, as well as type of IL and nanoparticles/nanoparticles concentration.

It should be noted that discussion on whether a material is good or not is strongly dependent on the specific application for the HTFs. Our recommendation is to use ILs in moderately high temperature (above 100 K, up to 400 K) in which pressure control is problematic (and can be neglected due to very low vapour pressure of ILs).

The modelling of physical properties of materials considered as HTFs might result in a significant reduction in time and cost of design. In this chapter, the presented calculations and the comparison to experimental data (density and thermal conductivity) show that the presented models are capable to predict those physical properties. In terms of heat capacity, empirical equations designed for specific nanomaterials where used, which shows that further work on more versatile approach is needed.

Bibliography

[1] J. JACQUEMIN, R. GE, P. NANCARROW, D. W. ROONEY, M. F. COSTA GOMES, A. A. H. PÁDUA, and C. HARDACRE, *Journal of Chemical & Engineering Data* **53**, 716 (2008).

[2] A. HEINTZ, J. K. LEHMANN, C. WERTZ, and J. JACQUEMIN, *Journal of Chemical & Engineering Data* **50**, 956 (2005).

[3] J. JACQUEMIN, P. HUSSON, V. MAYER, and I. CIBULKA, *Journal of Chemical & Engineering Data* **52**, 2204 (2007).

[4] M. CHORĄZEWSKI, E. B. POSTNIKOV, K. OSTER, and I. POLISHUK, *Industrial & Engineering Chemistry Research* **54**, 9645 (2015).

[5] I. MAHBUBUL, R. SAIDUR, and M. AMALINA, *International Journal of Heat and Mass Transfer* **55**, 874 (2012).

[6] R. PRASHER, D. SONG, J. WANG, and P. PHELAN, *Applied Physics Letters* **89**, 1 (2006).

[7] S. ATASHROUZ, G. PAZUKI, and Y. ALIMORADI, *Fluid Phase Equilibria* **372**, 43 (2014).

[8] M. CORCIONE, *Energy Conversion and Management* **52**, 789 (2011).

[9] N. MASOUMI, N. SOHRABI, and A. BEHZADMEHR, *Journal of Physics D: Applied Physics* **42**, 1 (2009).

[10] P. M. KUMAR, J. KUMAR, and S. SURESH, *International Journal of Engineering Innovations and Research* **1**, 182 (2012).

[11] M. SADI, *Heat Transfer Engineering* **38**, 1561 (2017).

[12] G. KNOTHE and K. R. STEIDLEY, *Fuel* **84**, 1059 (2005).

[13] D.-G. LI, H. ZHEN, L. XINGCAI, Z. WU-GAO, and Y. JIAN-GUANG, *Renewable Energy* **30**, 967 (2005).

[14] S. Z. ERHAN and S. ASADAUSKAS, *Industrial Crops and Products* **11**, 277 (2000).

[15] E. K. SICHEL, R. E. MILLER, M. S. ABRAHAMS, and C. J. BUIOCCHI, *Physical Review B* **13**, 4607 (1976).

[16] R. TAYLOR, *Philosophical Magazine* **13**, 157 (1966).

[17] D. FENG, Y. FENG, X. ZHANG, and G. WANG, Effective Thermal Conductivity of Ordered Mesoporous Carbon CMK-3, in *ASME 2013 Heat Transfer Summer Conference collocated with the ASME 2013 7th International Conference on Energy Sustainability and the ASME 2013 11th International Conference on Fuel Cell Science, Engineering and Technology*, pp. V001T02A002–V001T02A002, American Society of Mechanical Engineers, 2013.

[18] Y. U. PAULECHKA, A. V. BLOKHIN, and G. J. KABO, *Thermochimica Acta* **604**, 122 (2015).

[19] J. M. P. FRANÇA, F. REIS, S. I. C. VIEIRA, M. J. V. LOURENÇO, F. J. V. SANTOS, C. A. N. DE CASTRO, and A. A. H. PADUA, *The Journal of Chemical Thermodynamics* **79**, 248 (2014).

[20] C. A. NIETO DE CASTRO, M. J. V. LOURENÇO, A. P. C. RIBEIRO, E. LANGA, S. I. C. VIEIRA, P. GOODRICH, and C. HARDACRE, *Journal of Chemical & Engineering Data* **55**, 653 (2009).

[21] J. M. P. FRANÇA, S. I. C. VIEIRA, M. J. V. LOURENÇO, S. M. S. MURSHED, and C. A. NIETO DE CASTRO, *Journal of Chemical & Engineering Data* **58**, 467 (2013).

[22] S.-Q. ZHOU and R. NI, *Applied Physics Letters* **92**, 93123 (2008).

[23] J. BUONGIORNO, *Journal of Heat Transfer* **128**, 240 (2006).

[24] L.-P. ZHOU, B.-X. WANG, X.-F. PENG, X.-Z. DU, and Y.-P. YANG, *Advances in Mechanical Engineering* **2**, 172085 (2010).

[25] D. SHIN and D. BANERJEE, *The International Journal of Structural Changes in Solids* **2**, 25 (2010).

[26] R. HENTSCHKE, *Nanoscale Research Letters* **11**, 88 (2016).

[27] G. HUMMER, J. C. RASAIAH, and J. P. NOWORYTA, *Nature* **414**, 188 (2001).

[28] T. MORIMOTO and K. MIURA, *Langmuir* **1**, 658 (1985).

[29] G. GIOVANNETTI, P. A. KHOMYAKOV, G. BROCKS, P. J. KELLY, and J. VAN DEN BRINK, *Physical Review B* **76**, 73103 (2007).

[30] G. TAO, L. ZHANG, Z. HUA, Y. CHEN, L. GUO, J. ZHANG, Z. SHU, J. GAO, H. CHEN, and W. WU, *Carbon* **66**, 547 (2014).

[31] I. SUMIRAT, Y. ANDO, and S. SHIMAMURA, *Journal of Porous Materials* **13**, 439 (2006).

[32] C. A. N. DE CASTRO, S. M. S. MURSHED, M. J. V. LOURENÇO, F. J. V. SANTOS, M. L. M. LOPES, and J. M. P. FRANÇA, *International Journal of Thermal Sciences* **62**, 34 (2012).

[33] C. A. N. DE CASTRO, E. LANGA, A. L. MORAIS, M. L. M. LOPES, M. J. V. LOURENÇO, F. J. V. SANTOS, M. S. C. S. SANTOS, J. N. C. LOPES, H. I. M. VEIGA, and M. MACATRÃO, *Fluid Phase Equilibria* **294**, 157 (2010).

[34] M. MUSIAŁ, K. MALARZ, A. MROZEK-WILCZKIEWICZ, R. MUSIOL, E. ZORĘBSKI, and M. DZIDA, *ACS Sustainable Chemistry & Engineering* **5**, 11024 (2017).

[35] M. S. WANG and T. J. PINNAVAIA, *Chemistry of Materials* **6**, 468 (1994).

[36] D. M. FOX, J. W. GILMAN, H. C. DE LONG, and P. C. TRULOVE, *The Journal of Chemical Thermodynamics* **37**, 900 (2005).

Chapter 7

Ionic Liquid-Based *versus* Commercial Heat Transfer Fluids

7.1 Economic Analysis

7.1.1 Pure Ionic Liquids

Physical properties are very important to ascertain whether some material can be used as HTFs. The most important are thermal conductivity, isobaric heat capacity, density and viscosity. Further investigation of these properties can lead to estimation of the heat exchange reactor cost. For the sake of comparison between materials in this work and those commercially used, assumptions described in Section 2.3.3 are done (degree of freedom reduction by selecting shell and tube type heat exchange units as references, neglecting the pressure drop across the fluid ducts). In this work an extensive analysis of thermal conductivity, heat capacity, density and viscosity were performed.

The comparison of ILs thermal conductivity depends on the composition of commercial fluid, for example water-based materials have higher thermal conductivity (*i.e.* Dynalene PG series, Dowtherm 4000 or Dynalene EG series), while those based on organic compounds have lower or similar thermal conductivity (*i.e.* Therminol ADX10 or Dynalene SF). In case of density, the comparison also depends on the type of material, for example the values in this work are similar to synthetic aromatic hydrocarbon mixtures (*i.e.* Therminol ADX10 or Dynalene SF), slightly lower than water, or significantly lower than glycol-based HTFs (for example Dowtherm 4000 or Dynalene EG series). In terms of heat capacity, it is similar or higher than organic-based HTFs (*i.e.* Therminol ADX10 or Dynalene SF), or lower than those with with (for example Dowtherm 4000 or Dynalene

EG series). Unfortunately, the viscosity is significantly higher than commercial HTFs, which is the main drawback. Therefore, the price of heat exchange unit for materials in this work would be higher than commercial HTFs.

The application of ILs as HTFs is still a discursive matter, mainly due to high cost of these materials. França *et al.* (**2009**) [1] used a simple approach to predict the cost of the shell and tube heat exchangers, originally proposed by Mendonça *et al.* (**1981**). [2] This is based only on the thermophysical properties of substances (density, viscosity, heat capacity and thermal conductivity). This procedure has been used, herein, to compare the thermophysical properties of investigated ILs to commonly used HTFs. The estimated costs of all considered heat exchangers (at 298.15 K and 363.15 K) are summarized in **Table 7.1.1** and shown in **Figure 7.1.1**.

Table 7.1.1. The results of economic analysis in the meaning of the heat exchange reactor cost, C_E, at 298.15 K and 363.15 K, along with the temperature effect.

	C_E 298.15 K (k$)	C_E 363.15 K (k$)	Temperature effect (%)
$[P_{14,6,6,6}]$[AcO] Neat	1130.7	542.2	108.54
$[P_{14,6,6,6}]$[AcO] + 0.5 wt% MWCNT	1163.0	575.0	102.26
$[P_{14,6,6,6}]$[AcO] + 1.0 wt% MWCNT	1234.5	596.3	107.03
$[P_{14,6,6,6}]$[AcO] + 3.0 wt% MWCNT	1280.6	632.1	102.59
$[P_{14,6,6,6}]$[AcO] + 0.5 wt% G	1166.0	565.2	106.30
$[P_{14,6,6,6}]$[AcO] + 1.0 wt% G	1180.4	573.0	106.00
$[P_{14,6,6,6}]$[AcO] + 3.0 wt% G	1286.3	632.2	103.46
$[P_{14,6,6,6}]$[AcO] + 0.5 wt% BN	1155.2	555.1	108.11
$[P_{14,6,6,6}]$[AcO] + 1.0 wt% BN	1164.9	562.4	107.13
$[P_{14,6,6,6}]$[AcO] + 3.0 wt% BN	1273.0	591.2	115.32
$[P_{14,6,6,6}]$[AcO] + 0.5 wt% MC	1181.5	552.6	113.81
$[P_{14,6,6,6}]$[AcO] + 1.0 wt% MC	1217.7	566.2	115.07
$[P_{14,6,6,6}]$[AcO] + 3.0 wt% MC	1311.9	601.4	118.14
$[P_{14,6,6,6}]$[ButO] Neat	1245.8	584.1	113.29
$[P_{14,6,6,6}]$[ButO] + 16.680 wt% H_2O	655.9	362.0	81.19
$[P_{14,6,6,6}]$[ButO] + 0.5 wt% MWCNT	1280.6	604.6	111.81
$[P_{14,6,6,6}]$[ButO] + 1.0 wt% MWCNT	1351.3	636.7	112.23
$[P_{14,6,6,6}]$[ButO] + 3.0 wt% MWCNT	1482.4	691.9	114.25
$[P_{14,6,6,6}]$[ButO] + 0.5 wt% G	1251.5	587.0	113.20
$[P_{14,6,6,6}]$[ButO] + 1.0 wt% G	1262.7	599.8	110.52
$[P_{14,6,6,6}]$[ButO] + 3.0 wt% G	1432.8	668.5	114.33
$[P_{14,6,6,6}]$[ButO] + 0.5 wt% BN	1279.9	606.1	111.17
$[P_{14,6,6,6}]$[ButO] + 1.0 wt% BN	1359.9	638.3	113.05
$[P_{14,6,6,6}]$[ButO] + 3.0 wt% BN	1375.2	654.9	109.99
$[P_{14,6,6,6}]$[ButO] + 0.5 wt% MC	1257.0	596.5	110.73
$[P_{14,6,6,6}]$[ButO] + 1.0 wt% MC	1308.7	631.5	107.24
$[P_{14,6,6,6}]$[ButO] + 3.0 wt% MC	1459.9	678.1	115.29
$[P_{14,6,6,6}]$[HexO] Neat	1385.7	643.2	115.44

$[P_{14,6,6,6}]$[HexO] + 15.825 wt% H_2O	719.4	395.0	82.13
$[P_{14,6,6,6}]$[HexO] + 0.5 wt% MWCNT	1450.3	685.5	111.57
$[P_{14,6,6,6}]$[HexO] + 1.0 wt% MWCNT	1540.4	726.0	112.18
$[P_{14,6,6,6}]$[HexO] + 3.0 wt% MWCNT	1604.2	750.0	113.89
$[P_{14,6,6,6}]$[HexO] + 0.5 wt% G	1411.3	654.0	115.80
$[P_{14,6,6,6}]$[HexO] + 1.0 wt% G	1477.4	692.3	113.40
$[P_{14,6,6,6}]$[HexO] + 3.0 wt% G	1626.2	744.9	118.31
$[P_{14,6,6,6}]$[HexO] + 0.5 wt% BN	1447.9	664.9	117.76
$[P_{14,6,6,6}]$[HexO] + 1.0 wt% BN	1488.9	692.9	114.88
$[P_{14,6,6,6}]$[HexO] + 3.0 wt% BN	1521.8	701.8	116.84
$[P_{14,6,6,6}]$[HexO] + 0.5 wt% MC	1422.0	663.9	114.19
$[P_{14,6,6,6}]$[HexO] + 1.0 wt% MC	1477.7	693.0	113.23
$[P_{14,6,6,6}]$[HexO] + 3.0 wt% MC	1542.5	719.3	114.44
$[P_{14,6,6,6}]$[OctO] Neat	1460.9	668.4	118.57
$[P_{14,6,6,6}]$[OctO] + 14.783 wt% H_2O	738.8	429.5	72.25
$[P_{14,6,6,6}]$[OctO] + 0.5 wt% MWCNT	1508.8	696.0	116.78
$[P_{14,6,6,6}]$[OctO] + 1.0 wt% MWCNT	1539.1	708.7	117.17
$[P_{14,6,6,6}]$[OctO] + 3.0 wt% MWCNT	1596.0	737.0	116.55
$[P_{14,6,6,6}]$[OctO] + 0.5 wt% G	1492.5	699.1	113.49
$[P_{14,6,6,6}]$[OctO] + 1.0 wt% G	1549.6	724.9	113.77
$[P_{14,6,6,6}]$[OctO] + 3.0 wt% G	1663.3	789.4	110.70
$[P_{14,6,6,6}]$[OctO] + 0.5 wt% BN	1529.5	700.0	118.50
$[P_{14,6,6,6}]$[OctO] + 1.0 wt% BN	1533.0	710.4	115.79
$[P_{14,6,6,6}]$[OctO] + 3.0 wt% BN	1555.6	724.9	114.60
$[P_{14,6,6,6}]$[OctO] + 0.5 wt% MC	1476.7	700.4	110.84
$[P_{14,6,6,6}]$[OctO] + 1.0 wt% MC	1513.8	725.4	108.68
$[P_{14,6,6,6}]$[OctO] + 3.0 wt% MC	1641.8	734.9	123.40
$[P_{14,6,6,6}]$[DecO] Neat	1482.4	696.1	112.96
$[P_{14,6,6,6}]$[DecO] + 14.150 wt% H_2O	832.5	454.7	83.09
$[P_{14,6,6,6}]$[DecO] + 0.5 wt% MWCNT	1553.9	730.2	112.80
$[P_{14,6,6,6}]$[DecO] + 1.0 wt% MWCNT	1604.5	749.8	113.99
$[P_{14,6,6,6}]$[DecO] + 3.0 wt% MWCNT	1719.0	815.5	110.79
$[P_{14,6,6,6}]$[DecO] + 0.5 wt% G	1514.0	709.7	113.33
$[P_{14,6,6,6}]$[DecO] + 1.0 wt% G	1605.9	740.4	116.90
$[P_{14,6,6,6}]$[DecO] + 3.0 wt% G	1695.6	807.0	110.11
$[P_{14,6,6,6}]$[DecO] + 0.5 wt% BN	1556.8	751.1	107.27
$[P_{14,6,6,6}]$[DecO] + 1.0 wt% BN	1641.4	757.1	116.80
$[P_{14,6,6,6}]$[DecO] + 3.0 wt% BN	1657.5	786.3	110.80
$[P_{14,6,6,6}]$[DecO] + 0.5 wt% MC	1572.7	746.0	110.82
$[P_{14,6,6,6}]$[DecO] + 1.0 wt% MC	1620.4	772.8	109.68
$[P_{14,6,6,6}]$[DecO] + 3.0 wt% MC	1769.6	834.8	111.98
Therminol VLT[a]	285.4	255.6	11.66
Dowtherm MX[b]	612.1	365.3	67.56
Therminol LT[c]	273.0	241.0	13.28
Dowtherm J[d]	271.1	241.7	12.16
Therminol D12[e]	322.1	270.4	19.12
Dowtherm A[f]	362.8	272.6	33.09
Dynalene PG50[g]	263.7	179.3	47.07
Dynalene FC-EG[h]	224.2	166.6	34.57
Water	152.4	129.8	17.48

[a] methylcyclohexane/trimethylpentane mixture
[b] mixture of alkylated aromatics
[c] alkyl-substituted aromatics
[d] mixture of isomers of alkylated aromatics
[e] synthetic hydrocarbons
[f] mixture of biphenyl and diphenyl oxides
[g] inhibited propylene glycol:water mixture (60:40 vol%)
[h] mixture of ethylene glycol:water (50:50 vol%) and nanoparticles (trade secret)

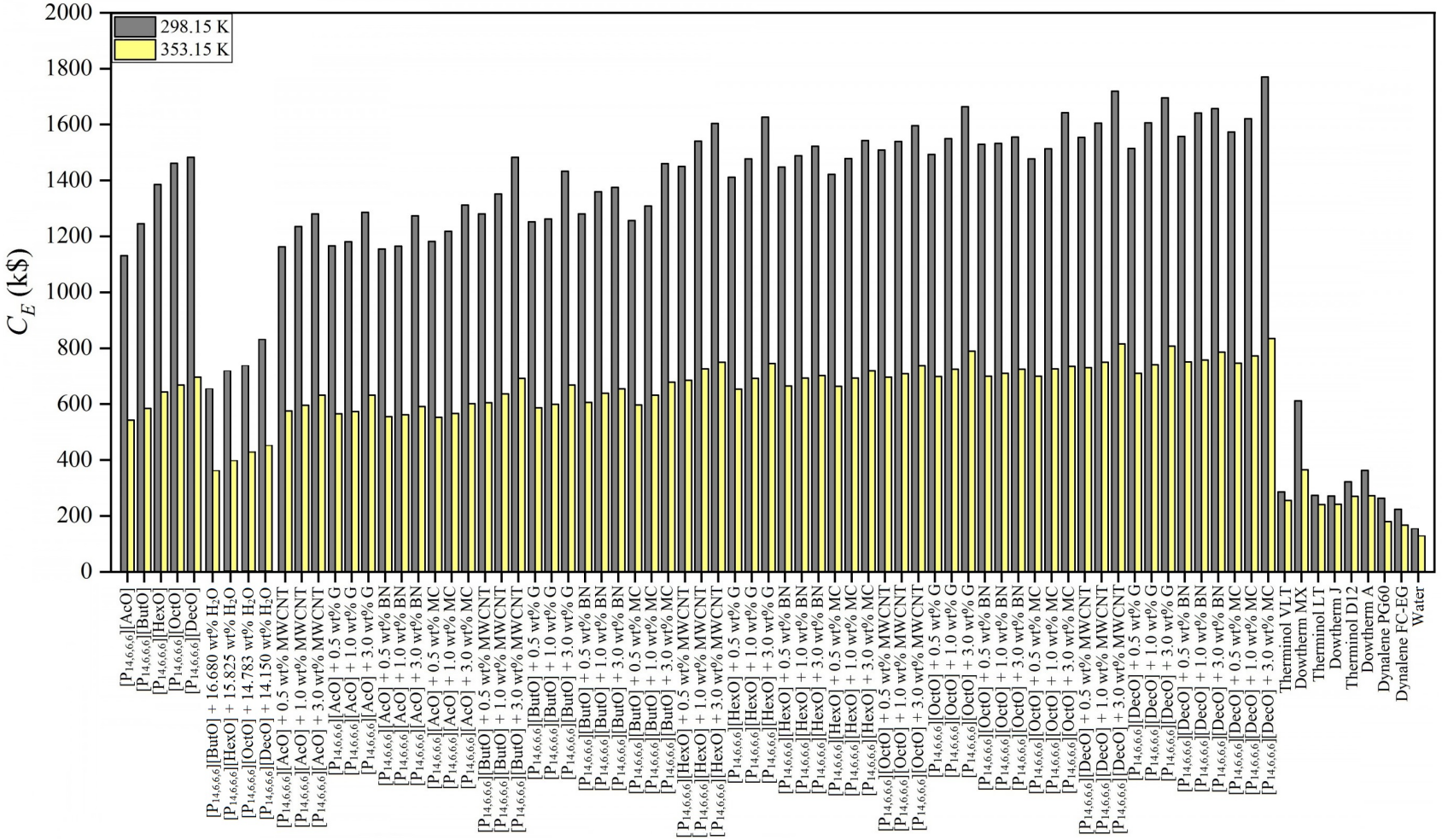

Figure 7.1.1. The results of economic analysis in the meaning of the heat exchange reactor cost, C_E, at 298.15 K and 363.15 K.

Firstly, the prices for all pure ILs are higher than those of selected HTFs, for example (1130.7, 1245.8, 1385.7, 1460.9 and 1482.4) k$ for $[P_{14,6,6,6}]$[AcO], $[P_{14,6,6,6}]$[ButO], $[P_{14,6,6,6}]$[HexO], $[P_{14,6,6,6}]$[OctO] and $[P_{14,6,6,6}]$[DecO] at 298.15 K, and (542.2, 584.1, 643.2, 668.4 and 696.1) k$ for $[P_{14,6,6,6}]$[AcO], $[P_{14,6,6,6}]$[ButO], $[P_{14,6,6,6}]$[HexO], $[P_{14,6,6,6}]$[OctO] and $[P_{14,6,6,6}]$[DecO] at 363.15 K, respectively, as in **Table 7.1.1** and **Figure 7.1.1**. While the values for selected HTFs are for example (285.4, 612.1 or 362.8) k$ for Therminol VLT, Dowtherm MX or Dowtherm A at 298.15 K, and (255.6, 365.3 or 272.6) k$ for Therminol VLT, Dowtherm MX or Dowtherm A at 363.15 K, respectively. The ILs are more expensive by up to 5 times. This is caused by very high viscosity.

On the other hand, the price of pure ILs is decreasing with temperature, within about 100 K they tend to decrease for over 100%. The decrease for commercial HTFs is not that significant as they already have quite low viscosity, and as discussed before, the viscosity in this work is decreasing for about 1000% within the investigated temperature range. At higher temperatures, the price for ILs and commercial HTFs would be very similar. Moreover, in industrial purposes the fluids are usually used at high temperature which is more promising for ILs.

Despite the decreasing viscosity, other properties also contribute to the decrease of the price, for instance the isobaric heat capacity (7-9 % of increase within 100 K temperature change). Unfortunately, thermal conductivity and density counteract the beneficial changes in viscosity and isobaric heat capacity, to quantify - about 5% and 7% decrease of density and thermal conductivity in 100K temperature change.

Despite the high cost of the ILs, they also have other important properties, namely low vapour pressure, [3] low freezing point, [4] high thermal stability, [5] or wide liquid range. [6] Therefore, the application of them as HTFs is beneficial as they can help to overcome many limitations associated with the engineering issues of the heat exchange.

7.1.2 Ionic Liquid Mixtures with Water

As can be seen, water is the cheapest material (152.4 and 129.8) k$ at 298.15 K and 363.15 K, respectively, because of its very low viscosity, high heat capacity and

thermal conductivity, and moderate density. Taking into account the features of above presented ILs, an obvious conclusion is that these have higher predicted heat exchange unit price, as in **Table 7.1.1** and **Figure 7.1.1**.

One of the solutions for this problem (mainly viscosity) was introducing water as a mixture of IL and water. [7, 8] The viscosity is significantly reduced (up to 560%), and heat capacity, thermal conductivity and density are enhanced simultaneously (~80%, ~19% and ~2.5%, respectively). Consequently, the price of heat exchange unit is much lower for mixtures with water than pure ILs, for even up to almost 100%.

Nevertheless, the thermophysical properties are better in the meaning of application as HTFs, other properties are much less attractive, for example the liquidus range is significantly reduced (from over 150 K to 100 K, as for water liquidus range), [9] or increased corrosivity. [10, 11]

As for pure ILs, the decrease of viscosity caused by the increasing temperature is much higher for mixtures than water (~80% and ~17%, respectively). Also, it should be noted that water (in a liquid state) cannot be used over 373.15 K (due to boiling) which is an enormous disadvantage because, as mentioned above, most processes in industry occur at higher temperature, and the control of pressure in the system becomes problematic (isobaric thermal expansion and evaporation).

7.1.3 Ionanofluids

Furthermore, the addition of nanoparticles causes an increase in the price (**Table 7.1.1** and **Figure 7.1.1**). It was observed that the enhancement was independent on the type of IL or nanoparticle, average as (3.1, 6.8 and 13.7) % for ionanofluids containing 0.5 wt%, 1.0 wt% and 3.0 wt% nanoparticles, respectively. This is a very significant shift, for example above enhancements are at least (35 000, 77 000 and 155 000) $. These shifts are mainly caused by the increase in viscosity (of even up to 150%), even though the other properties are improved, for example density (up to ~3%), isobaric heat capacity (up to ~35%) and thermal conductivity (up to ~20%). Unfortunately, as can be seen, the viscosity is still a remaining problem and it influences the thermal performance of ionanofluids, even though other properties are improved. On the other hand, the temperature effect

on the price (and physical properties, particularly viscosity) is similar to this of pure ILs (slightly above 100% of decrease).

Unfortunately, based on the conducted economic studies, ionic liquid-based nanofluids do not seem to be promising materials for heat transfer applications. Despite the enhanced thermal conductivity, density and heat capacity, which are very favoured, the viscosity is also enhanced which significantly increases the price of the unit. Also, including the decrease of the price induced by the increasing temperature, it does not seem to be as promising for ionanofluids as for pure ILs (for ionanofluids pure ILs are used, and very expensive nanoparticles to purchase and synthesise). Better combined heat transfer performance is achieved for ILs than for ionanofluids (mainly due to viscosity).

Therefore, pure ILs could be very promising materials for heat transfer applications. The physical properties are not very spectacular at room temperature, however, at higher temperature (where most processes occur), the viscosity is significantly decreased which makes them a viable applicable option. Additionally, the properties of ILs (low vapour pressure or wide liquid range) makes them even a more attractive solution. Mixtures of ILs and water, in terms of their application as HTFs, seem to be more promising materials: **a)** heat capacity and thermal conductivity are enhanced to higher values; **b)** viscosity is significantly reduced. However, the unique properties of ILs are lost in that case. Reliable data over the entire concentration range are thus a necessary prerequisite for the use of such mixtures. Furthermore, we may have negative effect in term of excess properties especially in the water rich region, which may have a negative impact on heat capacity thermal properties. [12, 13]

7.2 Impact of the Thermophysical Properties Measurement Errors

The accuracy of determined thermophysical properties has an enormous impact on the heat exchange units design. This was also investigated based on this methodology by Mendonça *et al.* (**1981**) that showed 25% of misestimation of the unit cost, [2] Nunes *et al.* (**2003**) studied the importance of viscosity and thermal conductivity accuracy which might result in the heat exchanger cost misestimation of 16%, [14] França *et al.* (**2009**) combined the uncertainties of all four thermophysical properties and reported the misestimation of 15%. [1] However, all these authors set the measurmement uncertainties as constant values (10, 15, 20, *etc.*) %, whereras in this work the real uncertainties are considered.

The measurement of thermophysical properties is undoubtedly the most accurate way to perform the HTFs design. Nevertheless, it does not remain the most efficient, fastest, robust and cheapest option. The other approach that is very well-known is to calculate the properties of investigated materials where the physical properties of several systems without any prior knowledge of those properties.

It is also in high importance to know the impact of each of these properties on the calculated combined price of heat exchange unit. The percentage relative deviation shows the error of physical property influence on the HTFs design, but it also gives an idea of the physical property impact/importance on the combined heat exchange unit price. The results can be seen in **Figure 7.2.1**.

For the density (**Figure 7.2.1a**), the property's error impact was found to be about 0.11% for all samples. Interestingly, it is very close to the standard uncertainty of density (± 0.1%). Moreover, increasing the density values results in decreasing the heat exchange cost. In terms of heat capacity (**Figure 7.2.1b**), average of 1.37% of error impact on the heat exchange unit can be observed. As can be seen, this impact is much smaller than the standard uncertainty of heat capacity measurement (± 3%). Also, it can be seen that increasing the heat capacity results in reducing the cost. The impact of the thermal conductivity error was found to be about 3.01% (**Figure 7.2.1c**) which is very close to the average standard uncertainty of thermal conductivity (~3.44%). Moreover, the increase of thermal conductivity values decreases the cost. The last property's error, viscosity, was found to influence the cost by -1.88% in case of the errors, while the experimental standard uncertainty was ±3%. As can be seen, the thermal conductivity is the least

accurate property among all of the determined physical properties.

For the future aspects, the prediction of physical properties should be performed in the meaning of economic analysis, including all literature data available, including mixtures with solvents, water and nanoparticles (while for the latter case models for viscosity must be first developed).

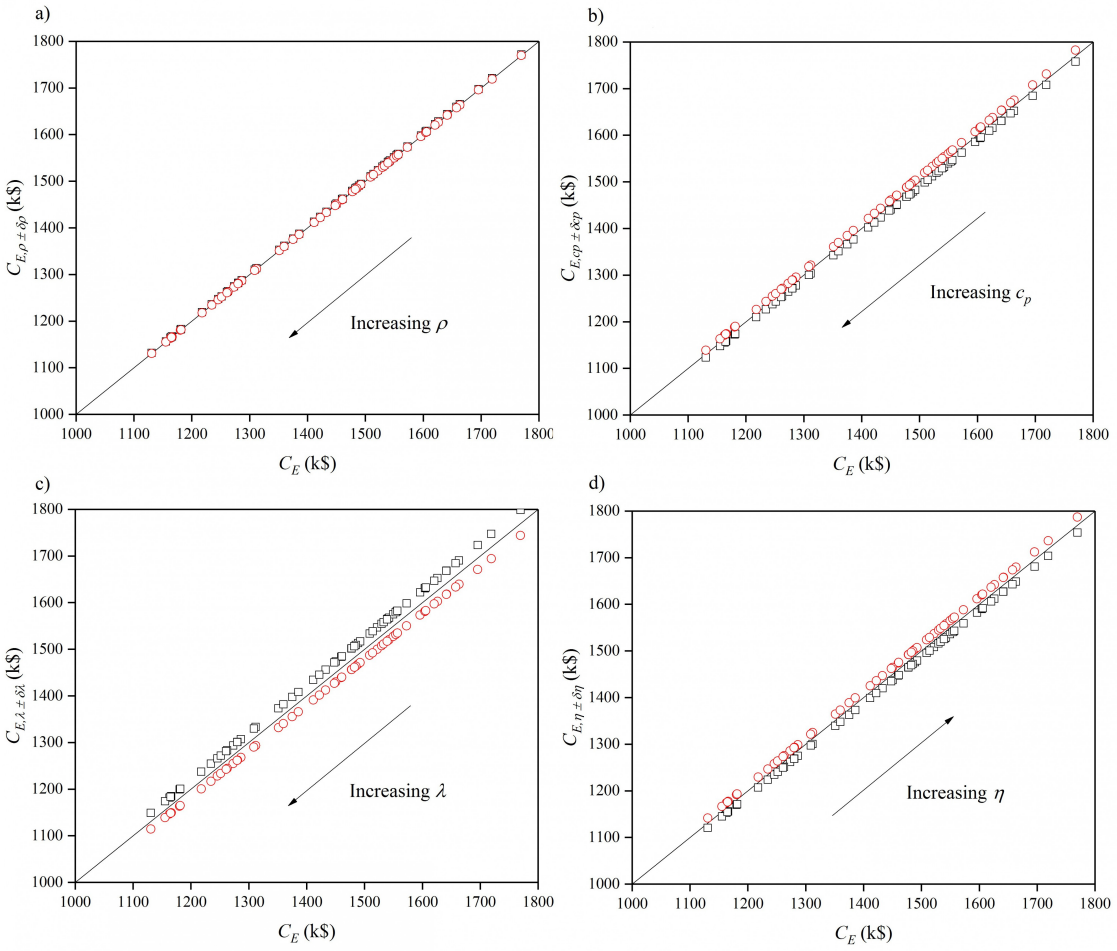

Figure 7.2.1. Effect of physical properties errors on the heat exchange unit price for **a)** density; **b)** heat capacity; **c)** thermal conductivity; **d)** viscosity; $x + \delta x$, □, x-δx, ○.

7.3 Conclusions

This chapter included the comparison of investigated ILs and their mixtures with water and nanoparticles to commonly used HTFs purely based on the physical properties. A property, so-called heat exchange unit price, which combines the most important physical properties - thermal conductivity, heat capacity, density and viscosity, was used to perform such studies. A few conclusions can be drawn.

First of all, the physical properties of pure ILs does not appear in better thermal performance than other HTFs, and in particular water, due to high viscosity values. Whereas the addition of water significantly reduces viscosity - therefore, the price of heat exchange unit, and then the IL + water mixtures seem to be more promising.

The impact of temperature on the thermal performance was also investigated, and it was shown that temperature has a significant impact. Above 373.15 K, the physical properties of ILs appear to be very similar to HTFs - including viscosity. Which indicated the possibility to use ILs (in a pure state) at high temperatures.

ILs with nanoparticles as additives were also investigated in terms of the application as HTFs. Thermal conductivity, density and heat capacity were found to enhance the thermal performance. On the other hand, viscosity was also shifted to higher values by the addition of nanoparticles which significantly increased the heat exchange unit cost. As a final result including all these effects, the thermal performance of ionanofluids in comparison to ILs is not better.

Taking into account other properties of ILs, such as negligible vapour pressure, wide liquid range or low flammability, they might be a solution for several issues in the industry. These properties are also lost in mixtures with water.

Finally, the impact of physical properties errors on the heat exchange unit design was assessed, and it was shown that thermal conductivity errors seem to be the most influencing the calculations.

Bibliography

[1] J. M. P. FRANÇA, C. A. NIETO DE CASTRO, M. M. LOPES, and V. M. B. NUNES, *Journal of Chemical & Engineering Data* **54**, 2569 (2009).

[2] A. J. F. MENDONCA, C. A. NIETO DE CASTRO, M. J. ASSAEL, and W. A. WAKEHAM, *Revista Portuguesa de Química* **23**, 7 (1981).

[3] M. J. EARLE, J. M. S. S. ESPERANÇA, M. A. GILEA, J. N. C. LOPES, L. P. N. REBELO, J. W. MAGEE, K. R. SEDDON, and J. A. WIDEGREN, *Nature* **439**, 831 (2006).

[4] S. ZHANG, N. SUN, X. HE, X. LU, and X. ZHANG, *Journal of Physical and Chemical Reference Data* **35**, 1475 (2006).

[5] C. MATON, N. DE VOS, and C. V. STEVENS, *Chemical Society Reviews* **42**, 5963 (2013).

[6] M. FREEMANTLE, *An Introduction to Ionic Liquids*, Royal Society of Chemistry, London, The United Kingdom, 2010.

[7] C. M. S. S. NEVES, P. J. CARVALHO, M. G. FREIRE, and J. A. P. COUTINHO, *The Journal of Chemical Thermodynamics* **43**, 948 (2011).

[8] M. A. R. MARTINS, C. M. S. S. NEVES, K. A. KURNIA, P. J. CARVALHO, M. A. A. ROCHA, L. M. SANTOS, S. P. PINHO, and M. G. FREIRE, *Fluid Phase Equilibria* **407**, 188 (2016).

[9] J. G. HUDDLESTON, A. E. VISSER, W. M. REICHERT, H. D. WILLAUER, G. A. BROKER, and R. D. ROGERS, *Green Chemistry* **3**, 156 (2001).

[10] M. UERDINGEN, C. TREBER, M. BALSER, G. SCHMITT, and C. WERNER, *Green Chemistry* **7**, 321 (2005).

[11] Q. B. ZHANG and Y. X. HUA, *Electrochimica Acta* **54**, 1881 (2009).

[12] G. GARCÍA-MIAJA, J. TRONCOSO, and L. ROMANÍ, *The Journal of Chemical Thermodynamics* **41**, 161 (2009).

[13] L. E. FICKE, H. RODRÍGUEZ, and J. F. BRENNECKE, *Journal of Chemical & Engineering Data* **53**, 2112 (2008).

[14] V. M. B. NUNES, M. J. V. LOURENÇO, F. J. V. SANTOS, and C. A. NIETO DE CASTRO, *Journal of Chemical & Engineering Data* **48**, 446 (2003).

Final Remarks and Future Work

The main aim of this work was to study the potential application of ionic liquids and nanoparticles mixtures as heat transfer fluids. Moreover, other types of ionic liquid-based systems were investigated, such as pure ionic liquids and mixtures with water.

In **Chapter 1**, the introduction and basic theories necessary to understand the outcome of studies carried out were presented. Those included the literature review on ionic liquids, nanoparticles, nanofluids and heat transfer fluids. In **Chapter 2**, the experimental and calculation details were presented, including the synthesis and purification of ionic liquids, preparation of ionic liquid-nanoparticles and ionic liquid-water mixtures, techniques used for characterization, quantum chemical basics, and prediction/correlation models. In **Chapter 3**, studies on imidazolium- and pyrrolidinium-based ionic liquids with nanoparticles were studied. The initial conclusions on density, heat capacity and thermal conductivity were drawn therein. In **Chapter 4**, thermophysical properties (density, isobaric heat capacity, ionic conductivity, thermogravimetric analysis, thermal conductivity and viscosity) of quaternary phosphonium-based ionic liquids and their mixtures with water were investigated. This novel class of ionic liquids was chosen to make further development of the knowledge on ionic liquids and their mixtures with water. In **Chapter 5**, the modelling of isobaric heat capacity and thermal conductivity was performed. The previously studied quaternary phosphonium-based ionic liquids (from Chapter 4) were used as a testing set as those were not used in any models considered. Furthermore, the models for those properties were improved by including quantum chemical calculations. In **Chapter 6**, novel mixtures of quaternary phosphonium-based ionic liquids and nanoparticles (carbon nanotubes, graphite, boron nitride and mesoporous carbon) were studied in terms of their density, viscosity, heat capacity, thermal conductivity and thermal stability. The initial results from Chapter 3 were additionally discussed and confirmed in Chapter 6 which resulted in more insight into the phenomena occurring in these systems, such as

physical properties enhancement. In **Chapter 7**, a comparative economic analysis was performed between investigated ionic liquids, their mixtures with water and nanoparticles, and commercially available heat transfer fluids and water.

A persistent question which scientists ask in heat transfer community is: How can we improve the existing heat transfer fluids? One of the well-known solutions was proposed by Choi and Eastman in 1995 by mixing those heat transfer fluids with nanoparticles (so-called nanofluids). Several advantages were presented - mainly focued on the thermophysical properties enhancement. Nowadays, there is a commercially available nanofluid (of which composition is an industrial secret). After 15 years, in 2010, Nieto de Castro and co-workers published a research publication on mixtures of ionic liquids (which were discovered in 1914 by Walden) and nanoparticles, providing a potential applicability (resulting from ionic liquids specific properties and physical properties enhancement caused by the dispersed nanoparticles). However, even though some results were presented, the assessment of the real possibility to use as heat transfer fluids was not performed, mainly due to the lack of full experimental characterisation. In 2018, in this work, the full characterization of physical properties of ionic liquid-nanoparticle mixtures, theoretical investigation and comparison to commercial heat transfer fluids, were presented. This was the first work in which such comprehensive studies were conducted.

After the analysis and economical comparison to commercial heat transfer fluids, unfortunately, ionic liquid-nanoparticle mixtures do not represent better heat transfer efficiency than commercial heat transfer fluids (or pure ionic liquids) which was mainly caused by large viscosity enhancement. However, based on the studies carried out, ionic liquid-water mixtures seem to be very promising materials.

For the future plans, studies performed in Chapter 3 should be done for a wider range of ionic liquids, including different cation/anion chain length/type and/or functionalisation. In terms of Chapter 4, because of the beneficial improvement of the physical properties of ionic liquid-water mixtures than pure ionic liquids, more mixtures should be studied, including the effect on heat capacity and thermal conductivity (particularly the excess properties). Regarding Chapter 5, more ionic liquids should be studied in terms of thermal conductivity and heat capacity, and further improvement of these models should be performed. However, an emphasis should be put on the prediction of viscosity which is still very inaccurate. More ionic liquid-nanoparticle mixtures should be studied, as in

Chapter 6, therefore, more accurate discussion could be done on the physical properties enhancement, and the driving forces responsible for these. Finally, all above considerations should be performed in comparison to commercial heat transfer fluids, including the prediction models capabilities, as in Chapter 7.

Appendix A

Table A1 Chemicals description.[a]

Chemical name [CAS]	Supplier	Mass fraction purity	Purification method	Analysis method	Halide content ppm[b]
Trihexyl(tetradecyl)phosphonium acetate [872700-58-8]	In houses	≥ 0.98	Washing-extraction Vacuum	^{1}H, ^{13}C and ^{31}P NMR CHNS analysis KF titration	< 5
Trihexyl(tetradecyl)phosphonium butanoate [1393375-56-8]	In house	≥ 0.98	Washing-extraction Vacuum	^{1}H, ^{13}C and ^{31}P NMR CHNS analysis KF titration	< 5
Trihexyl(tetradecyl)phosphonium hexanoate [1393375-57-9]	In house	≥ 0.98	Washing-extraction Vacuum	^{1}H, ^{13}C and ^{31}P NMR CHNS analysis KF titration	< 5
Trihexyl(tetradecyl)phosphonium octanoate [1393375-58-0]	In house	≥ 0.98	Washing-extraction Vacuum	^{1}H, ^{13}C and ^{31}P NMR CHNS analysis KF titration	< 5
Trihexyl(tetradecyl)phosphonium decanoate [465527-65-5]	In house	≥ 0.98	Washing-extraction Vacuum	^{1}H, ^{13}C and ^{31}P NMR CHNS analysis KF titration	< 5
Trihexyl(tetradecyl)phosphonium chloride [258864-54-9]	Cytec Inc.	> 0.95			
Ethanol [64-17-5]	Sigma-Aldrich	> 0.998			
Strongly basic anion resin IRN-78 [11128-95-3]	Alfa Aesar	≤ 0.0005 Cl^-; ≤ 0.0001 SiO_2; ≤ 0.0006 SO_4			
Silver nitrate [7761-88-8]	Sigma-Aldrich	≥ 0.999999			
Acetic acid [64-19-7]	Sigma-Aldrich	≥ 0.99			
Butanoic acid [107-92-6]	Sigma-Aldrich	≥ 0.99			
Hexanoic acid [142-62-1]	Sigma-Aldrich	≥ 0.995			
Octanoic acid [124-07-2]	Sigma-Aldrich	≥ 0.99			
Decanoic acid [334-48-5]	Sigma-Aldrich	≥ 0.98			
1-octyl-3-methylimidazolium bis[(trifluoromethyl)sulfonyl]imide [178631-04-4]	In house	≥ 0.98	Washing-extraction Vacuum	^{1}H and ^{13}C NMR KF titration	< 5
Water [7732-18-5]	Deionisator	Ultrapure, type 1	Deionisation	UV, conductivity measurement[c]	
1-butyl-3-methylimidazolium dicyanamide [448245-52-1]	Merck	≥ 0.98	Washing-extraction Vacuum	^{1}H and ^{13}C NMR KF titration	< 5
1-Butyl-3-methylimidazolium	Merck	≥ 0.98	Washing-	^{1}H and ^{13}C NMR	< 5

bis[(trifluoromethyl)sulfonyl]imide [174899-83-3]			extraction Vacuum	KF titration	
1-Butyl-1-methylpyrrolidinium bis[(trifluoromethyl)sulfonyl]imide [223437-11-4]	In house	≥ 0.98	Washing-extraction Vacuum	^{1}H and ^{13}C NMR KF titration	< 5
1-Hexyl-3-methylimidazolium hexafluorophosphate [304680-35-1]	In house	≥ 0.98	Washing-extraction Vacuum	^{1}H and ^{13}C NMR KF titration	< 5
1-Ethyl-3-methylimidazolium ethylsulfate [342573-75-5]	In house	≥ 0.98	Washing-extraction Vacuum	^{1}H and ^{13}C NMR KF titration	< 5
Multi-walled carbon nanotubes [308068-56-6]	Bayer Material Science	≥ 0.99		Ashing,[d] TEM,[d] SEM,[e] EN ISO 60,[d] XRD, laser diffraction technique	
Boron nitride [10043-11-5]	US Research Nanomaterials, Inc.	≥ 0.998		SEM,[e] XRD[e]	
Graphite [7782-42-5]	US Research Nanomaterials, Inc.	≥ 0.999		SEM,[e] XRD[e]	
Mesoporous carbon [7440-44-0]	US Research Nanomaterials, Inc.	≥ 0.95		SEM,[e] XRD[e]	
Toluene [108-88-3]	Sigma-Aldrich	≥ 0.995			
Glycerine [56-81-5]	Sigma-Aldrich	≥ 0.99			
Sodium chloride [7647-14-5]	Sigma-Aldrich	≥ 0.99			
Synthetic sapphire [1317-82-4]	TA Instruments	Ultrapure[d]			

[a] ^{1}H and ^{13}C NMR refer to proton, carbon and nuclear magnetic resonance spectroscopy, respectively;

[b] determined by $AgNO_3$ titration;

[c] Merck Millipore Direct-Q 3UV equipment;

[d] as reported by the supplier;

[e] as reported by supplier and confirmed by measurement.

Table A2 ^{1}H, ^{13}C and ^{31}P NMR analysis results for $[P_{14,6,6,6}][AcO]$, $[P_{14,6,6,6}][ButO]$, $[P_{14,6,6,6}][HexO]$, $[P_{14,6,6,6}][OctO]$, $[P_{14,6,6,6}][DecO]$, $[C_8C_1Im][NTf_2]$, $[C_4C_1Im][Dca]$, $[C_4C_1Im][NTf_2]$, $[C_4C_1Pyrr][NTf_2]$, $[C_6C_1Im][PF_6]$ and $[C_2C_1Im][C_2SO_4]$.

$[P_{14,6,6,6}][AcO]$

^{1}H NMR (400 MHz, $CDCl_3$): δ (ppm) = 0.81 (m, 12H, CH_3 (P)), 1.22 (m, 32H, CH_2 (P)), 1.43 (m, 16H, CH_2 (P)), 1.87 (s, 3H, CH_3 (AcO)), 2.35 (m, 8H, CH_2 (P));

^{13}C NMR (400 MHz, $CDCl_3$): δ (ppm) = 14.09, 14.28, 18.75, 19.37, 22.03, 22.09, 22.52, 22.85, 25.67, 29.14, 29.47, 29.51, 29.67, 29.80, 30.58, 30.77, 30.89, 31.09, 31.39, 32.08, 176.68;

^{31}P NMR (400 MHz, $CDCl_3$): δ (ppm) = 34.09;

Molar mass: 542.90 g/mol; **C** – experimental: 74.99 %, theoretical: 75.22 %, **H** – experimental: 13.40 %, theoretical: 13.18 %.

$[P_{14,6,6,6}][ButO]$

^{1}H NMR (400 MHz, $CDCl_3$): δ (ppm) = 0.89 (m, 15H, CH_3 (P) + (ButO)), 1.30 (m, 32H, CH_2 (P)), 1.53 (m, 16H, CH_2 (P)), 1.65 (m, 2H, CH_2 (ButO)), 2.21 (t, 2H, CH_2 (ButO)), 2.40 (m, 8H, CH_2 (P));

^{13}C NMR (400 MHz, $CDCl_3$): δ (ppm) = 14.06, 14.25, 14.55, 18.73, 19.35, 20.16, 21.98, 22.04, 22.50, 22.82, 29.11, 29.49, 29.66, 29.78, 30.54, 30.73, 30.85, 31.05, 31.25, 32.06, 40.36, 178.61;

^{31}P NMR (400 MHz, $CDCl_3$): δ (ppm) = 34.10;

Molar mass: 570.95 g/mol; **C** – experimental: 76.01 %, theoretical: 75.73 %, **H** – experimental: 13.18 %, theoretical: 13.24 %.

$[P_{14,6,6,6}][HexO]$

^{1}H NMR (400 MHz, $CDCl_3$): δ (ppm) = 0.88 (m, 15H, CH_3 (P) + (HexO)), 1.30 (m, 36H, CH_2 (P) + (HexO)), 1.47 (m, 16H, CH_2 (P)), 1.63 (m, 2H, CH_2 (HexO)), 2.24 (t, 2H, CH_2 (HexO)), 2.36 (m, 8H, CH_2 (P));

^{13}C NMR (400 MHz, $CDCl_3$): δ (ppm) = 14.02, 14.21, 14.29, 18.71, 19.34, 22.00, 22.06, 22.46, 22.78, 22.88, 27.12, 29.09, 29.44, 29.61, 29.74, 30.53, 30.72, 30.84, 31.04, 31.24, 32.02, 32.55, 39.39, 179.02;

^{31}P NMR (400 MHz, $CDCl_3$): δ (ppm) = 34.02;

Molar mass: 599.00 g/mol; **C** – experimental: 76.47 %, theoretical: 76.19 %, **H** – experimental: 13.06 %, theoretical: 13.29 %.

$[P_{14,6,6,6}][OctO]$

^{1}H NMR (400 MHz, $CDCl_3$): δ (ppm) = 0.88 (m, 15H, CH_3 (P) + (OctO)), 1.28 (m, 40H, CH_2 (P) + (OctO)), 1.51 (m, 16H, CH_2 (P)), 1.61 (m, 2H, CH_2 (OctO)), 2.22 (t, 2H, CH_2 (OctO)), 2.39 (m, 8H, CH_2 (P));

^{13}C NMR (400 MHz, $CDCl_3$): δ (ppm) = 13.71, 13.91, 18.39, 19.02, 21.72, 22.17, 22.48, 22.53, 27.38, 28.78, 29.15, 29.31, 29.44, 30.06, 30.23, 30.43, 30.54, 30.73, 30.94, 31.72, 31.81, 39.62, 178.58;

^{31}P NMR (400 MHz, $CDCl_3$): δ (ppm) = 33.65

Molar mass: 627.06 g/mol; **C** – experimental: 76.70 %, theoretical: 76.62 %, **H** – experimental: 13.30 %, theoretical: 13.34 %.

$[P_{14,6,6,6}][DecO]$

^{1}H NMR (400 MHz, $CDCl_3$): δ (ppm) = 0.88 (m, 15H, CH_3 (P) + (DecO)), 1.28 (m, 44H, CH_2 (P) + (DecO)), 1.49 (m, 16H, CH_2 (P)), 1.60 (m, 2H, CH_2 (DecO)), 2.20 (t, 2H, CH_2 (DecO)), 2.38 (m, 8H, CH_2 (P));

^{13}C NMR (400 MHz, $CDCl_3$): δ (ppm) = 14.12, 14.30, 18.80, 19.42, 22.09, 22.15, 22.56, 22.89, 27.39, 29.20, 29.54, 29.62, 29.73, 29.84, 29.91, 30.00 30.35, 30.63, 30.82, 30.94, 31.14, 31.34, 32.11, 32.16, 39.22, 179.09;

^{31}P NMR (400 MHz, $CDCl_3$): δ (ppm) = 34.09;

Molar mass: 655.11 g/mol; **C** – experimental: 76.88 %, theoretical: 77.00 %, **H** – experimental: 13.89 %, theoretical: 13.39 %.

$[C_8C_1Im][NTf_2]$

^{1}H NMR (400 MHz, $CDCl_3$): δ (ppm) = 0.75 (t, 3H, CH_3), 1.19 (d, 10H, CH_2), 1.77 (m, 2H, CH_2), 3.82 (s, 3H, CH_3), 4.06 (t, 2H, CH_2), 7.28 (d, 2H, 2xCH), 8.53 (s, 1H, CH).

$[C_4C_1Im][Dca]$

^{1}H NMR (400 MHz, $CDCl_3$): δ (ppm) = 0.16 (t, 3H), 0.59 (m, 2H), 1.11 (m, 2H), 3.21 (s, 3H), 3.47 (t, 2H), 6.80 (d, 1H), 6.85 (d, 1H), 8.26 (s, 1H);

^{13}C NMR (400 MHz, $CDCl_3$): δ (ppm) = 12.91, 18.83, 31.38, 35.78, 49.14, 118.93, 122.01, 123.10, 135.45

$[C_4C_1Im][NTf_2]$

^{1}H NMR (400 MHz, $CDCl_3$): δ (ppm) = 0.95 (t, 3H), 1.33 (m, 2H), 1.88 (m, 2H), 3.92 (s, 3H), 4.15 (t, 2H), 7.36 (dt, 2H), 8.64 (s, 1H);

^{13}C NMR (400 MHz, $CDCl_3$): δ (ppm) = 12.99, 19.15, 31.77, 36.05, 49.75, 117.84, 121.06, 122.03, 123.17, 135.11.

$[C_2C_1Im][C_2SO_4]$

^{1}H NMR (400 MHz, $CDCl_3$): δ (ppm) = 1.03 (t, 3H), 1.39 (t, 3H), 3.79 (dd, 2H), 3.94 (s, 3H), 4.21 (dd, 2H), 7.79 (d, 2H), 9.08 (s, 1H);

	^{13}C NMR (400 MHz, $CDCl_3$): δ (ppm) = 14.93, 15.05, 35.69, 44.55, 62.42, 121.87, 123.37, 136.79.
[C_6C_1Im][PF_6]	**^{1}H NMR** (400 MHz, $CDCl_3$): δ (ppm) = 0.86 (t, 3H), 1.31 (m, 6H), 1.86 (m, 2H), 3.90 (s, 3H), 4.12 (t, 2H), 7.34 (dt, 2H), 8.44 (s, 1H);
	^{13}C NMR (400 MHz, $CDCl_3$): δ (ppm) = 14.01, 22.93, 27.37, 27.86, 31.56, 31.64, 47.53, 119.85, 123.55, 139.54.
[C_6C_1Im][PF_6]	**^{1}H NMR** (400 MHz, $CDCl_3$): δ (ppm) = 0.89 (t, 3H), 1.35 (m, 2H), 1.89 (m, 2H), 2.13 (m, 4H), 2.96 (s, 3H), 3.08 (m, 6H);
	^{13}C NMR (400 MHz, $CDCl_3$): δ (ppm) = 14.01, 21.32, 23.24, 25.38, 48.57, 57.85, 63.02, 122.30.

Appendix B

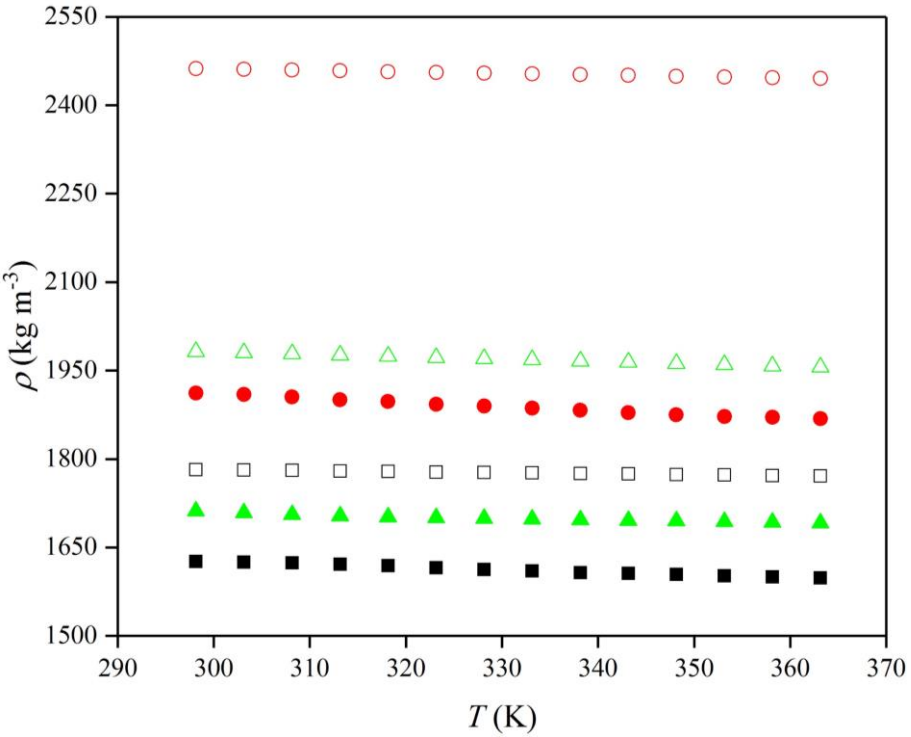

Figure B1 The density of investigated nanoparticles determined from the density measurement, for additivity model, full symbols ■, excess molar volume model, open symbols □, carbon nanotubes, black, boron nitride, red, graphite, green.

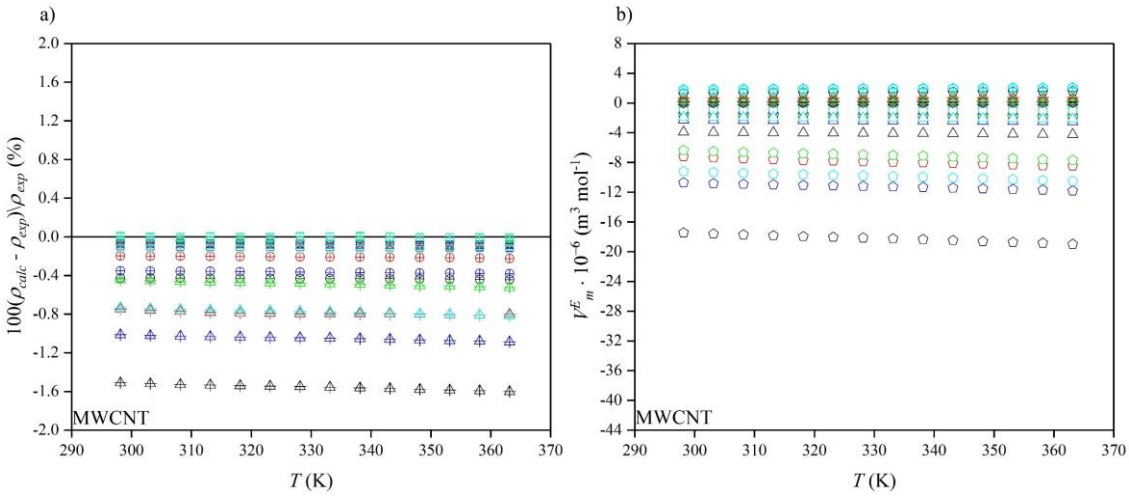

Figure B2 a) Deviations between calculated density, ρ_{calc}, and experimental values, ρ_{exp}, for ionanofluids with multiwalled carbon nanotubes (MWCNT) based on excess molar volume approach; **b)** excess molar volume, V^E_m, as a function of the temperature, T, calculated by using nanoparticle densities from empirical equation (2.2.45) and excess molar volume approaches for multiwalled carbon nanotubes (MWCNT) based ionanofluids, for additivity model, open symbols □, excess molar volume model, crossed symbols ⊗, 0.5 wt% NP, circles ○, 1.0 wt% NP, triangles △, 3.0 wt% NP, pentagons ⬠, $[C_4C_1Im][Dca]$, black, $[C_4C_1Im][NTf_2]$, red, $[C_4C_1Pyrr][NTf_2]$, green, $[C_2C_1Im][C_2SO_4]$, blue, $[C_6C_1Im][PF_6]$, cyan.

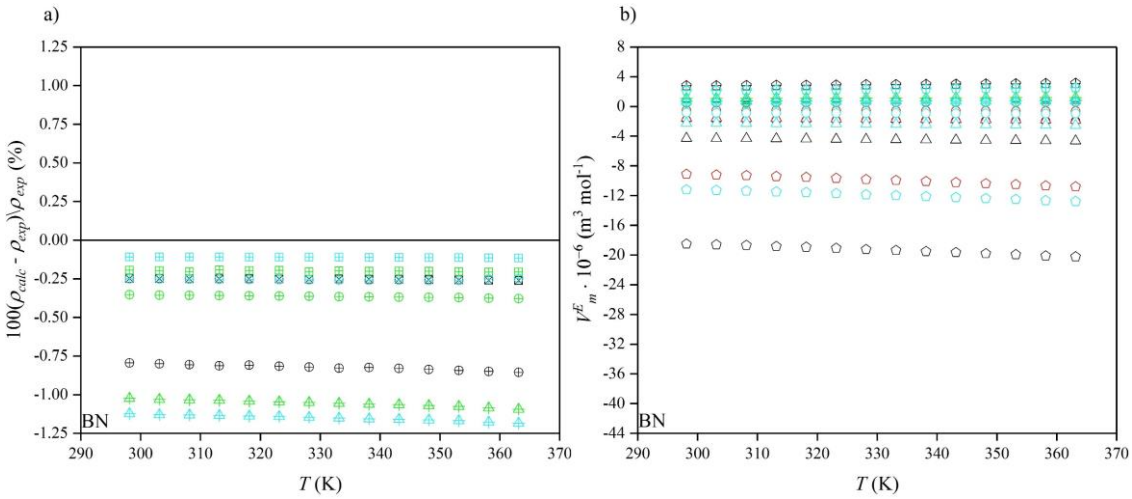

Figure B3 a) Deviations between calculated density, ρ_{calc}, and experimental values, ρ_{exp}, for ionanofluids with boron nitride (BN) based on excess molar volume approach; **b)** excess molar volume, V^E_m, as a function of the temperature, T, calculated by using nanoparticle densities from empirical equation (2.2.45) and excess molar volume approaches for boron nitride (BN) based ionanofluids, for additivity model, open symbols □, excess molar volume model, crossed symbols ⊠, 0.5 wt% NP, circles ○, 1.0 wt% NP, triangles △, 3.0 wt% NP, pentagons ⬠, $[C_4C_1Im][Dca]$, black, $[C_4C_1Im][NTf_2]$, red, $[C_4C_1Pyrr][NTf_2]$, green, $[C_2C_1Im][C_2SO_4]$, blue, $[C_6C_1Im][PF_6]$, cyan.

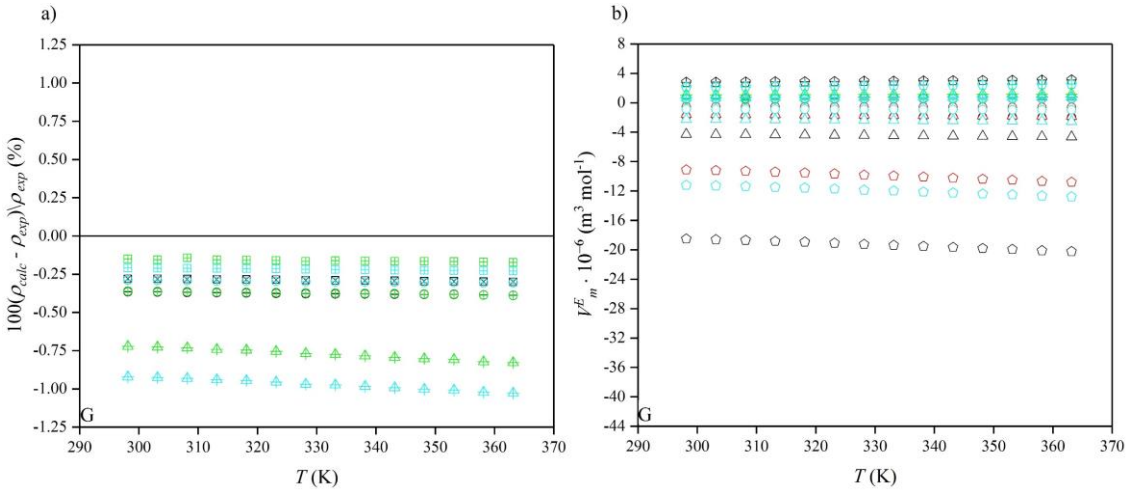

Figure B4 a) Deviations between calculated density, ρ_{calc}, and experimental values, ρ_{exp}, for ionanofluids with graphite (G) based on excess molar volume approach; **b)** excess molar volume, V^E_m, as a function of the temperature, T, calculated by using nanoparticle densities from empirical equation (2.2.45) and excess molar volume approaches for graphite (G) based ionanofluids, for additivity model, open symbols □, excess molar volume model, crossed symbols ⊠, 0.5 wt% NP, circles ○, 1.0 wt% NP, triangles △, 3.0 wt% NP, pentagons ⬠, $[C_4C_1Im][Dca]$, black, $[C_4C_1Im][NTf_2]$, red, $[C_4C_1Pyrr][NTf_2]$, green, $[C_2C_1Im][C_2SO_4]$, blue, $[C_6C_1Im][PF_6]$, cyan.

Appendix C

Table C1 The enhancements of density, ρ, dynamic visoscity, η, thermal conductivity, λ, isobaric heat capacity, c_p, for ionanofluids in comparison to pure ionic liquids.

	Enhancement (%)							
	Density (± 0.20 %)		Viscosity (0.5wt% = ± 2.4 %, 1.0wt% = ± 9.0 %, 3.0wt% = ± 13.3 %)		Thermal conductivity (± 4.5 %)		Heat capacity (± 5.3 %)	
	298.15 K	363.15 K	298.15 K	363.15 K	278.15 K	358.15 K	298.15 K	363.15 K
$[P_{14,6,6,6}][AcO]$ + 0.5 wt% MWCNT	0.40	0.45	19.1	27.9	2.8	0.8	6.1	3.6
$[P_{14,6,6,6}][AcO]$ + 1.0 wt% MWCNT	0.72	0.72	51.3	51.5	6.3	3.2	7.1	4.7
$[P_{14,6,6,6}][AcO]$ + 3.0 wt% MWCNT	1.99	2.05	116.2	135.4	19.9	18.0	11.7	9.3
$[P_{14,6,6,6}][AcO]$ + 0.5 wt% G	0.42	0.48	23.0	28.0	2.0	1.4	11.0	14.5
$[P_{14,6,6,6}][AcO]$ + 1.0 wt% G	0.76	0.83	39.7	50.4	4.4	4.5	17.1	21.9
$[P_{14,6,6,6}][AcO]$ + 3.0 wt% G	2.22	2.36	121.9	155.9	11.3	12.3	29.2	34.5
$[P_{14,6,6,6}][AcO]$ + 0.5 wt% BN	0.38	0.42	12.8	14.7	2.0	1.3	3.9	4.5
$[P_{14,6,6,6}][AcO]$ + 1.0 wt% BN	0.69	0.75	28.5	31.0	4.4	3.9	10.9	11.5
$[P_{14,6,6,6}][AcO]$ + 3.0 wt% BN	2.87	3.00	119.5	93.4	14.9	13.0	21.6	21.5
$[P_{14,6,6,6}][AcO]$ + 0.5 wt% MC	0.42	0.39	26.5	17.2	2.0	0.6	8.8	11.6
$[P_{14,6,6,6}][AcO]$ + 1.0 wt% MC	0.74	0.73	51.4	40.7	3.8	3.2	16.7	20.8
$[P_{14,6,6,6}][AcO]$ + 3.0 wt% MC	1.96	2.03	117.5	94.2	8.8	7.2	25.1	28.1
$[P_{14,6,6,6}][ButO]$ + 0.5 wt% MWCNT	0.30	0.27	21.8	23.0	3.8	4.6	5.2	3.1
$[P_{14,6,6,6}][ButO]$ + 1.0 wt% MWCNT	0.64	0.62	50.5	52.0	5.7	6.6	7.5	3.6
$[P_{14,6,6,6}][ButO]$ + 3.0 wt% MWCNT	2.10	2.14	156.7	154.0	22.6	21.4	10.3	7.0
$[P_{14,6,6,6}][ButO]$ + 0.5 wt% G	0.34	0.34	16.4	20.1	2.6	3.9	12.1	15.9
$[P_{14,6,6,6}][ButO]$ + 1.0 wt% G	0.70	0.71	28.5	38.9	5.1	5.9	18.3	22.4
$[P_{14,6,6,6}][ButO]$ + 3.0 wt% G	2.58	2.70	130.2	137.9	9.5	10.7	31.5	36.1
$[P_{14,6,6,6}][ButO]$ + 0.5 wt% BN	0.35	0.35	16.1	20.5	1.9	1.9	3.5	4.1
$[P_{14,6,6,6}][ButO]$ + 1.0 wt% BN	0.89	0.90	55.1	58.3	5.1	5.3	9.6	10.3
$[P_{14,6,6,6}][ButO]$ + 3.0 wt% BN	3.01	3.11	102.0	119.5	15.1	16.0	20.6	20.8
$[P_{14,6,6,6}][ButO]$ + 0.5 wt% MC	0.56	0.56	15.9	21.6	2.6	1.8	10.1	13.3
$[P_{14,6,6,6}][ButO]$ + 1.0 wt% MC	0.80	0.81	39.2	53.3	5.1	3.5	15.0	18.7
$[P_{14,6,6,6}][ButO]$ + 3.0 wt% MC	1.92	1.98	136.3	135.5	11.4	9.3	27.4	30.9
$[P_{14,6,6,6}][HexO]$ + 0.5 wt% MWCNT	0.22	0.23	28.8	31.5	3.8	2.3	5.7	3.3
$[P_{14,6,6,6}][HexO]$ + 1.0 wt% MWCNT	0.68	0.71	62.1	66.9	5.7	5.0	7.3	3.5
$[P_{14,6,6,6}][HexO]$ + 3.0 wt% MWCNT	2.29	2.29	133.1	138.2	21.4	20.0	11.4	8.1
$[P_{14,6,6,6}][HexO]$ + 0.5 wt% G	0.22	0.20	19.5	23.6	3.1	3.7	11.5	15.2
$[P_{14,6,6,6}][HexO]$ + 1.0 wt% G	0.52	0.51	50.6	63.6	5.0	6.4	18.7	23.1
$[P_{14,6,6,6}][HexO]$ + 3.0 wt% G	2.24	2.32	143.6	145.4	10.1	11.2	30.3	35.3
$[P_{14,6,6,6}][HexO]$ + 0.5 wt% BN	0.49	0.52	25.9	24.7	3.8	5.0	3.7	4.3
$[P_{14,6,6,6}][HexO]$ + 1.0 wt% BN	0.84	0.88	47.2	53.0	5.0	5.7	11.5	12.0
$[P_{14,6,6,6}][HexO]$ + 3.0 wt% BN	2.96	3.08	99.1	102.5	15.1	17.3	20.3	20.6
$[P_{14,6,6,6}][HexO]$ + 0.5 wt% MC	0.33	0.36	21.0	25.7	1.9	2.3	9.5	12.4
$[P_{14,6,6,6}][HexO]$ + 1.0 wt% MC	0.56	0.60	44.4	54.0	3.2	3.0	15.9	19.8
$[P_{14,6,6,6}][HexO]$ + 3.0 wt% MC	1.56	1.86	97.4	108.4	10.1	10.3	27.0	30.2
$[P_{14,6,6,6}][OctO]$ + 0.5 wt% MWCNT	0.37	0.36	17.8	20.2	1.9	1.6	5.1	2.8
$[P_{14,6,6,6}][OctO]$ + 1.0 wt% MWCNT	0.65	0.69	36.8	40.1	7.4	7.1	6.2	4.6
$[P_{14,6,6,6}][OctO]$ + 3.0 wt% MWCNT	2.40	2.45	92.9	98.5	19.8	19.1	11.5	10.0
$[P_{14,6,6,6}][OctO]$ + 0.5 wt% G	0.29	0.34	17.2	31.3	1.9	1.6	9.8	14.0
$[P_{14,6,6,6}][OctO]$ + 1.0 wt% G	0.65	0.71	43.6	59.1	4.7	3.6	15.8	19.9
$[P_{14,6,6,6}][OctO]$ + 3.0 wt% G	2.25	2.38	121.0	159.3	12.0	11.6	28.7	32.7
$[P_{14,6,6,6}][OctO]$ + 0.5 wt% BN	0.51	0.50	24.1	27.7	2.5	3.6	3.5	4.5
$[P_{14,6,6,6}][OctO]$ + 1.0 wt% BN	0.79	0.78	38.3	46.1	5.6	5.6	11.4	12.6
$[P_{14,6,6,6}][OctO]$ + 3.0 wt% BN	2.94	3.08	78.2	94.5	14.9	15.6	20.3	20.8
$[P_{14,6,6,6}][OctO]$ + 0.5 wt% MC	0.36	0.36	13.5	28.5	1.8	1.4	10.0	12.7
$[P_{14,6,6,6}][OctO]$ + 1.0 wt% MC	0.68	0.80	33.1	55.7	3.8	3.2	16.2	18.3
$[P_{14,6,6,6}][OctO]$ + 3.0 wt% MC	1.93	2.08	97.3	92.6	7.6	9.5	25.2	27.5
$[P_{14,6,6,6}][DecO]$ + 0.5 wt% MWCNT	0.40	0.41	27.6	25.3	3.3	2.5	5.2	3.3
$[P_{14,6,6,6}][DecO]$ + 1.0 wt% MWCNT	0.83	0.89	50.7	45.8	7.2	6.4	7.0	3.8
$[P_{14,6,6,6}][DecO]$ + 3.0 wt% MWCNT	2.31	2.44	137.8	144.9	22.0	20.6	11.6	8.9
$[P_{14,6,6,6}][DecO]$ + 0.5 wt% G	0.31	0.37	20.6	23.6	3.4	3.3	9.8	14.2
$[P_{14,6,6,6}][DecO]$ + 1.0 wt% G	0.79	0.88	60.9	57.0	5.9	6.4	18.7	22.1
$[P_{14,6,6,6}][DecO]$ + 3.0 wt% G	2.26	2.41	121.0	135.0	10.6	8.8	29.0	32.7
$[P_{14,6,6,6}][DecO]$ + 0.5 wt% BN	0.52	0.58	26.1	38.8	1.9	2.5	4.3	4.2
$[P_{14,6,6,6}][DecO]$ + 1.0 wt% BN	0.87	0.94	66.0	60.7	6.2	7.0	11.4	12.2
$[P_{14,6,6,6}][DecO]$ + 3.0 wt% BN	3.15	3.33	106.4	117.2	13.2	13.5	20.5	20.7
$[P_{14,6,6,6}][DecO]$ + 0.5 wt% MC	0.42	0.51	32.6	38.9	1.7	0.8	8.8	11.7
$[P_{14,6,6,6}][DecO]$ + 1.0 wt% MC	0.75	0.80	57.9	69.0	4.3	2.9	15.4	18.8
$[P_{14,6,6,6}][DecO]$ + 3.0 wt% MC	2.32	2.42	144.0	153.1	9.2	7.3	26.4	29.4

Appendix D

Table D1 Mulliken charges for investigated cations.

Group	Charge
Trimethyl(tetradecyl)ammonium	
N^+	-0.143
C1	C -0.376; H 0.280, 0.281
C2	C -0.519; H 0.266, 0.266, 0.264
C3	C -0.537; 0.268, 0.265, 0.274
C4	C-0.535; H 0.268, 0.273, 0.265
C5	C -0.423; H 0.234, 0.233
C6	C -0.389; H 0.212, 0.212
C7	C -0.391; H 0.203, 0.203
C8	C -0.390; H 0.201, 0.201
C9	C -0.388; H 0.198, 0.198
C10	C -0.387; H 0.197, 0.196
C11	C -0.386; H 0.195, 0.195
C12	C -0.385; H 0.194, 0.194
C13	C -0.382; H 0.192, 0.192
C14	C -0.378; H 0.190, 0.190
C15	C -0.374; H 0.188, 0.188
C16	C -0.364; H 0.192, 0.192
C17	C -0.626; H 0.198, 0.198, 0.220
1-Octyl-1-methylpyrrolidinium	
N^+	-0.132
C1	C -0.385; H 0.283, 0.276
C2	C -0.550; H 0.271, 0.267, 0.278
C3	C -0.384; H 0.300, 0.283
C4	C -0.473; H 0.269, 0.285
C5	C -0.469; H 0.268, 0.284
C6	C -0.400; H 0.305, 0.283
C7	C -0.413; H 0.234, 0.231
C8	C -0.390; H 0.209, 0.210
C9	C -0.387; H 0.201, 0.201
C10	C -0.381; H 0.196, 0.197
C11	C -0.376; H 0.191, 0.192
C12	C -0.366; H 0.194, 0.194
C13	C -0.623; H 0.200, 0.227, 0.200

Group	Charge
Trihexyl(tetradecyl)phosphonium	
P^+	0.928
C1	C -0.706; H 0.299, 0.298
C2	C -0.409; H 0.227, 0.226
C3	C -0.386; H 0.209, 0.210
C4	C -0.385; H 0.198, 0.198
C5	C -0.390; H 0.200, 0.200
C6	C -0.386; H 0.195, 0.196
C7	C -0.387; H 0.196, 0.196
C8	C -0.385; H 0.194, 0.194
C9	C -0.385; H 0.193, 0.194
C10	C -0.382; H 0.192, 0.191
C11	C -0.377; H 0.190, 0.190
C12	C -0.374; H 0.187, 0.188
C13	C -0.364; H 0.192, 0.191
C14	C -0.626; H 0.198, 0.220, 0.198
C15	C -0.704; H 0.297, 0.298
C16	C -0.405; H 0.225, 0.225
C17	C -0.378; H 0.205, 0.205
C18	C -0.374; H 0.193, 0.193
C19	C -0.367; H 0.197, 0.197
C20	C -0.620; H 0.200, 0.232, 0.200
C21	C -0.704; H 0.297, 0.297
C22	C -0.405; H 0.225, 0.225
C23	C -0.378; H 0.104, 205
C24	C -0.374; H 0.193, 0.193
C25	C -0.366; H 0.197, 0.197
C26	C -0.621; H 0.200, 0.200, 0.232
C27	C -0.404; H 0.226, 0.225
C28	C -0.378; H 0.205, 0.205
C29	C -0.375; H 0.193, 0.192
C30	C -0.367; H 0.197, 0.197
C31	C -0.620; H 0.200, 0.200, 0.232

Group	Charge
1-Hexylquinolinium	
N^+	-0.111
C1	C -0.115; H 0.277
C2	C -0.208; H 0.276
C3	C -0.212; H 0.278
C4	0.240
C5	0.306
C6	C -0.308; H 0.270
C7	C -0.216; H 0.267
C8	C -0.228; H 0.271
C9	C -0.299; H 0.260
C10	C -0.486; H 0.281, 0.287
C11	C -0.381; H 0.235, 0.231
C12	C -0.385; H 0.205, 0.208
C13	C -0.380; H 0.196, 0.199
C14	C -0.367; H 0.198, 0.197
C15	C -0.620; H 0.200, 0.233, 0.201
1-Methyl-3-tetradecylimidazolium	
$N1^+$	-0.036
$N2^+$	-0.057
C1	C -0.377; H 0.255, 0.278
C2	C -0.043; H 0.288
C3	C -0.630; H 0.251, 0.269, 0.269
C4	C -0.161; H 0.284
C5	C -0.128; H 0.286
C6	C -0.387; H 0.224, 0.226
C7	C -0.387; H 0.209, 0.211
C8	C -0.390; H 0.204, 0.203
C9	C -0.390; H 0.200, 0.200
C10	C -0.388; H 0.197, 0.197
C11	C -0.387; H 0.196, 0.196
C12	C -0.386; H 0.194, 0.194
C13	C -0.385; H 0.194, 0.194
C14	C -0.383; H 0.192, 0.192
C15	C -0.377; H 0.190, 0.190
C16	C -0.374; H 0.188, 0.187
C17	C -0.364; H 0.191, 0.192
C18	C -0.626; H 0.198, 0.219, 0.198

Group	Charge
1-Octyl-3-methylpyrrolidinium	
N^+	-0.026
C1	C -0.441; H 0.277, 0.277
C2	C -0.115; H 0.288
C3	C -0.188; H 0.281
C4	C -0.229; H 0.281
C5	-0.205
C6	C -0.661; H 0.246, 0.252, 0.249
C7	C -0.162; H 0.286
C8	C -0.441; H 0.277, 0.277
C9	C -0.370; H 0.227, 0.229
C10	C -0.392; H 0.211, 0.213
C11	C -0.390; H 0.202, 0.203
C12	C -0.381; H 0.197, 0.197
C13	C -0.377; H 0.192, 0.192
C14	C -0.366; H 0.194, 0.195
C15	C -0.623; H 0.199, 0.227, 0.199

Table D2 Mulliken charges for investigated anions.

Group	Charge
Butanoate	
C1	0.286
$O1^-$	-0.552
$O2^-$	-0.540
C2	C -0.446; H 0.170, 0.156
C3	C -0.371; H 0.178, 0.210
C4	C -0.639; H 0.182, 0.183, 0.182
Ethylsulfate	
S1	1.392
$O1^-$	-0.664
$O2^-$	-0.688
$O3^-$	-0.688
O4	-0.534
C1	C -0.153; H 0.193, 0.194
C2	C -0.633; H 0.205, 0.205, 0.170
Octylsulfate	
S1	1.396
$O1^-$	-0.687
$O2^-$	-0.661
$O3^-$	-0.688
O4	-0.538
C1	C -0.137; H 0.184, 0.185
C2	C -0.402; H 0.194, 0.194
C3	C -0.387; H 0.185, 0.186
C4	C -0.375; H 0.186, 0.186
C5	C -0.373; H 0.186, 0.185
C6	C -0.373; H 0.185, 0.186
C7	C -0.363; H 0.190, 0.190
C8	C -0.633; H 0.197, 0.207, 0.197
Decanoate	
C1	0.284
$O1^-$	-0.540
$O2^-$	-0.547
C2	C -0.447; H 0.152, 0.173
C3	C -0.382; H 0.209, 0.169
C4	C -0.367; H 0.170, 0.172
C5	C -0.377; H 0.186, 0.181
C6	C -0.375; H 0.183, 0.182
C7	C -0.374; H 0.186, 0.184
C8	C -0.372; H 0.184, 0.184
C9	C -0.364; H 0.190, 0.190
C10	C -0.633; H 0.197, 0.207, 0.196
Hexylphosphate	
P-	1.568
F1-F6	-0.428
Bis[(trifluoromethyl)sulfonyl]imide	
N^-	-0.781
S1-S2	1.234
O1, O3	-0.584
O4, O2	-0.602
C1	0.463
C2	0.463
F1, F5	-0.205
F2, F4	-0.197
F3, F6	-0.217